T.C.
AKDENİZ ÜNİVERSİTESİ
SAĞLIK BİLİMLERİ ENSTİTÜSÜ
Histoloji ve Embriyoloji Anabilim Dalı

PRO-İNFLAMATUVAR SİTOKİN MAKROFAJ MİGRASYONUNU İNHİBE EDİCİ FAKTÖR (MIF)'ÜN İLİŞKİDE OLDUĞU PROTEİNLERİN TANIMLANMASI VE BUNLARIN MOLEKÜLER ÖZELLİKLERİNİN BELİRLENMESİ

Sevil ÇAYLI

Doktora Tezi

Antalya, 2009

T.C.
AKDENİZ ÜNİVERSİTESİ
SAĞLIK BİLİMLERİ ENSTİTÜSÜ
Histoloji ve Embriyoloji Anabilim Dalı

PRO-İNFLAMATUVAR SİTOKİN MAKROFAJ MİGRASYONUNU İNHİBE EDİCİ FAKTÖR (MIF)'ÜN İLİŞKİDE OLDUĞU PROTEİNLERİN TANIMLANMASI VE BUNLARIN MOLEKÜLER ÖZELLİKLERİNİN BELİRLENMESİ

Sevil ÇAYLI

Doktora Tezi

Tez Danışmanları
Prof.Dr.Ramazan Demir
Prof.Dr. Andreas Meinhardt

Bu çalışma Akdeniz Üniversitesi Bilimsel Araştırma Projeleri Yönetim Birimi Tarafından Desteklenmiştir. (Proje No: 2006.03.0122.003)

Antalya, 2009

Sağlık Bilimleri Enstitüsü Kurul ve Senato Kararı

Sağlık Bilimleri Enstitüsünün 22/06/2000 tarih ve 02/09 sayılı enstitü kurul kararı ve 23/05/2003 tarih ve 04/44 sayılı senato kararı gereğince 'Sağlık Bilimleri Enstitülerinde lisanüstü eğitim gören doktora öğrencilerinin tez savunma sınavına girebilmeleri için, doktora bilim alanında en az bir yurtdışı yayın yapması gerektiği' ilkesi gereğince yapılan yayınların listesi aşağıdadır (Orjinalleri ekte sunulmuştur).

1. Cayli S, Klug J, Frohlich S, Krasteva G, Orel L, Meinhardt A. (2009). The COP9 signalosome interacts ATP-dependently with p97/VCP and controls the ubiquitination status of proteins bound to p97/VCP. EMBO reports (baskı için revizyonda)

2. Filip AM, Klug J, **Cayli S**, Frohlich S, Henke T, Lacher P, Eickhoff R, Bulau P, Linder M, Carlsson-Skwirut C, Leng L, Bucala R, Kraemer S, Bernhagen J, Meinhardt A. (2009). Ribosomal Protein S19 Interacts with Macrophage Migration Inhibitory Factor and Attenuates Its Pro-inflammatory Function. J Biol Chem 284:7977-7985.

3. Kayisli, U. A., **Cayli, S.,** Seval, Y., Tertemiz, F., Huppertz, B., and Demir, R. (2006). Spatial and temporal distribution of Tie-1 and Tie-2 during very early development of the human placenta. Placenta *27*, 648-659.

4. Cayli, S., Sakkas, D., Vigue, L., Demir, R., and Huszar, G. (2004). Cellular maturity and apoptosis in human sperm: creatine kinase, caspase-3 and Bcl-XL levels in mature and diminished maturity sperm. Mol Hum Reprod *10*, 365-372.

5. Cayli, S., Jakab, A., Ovari, L., Delpiano, E., Celik-Ozenci, C., Sakkas, D., Ward, D., and Huszar, G. (2003). Biochemical markers of sperm function: male fertility and sperm selection for ICSI. Reprod Biomed Online *7*, 462-468.

6. **Cayli, S.,** Ustunel, I., Celik-Ozenci, C., Korgun, E. T., and Demir, R. (2002). Distribution patterns of PCNA and ANP in perinatal stages of the developing rat heart. Acta Histochem *104*, 271-277.

Sağlık Bilimleri Enstitüsü Müdürlüğüne;

Bu çalışma jürimiz tarafından Histoloji ve Embriyoloji Anabilim Dalı, Histoloji ve Embriyoloji doktora Programında doktora tezi olarak kabul edilmiştir. 12/06/2009

Danışman:
Prof.Dr.Ramazan Demir
Akdeniz Universitesi
Tıp Fakültesi Histoloji ve Embriyoloji Anabilim Dalı

Üye:
Prof.Dr.Mevlüt Asar
Akdeniz Universitesi
Tıp Fakültesi Histoloji ve Embriyoloji Anabilim Dalı

Üye:
Prof.Dr. Zeynep Kahveci
UludağÜniversitesi
Tıp Fakültesi Histoloji ve Embriyoloji Anabilim Dalı

Üye:
Prof.Dr.İsmail Üstünel
Akdeniz Universitesi
Tıp Fakültesi Histoloji ve Embriyoloji Anabilim Dalı

Üye:
Doç.Dr.Mustafa Usta
Akdeniz Universitesi
Tıp Fakültesi Üroloji Anabilim Dalı

ONAY:

Bu tez, Enstitü Yönetim Kurulunca belirlenen yukarıdaki jüri üyeleri tarafından uygun görülmüş ve Enstitü Yönetim Kurulu'nun …/…/2009 tarih ve …/…/…sayılı kararıyla kabul edilmiştir.

Prof.Dr.İsmail Üstünel
Enstitü Müdürü

ÖZET

Makrofaj göçünü engelleyici faktör (MIF) birçok hücre tipi tarafından sentezlenen ve ismi insan monositlerinin göçünü engellemesi nedeniyle verilmiş olan bir immun mediatördür. Son yıllarda, MIF'in Jab1/CSN5 (c-Jun-aktive edici domain-bağlayıcı protein 1)'e bağlanarak, COP9 (constitutive photomorphogenesis: sürekli ışıkla değişim 9) signalozomun (CSN) denedilaz (Cullin proteininden Nedd8 proteinin uzaklaştırılması) aktivitesini durdurduğu ortaya konulmuştur. CSN'nin hedef proteinlerinden biri Cullin proteini SCF (Skp1-Cullin-F box) E3 übikütin ligaz ailesine aittir. SCF E3 übikütin ligazlar, 26S protazomda yıkıma uğratılan substratların übikütinlenmesinden sorumludurlar. MIF'in UPS'deki biyolojik rolünü daha iyi anlamak amacıyla, bu çalışmada MIF'i sürekli olarak ekspre eden NIH3T3 (fare fibroblast hücre dizisi) hücrelerinde biyotinlenmiş MIF ile ilişkide olan proteinleri araştırdık.

Biyotinlenmiş MIF ve onun ilişkide olduğu proteinler, streptavidin ile saflaştırıldı. MIF'e bağlanan proteinlerin kütle spektrometrisi ile tanımlanması sonucu, MIF ile birlikte peroksiredoksin 1 ve RP S19 (ribozomal protein S19) gibi MIF'e bağlandığı bilinen proteinlerin de belirlenmesi kullandığımız metodun güvenilirliğini gösterdi. Belirlenen yeni proteinler yanında Valosin-içeren protein (valosin-containing protein, VCP) gibi endoplasmik retikulum (ER)'la ilişkili ve UPS'de çalışan proteinler de saptandı. Belirlenen proteinlerin büyük bir çoğunluğunun UPS'de görevli olduğunun bulunması, bundan sonraki araştırmaların MIF ile VCP arasındaki ilişki üzerine yoğunlaşmasına neden oldu. MIF'in VCP'ye Jab1/CSN5 aracılı bağlandığı, VCP ve Jab1/CSN5 arasındaki bağlanmanın ise direk olduğu immun çökeltme (ko-immunopresipitasyon), *in vitro* çökeltme (*in vitro* presipitasyon) ve floresan rezonans enerji transferi (FRET) yöntemleriyle kanıtlandı.

VCP ve Jab1/CSN5 arasındaki bağlanma, her iki proteine ait mutant ve vahşi tip proteinlerin hücreye transfeksiyonu ve sonra da onların immun çökertmeleri ile belirlendi. Jab1/CSN5'in MPN (Mpr1 Pad1-N-terminal) domainin, VCP'nin ND1 domaini ile bağlandığı belirlendi. Ayrıca, bağlanmanın izopeptidaz aktivitesine sahip MPN domainindeki JAMM (Jab1/MPN domain-associated metalloisopeptidase: Jab1/MPN domain-ilişkili metaloizopeptidaz) motifine bağlı olmadığı da gösterildi. Jel filtrasyon kromatografisi kullanılarak da, VCP'nin sadece Jab1/CSN5'a değil de tüm CSN kompleksine bağlandığı ortaya konuldu.

RNA interferans aracılı gen susturma (nakdavn: gen ekspresyonunun azaltılması) çalışmaları ile, Jab1/CSN5'ın JAMM motifinin, CSN kompleksi subunitelerinin ve CSN'e bağlı deübikütinlaz USP15 (ubikütin spesifik proteaz 15)'in VCP'ye bağlı substratların deübikütinlenmesi (übikütin zincirlerinin uzaklaştırılması) için gerekli oldukları gösterildi.

Kısacası, bu sonuçlar, VCP'nin CSN ile birlikte bir kompleks oluşturduğunu ortaya çıkardı. Bu kompleksin görevi ise, übikütinlenmiş ve yanlış katlanma gösteren proteinlerin kaderlerini belirlemede görev yaparak, bu proteinleri bağlı bulundukları komplekslerden uzaklaştırmaktır.

Anahtar kelimeler: MIF, VCP, Jab1/CSN5, UPS

ABSTRACT

Macrophage migration inhibitory factor (MIF) is an immune modulator which is synthesized by various cell types and originally has been named by its ability to inhibit the random migration of human monocytes. More recently, evidence has accumulated that MIF may function in the inhibition of the deneddylase activity of the COP9 signalosome (CSN) by interacting with its subunit Jab1/CSN5. The target of the CSN deneddylase activity is the cullin component of SCF E3 ubiquitin ligases that are significantly more active when neddylated. These ligases are responsible for the selective ubiquitinylation of substrates which are hydrolysed in the 26S proteasome. Thus, ubiquitinylating enzymes and the proteasome form the two main components of the ubiquitin proteasome system (UPS). To better understand the biological role of MIF in the UPS, a systematic interactome screen was performed in NIH3T3 cells that are constitutively expressing biotinylated MIF.

Biotinylated MIF and its associated proteins were purified by streptavidin binding. Subsequent identification of MIF interacting proteins by mass spectrometry detected a number of already known MIF interacting proteins including MIF itself, peroxiredoxin 1 and RPS19, thus emphasizing the validity of the approach. Besides other new candidates, endoplasmic reticulum (ER) associated chaperones and the AAA ATPase valosin-containing protein (VCP), which are all involved in ER-associated degradation were identified. As many new MIF interacting partners are involved in the UPS, further investigations were concentrated on the association of MIF with Jab1/CSN5 and VCP. While the binding of MIF to VCP is mediated by Jab1/CSN5, the interaction of VCP with Jab1/CSN5 is direct as verified independently by co-immunoprecipitation (co-IP), *in vitro* pull-down assays and fluorescence resonance energy transfer experiments.

The interaction interface between VCP and Jab1/CSN5 was investigated by transient transfection of wild type and mutant proteins followed by co-IP. It emerged that Jab1/CSN5 associates with VCP via the core of its MPN domain that is contacting the ND1 domain of VCP. Its binding is independent of the JAMM motif harboring the NEDD8 isopeptidase activity. Using gel filtration chromatography, VCP co-migrated with the CSN and co-IP experiments confirmed that the interaction of VCP is not restricted to Jab1/CSN5, but involves the whole CSN complex in the association.

RNA interference mediated knockdowns demonstrated that the JAMM motif of CSN5, a functional CSN complex and the CSN-associated deubiquitinase USP15 are all required for deubiquitinylation of substrates bound to VCP.

Taken together, these results suggest that the CSN together with VCP forms a complex. Therefore, the CSN together with VCP could have the function to extract ubiquitinylated and abnormal folded proteins from larger protein complexes or membranes and to determine their fate.

Key words: MIF, VCP, Jab1/CSN5, UPS

TEŞEKKÜR

Yazar, bu çalışmanın gerçekleşmesine katkılarından dolayı, aşağıda adı geçen kişi ve kuruluşlara içtenlikle teşekkür eder.

Tez danışmanlarım Prof. Dr. Ramazan Demir ve Prof. Dr. Andreas Meinhardt tezimin gerçekleşmesi için her türlü desteği sağlamışlardır.

Prof. Dr. Andreas Meinhardt tezin maddi desteğinin büyük bir kısmını karşılaşmıştır ve Dr. Meinhardt'ın diğer çalışma arkadaşlarından teknik destek alınmıştır.

Histoloji ve Embriyoloji Anabilim Dalı'nın tüm çalışanları, ihtiyacım olduğunda yardımlarını esirgemeden destek olumuşlardır.

Son olarak eşim Fatih Çaylı tezimin gerçekleşmesinde manevi destek vermiştir.

İÇİNDEKİLER DİZİNİ

Ek 1. Cayli S, Klug J, Frohlich S, Krasteva G, Orel L, Meinhardt A. (2009). The COP9 signalosome interacts ATP-dependently with p97/VCP and controls the ubiquitination status of proteins bound to p97/VCP. EMBO reports

Ek 2. Filip AM, Klug J, **Cayli S**, Frohlich S, Henke T, Lacher P, Eickhoff R, Bulau P, Linder M, Carlsson-Skwirut C, Leng L, Bucala R, Kraemer S, Bernhagen J, Meinhardt A. (2009). Ribosomal Protein S19 Interacts with Macrophage Migration Inhibitory Factor and Attenuates Its Pro-inflammatory Function. J Biol Chem 284:7977-7985.

Ek 3. Kayisli, U. A., **Cayli, S.,** Seval, Y., Tertemiz, F., Huppertz, B., and Demir, R. (2006). Spatial and temporal distribution of Tie-1 and Tie-2 during very early development of the human placenta. Placenta *27*, 648-659.

Ek 4. Cayli, S., Sakkas, D., Vigue, L., Demir, R., and Huszar, G. (2004). Cellular maturity and apoptosis in human sperm: creatine kinase, caspase-3 and Bcl-XL levels in mature and diminished maturity sperm. Mol Hum Reprod *10*, 365-372.

Ek 5. Cayli, S., Jakab, A., Ovari, L., Delpiano, E., Celik-Ozenci, C., Sakkas, D., Ward, D., and Huszar, G. (2003). Biochemical markers of sperm function: male fertility and sperm selection for ICSI. Reprod Biomed Online *7*, 462-468.

Ek 6. Cayli, S., Ustunel, I., Celik-Ozenci, C., Korgun, E. T., and Demir, R. (2002). Distribution patterns of PCNA and ANP in perinatal stages of the developing rat heart. Acta Histochem *104*, 271-277.

SİMGELER VE KISALTMALAR

aa	:	Aminoasit
Amp	:	Ampisillin
AP-1	:	Aktivatör protein 1
APS	:	Amonyum persülfat
ATP	:	Adenosin 5'-trifosfat
bp	:	Baz çifti
BSA	:	Sığır serum albumin
cDNA	:	Komplementer DNA
COP	:	Sürekli fotomorfogenez
cPLA2	:	sitosolik fosfolipaz
CXCR2	:	CXC kemokin reseptörü 2
DMSO	:	Dimetil sülfoksit
DNA	:	Deoksiribonükleik asit
DTT	:	Ditiotereitol
DUB	:	Deübikütinaz
E. coli	:	*Escherichia coli*
ECL	:	Kemiluminisans
EDTA	:	Etil diamin tetraasetik asit
ERAD	:	Endoplasmik retikulum ilişkili yıkım
ERK1/2	:	Ekstrasellular sinyal-regüle edici kinaz1/2
FCS	:	Fetal sığır serumu
FLAG	:	N-DYKDDDDK-C (oktapeptid)
FRET	:	Floresan Rezonans Enerji Transferi
GST	:	Glutatyon S-Transferaz
HIF-1	:	Hipoksi indükleyici transkripsiyon faktör 1
His	:	Histidin
HRP	:	Horse radish peroksidaz
IPTG	:	Izopropil β-D-tihogalaktopranosit
IEF	:	Isoelektrik fokuslayıcı faktör
JAB1	:	c-Jun-aktivasyon domain-bağlayıcı protein 1
JNK	:	c-Jun N-terminal kinaz
kb	:	Kilo baz.
kD	:	Kilo Dalton
LB	:	Luriya Bertani medyum
LPS	:	Lipopolisakkarid
M	:	Molar
MAPK	:	Mitojen-aktive edici protein kinaz
MES	:	Morfolin etan sülfonik asit
MIF	:	Makrofaj göçünü engelleyici faktör
MOPS	:	3-(N-Morpolin)-propan sülfonik asit

mRNA	:	*haberci* RNA
NaCl	:	Sodyum klorit
NCBI	:	Uluslarası Biyoteknoloji Bilgi Servisi
NHS	:	Normal at serumu
NP-40	:	Nonidet P-40
PAG	:	Proliferasyonla ilgili-gen
PAGE	:	Poliakrillamit jel elektroforesi
PBS	:	Fosfat buferli tuz
PCR	:	Polimeraz zincir reaksiyonu
PFA	:	Paraformaldehit
PGE2	:	Prostaglandin E2
Pgk-1	:	Fosfogliserat kinaz 1
pH	:	-log c[H^+]
PMSF	:	Fenilmetilsülfonil florit
PVDF	:	Polivinlidenflorit
RISC	:	RNA-indüklü susturucu kompleks
RNA	:	Ribonükleik asit
RNAi	:	RNA interferans
RNase	:	Ribonükleaz
rpm	:	Revolutions per minute
RP S19	:	Ribosomal protein S19
SCF	:	Skp1-Cullin-F-box protein
SDS	:	Sodyum dodesilsülfat
siRNA	:	short (kısa) interferans RNA
shRNA	:	short (kısa) hairpin (U şekilli) RNA
STAM	:	sinyal iletici adaptör molekül
TAE	:	Tris-asetat-EDTA
TAP	:	Çok aşamalı afinite saflaştırması
TBE	:	Tris-borat-EDTA
TE	:	Tris-EDTA
TEMED	:	N-N'-N'-Tetrametilendiamin
TLR	:	Toll benzeri reseptör
TNF-α	:	Tümor nekroz faktörü alfa
Tris	:	Tris (hidroksimetil)-amino-methan
UPS	:	Übikütin protazom sistem
USP15	:	Übikütin spesifik proteinaz 15
UV	:	Ultraviolet
V	:	Volt
VCP	:	Valosin-içeren protein
wt	:	vahşi tip
µ	:	Mikro

ŞEKİLLER DİZİNİ

ÇİZELGELER DİZİNİ

GİRİŞ VE KONU İLE İLGİLİ KAYNAK BİLGİLER

1.1. MIF'in Keşfi

Makrofaj migrasyonunu inhibe edici faktör (Macrophage migration inhibitory factor: Makrofaj göçünü engelleyici faktör, MIF), bilinen en eski immunolojik mediatörlerden bir tanesidir. MIF ismi, yapılan *in vitro* çalışmalar sonucu bu faktörün makrofaj göçünü engellediğinin görülmesi nedeni ile verilmiştir [1, 2]. 1989'da MIF proteini, başarılı bir şekilde klonlanmış [3], biyoaktif MIF proteini ve nötralize edici MIF antikorları üretilmiştir [4].

İnflamasyonda görevli glukokortikoidlerin araştırılması sırasında, MIF'in ön hipofiz bezi hücrelerinden tıpkı bir hormon gibi salgılanabilen yeni bir protein olduğu açığa çıkarılmıştır [5]. İntraperitonel olarak farelere MIF enjeksiyonunun, önhipofizdeki MIF içeriğinde bir düşüşe neden olduğunun gösterilmesi MIF'in immun ve inflamatuvar sistem arasında çalışan bir mediatör olduğunu açığa çıkarmıştır.

1.2. MIF Geni ve Protein Yapısı

MIF geni, insan genomunun 22. kromozomunda lokalize olmuştur. Bu gen, üç kısa ekzon ve 2 kısa intron içermektedir. 5'regulator bölgesi, aktivatör protein (AP-1) ve nüklear faktör κB (NF-κB) gibi insan MIF geninin regülasyonunda görevli çeşitli transkripsiyon faktörleri için DNA'ya bağlanma bölgeleri içermektedir. MIF'in homoloğu olan genlerin araştırılması sırasında, *D*-dopakrom tatomeraz (DDT)'ın MIF ile homoloji gösterdiği belirlenmiştir [6] Tüm memeli MIF'leri (insan, fare, kedi, sıçan), %90 homoloji göstermektedir. MIF geninin bu şekilde korunmuş olması, bu genin önemli biyolojik aktivitelere sahip olduğunu göstermektedir. MIF cDNA'sı 12,5kDA luk moleküler ağırlıklı, 114 aminoasitlik proteini kodlamaktadır.

X-ray kristallografisi ile birlikte, sıçan ve insan MIF proteininin kurdele yapısı belirlenmiştir [7-9]. Yapılan çalışmalar, MIF'in hem trimer olarak kristal yapıda [10] hem de dimer olarak eriyik formda [9] bulunduğunu göstermiştir. Son çalışmalar, fizyolojik şartlar altında, MIF'in monomer, dimer ve trimer olduğunu göstermektedir.

1.3. MIF'in Enzimatik Aktivitesi

Üç boyutlu yapısı ve de prokaryatik enzime benzemesi nedeniyle MIF'in enzimatik aktivitesi ile ilgili çalışmalar hız kazanmıştır. MIF, hem totameraz [11-13] hem de oksidoredüktaz [14-16] aktivitelerine sahiptir.

1.4. MIF'in Biyolojik Aktiviteleri

1.4.1. MIF Aracılı ERK1/ERK2 Yolağının Aktivasyonu

MIF'in mitojen aktive edici protein kinaz (MAPK) ailesine ait ekstrasellular sinyal-düzenleyici kinaz 1 (ERK1)/ERK2'i aktive ederek hücre proliferasyonuna neden olduğu ortaya konulmuştur [17]. MIF indüklü ERK1/ERK2 aktivasyonu protein kinaz A'ya ve de aynı zamanda da sitoplazmik fosfolipaz A2 (PLA2) enzim aktivitesindeki artışa bağlıdır. PLA2 proinflamatuvar yolakların aktivasyonunda önemli bir hücreiçi aracı moleküldür ve glukokortikoidlerin anti-inflamatuvar etkilerinin gösterilmesinde hedef bir proteindir. ERK1/ERK2 aracılı PLA2'nın aktivasyonu, MIF'in steroidler üzerindeki immun baskılayıcı etkilerini nasıl ortaya çıkardıklarını gösteren bir mekanizma olmuştur [17].

CD74'un ekstrasellüler domaininin, MIF'e bağlandığı ispatlanmıştır [18]. CD74 prostaglandin E2 (PGE2) üretimi, hücre çoğalması, ERK1/ERK2 aktivasyonu gibi MIF'in direk içinde bulunduğu birçok aktivitede görev yapmaktadır. Fakat, CD74'ün hücreiçi domaininin MIF ile bağlantısı gösterilemediği için, CD74'un MIF için belirlenmiş bir reseptör olduğu buluşu tartışma yaratmıştır.

1.4.2. MIF'in p53'ü İnhibisyonu

MIF'in p53 aracılı büyüme geriliği ve apoptozu negatif yönde etkilediğini gösteren çalışmalar inflamasyon ve tümorogenez arasında bir bağlantı kurulmasını sağlamıştır [19]. Bu çalışmayı takiben, LPS (lipopolisakkarit) stimulasyonu sonrası MIF geni susturulmuş makrofajların proinflamatuvar fonksiyonlarının ve canlılıklarının normal hücrelere göre düştüğünü göstermiştir [20]. MIF geni susturulmuş makrofajlar, normal hücrelerle karşılaştırıldıklarında, heriki hücreninde eşit NO (nitrik oksit) ürettikleri bilinse de, NO'in MIF geni susturulmuş makrofajlarda apoptozu artırıcı önemli bir aracı molekül olduğu düşünülmüştür. Dahası, MIF'in hücre içinde p53'in intraselüler birikimini engellediği de bulunmuştur. MIF tarafından p53'nin inhibisyonu ERK1/ERK2, PLA2, sikloksijenaz 2 (COX2) and PGE2'nin ardı ardına aktivasyonunu gerektirmektedir (Şekil 1.4.2.1). Bu çalışmalara ek olarak, MIF'in normal ve tümorlü hücre gelişimini sağlamak için E2F–p53 yolağı ile de etkileşimde olduğunu göstermiştir [21].

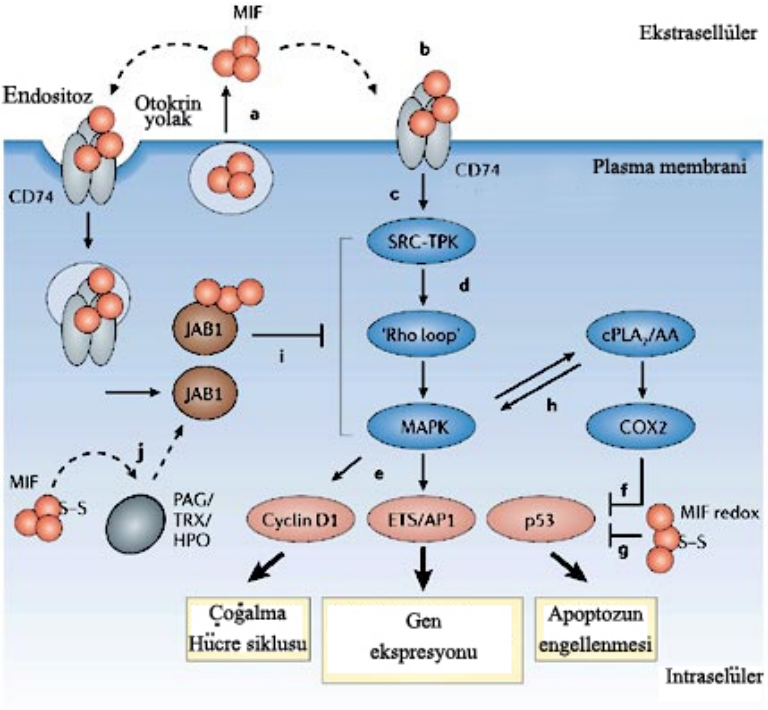

Şekil 1.4.2.1. MIF'in ekstraselüler reseptör aracılı ve intrasellüler etkileşimlerini gösteren hücre yolağı.

(a) Ekstraselüler MIF hücre yüzeyinde CD74 ile etkileşir. (b) MIF, CD74 aracılı, p38 mitojen aktive edici protein kinaz (MAPK) yolağını ve ekstraselüler sinyal kontrolünü sağlayan kinaz 1 ve 2 (ERK1/2)'i aktive eder. (b, c, d) CD74 ve MIF arasında bu yolakta çalışan proteinlerin bazıları (SRC ailesine ait tirozin kinaz ve Rho kinaz ailesine ait tirozin kinaz) izlenmektedir. (e) CD74/MIF yolağının aktivasyonu, siklin D1, ETS domainini içeren transkripsiyon faktörünü de aktive ederek gen ekspresyonunu, hücre çoğalmasını ve hücre siklusunun çalışmasını başlatmaktadır. (f) MIF tarafından p53 yolağının inhibisyonu MIF ve CD74 etkişiminin başlaması ve de sitosolik fosfolipaz A2 (cPLA2), araknoik asit, siklooksijenaz 2 (COX2) ile olmaktadır. Oksidatif stres ile indüklenen apoptoz MIF'in antioksidant aktivitesi ile inhibe edilmektedir. (g, h) Araknoik asit, MAPK aktivasyonuna ve AP1 düzenleyici gen ekspresyonuna neden olmaktadır. (i) Yüksek konsantrasyonlardaki endositoz ile hücre içine alınan MIF, c-jun aktive edici domain bağlayıcı protein 1 (JAB1)'ne bağlanır ve MIF sinyal yolunu negatif yönde etkiler. (j) Hücreiçi MIF, JAB1 yanında peroksiredoksin 1(PAG), tihoredoksin (TRX) ve hepatopoetin (HPO)'e bağlanır.

1.4.3. MIF'in Toll Benzeri Reseptör-4 Ekpresyonunu Kontrol Etmesi

Toll benzeri reseptörler (Toll-like receptor, TLR) mikroorganizmaların ürünü olan maddeleri tanıyarak immun sistemde temel rol alırlar [22, 23]. TLR4 gram negatif bakterilerin hücre duvarının temel bir elemanı olan LPS için bir reseptördür [24]. MIF ekspre etmeyen makrofajların LPS ve gram negatif bakterilere yanıt vermedikleri ve TLR4 ekspresyonundaki düşüşden dolayı da sitokin üretiminlerinde de düşüş gösterdikleri ortaya çıkarılmıştır [25, 26]. MIF, fare TLR4 geninin transkripsiyonu için temel olan ETS ailesine ait transkripsiyon faktörleri üzerinde etki göstererek TLR4

ekspresyonunu artırmaktadır. Bu nedenle, MIF invasif bakterilere hızlı cevap verilmesini sağlayarak endotoksin içeren bakterilerin saptanmasına yardımcı olur.

1.4.4. MIF'in Glikolizi Uyarması

MIF'in glikolozisi regüle ettiği *in vivo* ve *in vitro* çalışmalarla kanıtlanmıştır [27]. MIF periferal glukoz metabolizmasını ve inflamatuvar cevaplar tarafından indüklenen katabolik etkileri kontrol eder. Rekombinant MIF'ın farklılaşmış sıçan kas hücrelerine eklenmesi, früktoz bifosfat sentezini artırmıştır. Aynı çalışmada, TNF-α'nın kas hücrelerine olan katobolik etkisinin MIF aracılı olduğu ve bu etkinin früktoz bifosfat üretimini sağladığı belirtilmiştir. Farelere TNF-α verilmesi serum glukoz düzeyinin düşmesine ve kas fruktoz bifosfat düzeylerinin yükselmesine neden olmuştur. Buna ek olarak, nötralize edici anti-MIF antikorunun uygulanması, bu etkieri tamamiyle ortadan kaldırmıştır. Aynı zamanda, anti-MIF antikorunun uygulanması hipoglisemiyi de engellemiş ve LPS ile muamele edilmiş TNF-α–nakavt farelerde, kas fruktoz bifosfat düzeyleri de yükselmiştir. Bu sonuç, MIF'in bu inflamasyon indüklü metabolik değişikliklere katkısını da desteklemektedir. Kısacası, MIF insulin salınımının otokrin uyarıcısı olarak bilinmektedir ve glukoz, karbonhidrat metabolizmasının kontrolünde önemli bir rol oynadığı kanıtlanmıştır.

1.4.5. MIF'in JAB1/CSN5 Aktivitesini Engellemesi

MIF ve COP9 signalozomun beşinci komponenti olarak bilinen c-Jun-aktive edici domain-bağlayıcı protein 1 (JAB1) arasındaki bağlanma, protein-protein bağlanmasını saptamada kullanılan maya iki-hibrit sistemi (yeast two-hybrid sistemi) ile gösterilmiştir [28]. Jab1/CSN5, Jun N-terminal kinaz (JNK) ve c-Jun'u aktive eder ve hücre büyümesi, transformasyonu ve ölümünde görev alan aktivatör protein 1 (AP1)'i uyarır [29]. MIF ve Jab1/CSN5'in sitoplâzmada birlikte bulundukları, MIF'in JNK ve AP1'nin regülator etkisini engellediği ortaya çıkarılmıştır [28].

1.4.6. MIF'in AKT Yolağını Uyarması

MIF tarafından p53 aracılı apoptozun engellendiği gösterilmiş olmasına rağmen, MIF indüklü AKT (serin/tirionin-spesifik protein kinaz) yolağının da, apoptozu engelleyip fibroblast, HeLa serviks karsinoma hücreleri ve birçok göğüs kanseri hücrelerinde hücre yaşamını sağladığı gösterilmiştir [30]. Fosfoinositol-3-kinaz (PI3K)/AKT sinyal yolağı, büyüme, metabolizma, migrasyon, apoptoz ve hücre yaşamı gibi hücresel fonksiyonları kontrol etmede önemli bir rol oynamaktadır [31]. Bu sinyal yolağı, reseptör tirozin kinaz ve ya G-protein eşli reseptörlerin indüklenmesi ile başlatılmaktadır [32]. PI3K/AKT aktivasyonu birçok hücresel yolağın çalışmasını başlatmakla beraber, en önemlisi, hücre yaşamını sağlayarak apoptozu engellemektedir. MIF indüklü AKT yolağı, sinyalini MIF reseptörü CD74 ile ve de Src, PI3K kinazlar yoluyla iletmektedir. Bunlara ek olarak, MIF indüklü AKT aktivasyonu, proapoptotik proteinlerden BAD ve Foxo3a'nın inaktivasyonuna neden olmaktadır. Bu sonuçlara paralel, MIF tarafından apoptozun baskılanması AKT yolak inhibitörü PTEN (Fosfotaz ve tensin homoloğu olan gen, Phosphatase and tensin homolog gen) tarafından da

engellenmiştir. Bu sonuç, apoptozun inhibisyonunun p53 yardımıyla olmadığını kanıtlamıştır. Kısacası, MIF'in hücre yaşamı üzerine olan etkisinin birçok hücrede, PI3K/AKT ve onun altyolakları aracılığıyla olduğu kanıtlanmıştır.

1.4.7. MIF'in Lökosit Göçünü Düzenlemesi

MIF'in makrofaj göçünü engellediği keşfedilmiş olmasına rağmen [2], MIF'in regüle ettiği hücre göçünün mekanizması ve bu göçde görev alan proteinler uzun yıllardır çalışılmamıştır. Son çalışma, MIF'in kemokin reseptörleri olan CXCR2 (kemokin reseptörü 2) ve CXCR4 için fonksiyonel bir bağlayıcı molekül olduğunu ve bu nedenlede inflamatuvar ve atherojenik lökosit alınımını kontrol ettiği ortaya çıkarılmıştır [33]. Bu çalışmada, MIF'in CXCR2 ve CXCR4 aracılı monosit ve T hücrelerinin kemotaksisine, hızlı integrin aktivasyonuna ve kalsiyum akışına yardımcı olduğu gösterilmiştir. MIF direk olarak CXCR2'ya bağlanır, CXCR2 ve CXCR4'e bağlanmak için rekabete girer. Bu çalışmada aynı zamanda, CXCR2 ve CD74 interaksiyonun da bulunması, CXCR2-CD74 kompleksi için yeni bir sinyal yolağı oluşturacağını önermektedir. Bunlara ek olarak, *in vivo* çalışmalar, MIF eksikliğinin atherosiklorotik farelerde, monositlerin arterial duvara adhezyonunu azalttığını göstermiştir. Kısacası, MIF atherosiklerozda temel bir CXCR2 ligandı olarak tanımlanmıştır. İleri düzeyli arterosiklerozlu farelerde MIF blokajı plak gerilemesine ve plaklarda monosit ve T hücre içeriğinde azalmaya neden olmuştur. Bu önemli buluşlar ışığında, MIF'in kemokin benzeri özellikleri, inflamasyon ve arterosiklerozdaki düzenleyici rolü keşfedilmiştir [33].

1.4.8. MIF'in AMPK Yolağını Aktive Etmesi

MIF'in metabolik etkilerinden bir tanesi de AMP-aktiveli protein kinaz (AMPK) yolağı üzerinde çalışmış olmasıdır [34]. AMPK yolağı, hücresel stress sırasında hem glukoz alımının hem de glikolizin kontrolünde ve de apoptoz ve iskemik hasara karşı kalbin korunmasında rol oynamaktadır. AMPK farklı yolaklar üzerinde etki göstermektedir. Örneğin, AMPK glikolizi ve 6-fosfofruktoz-2-kinaz aktivitesini uyarır [35], glukoz taşıyıcısı-4 (GLUT-4) translokalizasyonunu indükler, miyokardiyal hasarı ve apoptozu engeller [36].

MIF'in CD74 aracılığıyla, AMPK aktivasyonunu uyardığı ve iskemik kalpden salındığı gösterilmiştir. Bu uyarı, glukoz alınımını indüklediği gibi, kalbi iskemi-reperfüzyon hasarı boyunca da korur. MIF geninin delesyonu, fare kalbinde iskemik AMPK sinyalini engellemektedir. Buna ek olarak, insan fibroblastlarında MIF salınımı ve AMPK uyarısı hipoksiya boyunca azalmıştır. Bu nedenlerden dolayı, MIF, iskemi boyunca, kalbi koruyucu AMPK yolağı uyaran bir düzenleyici olarak kabul edilmektedir. Bu sonuçlar, kalbde metabolizma ve inflamasyon arasında bir bağlantı olduğunu göstermektedir. Ayrıca, MIF'in AMPK yolağı aracılığıyla insan kalbinin iskemiye cevabında önemli bir role sahip olduğunu da düşündürmektedir.

AMPK, iskelet kas glukoz alınımını arttırması ve hepatik glukoz üretimini baskılaması gibi metabolik etkilerinden dolayı birçok hastalığın tedavisinde hedef moleküllerden birisidir. AMPK'nin, iskemik şartlardaki rolü ve kalbi koruyucu etkisi de bilinmektedir [37]. Bu nedenlerden dolayı, miyokardiyal iskemi ve hasarına karşı, MIF ve MIF agonistlerinin uygulanması, AMPK aktivasyonunu hedef alan bir tedavi olabilir.

1.5. MIF Ve Patalojisi

MIF kronik ve akut birçok hastalığın patogenezinde rol oynamaktadır. MIF ile ilişkili, birçok hastalığın farklı sistem ve organlardaki dağılımı Tablo 1.6.1'de gösterilmiştir [38].

Tablo 1.5.1. MIF ile İlişkili Patolojiler

Sistem ve organlar	Patoloji
Immün sistem	sepsis, septik şok ve allograft rejeksiyonu
Akciğer	astım, tüberkulosis ve Wegenerin granulomatosis
Böbrek	glomerulonefritis
Kemik ve eklemler	rheumatoid arthritis, polikondiritis
Gastrointestinal kanal	kolitis ve Crohn hastalığı
Deri	atopik dermatitis, psoriasis ve sistemik sklerosis
Endokrin sistem	tip–2 diabet ve pankreatis
Beyin	multiple sklerosis ve nöro-Behçet hastalığı
Göz	uvitis ve iridosistis
Kalp ve damarlar	atherosklerosis
Kulak	otitis

1.6. MIF'in Hücre Ve Dokulardaki Dağılımı

İmmun sistem yanında, MIF'in geniş bir hücre ve doku dağılımı vardır (Tablo 1.6.1). Önceleri, MIF'in kaynağının immune sistem T hücreleri olduğu düşünülürdü. Fakat monosit, makrofaj, kan dendritik hücreleri, B hücreleri, nötrofiller, eozinofiller, mast hücreleri ve hipofiz ön lobu kortikotropik hücrelerinin MIF ekspre ettikleri gösterilmiştir [38, 39]. MIF aynı zamanda, akciğer, derinin epitel tabakası, gastrointestinal ve ürogenital kanallar gibi doğal ortamla direk kontakta olan hücre ve dokular tarafından da ekspre edilir. Bunlara ek olarak, yüksek düzey MIF ekspresyonu, hipotalamus ve adrenal bezlerde de görülmüştür [40-43].

Tablo 1.6.1. MIF'ın hücre ve dokulardaki dağılımı

Hücre tipi	Stimülasyon	Referanslar
Ön hipofiz		
Kortikotropik hücreler	RF, LPS	[5] [44]
Immün sistem		
Monosit/makrofajlar	LPS, TNFα, IFNγ, Glukokortikoidler	[45]
	TSST-1, ekzotoksin	[46]
T hücreleri, mast hücreleri	PMA/ionomycin, PHA	[47]
Eozinofiller	PMA, C5a, IL-5	[48]
HL-60, miyelomonosistik	LPS	[49]
Adrenal bezler		
Korteks-zona glomeruloza, zona fasikülata	LPS	[41]
Akciğer		
Bronş epitel hücresi	LPS	[41]
Alveolar makrofajlar		[50]
Böbrek		
Tübül epitel hücreleri, proksimal tübüller	LPS	[51]
Glomerul epitel hücreleri, endotel	LPS	[43]
Kupfer hücreleri		
Tübüler epitel hücreleri	LPS	[52]
Mezangiyal hücreler	LPS, PDGF-AB, IFNγ	[53]
Karaciğer		
Sentral ven etrafındaki hepatositler	LPS	[41]
Deri		
Keratinositler, sebaköz bezleri,	LPS, kroton yağı	[54]
Kıl folekülünün örtüsü,	UV B	[54]
epidermal tabaka, endotel hücreleri	Akut inflamasyon	[55]
Testis		
Leydig hücreleri		[56]
Pankreas		
β hücreleri	Glukoz	[57]
Göz		
Korneyal epitel hücreleri		[58]
Endotel hücreleri, lens		[59]
Iris, siliar epitel		[59]
Beyin		
Korteks, hipotalamus	LPS	[60]
Glial hücreler, ependima, astrositler Telensephalon		[61]
Kemik		
Neonatal kemik ve osteoblastlar,	LPS	[62]
Yağ hücreleri		
3T3L1 adipositler	TNFα	[63]
Prostat		
Epitel hücreleri		[64] [65]
Damarlar		
Endotel hücreleri	LPS	[66]

1.7. MIF ile İlişkide Olan Proteinler

Birçok proteinle olan ilişkisi nedeniyle, MIF hücrede çok çeşitli aktiviteler göstermektedir (Tablo 1.7.1). MIF'in Jab1/CSN5'a direk olarak bağlanması ile, JNK ve AP1 aktivitelerinde değişiklikler görülmüştür [28]. Son bir çalışma, MIF'in MPN domainin, sadece COP9 signalozomun (detaylar için 1.9'a bakınız) beşinci komponenti olan Jab1/CSN5 ile değil, aynı zamanda, CSN6 ile de etkileştiğini göstermiştir [67]. Jab1/CSN5, CSN kompleksinin bir subunitesi olarak, bitkilerde ve hayvanlarda da önemli bir rol oynamaktadır. CSN kompleksi, SCF (Skp1/Cullin/F-box protein) E3 übikütin ligaz ile etkileşmekte ve Cullin proteininden Nedd8'in ayrılmasını sağlamaktadır [68]. Özellikle, Cullin 1'den Nedd8'in ayrılması, Jab1/CSN5'in MPN domainindeki JAMM motifin isopeptidaz aktivitesi tarafından sağlanmaktadır. Bu motif sadece CSN kompleksi ile bir bütün olduğu zaman fonksiyon görmektedir [69]. Cullin'den Nedd8'in ayrılması (denedilasyon), p27 ve Cyclin E'nin übikütin proteozomal sisteme yönlenmesini sağlayarak, SCF ligazın aktivitesinin artışıyla sonuçlanır [69, 70].

MIF'in, tihol-spesifik antioksidant olan PAG (proliferation associated gen: çoğalma ile ilişkili gen) ile etkileşimi gösterilmiştir. MIF ve PAG arasındaki bağlanma, MIF'in dopakrom totameraz aktivitesinin düşüşüne neden olmaktadır [71]. Bir başka çalışmada, hepatopoetin (HPO)'nin, hem Jab1/CSN5 hem de MIF ile etkileşimde olup, AP-1 yolağının düzenlenmesinde görev aldığı gösterilmiştir [72].

Son çalışmalardan bir tanesi, CD74'u MIF'in reseptörü olarak tanımlamıştır [18]. Fakat MIF eksprese eden tüm hücreler hücre yüzeylerinde CD74'ü bulundurmamaları ve de CD74'ün sinyal iletimi için hücreiçi domainini içermemesi nedeniyle, CD74'un reseptörden daha çok, MIF'in diğer proteinlerle etkileşmesini sağlayacak aracı bir protein olabileceği önerilmiştir.

MIF ve insulin arasındaki direk bağlantı belirlenmemiş olmasına rağmen, insulinin MIF ile birlikte pankreatik adacığın salgı granüllerinde lokalize olduğu ve de MIF'in glukoz uyarımlı insülin salınımının düzenlenmesinde rol oynadığı çalışılmıştır [57].

Son zamanlarda, MIF'in miyozin-hafif-zincir-kinaz isoformu (MLCK) ile olan direk etkileşimi tanımlanmıştır [73].

Tablo 1.7.1. MIF'e bağlanan proteinler

Proteinin ismi	Fonksiyonu	Bağlanmanın etkileri
Jab1/CSN5	AP1 uyaranı P27KIP1'a bağlanır ve yıkımını indükler Glukokortikoidlere ve progesteron reseptörlerine bağlanır P53 yıkımını indükler	MIF, Jab1 uyarımını engeller JNK aktivasyonunu azaltır c-jun fosforilasyonunu engeller
PAG	Tihol özgün antioksidant protein Sistein gruplarına sahiptir ve indirgeyici olarak Tiholü kullanır	MIF'in tatomeraz aktivitesini azaltır
BNIPL	Apoptoza neden olan bir proteindir	BNIPL MIF aracılı tümör hücre çoğalmasını engeller
CD74	ER'den golgiye MHC sınıfı II proteinlerinin taşınmasında rol oynar CD44'a bağlanarak immun hücre uyarılmasında rol alır	CD74, MIF aracılı ERK1-2 fosforilasyonunda, hücre çoğalmasında gereklidir
HPO	Karaciğere özgü rejenerasyon başlatıcısıdır	Jab1'a bağlanarak AP-1 yolağını kontrol eder

1.8. MIF'in Übikütin Protazom Sistemindeki (UPS) Rolü

Son bir araştırma, UPS'de önemli fonksiyon gördüğü bilinen SCF übikütin ligazın aktivitesinin sağlanmasında, Jab1/CSN5-MIF etkileşiminin önemli rol oynadığını göstermiştir [74]. MIF, Jab1/CSN5'in Cullin proteinleriyle olan etkileşimini engelleyerek, Jab1/CSN5'in fonksiyonunu engellemektedir [74]. Cullin 1, hem substrat özgünlüğü olan hem de übikütinlenmeyi kontrol eden SCF E3 übikütin ligaz ailesine ait bir proteindir. SCF kompleksi, üç farklı komponentden oluşmuştur: Rbx1 (Ring box-1), Cullin1 (Cul1, scaffold: iskelet protein), Skp1 (adaptör protein) ve substrat tanınmasından sorumlu F-box ailesine ait proteinlerdir (Şekil 1.8.1b) [75]. SCF'nin temel katalitik merkezi ise Rbx1 ve Cul1 subunitleridir. SCF'nin aktivitesi, Cullin1 proteinine übikütin benzeri bir protein olan Nedd8'in eklenmesi (nedilasyon) ile

uyarılmaktadır [76]. Buna zıt olarak da, Cullin proteininden Nedd8'in ayrılması (denedilasyon), COP9 signalozomun bir subuniti olan Jab1/CSN5 tarafından gerçekleşmektedir [68]. Denedile olan Cullinler, inhibitor protein Cand1 tarafından ayrılmaktadır (Şekil 1.8.1b) [77]. Böylelikle, SCF aktivitesi, Cand1 ve CSN ile etkileşimde olan MIF tarafından inhibe edilmektedir [78]. Bu bağlamda, MIF-Jab1/CSN5 etkileşimi SCF kompleksinin aktivitesini etkilemektedir. Kısaca, MIF'in UPS aktivitesini nasıl etkilediği Şekil 1.8.1a üzerinde gösterilmiştir.

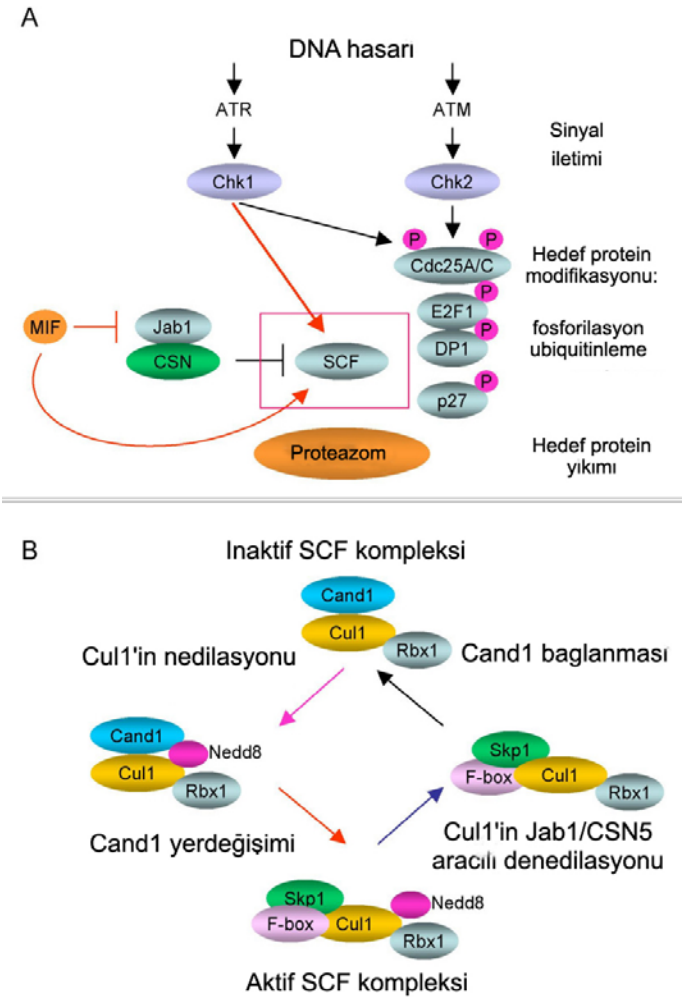

Şekil 1.8.1. SCF aktivitesinin MIF-Jab1/CSN5 etkileşimi ile kontrolü.

(A) DNA hasarının kontrol yolakları, temel hücre siklusu proteinlerinin yıkımı için SCF tarafından kontrol edilmektedir. Bu yolaktaki sinyal ileticiler (ATM, ATR, Chk1 ve Chk2) ve etkili yapılar (SCF, CSN ve 26S proteazom) gösterilmiştir. (B) SCF E3 übikütin ligaz Cullinler, Skp1 and F-box proteinlerinden oluşmuştur. Denedilasyon (Cullin1'den Nedd8'in ayrılması) Jab1/CSN5 sayesinde gerçekleşir. Nedilasyonu takiben, Skp1 ve F-box proteinleri inhibitör protein Cand-1'nin Cullin'e bağlanması ile yerdeğiştirirler ve SCF kompleksi inaktif hale gelir. Aynı şekilde MIF'in Jab1/CSN5'a bağlanması Cullin-Jab1/CSN5 etkileşimini engeller ve SCF kompleksi inaktif hale gelir [79].

1.9. COP9 Signalozom (CSN)

CSN, UPS'in en önemli üyelerinden birisidir. Deng ve arkadaşları, 1994 ilk olarak, Arabidops'larda (COP: constitutive photomorphogenesis: sürekli ışıkla değişim), ışık bağımlı gelişimin baskılayıcısı olarak tanımlanmıştır [80, 81]. Jab1/CSN5 içeren signalozom olarak da bilinen memeli CSN kompleksi, izole edilip, 26S proteazom ile birlikte saflaştırılmıştır [82].

CSN, gel filtrasyon kolonlarında, 450-550 kDa moleküler ağırlığında olduğu saptanmış ve CSN1'den CSN8'e kadar 8 subuniteden oluşmuştur (Şekil 1.9.1). CSN subunitelerinin en belirgin karakteristik özellikleri, PCI/PINT (Proteazom, COP9 signalozom, Initiation factor 3/Proteazom subunits, Int-6, Nip-1, and TRIP-15) ve MPN/MOV34 (Mpr1 Pad1-N-terminal) domainlerinin bulunmasıdır [83]. Bu iki domain aynı zamanda, CSN yanında, 26S proteazom kapak kompleksinde ve ökaryotik translasyon başlatıcı faktör 3 (eIF3)'de de bulunmuştur [84, 85]. Ökaryatik hücrelerde, lizozomal olmayan protein yıkımından sorumlu 26S proteazom (detaylar için 1.10'da Şekil 1.10.1C'ye bakınız,), 20S kor ve 19S düzenleyici iki kısımdan oluşmuştur. İlginç olarak, sekiz CSN subunitelerinin herbiri, 19S düzenleyici bölümün kapak kısmındaki unitelerle homoloji göstermektedir. Bu homoloji, CSN ve proteazom kapağının, evrimsel olarak aynı atadan gelebileceğini göstermektedir.

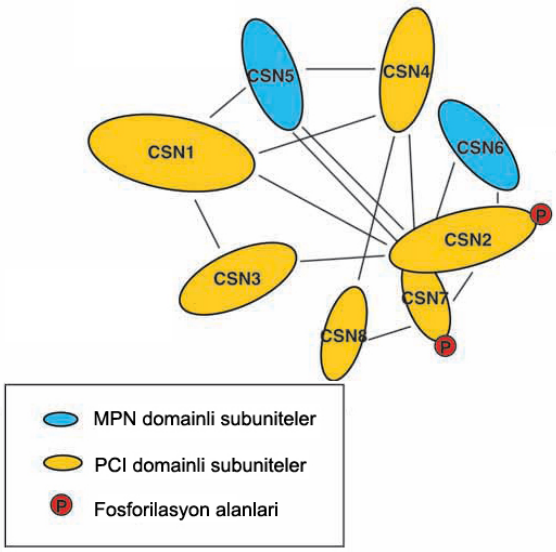

Şekil 1.9.1. CSN subunitelerinin birbiriyle ilişkileri.
MPN domainine sahip olan subuniteler mavi, PCI domainine sahip olanlar ise sarı ile gösterilmiştir. CSN2 ve CSN7'nin fosforilasyonu ise kırmızı ile belirtilmiştir.

CSN'nin aşağıda açıklanan birçok biyokimyasal aktiviteleri vardır:

1.9.1. CSN'in Metalloproteaz Ve Denedilaz Aktivitesi

Jab1/CSN5, JAMM (Jab1/MPN domain-associated metalloisopeptidase: Jab1/MPN domain-ilişkili metaloizopeptidaz) ya da MPN olarak bilinen metalloproteaz motifini içerir. Bu motifdeki mutasyonun, metalloproteaz aktivitesini engellediği görülmüştür. Benzer bir şekilde, proteazom kapağında yer alan, Jab1/CSN5 paralogu olan ve 26S proteasomun deübikütinleme aktivitesinden sorumlu RPN 11'nın da, aynı motifi içerdiği bilinmektedir [86]. Diğer bazı proteinlerde, JAMM/MPN motifine sahip olmalarına rağmen [87-89], bu proteinlerin metalloproteaz aktivitesi göstermedikleri saptanmıştır. Hem Jab1/CSN5 hem de RPN11, ancak CSN kompleksi ya da 26S proteazom yapısında bulundukları zaman bu aktiviteyi gösterdikleri belirlenmiştir [68]. Jab1/CSN5 ve RPN11'in metalloproteaz aktiviteleri, deübikütinleme ve denedilasyon aktiviteleri ile uyumlu bir şekilde yönetilmektedir.

Moleküler biyololojide ilgileri çeken CSN'nin diğer bir önemli fonksiyonu da, Jab1/CSN5'in MPN motifinden dolayı, SCF kompleksinin denedilasyonunda görev almasıdır. SCF übikütin ligaz kompleksi, CSN'nin temel hedefidir. SCF, hedef proteine übikütinin eklenmesinde görev yapan bir E3 übikütin ligazdır. Übikütin eklenmesine benzer bir şekilde, nedilasyon, Nedd8 aktive edici enzimler ile katalize edilmektedir. Fakat, denedilasyon ise Jab1/CSN5'in metaloisopeptidaz aktivitesi ile katalize edilmektedir [68]. Nedilasyon ve denidilasyonun aktif bir şekildeki bu siklusu, SCF aktivitesinin sağlanması için gereklidir.

1.9.2. CSN İlişkili Protein Kinaz Ve Deübikütinlasyon Aktivitesi

CSN'nin c-Jun (Ser63 and Ser73), IκBα, NF-κB prekürsörü p105'i ve de tümör supresörü p53 (Ser149, Thr 150 ve Thr 155)'ü fosforladığı *in vitro* olarak gösterilmiştir [82, 90]. Aynı zamanda, bazı CSN subuniteleri üzerinde fosforlanma alanları bulunmasından dolayı da, CSN'nin kendisi de fosforlanmaya hedefdir [91].

Son olarak, übikütin isopeptidaz aktivitelerinin CSN ile ilişkili olduğu gösterilmiştir [92-95]. CSN'nin deübikütinleme aktivitesi iki yolla açıklanmaktadır: CSN ya mono-übikütinlenmiş substratlardan übikütinin ayrılmasını ya da poliübikütin zincirlerinin depolimerize olmasını sağlar [93]. CSN'nin bu ilk aktivitesi, Jab1/CSN5'indeki metaloproteaz domainine ihtiyaç duyarken [93], sonraki aktivitesi ise tüm CSN ile ilişkilidir [92, 94, 95]. Kısacası, CSN hem denidilasyon hem de deübikütinlasyon aktivitelerine ya kendisi sahiptir ya da diğer deübikütinleyici enzimlerle ilişkide olması nedeniyle yürütmektedir.

1.9.3. Protein Yıkımı

Jab1/CSN5, p27Kip, Lutenize edici hormon reseptörü (LHR), p53, östrojen reseptörü, Smad4, Smad7, Id1, Id3 ve IκBα gibi birçok proteinin proteazoma bağlı yıkılımına yardımcı olmaktadır [96-101].

Protein yıkımı, hücre içerisindeki proteinlerin steady-state diye adlandırılan normal düzeylerinde fonksiyon görmelerini sağlamak amacıyla işleyen düzenli bir mekânizmadır. Ökaryotlarda protein yıkımı, hem sitoplâzmada hem de çekirdek UPS ve onun düzenleyici proteinleri sayesinde gerçekleşmektedir. Bu düzenleyici proteinler arasında hem CSN hem de VCP belirli substratların yıkımı kontrol etmektedirler [102, 103].

1.10. Übikütin Protazom Sistemi (UPS)

UPS, ökaryotlarda hücreiçi düzenleyici proteinlerin seviyelerini kontrol etmede önemli bir fonksiyona sahiptir. UPS'in übikütinleme ve übikütinlenmiş proteinlerin yıkımı olmak üzere iki temel fazı vardır. İlk übikütinleme fazında, übikütin (Ub) ATP yardımıyla übikütin aktive edici enzimin (E1) sistein kuyruğuna eklenir ve sonra übikütin bağlayıcı edici enzimin (E2) sistein kuyruğuna transfer edilir. Son olarak ise, übikütin, protein ligaz (E3) sayesinde substratın lizin kuyruğuna transfer edilir. Ub, substrata izopeptid bağı ile bağlanır. Ub aktivasyonu ve ligasyonu, Ub'nin son aminoasidinin (G76) karboksil grubunda gerçekleşir (Şekil 1.10.1) [104, 105].

Tek bir übikütin molekülünün substrata eklenmesi (monoübikütinleme) ise, lizozomal sınıflandırma, gen ekspresyonu ve endositoz gibi substratın farklı görevlerde iş yapmasına neden olmaktadır [106]

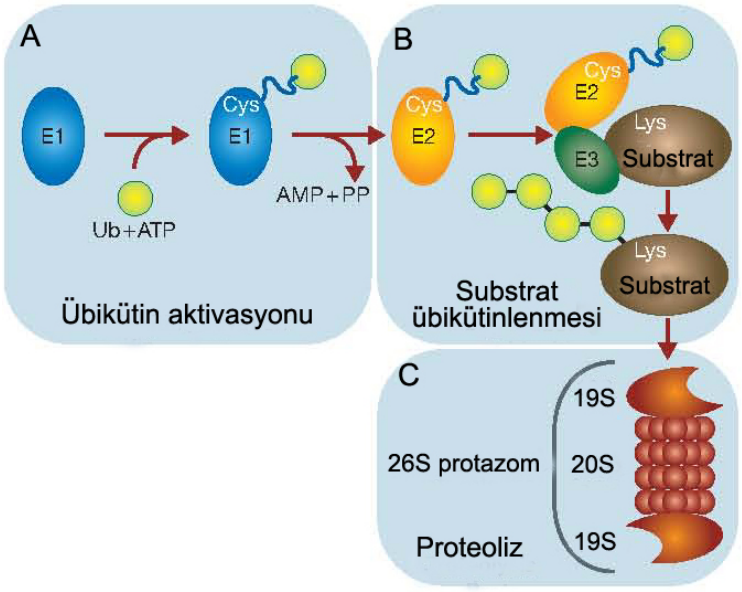

Şekil 1.10.1. Übikütin Sinyali

A: Übikütin, übikütin aktive edici enzim (E1) ile aktive edilip ve sonra übikütin bağlayıcı enzime (E2) transfer edilir. Substrat (mavi kutu) ve E2 enzimi özgün olarak übikütin protein ligaza bağlanabilirler ve de aktive olmuş übikütin substrata transfer olur. **B:** E3, substrata ve E2'ye farklı alanlarda bağlanır. Substrat, übikütinlenme sinyalı ile tanınır. **C:** Proteolizin gerçekleştiği 26S protazom, 19S kapak kısmı ve esas proteolitik aktiviteye sahip 20S kısmından oluşur. Proteoliz öncesi 19S kapakla bağlantılı deübikütinleyici enzimler ile substratdan übikütin zincirlerinin uzaklaşması sağlanır [107].

UPS siklusunun ikinci fazında, protazom poliübikütin zincirleri sayesinde, substratı tanır. Substrat, küçük peptidlerine yıkılır ve Ub'nin özgün deübikütinleyici enzimi sayesinde geri eldesi sağlanır. Ub'nin substrata konjugasyonu gibi, proteazomal yıkım da, ATP bağımlıdır. 26S proteazomun, hem übikütinlenmiş proteinlerin übikütinden ayrılması hem de onların yıkımlarının katalizlenmesinde önemli bir görevi vardır [108, 109]. Protazom, birbirine bağlı 2 farklı bölümden oluşmuştur (Figure 1.10.1C). 20S silindirik temel bölüm, proteolitik aktiviteye sahip iken, silindirik bölümün alt ve üst kısımlarına yerleşmiş 19S'lik proteazom kapakları poliübikütinlenmiş substratın tanınması ve proteoliz görevini üstlenmişlerdir. Herbir 19S kompleksi, 6 tanesi ATP az aktivitesine sahip 15-20 subuniteden oluşmuştur.

1.11. VCP Bağımlı Protein Yıkımı

97-kDa'luk Valosin-içeren protein (p97 ve ya VCP), übikütin-protazom sistemine bağlı proteolizde önemli fonksiyonlara sahiptir. Bu proteoliz, VCP'nin, übikütin ve kofaktörleri ile ilişkisine bağlıdır. VCP, UPS'de şaperon protein olarak görev yapmaktadır. Toplam hücresel proteinin 1% den fazlasının VCP olduğu bilinmektedir.

VCP, tip II AAA (ATPases Associated with a variety of Activities: Birçok aktivitesi bulunan ATPazlar) ATPaz ailesine ait bir proteindir ve AAA domaini olarak adlandırılan iki ATPaz domainine sahiptir [110-114]. VCP çeşitli türlerde farklı isimlerle anılmaktadır. Örneğin: arkebakteride VAT, mayada CDC48, Drosophilada TER94, memeli ve bitkilerde ise p97 ve ya VCP olarak bilinmektedir [115, 116].

VCP, N-terminal domain (N), iki tane ATPaz domaini (D1 and D2) ve de C-terminal domaini (C) olmak üzere dört domainden oluşmuştur. N terminal domaini, poliübikütin zincirlerine bağlanma ve substrat tanınmasından sorumlu iken, D1 ve D2 domainleri, VCP'nin şaperon aktivitesinden sorumludur (Figure 1.11.1) [117].

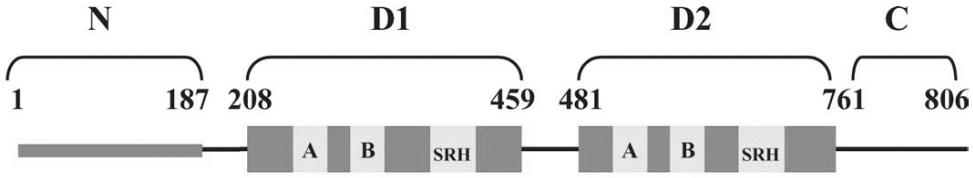

Şekil 1.11.1. VCP'nin yapısal domainleri.
A: Walker A, B: Walker B ve SRH: VCP'nin D1 ve D2 domainlerindeki ikinci bölge homoloji motifleri. [118].

Elektron mikroskobu çalışmaları, VCP'nin silindirik şekilli homo hekzemerik yapıda olduğunu kanıtlamıştır [117].

VCP, hücre içerisinde birçok aktivitede görev yapmaktadır: hücresiklusu gelişimi [119], mitoz sonrası membrane kaynaşması ve iğ ipliklerinin ayrılması [120-122], yanlış katlanmış proteinlerin ER'dan geri atılımı [103, 123, 124], proteazomda poliübikütinlenmiş proteinlerin degrade edilmesi [125, 126] ve transkripsiyon faktörlerinin aktivasyonu [127, 128].

VCP, kofaktörlerinin de yardımıyla, übikütinlenmiş proteinlere özgün olarak bağlanır ve bu proteinlere 26S protazomda degrede olmadan önce, şaperonluk yaparak onlara yol gösterir. Substrat übikütinlenmesinden sonra, VCP protein komplekslerini birbirinden ayırmak için ATP'yi kullanır ve proteinlerin protazoma yönlenmesini sağlar. Örneğin: Herhangi bir şekilde stimüle edilmeyen hücrelerde, NF-κB sitoplâzmada inaktif formda inhibitör IκB proteini ile etkileşim halindedir [129, 130]. Sitimulasyona cevap olarak, NF-κB aktive olur ve IκBα hızlıca fosforile olup, poliübikütinlenir [129]. Bunu takiben, VCP, poliübikütinlenmiş IκBα'ya bağlanır ve onu NF-κB kompleksinden ayırır [131]. IκBα'nın NF-κB'dan ayrılmasından sonra, NF-κB hedef genin regülâsyonu nedeniyle nükleusa transfer edilir. Bu arada, VCP, poliübikütinlenmiş IκBα'ya şaperonluk yaparak, onun 26S proteazomda yıkımı için yol gösterir [131].

1.12. Tezin Amacı

Makrofaj göçünü engelleyici faktör (MIF), temel olarak sitoplazmik bir proteindir ve hücre gelişimi, büyümesi ve birçok akut ve kronik inflamatör hastalığın kontrolünde görev yapmaktadır [38, 132]. Hücre içi MIF ile ilişkide olan proteinleri bulmak amacıyla yapılan 'maya iki-hibrit: yeast two-hybrid' taramasında Jab1/CSN5'ın MIF'e bağlandığı bulunmuştur [28]. MIF'in Jab1/CSN5'ın MPN domainine bağlandığı ve MIF'e bağlanarak MIF'in diğer proteinlerle olan ilişkisini etkilediği bilinmektedir. Son çalışmalar, MIF'in UPS aktivitesinin kontrolündeki rolüne işaret ederken, MIF'in Jab1/CSN5'in denedilaz aktivitesini inhibe ederek, proteazomal aktiviteyi kontrol altına aldığını göstermiştir [79].

MIF aracılı sinyal yollarındaki bu son gelişmelere rağmen, MIF üzerinden işleyen moleküler yolaklar, özellikle de UPS ve ERAD'da MIF ile etkileşimde fonksiyon gören diğer proteinler çalışılmamıştır.

Bu çalışmanın amacı, MIF'e bağlanan yeni proteinlerin tanımlanması ve bu tanımlanan proteinlerin hücresel fonksiyonlarının araştırılmasıdır.

MATERYAL VE METOD

Tezin bu bölümünde, deneyler boyunca kullanılan sarf malzemeler ve ait oldukları kaynaklar ayrı başlıklar halinde verildi.

2.1. Kimyasallar Ve Ait Oldukları Kaynaklar

Asetik asit	Merck, Darmstadt
Akrilamid 30%	Roth, Karlsruhe
Agaroz	Invitrogen, Karlsruhe
Bakto-Tripton	BD Bioscience, Sparks
Bakto-yeast ekstrakt	BD Bioscience, Sparks
Biyotin	Sigma-Aldrich, Steinheim
Bromofenol blue sodyum tuzu	Sigma-Aldrich, Steinheim
CHAPS	AppliChem, Darmstadt
Kloroform	Merck, Darmstadt
Komasi Mavisi Boyası	Sigma-Aldrich, Steinheim
Deksamethazon	Sigma Aldrich, Steinheim
1,4-Ditiotetritol	Roche, Mannheim
Etanol	Sigma-Aldrich, Steinheim
Etidyumbromid	Roth, Karlsruhe
Genetisin	Invitrogen, Karlsruhe
Glutatyon	Amersham, Freiburg
Gliserol	Merck, Darmstadt
Glisin	Sigma-Aldrich, Steinheim
Guanidin hidroklorid	Sigma-Aldrich, Steinheim
Igepal CA-630 (NP-40)	Sigma-Aldrich, Steinheim
Izopropiltiyo-β-D-galaktosid	Serva, Heidelberg
Iyoasetamid	Bio-Rad, München
Imidazol	Fluka, Steinheim
Lipopolisakkarid	Sigma-Aldrich, Steinheim
Magnezyum klorid	Merck, Darmstadt
Magnezyum sülfat	Sigma-Aldrich, Steinheim
Mangan klorid	Merck, Darmstadt
β-Merkaptoethanol	AppliChem, Darmstadt
Methanol	Sigma-Aldrich, Steinheim
MG132 (proteazom inhibitörü)	Calbiochem, Germany
Morfolinethan sülfonik asit	Serva, Heidelberg
Süttozu	Bio-Rad, München
Paraformaldehit	Merck, Darmstadt
Fenilmetilsülfonilflorid	Sigma-Aldrich, Steinheim
Ponseu S	Roth, Karlsruhe

Potasyum klorit	Merck, Darmstadt
Rotiforez Jel 30	Roth, Karlsruhe
Sodyum asetat	Roth, Karlsruhe
Sodyum azid	Merck, Darmstadt
Sodyum klorid	Sigma-Aldrich, Steinheim
Sodyum sitrat	Merck, Darmstadt
Sodyum karbonat	Roth, Karlsruhe
Sodyum dodesil sülfat	Merck, Darmstadt
Sodyum periyodat	Sigma-Aldrich, Steinheim
Sodyum tiyosülfat	Roth, Karlsruhe
Tris	Roth, Karlsruhe
Triton X-100	Sigma-Aldrich, Steinheim
Tween-20	Roth, Karlsruhe
Ure	Merck, Darmstadt
Zeosin	Invitrogen, Karlsruhe

2.2. Enzimler Ve Ait Oldukları Kaynaklar

Taq Polimeraz	Promega, Mannheim
T4 DNA Polimeraz	Promega, Mannheim
EcoRI	Promega, Mannheim
XhoI	Promega, Mannheim
NdeI	Promega, Mannheim
BglII	Promega, Mannheim
HindIII	Promega, Mannheim
T4 DNA Ligaz	Promega, Mannheim
DNAaz	Promega, Mannheim
RNAaz	Promega, Mannheim
TEV proteaz	Invitrogen, Germany

2.3. Antikorlar, Ait oldukları Kaynaklar Ve Kullanım Oranları

Primer antikorlar	**Firması**	**Dilusyon oranı**
Rabbit α-rat MIF	Kendi üretimi	1:20,000
α-GST-HRP	Amersham, Freiberg	1:5,000
Rabbit α-Jab-1	Santa Cruz, USA	1:500
α-Biotin-HRP	Amersham, Freiburg	1:1,500
Mouse α-VCP	ABR, USA	1:1,000
Rabbit α-VCP	Santa Cruz, USA	1:200
Goat α-Pgk-1	Santa Cruz, USA	1:200
Goat α-Fetuin	Santa Cruz,USA	1:200
Mouse FLAGM2	Sigma, Stenheim	1:10,000
Rabbit α-CSN1	Biomol, Hamburg	1:1,000
Mouse α-Myc (9E10)	Santa Cruz, USA	1:3,000
Rabbit α-Cullin1	Abcam, UK	1:250

Rabbit α-Nedd8	Axxora, USA	1:500
Rabbit α-peroxiredoxin-1	Abcam, UK	1:500

Sekonder antikorlar

Goat α-rabbit-HRP	ICN, Ohio, USA	1:10,000
Donkey α-rabbit IgG-Cy3	Chemicon, Hampshire, UK	1:1,000
Donkey α-mouse IgG-FITC	Dianova, Hamburg	1:1,000
Donkey α-goat IgG	Santa Cruz, USA	1:1,000
Rabbit α-mouse IgG	Cell Signaling , USA	1:100

2.4. Rekombinant Proteinler Ve Ait Oldukları Kaynaklar

Human MIF	kendi üretimi
His-VCP	kendi üretimi
GST-Jab1/CSN5	kendi üretimi

2.5. Kitler Ve Ait Oldukları Kaynaklar

Bradford kiti	Roth, GmbH, Karlsruhe
Gel Ekstraksiyon Kiti	Qiagen, Hilden
Maxiprep Plasmid Saflaştırma Kiti	Genomed GmbH, Löhne
Miniprep Kiti	Genomed GmbH, Löhne
PCR Saflaştırma Kiti	Qiagen, Hilden
Silver boyası Kiti	Invitrogen, Karlsruhe
DNA ekstraksiyon Kiti	Qiagen, Hilden
FLAG purifikasyon Kiti	Sigma, Steinheim

2.6. Hücreler

NIH 3T3 (fare fibroblastları),
HEK293T (insan epitelyal böbrek hücresi),
264.7 RAW (fare makrofajları),
HeLa (insan servikal karsinoma hücresi) hücreleri.

2.7. Hücre Kültürü Medyumları, Antibiyotikler Ve Ait Oldukları Kaynaklar

Ampisillin sodyum tuzu	Ratiopharm, Ulm
Kanamisin sodyum tuzu	Ratiopharm, Ulm
Sığır serum albumini	Invitrogen, Karlsruhe
Dulbecco Minimal Essential Medyumu	PAA Laboratories, Cölbe
Fetal kalf serum	Invitrogen, Karlsruhe
L-Glutamin	PAA Laboratories, Cölbe
Penisillin/Streptomisin	PAA Laboratories, Cölbe
RPMI 1640 medyumu	PAA Laboratories, Cölbe
Tripsin	PAA Laboratories, Cölbe
Ultrasalin A	PAA Laboratories, Cölbe

Optimem-serumsuz medyum	Invitrogen, Karlsruhe

2.8. Deney Aletleri Ve Markaları

Hücre kültürü inkübatörü	Binder, Tullingen
Hücre kültürü bençi	BDK,Sonnenbühl
Konfokal lazer scanning mikroskobu TCS SP2	Leica, Wetzlar
Easypet 4420 Pipet Seti	Eppendorf, Hamburg
Electronik balans SPB50	Ohaus, Giessen
Gel Jet Imager 2000	Intas, Göttingen
Heater Block DB-2A	Techne, Cambridge, UK
Horizontal Mini Elektroforez Sistem	PEQLAB, Erlangen
Microdalga fırını	Samsung, Schwalbach
Mini santrifüj	VWR International
Floresan mikroskobu	Carl Zeiss, Jena
PCR sistemi	Biozyme, Oldendor
Potter S homojenizatör	B. Braun, Melsungen
Power supply uniteleri	Keutz, Reiskirchen
Pre-Kast Gel Sistemi	Invitrogen, Karlsruhe
SDS jel elektroforez uniteleri	Invitrogen, Karlsruhe
Semi-dry-elektroblotlama unitesi	PEQLAB, Erlangen
Vertikal elektroforez sistemi	PEQLAB, Erlangen
Ultrasonik homojenizatör	Bandelin, Berlin
2D-PAGE sistemi	BioRad, München

2.9. siRNA'ler

1. Negatif kontrol (kat#:AM4621), Applied Biosystems, Darmstadt
2. VCP (Cat#: AM16708), Applied Biosystems, Darmstadt
3. Jab1/CSN5 (hedef sequensi: GCUCAGAGUAUCGAUGAAAtt), Applied Biosystems, Darmstadt
4. CSN1 (hedef sequensi: GAACCUUUAACGUGGACAUtt), Applied Biosystems, Darmstadt
5. UPS 15 (hedef sequensi: GCACGUGAUUAUUCCUGUUtt), Applied Biosystems, Darmstadt

2.10. pSUPER Vektörüne Klonlanan Oligonükleotidler

Oligonükleotidlerin (Sigma, Steinheim, Germany) 19bp lik hedef sekansları altı çizili olarak belirtilmiştir. Kontrol olarak ise aynı vektöre, 19bplik kısmın sekans dizilimi değiştirilerek (scrambled: scr) klonlama yapılmıştır.

Tablo 2.10.1. MIF, VCP ve Jab1/CSN5 nakdavları için pSUPER vektörüne klonlanan 64 bplik oligonükleotidler

İsim	Sekanslar
MIF forward	5'-GATCCCC**CCGCAACTACAGTAAGCTG**TTCAAGAGA**CAGCTTACTGTAGTTGCGG**TTTTTGGAAA -3'
MIF reverse	5'AGCTTTTCCAAAAA**CCGCAACTACAGTAAGCTG**TCTCTTGAA**CAGCTTACTGTAGTTGCGG**GGG-3'
MIF scr.forward	5'-GATCCCC**GCCAACATCGACATATCGG**TTCAAGAGA**CCGATATGTCGATGTTGGC**TTTTTGGAAA-3'
MIF scr.reverse	5'AGCTTTTCCAAAAA**GCCAACATCGACATATCGG**TCTCTTGAA**CCGATATGTCGATGTTGGC**GGG-3'
VCP forward	5'-GATCCCC**GGGCACATGTGATTGTTAT**TTCAAGAGA**ATAACAATCACATGTGCCC**TTTTTGGAAA-3'
VCP reverse	5'AGCTTTTCCAAAAA**GGGCACATGTGATTGTTAT**TCTCTTGAA**ATAACAATCACATGTGCCC**GGG-3'
VCP scr.forward	5'-GATCCCC**GATCGGTATTAGCAGCTAG**TTCAAGAGA**CTAGCTGCTAATACCGATC**TTTTTGGAAA-3'
VCP scr.reverse	5'AGCTTTTCCAAAAA**GATCGGTATTAGCAGCTAG**TCTCTTGAA**CTAGCTGCTAATACCGATC**GGG-3'
Jab1/CSN5 forward	5'-GATCCCC**GCTCAGAGTATCGATGAAA**TTCAAGAGA**TTTCATCGATACTCTGAGC**TTTTTGGAAA-3'
Jab1/CSN5 reverse	5'AGCTTTTCCAAAAA**GCTCAGAGTATCGATGAAA**TCTCTTGAA**TTTCATCGATACTCTGAGC**GGG-3'
Jab1/CSN5 scr.forward	5'-GATCCCC**CGTGACTGAAGATAGACGA**TTCAAGAGA**TCGTCTATCTTCAGTCACG**TTTTTGGAAA-3'
Jab1/CSN5 scr.reverse	5'AGCTTTTCCAAAAA**CGTGACTGAAGATAGACGA**TCTCTTGAA**TCGTCTATCTTCAGTCACG**GGG-3'

2.11. Hücre Kültürü Teknikleri

2.11.1. Hücre Kültürü

Bu çalışmada NIH 3T3 (fare fibroblastları), HEK293T (insan epitelyal böbrek hücresi), 264.7 RAW (fare makrofajları) ve HeLa (insan servikal karsinoma hücresi) hücreleri kullanıldı. Hücreler 2 mM glutamin, ısı ile inaktive edildi. 10%'luk fetal sığır serumu, 100 U/ml penisilin/streptomisin, %2.7 ultrasalin A içeren Dulbecco'nın modifiye Eagle medyumu (DMEM) ile %5'lik CO_2 lik ve 37°C'lik inkübatöre yetiştirildi. Hücreler, her 2-4 gün sonunda %80-90'lik konfluensiye (doyum noktası) ulaştıktan sonra, iki kez PBS ile yıkandı ve sonra 1:8 oranında medyum ile suspanse edildiler. Sonra, hücrelerin 1 ml Trypsin/EDTA (0.5 g/L Trypsin, 0.2 g/L EDTA) ile 2-3 dakika 37°C de inkübasyonu sonucu, 75 $cm^{2'}$ lik hücre kültürü kaplarından ayrılması sağlandı. İnkübasyon süresi sonucu, 7 ml DMEM medyumu flasklara eklenerek, hücreler flaskdan toplandı. 15 ml'lik falkon tüplerinde toplanan hücreler santrifüye edilip (500 x g, 10 dakika, oda ısısında) ve elde edilen pellet medyum ile yeniden suspanse edilip, yeni flakslara ekildi.

2.11.2. Hücre Dondurulması ve Çözülmesi

Hücre süspansiyonu, 1:1 oranında taze olarak hazırlanmış dondurma medyumu (freezing medium: 70% DMEM, 10% FCS and 20% DMSO) ile yeniden suspanse edildi. Dondurma işlemi için, ilk olarak hücreler -80ºC'de geceboyu ve sonrada sıvı nitrojende depolandı. Dondurulan hücrelerin çözülmesi için, sıvı nitrojendeki tüp, 2, 3 dakikalığına 37ºC lik inkübatörde bekletilip, direk olarak taze medyum içeren kültür kaplarına ekildi.

2.11.3. Transfeksiyon

Tranfeksiyon, yabancı bir genetik materyalin (örneğin: virus, plasmid, faj veya DNA segmentleri) kompotent hücrelere özel yöntemler kullanılarak aktarılması işlemidir. Bu çalışmada kullanılan transfeksiyon metodlarında, hücre membramında geçici delik ya da porlar açılarak, plasmid DNA sının ya da siRNA konstraklarının hücre içine alınımı sağlandı. Bu çalışmada, üç farklı transfeksiyon yöntemi kullanıldı.

2.11.3.1. Geçici Transfeksiyon

Transfeksiyon öncesi, 2 x 10^5 hücre, 6 vellik hücre kültürü kaplarına ekildi. 1 µg plasmid DNA'sı FuGene 6 (Roche) transfeksiyon ajanı kullanılarak hücrelere verildi. Çiftli transfeksiyon için, transfekte edilecek konstrak başına 0.5 µg DNA ve üçlü transfeksiyon için ise konstrak başına 0.33 µg DNA kullanıldı. Vel başına ise total DNA miktarı sürekli 1 µg olarak sabit tutuldu. Transfeksiyondan 24 saat sonra, gen ekspresyonu immunoblot ile değerlendirildi.

2.11.3.2. Sabit Transfeksiyon

Bu deneyde uygulanan sabit transfeksiyon için, pBudCE4.1-birA ve pN3-CTB-MIF vektörleri tek başlarına ve çiftli olarak NIH 3T3 hücrelerine Lipofectamine (Invitrogen) transfeksiyon ajanı kullanılarak transfekte edildi. Antibiyotik seçimine pN3-CTB-MIF klonu için 800 µg/ml Geneticin ile pBudCE4.1-birA klonu için ise 600 µg/ml Zeocin ile başlanıp, 4 hafta sonunda dereceli bir şekilde antibiyotik miktarları 100 µg/ml Geneticin and 150 µg/ml Zeocin'e kadar azaltıldı. Daha sonra, klonlar 22 kDa luk biyotinlenmiş MIF'in ekpresyonunu gözlemlemek için rabbit anti-rat-MIF antiserumu ve streptavidin HRP ile muamele edildi. 5-8 hafta sonunda, klonlar tripsin solusyonu içinde steril filtreler kullanılarak izole edildiler. En yüksek düzeyde biyotinlenme 0.1 mg/ml biyotinin medyuma eklenmesi ile başarıldı. Biyotinlenmiş MIF ekspresyonu gösteren bir klon ve sadece birA ekspresyonu gösteren kontrol klonu %10 FKS, biotin (0.1 mg/L), Geniticin (100 µg/ml) ve Zeocin (150 µg/ml) içeren DMEM medyumu içerisinde 37°C'de kültüre edildi.

2.11.3.3. siRNA Transfeksiyonu

Hücredeki genlerin geçici nakdovnları (gen susturulması: gen ekspresyonunun bastırılması) için, hücreler 6 vellik kültür kaplarına 24 saat öncesinden % 30-50 lik konfluenz ile ekildiler. Transfeksiyon sonrası, hücreler 2 defa yıkandı ve serum içermeyen OptiMEM medyumu (Invitrogen) ile süspanse edildiler. siRNA (son konsantrasyon:100 pmol) transfeksiyonu, Opti-MEM medyumu içerisinde Lipofectamine 2000 ajanı kullanılarak (4µl transfeksiyon ajanı/100 pmol siRNA) gerçekleştirildi. Transfeksiyondan 6 saat sonra, medyum değiştirilerek, yerine serum içeren DMEM eklendi ve hücre kültürüne 72 saat kadar devam edildi.

2.12. Protein Biyokimyası İle İlgili Methodlar

2.12.1. Hücre Ekstraktının Hazırlanması

75 $cm^{2'}$lik hücre kültürü flakslarında % 80-90 konfluensiye kadar geliştirilen hücreler, soğuk PBS ile yıkandı ve 1 ml lizis solusyonu (50 mM Tris-Cl pH 8.0, 150 mM NaCl, 1 mM EDTA, 1% NP-40, 1 µM leupeptin, 1 mM PMSF) ile 15 dakika inkübe edildi. Sonrasında, hücreler skraper yardımıyla flakslardan ependorf tüplerine transfer edilerek, sonikasyona tabi tutuldu (iki kez 10 saniye, 200-300 W, herbir sonikasyon için 10 saniye örnekler buzda bekletildi). Sonikasyon sonrası, 13,000 x g'de 10 dakika, 4°C'de santrifüj edildiler. Santrifüj sonrası elde edilen supernatan hücre sitoplazmik ekstraktı olarak kullanılırken, pellet kullanılmadı.

2.12.2. Protein Konsantrasyonunun Belirlenmesi (Bradford Yöntemi)

Bradfort yöntemi, solusyondaki protein konsantrasyonunun belirlenmesi için kullanıldı. Deneyde kullanılan Bradfort boyası 1:4 oranında distile su ile diluye edildi (1 hacim stok Bradfort boyası, 4 hacim distile su). Diluye öncesi mavi olan boya, diluye işleminden sonra kahverengini aldı. Standart olarak, 0, 250, 500, 1000, 1500, 2000 µg/ml konsantrasyonlarında Bovine serum albumin (BSA) kullanıldı. Hem standartlar

hem de örnekler, PBS içerisinde hazırlandı ve 1ml lik diluye Bradfort solusyonu 20 µl örnek ve standart ile karıştırıldı. 5 dakika inkubasyon süresi sonunda 595nm absorbans altında spektrofotometrede ölçümler yapıldı.

2.12.3. Afinite Saflaştırılması

2.12.3.1. Biyotinlenmiş Proteinlerin Elusyonu (elenmesi) Ve Saflaştırılması

Biyotinlenmiş MIF (biotin.MIF) ve ilişkide olduğu proteinler, streptavidin agaroz boncukları kullanılarak, NIH 3T3 hücre ekstratlarından saflaştırıldı. Hem deney (biyotinlenmiş MIF ve biotin ligaz birA ekspre eden grup) hem de kontrol (sadece biotin ligaz birA) gruplarından hazırlanan hücre ekstratları, 50 µl streptavidin-agaroz boncukları (Novagen) ile 1.5 saat oda ısısında rotator üzerinde inkübe edildi. İnkübasyonu takiben, boncuklar üç kez lizis solusyonu ile yıkandı. Yıkama, boncukların santrifügasyon ile pellet halinde tübün dibine çöktürülmesinden sonra, streptavidin bocuklarına bağlı proteinler, 1 x SDS solusyonu (62.5 mM Tris pH 6.8, 2% SDS, 5% gliserol, 0.3% bromofenol mavisi, 0.9% (v/v) β-merkaptoetanol) ile 10 dakika 90^0C de kaynatılarak boncuklardan elüye edildi. Elüye edilen proteinler, % 4-12 NuPAGE Bis-Tris jelinde (Invitrogen) yürütülüp, moleküler ağırlıklarına göre ayrışmaları sağlandı.

2.12.3.2. Streptavidin Boncuklarının TEV-proteaz İle İnkübasyonu

Biyotinlenmiş MIF'in biyotin kuyruğunu uzaklaştırıp sadece biyotinlenmiş MIF ve ilişkide olduğu proteinleri elde etmek amacıyla, streptavidin boncuklarına bağlı proteinler Tobacco Etch Virus (TEV) proteaz ile inkübe edildi. TEV proteaz biyotin kuyruğu ve MIF arasına yerleştirilmiş Glu-X-X-Tyr-X-Gln-Ser olarak bilinen yedi aminoasitlik bir dizilimi tanıyan bakteriyel bir enzimdir. Streptavidin boncuklarıyla yapılan afinite saflaştırması sonrası, 150 µl'lik TEV solusyonu (Invitrogen, enzim firma tarafından sağlanan özel bir solusyon içinde, taze olarak hazırlandı) 30°C'de 1 saat boncuklar ile muamele edildi. TEV proteaz ile inkübasyon sonucunda, boncuklar santrifüj edilip, MIF ve MIF ile ilişkide olan proteinleri içeren supernatan toplandı. Protein konsantrasyonunu artırmak amacıyla, üç deney sonucu elde edilen supernatanlar birleştirilip, 450 µl'lik eluye supernatan aseton ile (aseton çöktürmeu, 4 volume asetonun bir volume supernatan ile inkübasyonu ile yapıldı) geceboyu -20ºC'de presipiye edildi. Presipiye edilen proteinler, 1D ve 2D SDS PAGE'de yürütüldü.

2.12.4. 1D-SDS Poliakrilamid Jel Elektroforezi

Sodyum-dodesil-sülfat (SDS) poliakrilamid jel elektroforezi [133], hücre ekstraktlarındaki protein ekspresyonlarını belirlemek amacıyla kullanıldı. %18'lik ayırıcı jel solusyonu (375 mM Tris-HCl pH 8.8, %0.1 SDS, %18 akrilamid, %0.05 APS, %0.05 TEMED), 1 mm aralıklı iki cam plaka arasına döküldü. Polimerasyon sonrası, üst ayrıştırıcı jel solusyonu (125 mM Tris-HCl pH 6.8, %0.1 SDS, %4 akrilamid, %0.05 APS, %0.1 TEMED), bölgeye yerleştirilen taraklar üzerine döküldü. Örnekler ise, 1 x SDS jel yükleme solusyonu (62.5 mM Tris pH 6.8, %2 SDS, %5 gliserol, %0.3 bromofenol mavisi, %0.9 (v/v) β-merkaptoethanol) içerisinde hazırlanıp,

5 dakika kadar kaynatılıp proteinlerin denature olması sağlandı. Üst jelin polimerazyonu sonucu tarak jelden uzaklaştırılıp, elektroforez kabı içerisine yerleştirildi. Kab 1x SDS elektroforez solusyonu (25 mM Tris, %1.44 glisin, %0.1 SDS) ile doldurulup, tarağın uzaklaşması ile oluşan veller yıkanmış ve örnekler herbir vele teker teker yüklendi. Elektroforez, 150V altında yürütüldü.

İmmunoçöktürme için, örnekler NuPAGE % 4-12 lik gradient-jelllerde, elektroforez solusyonu olarak 1x MES solusyonu (50 mM MES, 50 mM Tris, 3.46 mM SDS, 1.025 mM EDTA) ve ya 1x MOPS (50 mM MOPS, 50 mM Tris, 3.46 mM SDS, 1.025 mM EDTA) solusyonu kullanılarak 200 V'da 1saat yürütüldü.

2.12.5. 2D-SDS Poliakrilamid Jel Elektroforezi

2D-SDS poliakrilamid jel elektroforezinde yürütülmek istenen proteinler, 130 µl'lik izoelektrik fokuslayıcı (IEF) rehidrasyon solusyonunda (8 M üre, 50 mM DTT, %4 CHAPS, %0.2 kariyer amfolat, %0.0002 Bromofenol Mavisi) oda ısısında resuspanse edildiler. Resuspanse edilen örnekler rehidrasyon kaplarına yerleştirildikten sonra, şeritler halindeki linear stripler (IPG Strips, BioRad) ön yüzleri rehidrasyon kaplarındaki örneklerle yüz yüze gelecek şekilde yerleştirildi. Bu striplerin gece boyunca oda ısısında örnekle temas edip, örneğin olabildiğince strip tarafından emilimi sağlandı. Daha sonra, striplerin toplam 10.000 Volt-saat lik (250 V'da 15 dakika, 4000 V ve üstünde 2 saat, 4000 V da 3 saat) voltaj koşulları altında, yürütülmesi sağlandı. İkinci elektroforezin yürütülmesinden önce, stripler 15 dakika taze olarak hazırlanmış equilibirasyon solusyonu 1 (6 M üre, %20 gliserol, %2 SDS, 0.375 M Tris-HCl pH 8.8, 130 mM DTT) de ve tekrar bir 15 dakika equilibirasyon solusyonu II'de (6 M üre, %20 gliserol, %2 SDS, 0.375 M Tris-HCl pH 8.8, 135 mM iodoasetamid) inkübe edildiler. Daha sonra, stripler, iki kez 1x SDS elektroforez solusyonu (bakınız 4.2.4) ile yıkanıp, % 12.5'luk SDS jeline yerleştirildiler. %3'lük agaroz jele yerleştirilen strip üzerini kapatmak amacıyla ince bir tabaka halinde strip üzerine uygulandı. Bu ikinci elektroforezin ise 160V da 45 dakika yürümesi sağlandı. Elektroforez sonrası, amaca uygun şekilde jel ya Gümüş, Komasi mavisi gibi boyalarla boyandı ya da immunoblot için değerlendirildi.

2.12.6. İmmunoblotlama

Proteinler, % 8-18 lik SDS-PAGE jelinde yürütülüp, membran başına 100 mA lik akım altında, 90 dakika semi-dry (yarı kuru) blotlama yöntemi ile nitrosellüloz membrana transfer edildi. Proteinlerin membrana transferinden sonra, membran bloklama solusyonu (% 0.1 Tween-20 içeren PBS ile hazırlanmış %5 (w/v)'lik non-fat dry milk) ile oda ısısında 1 saat rotator üzerinde inkübe edildi. Hemen ardından, membran geceboyu oda ısısı veya 4°C'de bloklama medyumunda hazırlanmış primer antikorla inkübe edildi. Üç kez 10'ar dakika PBS-Tween ile yıkama sonrası, membran 1 saat bloklama solusyonu içerisinde hazırlanmış sekonder antikor ile inkübe edildi. Üç kez 10'ar dakika, PBS-Tween ile yıkandıktan sonra, membran ECL Deteksiyon Ajanı ile (1:1 oranında (v/v) Ajan 1: Ajan 2) 2-5 dakika kadar inkübe edildi. Daha sonra,

membran plastik folye arasına konulup, X-ray filmi üzerine ekspoz edilip, film geliştirildi.

2.12.7. SDS Jelinin Boyanması Ve Matriks-Yardımlı Lazer Desorpsiyon-İyonlaşmalı (MALDI) Kütle Spektrometrisi İle Protein Analizi

1D ve 2D SDS-PAGE'de örneklerin yürütülmesinden sonra, kütle spektrometrisi ile incelemenin yapılması için, jel öncelikle Gümüş ve Komasi mavisi ile boyandı.

2.12.7.1. Gümüş Boyası

1D- ve 2D-SDS poliakrilamid jel elektroforezinde yürütülen proteinler, Gümüş boyası ile boyandı [134]. Öncelikle jel, 1 saat fiksatif solusyonunda (%50 metanol, %10 asetik asit) inkübe edilip, 30 dakika % 30'luk etanol ile yıkandı. Daha sonra jel, 1 dakika kadar, %0.02 lik sodyum tihosülfat ile inkübe edilip, distile su ile çalkalanıp, Gümüş boya solusyonunda (%0.2 Gümüş nitrat, %0.075 formaldehit) inkübe edildi. Tüm inkübasyonlar rotator üzerinde gerçekleştirildi. İnkübasyon süresi sonunda, jel yeni temiz bir kaba alınıp, distile su ile yıkanıp, geliştirici solusyon (%6 sodyum karbonat, %0.03 formaldehit, %2 sodyum thiosülfat) içerisinde, protein noktaları belirene kadar bekletildi. Geliştirmeyi durdurmak amacıyla, 15 dakika fiksatif solusyonu ile inkübe edildi. Boyanmış jel, iki kez distile su ile yıkanıp, 2 saat kadar jel koruyucu solusyonu (%30 etanol, %5 gliserol) içerisinde bekletildi. Jelin uzun süreli saklanması için, koruyucu solusyon içinden, jel kurutucu (Sigma) selefan plakalar arasına alındıktan sonra 3 gün süre ile oda ısısında jellerin kuruması sağlandı.

2.12.7.2. Komasi Mavi Boyası

Elektroforez sonrası, jel 1 saat fiksatif solusyonu (40% metanol içinde hazırlanmış %7 glasial asetik asit) içerisinde inkübe edildi. Boyama solusyonu ise, 4 volüm 1X Brilliant Blue G-Colloidal (Sigma) ve 1 volüm metanolün karışımı ile hazırlandı. Boyama solusyonu içerisinde, gece boyu rotator üzerinde inkübe edildi. Daha sonra jel, 60 saniye fazla boyanın uzaklaştırılması amacıyla boya uzaklaştırıcı solusyon I (destaining solusyon: % 25 (v/v)'lik metanol içinde hazırlanmış %10 asetik asit) ve ardından boya uzaklaştırıcı solusyon II (% 25 metanol) ile yıkandı. Jelin saklanması için, skan edilip, iki sephalon arasında kurumaya bırakıldı.

2.12.7.3. Protein Analizi (MALDI)

Komasi ve Gümüş boyanmalarından sonra, 1D-SDS-PAGE'den elde edilen bantlar ve 2D-SDS-PAGE'den elde edilen noktalar küçük parçalara ayrılarak, tüm bu küçük jel parçaları tripsin ile muamele edildi [135]. Tripsinize edilen proteinler, Q-TOF cihazındaki (Q-TOF ultima, Waters), LC-coupled ESI-tandem MS programında sekans analizine tabi tutuldular. Proteinler, MASCOT programı altında NCBI datalarına (bilgilerine) uygun olarak peptid fragmentleri araştırılarak tanımlandı.

2.12.8. Immün-çökeltme (Ko-immunopresipitasyon)

Hücreler, soğuk PBS ile bir kez yıkandıktan sonra, proteinaz inhibitörü içeren 500 µl RIPA solusyonu (50 mM Tris-HCl pH 7.5, 150 mM NaCl, 5 mM EDTA, 10 mM K_2HPO_4, %10 gliserol, %1 NP–40, %0.15 SDS, 1 mM Na_3VO_4, 1 mM sodyum molibdat, 20 mM NaF, 0.1 mM PMSF) ile lizis edildi. Daha sonra hücreler, skraper yardımıyla bulundukları hücre kültürü kaplarından ependorf tüplere aktarılarak 21'lik insulin iğneleri ile süspansiyon haline getirilirler ve sonrada 10 dakika 4°C'de 13,000 x g de santrifüj edildiler. Santrifüj sonrası elde edilen supernatan (500µl), 1:2 oranında immunoçöktürme (IP) solusyonu [20 mM Tris-HCl pH 8.0, 150 mM NaCl, 2 mM EDTA, 1% NP-40, 20 mM NaF, proteaz inhibitor koktail (Sigma)] ile dilüye edildi. Bu arada, 30 µl Protein G-Sepharose 4B Fast Flow boncukları (Amersham), IP için kullanılacak 1-2 µg antikor ile odaısısı veya 4°C'de rotator üzerinde (10 r.p.m.) 3 saatten geceboyuna kadar inkübe edildi. Daha sonra, hazırlanan hücre ekstraktı, antikor ile yüklenmiş Protein G boncukları ile 4°C'de rotator üzerinde, 3 saatten geceboyuna kadar değişen sürelerde inkübe edildi. İnkübasyon sonunda, boncuklar 3 kez 1ml soğuk IP solusyonu ile yıkandı. Yıkama solusyonunun uzaklaştırılmasından sonra, boncuklar üzerinde toplanmış immun kompleksler, 25 µl'lik 3x SDS–PAGE yükleme solusyonu ile süspanse edilip, 10 dakika 95°C'de kaynatılmış ve immun kompleksler NuPAGE % 4-12 Novex Bis-Tris jelinde (Invitrogen) yürütüldü. Amaca uygun olarak, elektroforez sonunda jel ya immunoblot için Nitrosellulöz membrana aktarıldı ya da kollaidal Komasi mavi boyası ile boyandı.

2.12.9. Rekombinant GST-Jab1/CSN5 Ve His-VCP Proteinlerinin Ekpresyonu Ve Saflaştırılması

Jab1/CSN5, GST kuyruğu ile, VCP ise His kuyruğu ile füzyon proteini olarak ekspre edildiler. GST-Jab1/CSN5 ve His-VCP'nin ekspresyonu için kompotent haldeki *E. coli* BL21 DE3 hücreleri pET28$^{a\ (+)}$ His-VCP ve ya pGEX-4T_1-Jab1/CSN5 konstrakları ile transforme edildiler (bakteriyal transformasyon için bakınız 3.3.1). Transformasyon sonucu elde edilen pozitif klonlar, antibiyotik içeren (His-VCP için kanamisin ve GST-Jab1/CSN5 için ampisilin) 5 ml 2YT medyumu (%1.6 tripton, %1 yeast ekstrakt and %1 NaCl, pH 7.0) içerisine ekilip, 37°C'de geceboyu çalkalamalı etüvde kültüre edildi. Ekspresyon koşullarını optimize etmek amacıyla, 50 µg/ml antibiyotik (kanamisin ve ya ampisilin) içeren 50 ml 2YT medyumundan (%2 baktotripton, % 1 yeast ekstrakt, 100 mM NaCl, pH 7.0) 500 µl alınıp geceboyu kültür hazırlandı. Kültürler 37°C'de OD_{600} = 0,5'e ulaşana kadar tutuldular. Daha sonra kültürler iki kısma bölünüp, herbir kültürden 1ml SDS-PAGE analizi için korundu. Bir kültür, 0.5 mM IPTG ile indüklenip, 37°'de çalkalamalı inkübatörde 1, 2 ve 3 saatlik periyotlarla inkübe edildi. Her bir inkübasyon süresi sonunda 1 ml kültürden alınıp, SDS-PAGE analizi için saklandı. 1ml lik kültür örnekleri maksimum hızda 1 dakika kadar santrifüj edilerek elde edilen pellet 1x SDS yükleme solusyonu ile karıştırılıp, 95°C'de 3 dakika kaynatıldı. Örnekler %12.5'luk SDS-PAGE'e yüklenip, jel Komasi mavisi boyası ile boyandı.

Daha büyük düzeyde ekspresyon elde etmek için, 5 ml'lik gece boyu kültürü, 400 ml 2YT medyumunu (100 µg/ml ampisilin veya kanamisin içeren) inoküle etmek için kullanıldı. OD_{600}: 0.5'a ulaştığında, 0.5 mM IPTG ile indüklenip 3 saat 37°C'de inkübasyona devam edildi. İnkübasyon sonunda, hücreler 3,000 x g, 4°C'de 30 dakika santrifüj edildi, elde edilen supernatan atılıp ve pellet soğuk PBS ile süspanse edildi. Hücreler sonrasında sonikasyon ile lizis edilip, küçük bir aliquat (parça: kısım) saklandı. Lizise uğramış hücreler %1 lik Triton X-100 ile muamele edilip, 30 dakika kadar füzyon proteini solubilize etmek amacıyla nazik bir şekilde rotatorda döndürüldü. Daha sonra, 1200 x g 4°C'de 10 dakika santrifügasyon yapılıp, pellet atılıp supernatan temiz bir kaba aktarıldı. Füzyon proteinin hangi fraksiyonda olduğunu anlayabilmek için hem pellet hem de supernatandan bir miktar aliquat SDS-PAGE analizi için kullanıldı.

His-VCP veya GST-Jab1/CSN5 içeren supernatanlar, daha sonrasında lizis solusyonu (50 mM Tris-HCl, 1mM EDTA, 100 mM NaCl, pH 8.0) ile süspanse edilip, 1mg/ml lizozim ve DNAaz I ile 30 dakika buz üzerinde inkübe edilmeye bırakıldı.

Lizise edilen hücreler 14,000 x g 4°C'de 15 dakika santrifüj edildikten sonra inklüzyon badileri içeren pellet lizis solusyonu ile 4 kez yıkandı. Daha sonra inklüzyon badileri içeren temizlenmiş pellet denatürasyon solusyonu (6 M guanidyum hidroklorid, 10 mM DTT in PBS) ile 30 dakika oda ısısında rotator üzerinde inkübe edildi ve sonrasında 12.000 rpm 4°C'de 15 dakika santrifüj edildi. Santrifügasyon sonunda elde edilen temizlenmiş pellet, 0.5 mM PMSF and 1 mM DTT içeren PBS pH 7.8 solusyonuna karşı 4 saat diyaliz edildikten sonra, temizlenmiş hücre ekstraktı 4°C'de 60 dakika % 50 Ni-NTA (10 ml ekstrat için 1ml Ni-NTA kullanıldı) ile inkübe edildi. Daha sonra Ni-NTA matriksi 2 kez 50 mM NaH_2PO_4 pH 8.0, 300 mM NaCl ve 20 mM imidazol solusyonu ile yıkanıp, matrikse bağlı proteinler, 50 mM Na_2HPO4, 300 mM NaCl, 250 mM imidazol, pH 8.0 solusyonu ile eluye edildi. Eluye edilen proteinlerin saflığı, SDS-PAGE'de analiz edildi.

GST-Jab1/CSN5'nin saflaştırılması için, GST-Jab1/CSN5 içeren supernatan Glutatyon Sepharoz 4B kramotografisine 4°C'de 2 saat maruz bırakıldıktan sonra matriks, iki kez PBS (140 mM NaCl, 2.7 mM KCl, 10 mM Na_2HPO_4, 1.8 mM KH_2PO4) ile yıkandı ve bağlı proteinler 50 mM Tris-HCl pH 8.0 içerisinde hazırlanmış 10 mM Glutatyon ile eluye edildi.

2.12.10. *In vitro* Çökeltme

2.12.10.1. His-VCP Çökeltmesi

His-VCP (1 µg), 30 µl Ni-NTA boncukları ile oda ısısında 1 saat, rotator üzerinde inkübe edildi. Bağlanmamış proteinleri uzaklaştırmak için, boncuklar, 3 kez PBS ile yıkandıktan sonrasında, boncuklar, artan miktarlarda (0.5, 1 ve 2 µg sırasıyla)

rekombinant GST-Jab1/CSN5 ile 25 mM Tris-HCl pH 8.0, 200 mM KCl, 2 mM $MgCl_2$, 1 mM ATP, 1 mM ditioteitol, %5 gliserol and %1 Triton X–100 solusyonu içerisinde 2 saat 4°C inkübe edildi. Kontrol olarak, Ni-NTA boncukları His-VCP ile kaplanmadan, sadece 2 µg GST-Jab1/CSN5 kaplanmamış boncuklarla inkübe edildikten sonra, boncuklar yıkanarak, 3 X SDS yükleme solusyonunda 5 dakika kaynatıldı. Daha sonra, proteinler, SDS-PAGE'de yürütülüp ya kolloidal Komasi mavisi boyasıyla boyandı ya da immunoblot ile deneye devam edildi.

2.12.10.2. GST-Jab1/CSN5 Çökeltmesi

1 µg of GST-Jab1/CSN5, 30 µl glutatyon sepharoz boncukları ile oda ısısında 1 saat rotator üzerinde inkübe edildi. 3 kez PBS ile yıkandıktan sonra, boncuklar His-VCP proteini (0.5, 1 ve 2 µg sırasıyla) ile 2 saat 4°C'de rotator üzerinde inkübe edildi. Kontrol olarak, His-VCP kaplanmamış glutatyon boncukları ile inkübe edildi. Daha sonrasında boncuklar yıkanıp, GST-Jab1/CSN5'a bağlanmış proteinler immunoblot ile analiz edildi.

2.13. Molekülar Biyoloji Methodları

2.13.1. Kompetent *E. coli* Hazırlığı Ve Bakteriyal Transformasyon

Kompetent *E. coli* hazırlığı dondurulmuş gliserol stoğu halindeki *E. coli* DH5α hücrelerinin antibiyotik içermeyen LB agar kültür kaplarına ekilmesi ile başlatıldı. Ekim sonrası, kültür kapları 16 saat 37°C'de inkübe edilip hücrelerin üremesi sağlandı. İnkübasyon süresi sonunda, tek bir koloni 5 ml SOB medyumu içerisine alınıp geceboyu çalkalamalı etüvde 37°C'de inkübe edildi. 50 ml önceden 37°C'de ılıtılmış SOB medyumu (%2'lik baktotripton veya pepton, 0.5 %'lik yeast ekstrakt, 10 mM NaCl, 2.5 mM KCl) içine geceboyu kültürden 0.5 ml eklendi ve hücrelerin 2.5-3.0 saat kadar kültürdeki gelişimleri izlenerek OD_{600}: 0.45-0.50 olana kadar spektrofotometre altında okuma yapıldı. Hücreler sonrasında, 20 dakika buz üzerinde inkübe edildi. Hücreler 1075 x g'de 4°C'de 15 dakika santrifüj edildi, supernatan atıldı. Pellet 100 ml TFB solusyonu (10 mM MES, 45 mM $MnCl_2$, 10 mM $CaCl_2$, 100 mM KCl, pH 6.2) içerisinde buz üzerinde 10-15 dakika bekletildi ve sonrasında 1075 x g'de 15 dakika 4°C'de santrifüj edildi. Santrifüj sonrası, supernatan atıldı ve pellet nazik bir şekilde 3.9 ml TFB buffer içerisinde süspanse edilip, 5 dakika buz üzerinde inkübasyona bırakıldı. Sonra ardı ardına 140 µl DMSO ile 5 dakika, 140 µl 1M DTT ile 10 dakika ve tekrar 140 µl DMSO 5 dakika inkübe edildi. Transformasyon için, 200 µl lik komponent hücreler, Ependorf tübüne transfer edilip, buz üzerinde 3-7 µl lik 50 ng plasmid kompenent hücreler üzerine eklendi ve 30 dakika buz üzerinde inkübe edildi. İnkübasyon süresi sonunda, ependorf tübü, 42°C'de 45 saniye bekletilip hemen buz üzerine alındı. 2 dakika buz üzerinde soğutulduktan sonra, 200 µl lik komponent hücreler üzerine 800 µl lik ılıtılmış SOC medyumu (5 mM glukoz içeren SOB medyumu) eklendi. Daha sonrasında, 60 dakika çalkalamalı inkübatörde inkübe edilip, inkübasyon sonunda 200 µl lik transforme olmuş komponent hücreler, uygun

antibiyotik (50 µg/ml) içeren LB agar petrilerine ekildi. Petri kapları odaısısında 30 dakika kadar bekletilip, 37°C de geceboyu inkübe edildiler. İnkübasyon sonunda, petrilerden 1 koloni seçilerek 5ml'lik minikültür (Antibiyotik içeren SOB medyumu) içerisine ekildiler.

2.13.2. Plasmid DNA İzolasyonu (mini ve maksi bakteriyal kültür hazırlığı)

5 ml'lik mini kültür (antibiyotik içeren SOB medyumu) içerisine bir koloni konulup, bakteriyel kültür 37°C'de çalkalamalı inkübatörde geceboyu inkübe edildi. Promega Miniprep DNA izolasyon kitinde verilen protokole uygun bir şekilde geceboyu kültürden DNA izolasyonu yapıldı. Maksi kültürden DNA izolasyonunun tek farklı, kültür hacminin fazla olmasıydı. Promega DNA izolasyon Kitinde belirtilen aynı protokol uygulandı. Fakat minikültürdeki 5 ml lik kültür yerine 200 ml lik maksi kültür, plasmid içeren koloni ile 37°C'de 12-16 saat çalkalamalı inkübatörde inkübe edildi. İzole edilen plasmid DNA'sı agaroz jel elektroforezinde yürütüldü.

2.13.3. Agaroz Jel Elektroforezi

% 0.8-% 1'lik agaroz jeli, 100 bp ile 10 kb arasındaki DNA fragmentlerini ayırmak amacıyla kullanıldı. Hazırlanacak jelin yüzdesine göre, belli bir miktardaki agaroz 1x TAE solusyonu (40 mM Tris-asetat, 1 mM EDTA pH 8.0) içerisinde çözüldü ve mikrodalga fırını içerisinde ısıtılarak çözülmesi sağlandı. Jel kaplara dökülmeden önce, 1x SYBR green boyası eklenerek iyice karıştırıldı. Hazırlanan jel solusyonu tarağı yerleştirilmiş jel kaplarına döküldü ve 30 dakika sonra jelin polimerize olduğu görüldükten sonra, tarak jelden uzaklaştırıldı. Sonra, jel elektroforez kabı içerisine yerleştirilip, üzeri 1x TAE solusyonu ile kaplandı. DNA örnekleri ve markerlar, uygun oranda DNA örnek solusyonu (%3 gliserol, %0.025 bromofenol blue, 0.025% xylene cyanol FF) ile karıştırılıp, jeldeki veller içerisine yüklendi. Jel, 100V (2-10V/cm jel)'da yürütülüp, 305 nm UV transilluminatörü altında incelenip, fotograflandı.

2.13.4. shRNA Vektörü pSUPER'e Klonlama

MIF geninin nakdovnu (susturulması) için, shRNA vektörü pSUPER kullanıldı [136]. shRNA içerisine 64'lük oligonükleotid çiftinin annealing edilmesi ile elde edilen kısa insertler klonlandı. Vektör içerisine klonlanan bu 64 oligonükleotid, 19 nükleotidlik MIF mRNA sından alınmış bir kısım ve 9 bp lik ayırıcılar (spacer) içermekteydi.

Spesifik gen susturma (nakdavn) için kullanılan pSUPER vektörüne klonlama işleminin basamakları aşağıda özetlenmiştir:

- İnsertin üst ve alt dizilerinin annealing (ısı ile ayrıştırma) edildi.
- pSUPER vektörü Bgl II ve Hind III ile linear (düz) hale getirildi.
- Annealing edilmiş oligolar pSUPER vektörüne klonlandı.

- Bakteriye transformasyonu, pozitif klonların seçimi, plasmid DNA saflaştırılması, DNA sekanslanması yapıldı.
- pSUPER-MIF'in memeli hücrelerine transfekte edildi.
- Nakdavn etkisi protein ve mRNA düzeyinde kontrol edildi.

2.13.4.1. Oligoların Ayrıştırılması

MIF için seçilmiş olan 64'lük oligonükleotidler, Sigma firmasından satın alınıp, konsantrasyonları 100 pmol/µl olacak şekilde Tris-EDTA, pH 8.0 solusyonu içerisinde çözüldüler. 20 µl herbir oligonükleotitden (yaklaşık 20 µg), 10 µl 10x annealing solusyonu (100 mM Tris-HCl pH8.0, 10 mM EDTA, 300 mM KCl), 50 µl distile su reaksiyon tübü içerisinde karıştırıldı. Daha sonrasında, reaksiyon tübü, kaynatılmış su içerisinde inkübe edildi ve sıcak suyun ısısı oda ısısı sıcaklığına düşene kadar tüpler su içerisinde inkübe edilip, oligonükleotidlerin anneal olması sağlandı ve inkübasyon sonunda, ayrıştırılmış oligonükleotidler dilüye edilip, -20°C de kullanılana kadar saklandı.

2.13.4.2. pSUPER Vektörüne Ligasyon (bağlama)

20 µg pSUPER vektörü, Hind III ve Bgl II ile linearize edildi. Lineariye edilen vektör, %1'lik agaroz jelden purifiye edildikten sonra, DNA jel purifikasyon kiti kullanılarak, jel içerisinden DNA purifiye edildi. Ligasyon reaksiyonu, 1 µl pSuper (100 ng/µl), 2 µl anneal edilmiş oligolar (4 ng/µl), 5 µl 2x T4 DNA ligaz solusyonu, 1 µl H_2O ve 1 µl T4 DNA ligazların karıştırılmasıyla hazırlandı. Kontrol olarak ise, ligasyon reaksiyonu, ligaz enzimi reaksiyon içerisine konulmadan gerçekleştirildi. Ligasyon reaksiyonunun yarısı, kompotent *E. coli* DH5α'ya transform edildi. 5 ng standart plasmid vektör, transformasyon kontrolü olarak kullanıldı. Bakteri ampisilin içeren agar kaplarına yayılıp, geceboyu kültüre edildi. Koloniler, ertesi gün kültür kaplarından toplanıp, ampisilin içeren LB medyumu içerisinde yetiştirildi. Klonların, Bgl II enziminin bulunduğu reaksiyon solusyonu içerisinde kontrolü sağlandı (Bgl II alanı, pozitif klonlarda görülmemesi gerekmektedir Bgl II klonlamada kullanılan bir enzimdir ve klonlama sonunda Bgl II alanı kaybolmaktadır, dolayısıyla pozitif klonlar Bgl II ile seçildi). Daha sonrasında, DNA sekanslanması ile pozitif klonların gen dizilimleri doğrulandı (Seqlab, Göttingen).

2.13.4.3. Memeli Hücrelerine Transfeksiyon

Transfeksiyondan bir gün önce, hücreler, %10 fetal bovin serumu içeren Dulbecco'nun modifiye Eagle medyumu (DMEM) ile % 50-70 konfluent olacak şekilde kültüre edildiler. Transiyent (geçici) transfeksiyon Lipofectamine 2000 (Invitrogen) kullanılarak gerçekleştirildi. MIF geninin baskılanma derecesi, immunoblot yöntemi ile protein düzeyinde belirlendi.

2.14. FRET (Floresan Rezonans Enerji Transferi)

İki protein arasındaki yakınlığı saptamak amacıyla, konfokal mikroskobu altında, çiftli indirek immunofloresan ile proteinler işaretlendikten sonra FRET ölçümü gerçekleştirildi. Hücreler, 24 vellik kültür kaplarına ekildikten sonra, çiftli transfekte edildiler. Transfeksiyon herbir protein için hazırlanmış plasmidlerin hücrede overekspre edilmesi ile gerçekleştirildi. Transfeksiyondan 24 saat sonra, hücreler % 4'lük paraformaldehit ile 15 dakika fikse edildi. Jab1/CSN5 ve VCP indirek çiftli immunofloresan tekniği ile işaretlendiler (Jab1/CSN5, anti rabbit Cy5-konjuge sekonder antikor ile VCP ise, anti mouse Cy3- konjuge sekonder antikoru ile işaretlendi). Her iki primer antikor aynı zamanda uygulanıp, geceboyu 4^{o}C'de inkübe edildi. Ertesi gün, yıkama işleminden sonra, Cy3-konjuge donkey anti-mouse-Ig ile 1 saat oda ısısında inkübe edilip, ardından ikinci yıkamaya geçildi ve sonrasında, Cy5-konjuge donkey anti-rabbit-Ig ile 1 saat inkübe edildi. Kontrol olarak, sadece Jab1/CSN5 antikoru ve ardından da her iki sekonder antikorlar uygulandı.

FRET akseptörün söndürülmesi (photobleaching) temeline dayalı bir metod olup, konfokal altında hesaplandı. FRET sinyali, Cy5 işaretli alıcının (akseptörün: Jab1/CSN5) söndürülmesinden önce ve sonrasında, Cy3 işaretli verici (donor) kanalındaki floresan yoğunluğundaki artış olarak hesaplandı. Akseptör, 5 kez (1.28 s/scan) mümkün olan en yüksek fokuslama alanında, 633 nm lik HeNe lazer ışığı altında söndürüldü. FRET den kaynaklanmayan ölçümleri de değerlendirmek amacıyla, akseptörün söndürüldüğü alanlara yakın bölgeler (ROI: region of interest) de söndürüldü. Donor floresanındaki artış: $(\Delta IF)=I_{DA}$ (söndürülmeden sonraki floresan yoğunluğu)-I_{DB} (söndürülmeden önceki floresan yoğunluğu) şeklinde hesaplandı.

Konfokal mikroskobu için gerekli olan değerler: Cy3 nin deteksiyonu: 543 nm altında 52% lazer gücü; Cy5'in deteksiyonu: 633 nm altında, 20% lik lazer gücü kullanıldı.

İSTATİKSEL ANALİZ

3.1. FRET (Floresan Rezonans Enerji Transferi)

FRET deneyi sonunda, deney ve kontrol grupları arasındaki FRET farkı, SPSS programının, sürüm 12 (SPSS GmbH Software, Munich, Germany) ile Mann-Whitney testi ile hesaplandı.

BULGULAR

4.1. MIF'e bağlanan proteinlerin belirlenmesi

MIF'e bağlanan proteinlerin tanımlanması için, aşağıdaki stratejiler sırasıyla uygulandı. İlk olarak, *in vivo* biyotin ile işaretleme (*in vivo* biotin tagging) metodunu takiben, afinite temelli kromatografik methodlar ile MIF ve MIF'e bağlanan proteinler hücre ekstratlarından saflaştırıldı ve ardından saflaştırılan proteinlerin tanımlanması amacıyla kütle spektrometrisine başvuruldu. Ayrıca, MIF ve MIF ile ilişkide olan proteinlerin birbirlerine bağlanmaları Floresan Rezonans Enerji Transferi (FRET), *in vivo* immunçökeltme ve *in vitro* çökeltme metodlarıyla birkez daha doğrulandı.

4.1.1. MIF'in biyotin ile *in vivo* işaretlenmesi

In vivo MIF'in biyotinlenmesi, MIF'i eksprese eden vektör pN3-CTB-MIF ve BirA enzimini eksprese eden vektör pBudCE4.1-birA'nin birlikte NIH 3T3 hücrelerine sabit bir şekilde transfekte edilmesi ile sağlandı. Bu biyotinleme işinin temel prensibi Şekil 4.1.1.1'de gösterildi.

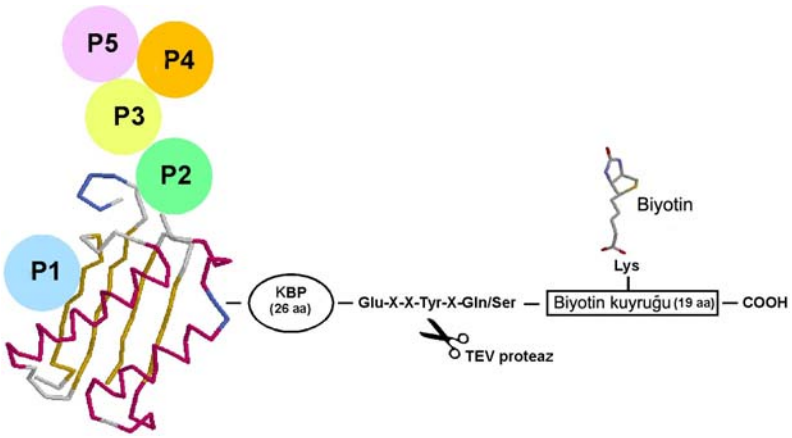

Şekil 4.1.1.1. NIH 3T3 hücrelerinde MIF'in *in vivo* biyotinlenmesinin temel prensibi. MIF ve P1, P2, P3 gibi MIF'le ilişkili proteinlerin biyotine bağlanması görülmektedir. MIF biyotine kalmoduline bağlanan peptid (KBP) ve TEV proteaz kesici kısım ile bağlanmış durumdadır. Biyotinlenme için gerekli olan bakteriyal biyotin ligaz birA'nın sabit olarak NIH 3T3 lerinde MIF ile birlikte aynı klonda ekspre edildiği görülüyor.

MIF hedef proteinin etkili bir şekilde biyotinlenmesi, SDS-PAGE analizi ile değerlendirildi (Şekil 4.1.1.2). Hedef MIF ve beraberinde BirA enzimiyle çiftli transfekte edilen (biyotin. MIF/BirA) ve de sadece BirA enzimiyle tekli transfekte edilen (BirA) hücrelerden elde edilen protein ekstraktları %18'lik SDS jelinde yürütüldü. Daha sonra proteinler, nitroselüloz membrana transfer edilip, endojenöz ve biyotinlenmiş MIF'i saptamak amacıyla anti-MIF antikoruyla inkübe edildi. Aynı membran, striplenip biyotinlenmiş MIF'i belirlemek amacıyla streptavidin-HRP (Şekil

4.1.1.2, alt panel) ile muamele edildi. Çiftli transfekte edilen grupdaki hücre ekstraktlarında, 22 kDa'luk biyotinlenmiş MIF (Şekil 4.1.1.2, üst panel, sıra 2, ok) ve de 12 kDa'luk endejenöz MIF (Şekil 4.1.1.2, üst panel, sıra 2, yıldız) Western blot ile belirlendi. Tekli transfekte edilen grupta ise, sadece endojenöz MIF saptandı (Şekil 4.1.1.2, üst panel, sıra 3). Ayrıca, MIF'in başarılı bir şekilde biyotinlendiği, streptavidin-HRP uygulanması ile de doğrulandı. Çiftli transfekte edilen grupda, biyotinlenmiş MIF'deki artan sinyal belirgin olarak saptanırken (Şekil 4.1.1.2, alt panel, sıra 2, ok), tekli transfekte edilen grupda biyotinlenme görülmedi (Şekil 4.1.1.2, alt panel, sıra 3). Bu sonuçlar, MIF'in NIH 3T3 hücrelerinde, etkili bir biçimde biyotinlendiğini gösterdi.

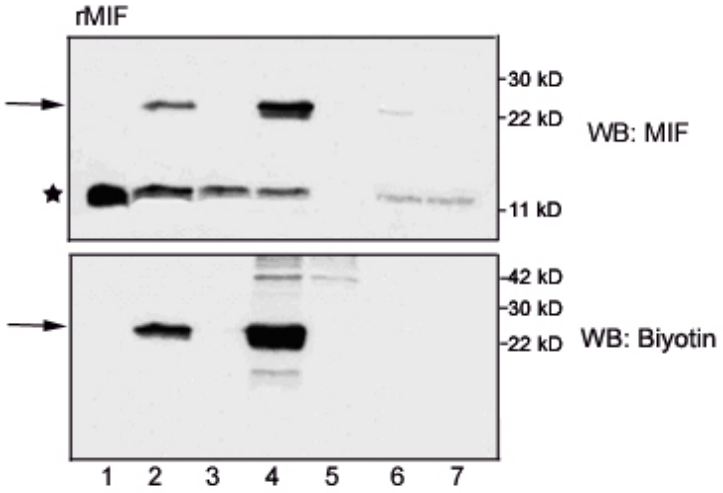

Şekil 4.1.1.2. MIF'in biyotinlenmesi ve saflaştırılmasını gösteren immunblot.
Biyotinlenmiş MIF ve biyotin ligaz bir A ekspre eden çiftli transfekte edilmiş (sıra 2, 4 ve 6) ve sadece birA ile transfekte edilmiş (sıra 3, 5 ve 7) hücrelerden elde edilen sitoplazmik ekstraktlar streptavidin agaroz boncukları ile inkübe edildiği gözlenmektedir. Supernatan (streptavidine bağlanmamış, sıra 6 ve 7), streptavidine bağlanmış proteinler (sıra 4 ve 5) ve hücre ekstraktının %5'i (sıra 2 and 3) % 18'lik SDS-PAGE analizine maruz bırakıldıktan sonra MIF ve biyotinlenmiş MIF'in saptanması Western blot (WB) ile gösterilmiştir. Yıldız: Endojenöz ve rekombinant MIF (rMIF), ok: biyotinlenmiş MIF

MIF'in etkili bir şekilde *in vivo* biyotinlendiğinin gösterilmesinden sonra, biyotinlenmiş MIF ve ilişkide olduğu proteinlerin hücre ekstraklarından saflaştırılması, streptavidin ile kaplı boncuklar ile afinite kromatografisi yardımıyla gerçekleştirildi. Total protein ekstraklarının streptavidin boncuklarına bağlanma oranı farklı miktarlardaki protein ekstraklarının ve farklı inkubasyon zamanlarının kullanılması ile saptandı. Total protein ekstrakları (Şekil 4.1.1.2, sıra 2 ve 3), streptavidine bağlanan materyal (Şekil 4.1.1.2, sıra 4 ve 5) ve bağlanmayan supernatan (Şekil 4.1.1.2, sıra 6 ve 7) Western blot ile analiz edildi. Şekil 4.1.1.2'de görüldüğü üzere (alt panel), birçok endojenöz olarak biyotinlenmiş proteinlerin de streptavidin-HRP'ye bağlandıkları

saptandı. Sonuç olarak, bu bulgular, biyotinlenmiş MIF'in tek adımlı afinite saflaştırması ile hücre ekstraktlarından geri elde edilebileceğini gösterdi.

4.1.2. MIF'e Bağlanan Proteinlerin Gözlenmesi Ve Saflaştırılması

Hücre ekstraklarından biyotinlenmiş MIF'in tek basamaklı saflaştırılması sonucu elde edilen biyotinlenmiş MIF ve onunla etkileşimde olan proteinler Komasi mavisi ve gümüş boyası ile boyandı (Şekil 4.1.2.1A ve B). Her iki boyama yöntemi ile de aynı boyanma paterni gözlendi ve gümüş boyasının Komasiden daha hassas olması nedeniyle, elde edilen protein bantlarında bir artış belirlendi. Biyotinlenmiş MIF sadece, çiftli transfekte edilen grubun hücre ekstratlarında gözlendi. Biyotinlenmiş MIF proteinini gösteren band, Komasi mavisi ile boyanmış jelden kesilip kütle spektrometresinde incelenmesi ile doğrulandı. Biyotinlenmiş MIF ve MIF ile ilişkide olan proteinlerin bulunduğu sıranın (sıra 3) boyanma paterninin, arkaplan boyanmasından (sıra 4) farklı olması, biyotinlenmiş MIF ile ilişkide olan proteinlerin saflaştırmanın başarı ile sonuçlandığını gösterdi. Çiftli ve tekli transfekte edilen hücre ekstratlarının SDS PAGE'de analiz edilip, Komasi mavisi ile boyanması sonrası gözlemlenen protein bandları, jelden kesilip, küçük parçalara ayrılıp, kütle spektrometresinde incelendi.

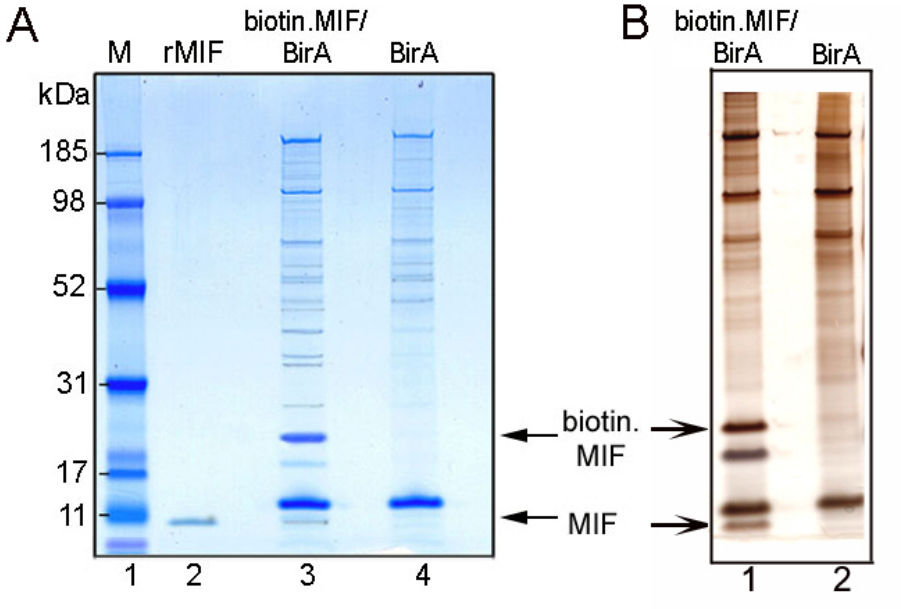

Şekil 4.1.2.1. Saflaştırılmış biyotinlenmiş MIF ve ilişkide olduğu proteinlerin Komasi mavisi ve gümüş ile gösterilmesi. Biyotinlenmiş MIF ve birA (A, sıra 3; B, sıra 1) ve de sadece birA (A, sıra 4; B, sıra 2) ekspre eden hücrelerden elde edilen proteinlerin streptavidin biyotin saflaştırması sonrası Komasi mavisi (A) ve gümüş (B) boyaları ile görüntülenmiştir. M = moleküler ağırlık standartı (sıra 1), rMIF (A, sıra 2).

Kütle spektrometri analizinden sonra, çiftli ve tekli transfekte edilen gruplardaki (Şekil 4.1.2.1, sıra 3 ve sıra 4) proteinler karşılaştırıldı. Biyotinlenmiş MIF ve onunla birlikte saflaştırılan proteinler (sıra 3), endojenöz olarak biyotinlenmiş proteinlerle (sıra 4) rekabet edebilecekleri için bu grupdaki proteinler listeden elimine edildi. Kütle spektrometrisi sonucu tanımlanan proteinler arasında, daha öncesinden bilinen MIF ile ilişkisi bilinen proteinlerden peroksiredoksin–1 and RPS 19 de yer almaktaydı.

MIF'in biyotinlenmesi sonucu, MIF'e eklenen biyotin işaretleyicisi, MIF'in üç boyutlu yapısını değiştirebileceği ihtimali göz önünde bulundurularak, biyotinlenmiş MIF'in hala protein-protein bağlantısını koruyup koruyamayacağı da test edildi. Biyotinlenmiş MIF, streptavidin boncuklarıyla pürifiye edildikten sonra, MIF ile ilişkisi bilinen proteinlerden Jab1/CSN5 ve peroksiredoksin-1'in de biotin.MIF ile birlikte saflaştırıldığı (Şekil 4.1.2.2, sıra 3) bulundu.

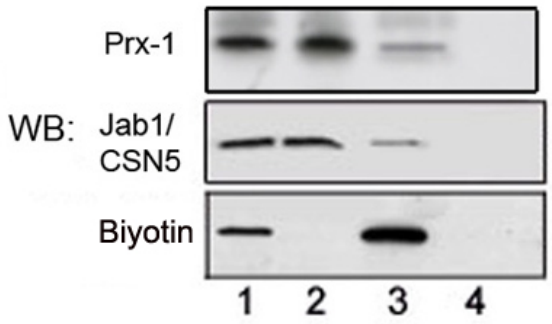

Şekil 4.1.2.2: Biyotinlenmiş MIF'e bağlanan proteinlerin gösterilmesi.Biyotinlenmiş MIF ve BirA (sıra 1 ve 3) ve de sadece BirA (sıra 2 ve 4) eksprese eden hücre ekstraktları streptavidin boncukları ile inkübe edildikten sonraki immunoblot analizi görülmektedir. Başlangıç materyali (sıra 1 ve 2) ve biyotinlenmiş MIF'e bağlanmış proteinler (sıra 3 ve 4) % 16'lik SDS jelde yürütülüp, Jab1/CSN5, peroksiredoksin-1 (Prx-1) ve biyotin antikorları kullanılarak immunoblot ile analiz sonuçları gözleniyor.

4.1.3. Streptavidin Boncuklarında TEV Proteaz Reaksiyonu Ve 1D-SDS-PAGE

Biyotin işaretleyici üzerinde yer alan spesifik TEV proteaz bölümü (Şekil 4.1.1.1'e bakınız), streptavidin boncuklarından MIF ve bağlı bulunduğu proteinleri ayırmak amacıyla kullanıldı. Çiftli ve tekli transfekte edilmiş hücrelerden elde edilen hücre ekstratları, streptavidin boncukları ile inkübe edildikten sonra, boncuklar yıkanıp, TEV proteaz ile inkübe edildiler. Farklı üç deneyden elde edilen TEV elusyonları birleştirilip, proteinler aseton ile çöktürüldü. Çöktürme sonucu proteinler, 1D ve 2D-SDS-PAGE'de analiz edildi.

4.1.4. TEV Proteaz Reaksiyonu Sonucu Elde Edilen Protein Komplekslerinin 2D-SDS-PAGE Analizi

Çiftli ve tekli transfeksiyon sonrası TEV elusyonlarından elde edilen proteinlerin 2D-SDS-PAGE'de ayrımı yapılıp, Gümüş boyanması ile görüntülenmeleri sağlandı (Şekil 4.1.4.1). Çiftli ve tekli transfeksiyon gruplarından elde edilen proteinler karşılaştırılıp, sadece çiftli transfeksiyonda gözlemlenen proteinler Gümüş boyası ile boyandı ve jelden çıkarılarak, tripsin uygulandıktan sonra kütle spektrometresi ile incelendi. Kütle spektrometrisi sonrası tanımlanan proteinlerin listesi Tablo 4.1.4.1'dedir. Toplam 30 protein inceleme altına alındı, bunlar arasında 4 gen ürünü 1D-SDS jelinde de saptandı.

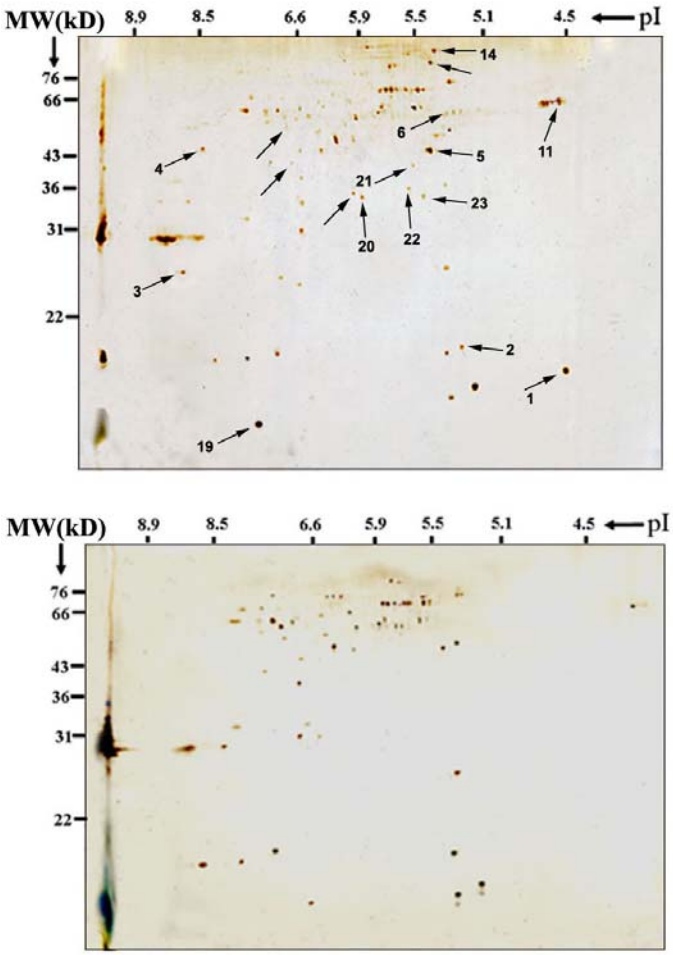

Şekil 4.1.4.1. TEV proteaz reaksiyonu sonrası elde edilen proteinlerin 2D-SDS-PAGE analizi. Biyotinlenmiş MIF ve BirA eksprese eden hücrelerden (üst panel) elde edilen proteinler, sadece BirA (alt panel). ekspre eden hücrelerdeki proteinlerle karşılaştırılıp, sadece biyotinlenmiş MIF ve BirA eksprese eden hücrelerdeki proteinler jelden çıkarılıp, kütle spektrometrisinde incelendikten sonra elde edilen protein noktaları gözleniyor. Üst panelde belirtilen numaralar, Tablo 4.1.4.1'de liste halinde belirtildi.

Tablo 4.1.4.1. 2D-SDS-PAGE analizi sonrası, MIF'e bağlanan proteinlerin MALDI-MS ile tanımlanmaları

Noktalar	Protein ismi	NCBI numaraları	M_r (kDa)	Eşleşen peptit sayısı
3	Peroksiredoksin 1	gi|56103807	22	10
14	Valosin-içeren protein	gi|55217	89	12
4	Fosfogliserat kinaz 1	gi|987048	45	11
5	Heterojen nüklear ribonükleoprotein F	gi|17390408	46	7
6	Serin proteinaz inhibitorü	gi|27806941	49	5
11	Alfa-2-HS-glikoprotein	gi|27806751	58	5
2	Ökaryatik translasyon başlatıcı faktör 5A-1 (eIF-5A-1)	gi|124231	19	3
20	Malat dehidrogenaz	gi|164543	36	4
19	MIF	gi|694108	11	4
1	Troponin C- protein	gi|223036	17	2
21	AHA1, 90kDa ısı şoku protein aktivatörü	gi|12653109	38	2
22	Pirofosfataz	gi|27754065	42	2
23	Asidik ribozomal fosfoprotein P0	gi|6671569	35	2

4.1.5. MIF'e Bağlı Proteinlerin NIH 3T3 Hücrelerinde İmmunoçökeltmesi

İn vivo biyotin ile işaretleme sonrası yapılan kütle spektrometri analizi sonucu belirlenen MIF'e bağlı proteinleri, başka yöntemlerle de doğrulamak amacıyla protein-protein bağlanmasını saptamada çok kullanılan birlikte-immunçökeltme (co-IP) yöntemine başvuruldu. Peroksiredoksin-1, Fetuin, Pgk-1, RPS 19 and VCP proteinleri, MIF ile çöktürüldü (Şekil 4.1.5.1). NIH 3T3 fibroblast hücre ekstratları, protein G-Sepharoz boncukları üzerine bağlanmış olan rabbit anti-rat MIF ve rabbit kontrol preimmun serumuna maruz bırakıldı. Daha sonra, immun kompleksler, Peroksiredoksin-1, VCP, Fetuin, RPS 19, Jab1/CSN5 and Pgk-1'nin saptanmaları için herbir proteine ait spesifik antikorlar ile muamele edilip, membranlar striplendikten sonra MIF için problandı. Şekil 4.1.5.1'de gösterildiği üzere, anti-MIF antikoru, MIF ile

birlikte NIH 3T3 hücre ekstratlarından Peroksiredoksin-1, VCP, Fetuin, Pgk-1 ve RPS 19'in çökmesini sağladı.

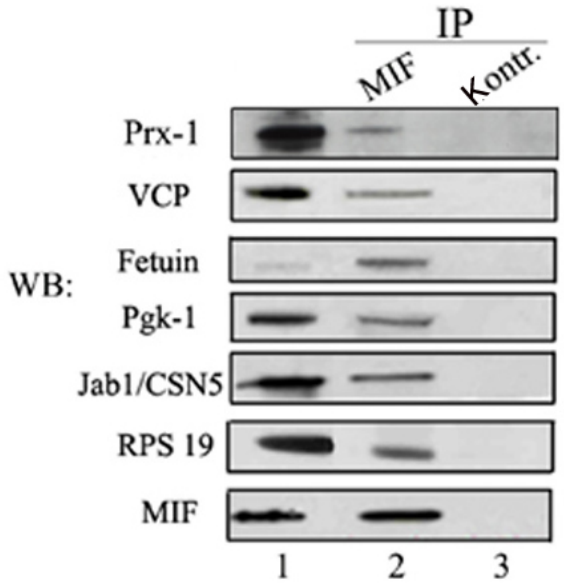

Şekil 4.1.5.1. Endejönez MIF ile birlikte MIF'e bağlanan proteinlerin NIH 3T3 hücrelerinde çöktürülmesini gösteren Western blot sonuçları.
Hücre ekstratları, rabbit anti-MIF antiserum (sıra 2) ve rabbit pre-immunserum (sıra 3) ile muamele edilerek, MIF ile çöktürülen proteinlerin (solda isimleri sıralanan), Western blot analiz sonuçları görülmektedir. İmmunçökeltmede hücre ekstratının %5'i başlangıç materyalı (sıra 1) olarak kullanıldı.

4.1.6. MIF ve MIF'e Bağlanan Proteinlerin Ortak Yerleşimleri

MIF ve MIF'e bağlanan proteinler arasındaki ilişki, konfokal mikroskobu ile bu proteinlerin ortak yerleşimlerinin gösterilmesi ile bir kez daha doğrulandı (Şekil 4.1.6.1).

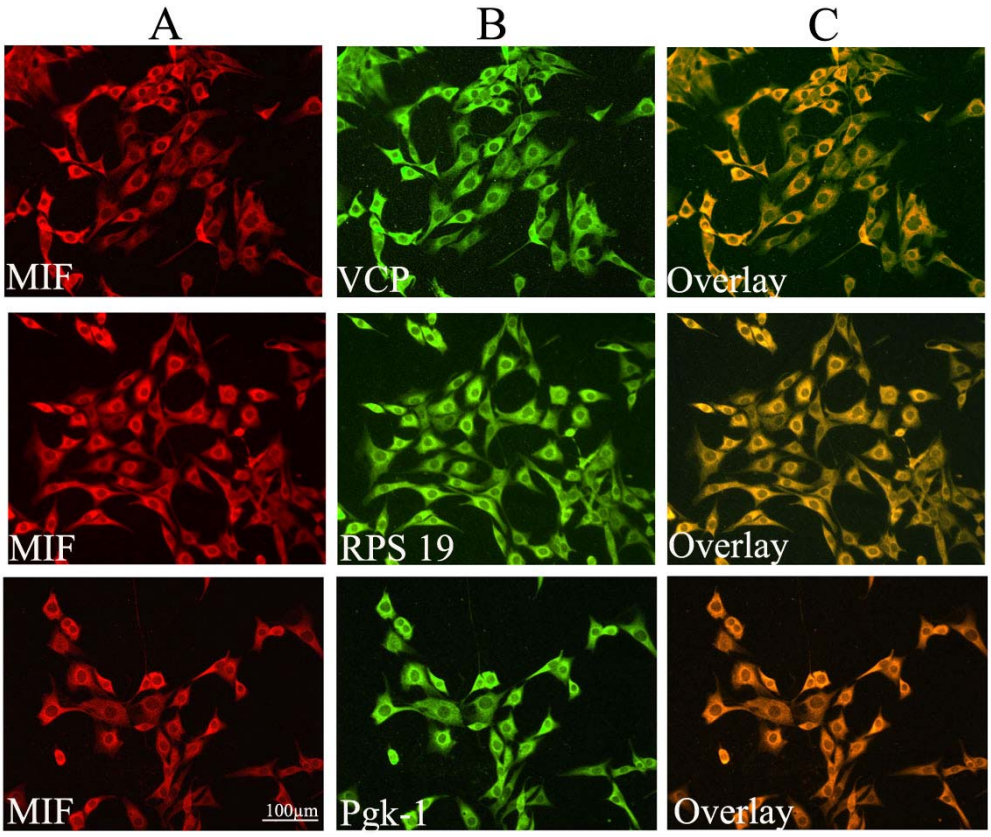

Şekil 4.1.6.1. MIF ve MIF'e bağlanan proteinlerin NIH 3T3 hücrelerindeki ortak yerleşimlerinin konfokal mikroskopta gösterilmesi. Hücreler, MIF ve VCP, RPS 19 ve ya Pgk-1'e karşı geliştirilmiş primer antikorlar ve ardından florasan ile işaretlenmiş sekonder antikorlar ile muamele edilerek çiftli lokalizasyonları gözlenmektedir. MIF kırmızı ile (A), MIF'e bağlanan proteinler yeşil ile (B), proteinlerin ortak yerleşimleri (overlay) turuncu ile gösterildi(C).

Bu çalışmada kullanılan *in vivo* biyotin ile işaretleme yöntemi, 1D- ve 2D-SDS-PAGE analizleri sonucu yapılan kütle spektrometrisi ile yeni MIF'e bağlanan proteinler belirlendi. Son bir çalışma, MIF'in UPS (Übikütin Protazom Sistem) de önemli bir rol oynadığı bilinen SCF übikütin ligaz aktivitesini kontrol ettiğini göstermiştir [74]. Bu çalışmayla uyumlu olarak, bu tezde de UPS'in önemli elemanlarından birisi olan VCP (Valosin-içeren protein) 2D-SDS-PAGE analizinde yüksek peptit skoru vermesi nedeni ile MIF'e bağlanan protein adayı olarak belirlendi. Bu nedenle, daha sonraki analizler MIF ve VCP arasındaki etkileşimi detaylı incelemek amacıyla yapıldı.

4.1.7. MIF Ve VCP Arasındaki Bağlanma Domainlerinin Belirlenmesi

MIF ve VCP arasındaki bağlanma domainlerini araştırmak amacıyla, VCP'nin FLAG işaretli N-terminal domaini (1–202 residuleri), D1 domaini (203–450 residuleri), D2 domaini (451–807 residuleri) ve ND1 domaini (1–450 residuleri) (Şekil 4.1.7.1A), MIF ile birlikte NIH 3T3 hücrelerinde, eksprese edildiler. Transfekte edilen hücrelerden hazırlanan ekstraklar, MIF'in çöktürülmesi amacıyla kullanıldı ve MIF ile birlikte çöktürülen proteinler anti-FLAG antikoru ile saptandı. Fakat VCP'nin çalışılan hiçbir domaininin MIF ile birlikte çökmediği belirlendi (Şekil 4.1.7.1B).

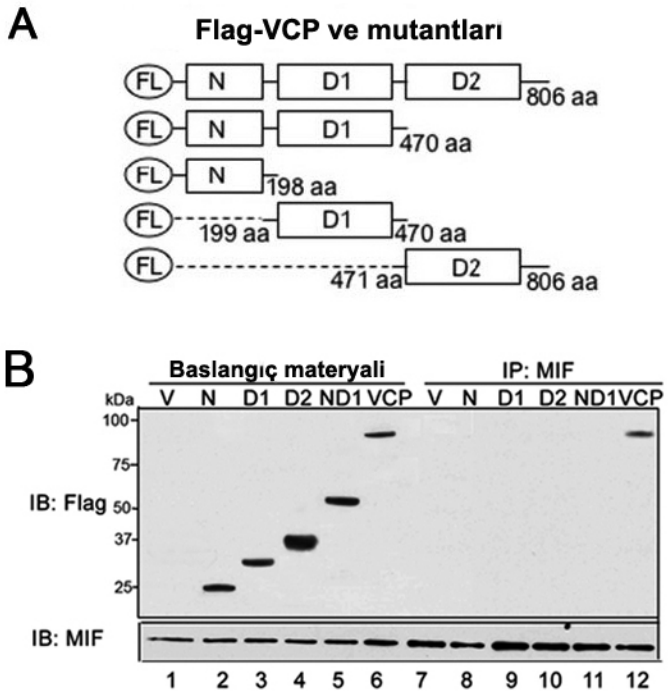

Şekil 4.1.7.1. VCP'nin MIF'e bağlandığı domainlerinin belirlenmesini gösteren şekil.
(A) VCP and onun N-terminal FLAG (FL) işaretleyicisi taşıyan delesyon mutantlarının şematik gösterimi (B) wt-VCP ve onun N-terminal domain (1–202 residuleri), D1 domain (203–450 residuleri), D2 domain (451–807 residuleri) ve ND1 domain (1–450 residuleri)'i ektopik olarak NIH 3T3 hücrelerinde FLAG ile işaretli proteinler olarak ekspre edildiği, kontrol olarak ise, hücrelerin, VCP expresyon vektörü (V) ile transfekte edildiği gözlenmektedir. Aynı anda, MIF, VCP ile birlikte ekspre edildikten sonra. anti-MIF antikorları (7-12) kullanılarak, hücre ekstratlarından MIF çöktürülüp, çöken proteinler, anti-FLAG antikoru ile saptantığı gösterilmektedir. Hücre ekstratlarındaki FLAG ve MIF proteinleri immunoblot (IB) ile saptandı (başlangıç materyali; 1–6).

Protein-protein bağlantısını bulmada kullanılan bir başka yöntem olan Floresan rezonans enerji transferi (FRET), VCP ve MIF arasındaki hücresel uzaklığın 10 nm'den daha yakın olup olmadığını saptamak amacıyla kullanıldı. MIF ve VCP heriki protein de sitoplâzmada yerleşmiş olmalarına rağmen, iki protein arasında herhangi bir anlamlı

FRET sinyali saptanamadı. Bütün bu sonuçlar, MIF ve VCP arasında direk değilde indirekt olarak bir kofaktör aracılı bağlanma olabileceğini akla getirdi. Bilinen MIF ile ilişkide olan proteinler arasından, Jab1/CSN5, VCP gibi UPS'de çalışması nedeniyle MIF ve VCP arasında kofaktör olarak bağlantıyı yapabilecek bir protein olarak düşünüldü. Jab1/CSN5'nin kofaktör olup olamayacağını anlayabilmek amacıyla, FLAG işaretleyicisi taşıyan VCP ve mutantları, wt-Jab1/CSN5'la birlikte NIH 3T3 hücrelerinde ko-ekspre edildiler (Şekil 4.1.7.2). Jab1/CSN5 presipitiye edildikten sonra, sadece ND1 domainin (sıra 11) ve wt-VCP'nin (sıra 12) Jab1/CSN5'a bağlandığı belirlendi.

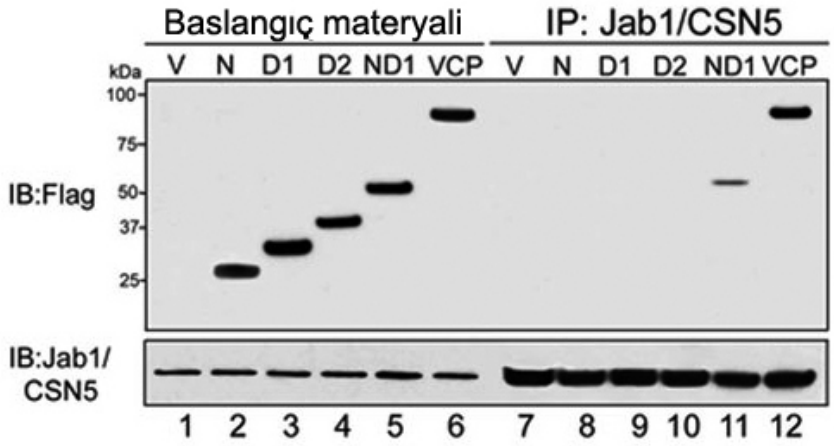

Şekil 4.1.7.2. VCP'nin Jab1/CSN5'e bağlandığı domainler.
Jab1/CSN5, VCP ve mutantları ile birlikte ekspre edildikten sonra anti-Jab1/CSN5 antikorları (7-12) kullanılarak, hücre ekstratlarından Jab1/CSN5 presipiye edilip, presipiye edilen proteinler, anti-FLAG antikoru ile saptanmalaı gözlenmktedir. Hücre ekstratlarındaki FLAG ve Jab1/CSN5 proteinleri immunoblot (IB) ile saptanmıştır (başlangıç materyali; 1–6).

4.2. MIF'in VCP'ye Jab1/CSN5 Aracılığıyla Bağlanması

4.2.1. Jab1/CSN5 VCP'ye İn vivo Ve İn vitro Bağlanır

VCP ve Jab1/CSN5'nın direk olarak bir kofaktöre ihtiyaç duymadan bağlandığını kanıtlamak amacıyla birlikte çöktürme (ko-IP) ve *in vitro* çöktürme deneyleri uygulandı. İlk olarak, iki protein arasındaki bağlanma, proteinlerin normal ekspresyon düzeylerine bakılarak *in vivo* olarak incelendi. Endojenöz Jab1/CSN5–VCP kompleksi, NIH 3T3 ve HEK293T hücre ekstratlarından anti-Jab1/CSN5 (Şekil 4.2.1.1A, sıra 2) ve anti-VCP (Şekil 4.2.1.1B, sıra 2) antikorları kullanılarak çöktürüldü. Ko-IP için kullanılan hücre ekstratları, VCP ve Jab1/CSN5 ekspresyonları için analiz edildi (Şekil 4.2.1.1A ve B, sıra 1). İzotip kontrol antikorları kullanıldığında (Şekil 4.2.1.1A ve B, sıra 3) çöktürme gözlenmedi.

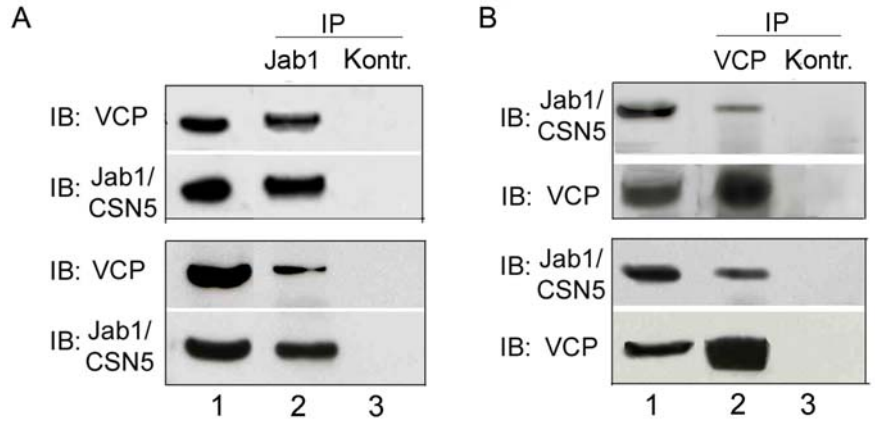

Şekil 4.2.1.1. Jab1/CSN5'ın VCP'ye *in vivo* bağlanması.

***(*A)** NIH 3T3 (üst panel) ve HEK293T (alt panel) hücre ekstratlarındaki, VCP ve Jab1/CSN5 proteinlerinin ekspresyonları immunoblot (IB) ile (başlangıç materyali, sıra 1). incelenmiştir. Hücre ekstraktları, anti-Jab1/CSN5 antikoru (2) ve izotip kontrol antikoru (kontrol, sıra 3) ile inkübe edilerek, Jab1/CSN5 çöktürüldü. **(B)** VCP, Anti-VCP antikoru (2) ile çöktürüldü. İzotip kontrol IgG (lane 3*)* ile ise çöktürme gözlenmemiştir. VCP ile birlikte çöktürülen proteinler, anti-VCP ve anti-Jab1/CSN5 antikorları ile saptandı.

Bunlara ek olarak, proteinler arasındaki direk etkileşim *in-vitro* çöktürme deneyi ile de incelendi. Bu amaçla, öncelikle rekombinant His-VCP ve GST-Jab1/CSN5 bakteriden saflaştırılarak, artan konsantrasyonlarda His-VCP (Şekil 4.2.1.2, sıra 1: 0.25 µg, sıra 2: 0.50 µg, sıra: 1 µg, sıra 4: 2 µg) glutatyon agaroz boncuklarına immobilize edilmiş 1µg GST-Jab1/CSN5 ile inkübe edildi. Kontrol olarak, glutatyon agaroz boncukları, sadece 2 µg of His-VCP (sıra 5) ile inkübe edildi. Boncukların yıkanmasından sonra, GST-Jab1/CSN5'a bağlanan proteinler, Western blot ile saptandı (Şekil 4.2.1.2). Bu deney sonucunda, artan miktarlardaki His-VCP'nin GST-Jab1/CSN5 ile çöktüğü gösterilerek, bu iki protein arasındaki direk etkileşim belirlendi.

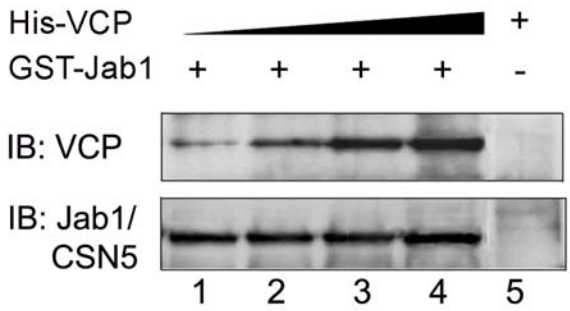

Şekil 4.2.1.2. Jab1/CSN5'ın VCP'ye in vitro bağlanması.
Rekombinant His-VCP'nin rekombinant GST-Jab1/CSN5'a bağlanması. Glutatyon boncuklarına bağlanmış olan GST-Jab1/CSN5, saflaştırılmış His-VCP'nin (sıra 1-4) artan miktarlarıyla inkübe edildiği gözlenmektedir. His-VCP'nin GST-Jab1/CSN5'a bağlanması anti-VCP antikoru ile saptandı (sıra 1-4, üst). Eşit miktarlarda, GST-Jab1/CSN5 (1 µg) (sıra 1-4, alt) kullanıldı. Kontrol olarak, sadece glutatyon boncukları, 2 µg of His-VCP (sıra 5) ile inkübe edildi. His-VCP: 0.25 µg (sıra 1); 0.5 µg (sıra 2); 1 µg (sıra 3); 2 µg (sıra 4 ve 5).

4.2.2. Jab1/CSN5 Ve VCP Arasındaki Bağlantı Domainlerinin Saptanması

Bundan önceki sonuçlar, Jab1/CSN5'ın VCP nin ND1 domainine bağlandığını gösterdi (bakınız 4.1.7, Şekil 4.1.7.2). Jab1/CSN5'nın hangi domaininin VCP ile etkileşdiğini bulmak amacıyla, FLAG-VCP, Myc-Jab1/CSN5 and Myc-Jab1/CSN5'nin delesyon mutantları (1–191, 1–110, 110–191), HEK293T hücrelerinde birlikte ekspre edildi. Şekil 4.2.2.1'da, Jab1/CSN5 ve onun delesyon mutantları şematik olarak gösterildi. Transfekte edilen hücrelerden elde edilen ekstraktlar, Flag-IP sine maruz bırakıldı (Şekil 4.2.2.1B). Anti-FLAG antikoru yardımıyla, FLAG-VCP, Myc-Jab1/CSN5 ile çöktürüldü, Jab1/CSN5 ve delesyon mutantları anti-Myc antikoru ile saptandı. Myc-Jab1/CSN5 ekspresyon vektörünün transfeksiyonu, immunoçöktürme (IP)'nin özgünlüğü için kontrol olarak kullanıldı. Deney sonuçları, wt-Jab1/CSN5'nın ve onun delesyon mutantlarından 1–110 ve 1–191'in FLAG-VCP'ye bağlandığını (Şekil 4.2.2.1B, sıra 7, 8, 9) fakat 110–191 mutantının (Şekil 4.2.2.1B, sıra 10) ise bağlanmadığını gösterdi. Bu sonuçlar, wt- Jab1/CSN5'nın ve MPN domainine sahip 1–191 delesyon mutantının VCP ile bağlandığını gösterdi.

Jab1/CSN5'nın 110-191 domainin VCP'ye bağlanmadığı saptandıktan sonra, bundan sonraki çalışmalar, VCP-Jab1/CSN5 bağlanmasının Jab1/CSN5'ın JAMM motifine bağlı olup olmadığını anlamak amacıyla yapıldı. Bu nedenle, Myc işaretli JAMM mutant Jab1/CSN5, HEK293T hücrelerinde, FLAG-VCP ile birlikte ekspre edildi ve transfekte edilen hücrelerden elde edilen ekstratlar, Myc ve FLAG-IP si için kullanıldı. Şekil 4.2.2.1C'de görüldüğü üzere, Myc-JAMM mutant Jab1/CSN5, FLAG-VCP ile birlikte çöktürüldü. Buna paralel olarak, FLAG-VCP, Myc- Jab1/CSN5 ile birlikte çöktürüldü (Şekil 4.2.2.1C, sıra 8). Hem FLAG hem de Myc çöktürme

sonuçları, Jab1/CSN5–VCP bağlanmasının JAMM motifinden bağımsız olduğunu gösterdi (Şekil 4.2.2.1C).

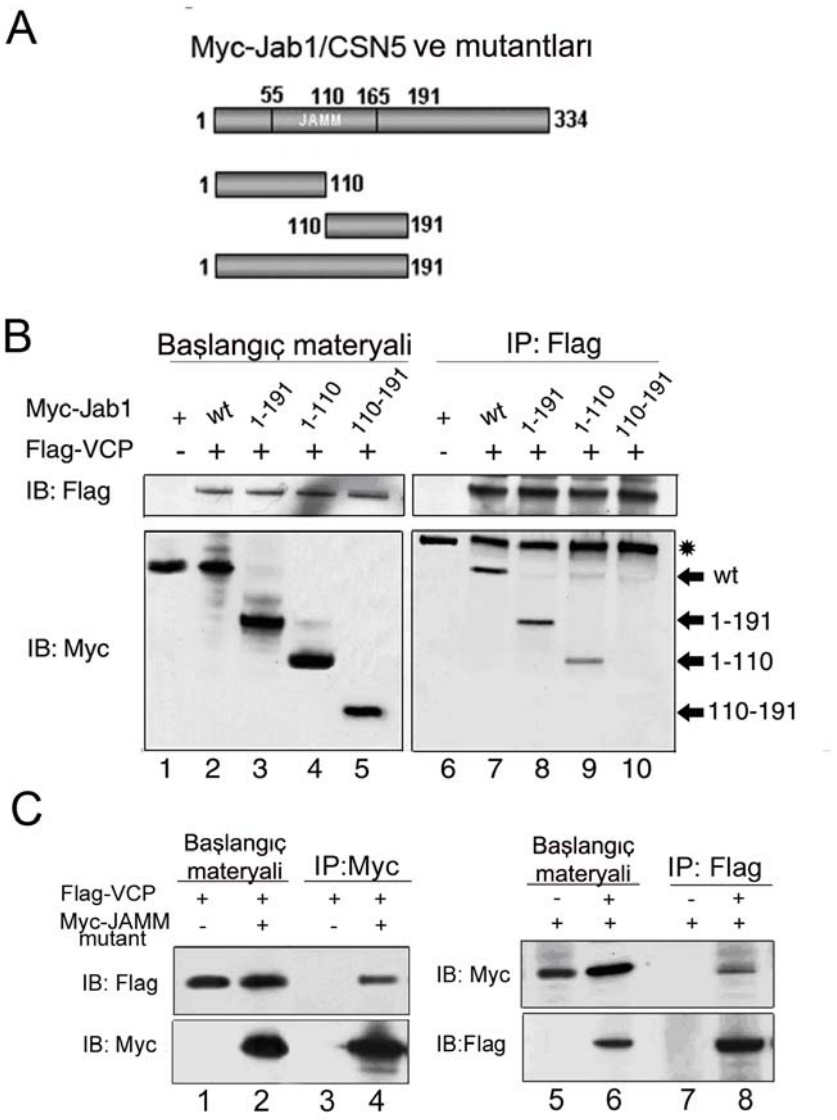

Şekil 4.2.2.1. Jab1/CSN5'nın VCP'e bağlandığı domainler

(A) Jab1/CSN5 ve onun delesyon mutantlarının şematik gösterimi. **(B)** FLAG-VCP'nin Jab1/CSN5'nın N-terminal domainine bağlanması. FLAG-VCP ve Myc-Jab1 (wt, 1-334), delesyon mutantları Myc–1–110, Myc–1–191, Myc–110–191 HEK293T hücrelerinde birlikte transfekte edildi. Anti-FLAG ve anti-Myc antikorları kullanılarak, Myc ve FLAG ekspresyonları hem hücre ekstratlarında (başlangıç materyeli, 1–5) hem de çöken materyallerde (6–10) saptandı. Yıldız, IgG'nin ağır zincirini göstermektedir. **(C)** JAMM mutant-Jab1/CSN5'nın VCP'ye bağlanması. FLAG-VCP ve Myc-Jab1/CSN5 mutant HEK293T hücrelerinde birlikte transfekte edildi. Başlangıç materyeli (sıra, 1, 2, 5 ve 6) ve çöken materyal (sıra, 3, 4, 7 ve 8) anti-Myc ve anti-FLAG antikorları kullanılarak, immunoblot ile saptandı.

4.2.3. Floresan Rezonans Enerji Transferi (FRET)

VCP ve Jab1/CSN5 proteinlerinin hücre içerisinde birbirine yakınlık derecelerini belirleyebilmek için konfokal mikroskobu altında Floresan Rezonans Enerji Transferi (FRET) tekniği uygulandı [137, 138]. İki protein NIH3T3 hücrelerinde birlikte ekspre edildi ve bu proteinler indirek çiftli-immunofloresan yöntemi ile saptandı. Overekspre edilen VCP ve Jab1/CSN5 proteinleri primer olarak sitoplâzmada gözlendi. FRET deneyinde, her iki proteinin birlikte ekspre edildiği bir bölge seçildikten sonra, o bölgedeki Cy3 işaretli verici floresan yoğunluğu, akseptör (alıcı) floresan sönmesi (bleaching) öncesi ve sonrasında hesaplanarak belirlendi. Akseptör (Jab1/CSN5) floroforun (Cy5) sönmesi, flurosan yoğunluğunun hemen hemen yok olmasını sağladı (Şekil 4.2.3, C ve D'deki ROI (ilgilenilen bölgeyi karşılaştırınız). Bu sırada, aynı bölgede Cy3 (donor) kanalında, flurosan yoğunluğunda bir artış görüldü (Şekil 4.2.3.1B). Her deney için, 18-20 hücre (n=76 deney grubu, n=85 kontrol grubu, 4 farklı deney) analiz edildi. Her deneyde pozitif FRET sinyalı saptandı. Cy3 fluroforundaki belirgin artış, Cy5 in fluroforunun söndüğü alanda 7,8 median değeri ile saptandı (Şekil 4.2.3.1E). Sekonder antikorun verdiği yalancı FRET sinyali ise, kontrol deneyleri kullanılarak belirlendi (median ΔIF = 2.75) (Şekil 4.2.3.1E).

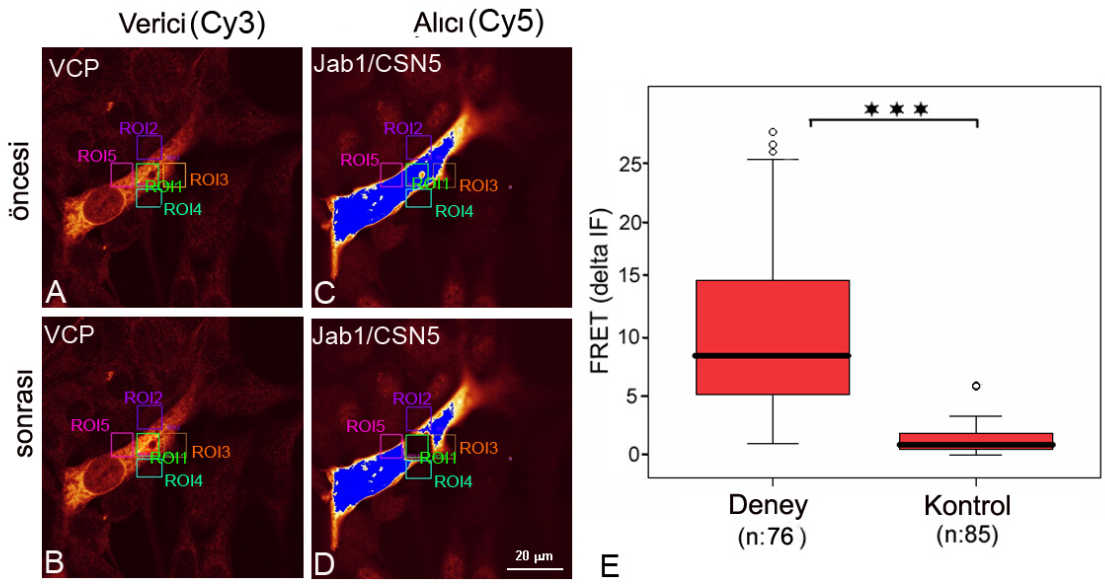

Şekil 4.2.3.1. VCP ve Jab1/CSN5 proteinlerinin birbirlerine olan hücresel yakınlık derecelerinin NIH 3T3 hücrelerinde, FRET analizi ile ölçümü. VCP (Cy3-konjuge sekonder antikor ile işaretlenmiş donor; **A and B**) ve Jab1/CSN5 (Cy5-konjuge sekonder antikor ile işaretlenmiş alıcı; **C+D**)'nın immunofloresan fotografı. Cy5 ilgili bölgede (ROI: Region of interest) söndürülmüş (**C** ve **D** deki ROI'leri karşılaştır). ROI 2-5: kontrol alanları **(E)** Deney grupları kontrol gruplarıyla karşılaştırılarak, ΔIF deki değişiklik belirlenmiştir. ***=p ≤ 0.001, Mann-Whitney test; n = deney sayısı (4 deney). O: verilerdeki ekstrem değerleri. Bar: 20µm

4.2.4. VCP'nin COP9 Signalozom (CSN) İle İlişkisi

Jab1/CSN5-içeren signalozom olarak da bilinen CSN kompleksi, CSN1'den CSN8'e kadar 8 subuniteden oluşmuştur [139]. Bu çalışmada bulunan Jab1/CSN5'nın VCP'ye bağlanması, CSN kompleksinin diğer subunitelerinin de VCP'ye bağlanıp bağlanamayacağı sorusunu akla getirdi. Bu soruya yanıt bulabilmek için CSN1 çöktürme deneyleri uygulanmıştır. CSN1 bazlı çöktürmelerin tüm CSN kompleksini çöktürebileceği önceki çalışmalarla gösterildi [140].
Bu çalışmada da, Anti-CSN1 antikoru ile tüm CSN kompleksinin çöktürülmesi, CSN'nin VCP'ye bağlandığını açığa çıkardı (Şekil 4.2.4.1). Çöktürmenin özgünlüğü, Jab1/CSN5'inde tüm CSN kompleksi ile birlikte çöktürülmesi ile doğrulandı (Şekil 4.2.4.1).

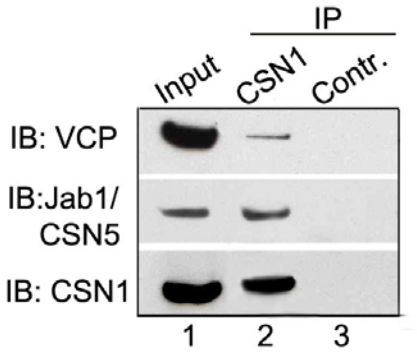

Şekil 4.2.4.1. VCP'nin CSN kompleksine bağlanması
HEK293T hücre ekstraktları VCP, Jab1/CSN5 ve CSN1 proteinlerinin ekspresyonları için immunoblot ile incelendi (IB, sıra 1). Sırasıyla, hücre ekstratları, anti-CSN1 antikoru (sıra 2) ve izotip kontrol antikoru (sıra 3) kullanılarak birlikte immunoçöktürme yapılarak sonuçlar doğrulndı. Immunoblot analizi ile çöktürülen proteinler, anti-VCP ve anti-Jab1/CSN5 antikoru ile saptandı, membran strip edilerek, anti-CSN1 antikoru ile yeniden muamele edildi.

4.3. Jab1/CSN5'ın VCP-poliübikütin Bağlanmasını Düzenlemesi

VCP'nin temel fonksiyonu, übikütinlenmiş proteinlere bağlanarak, onları ilişkide oldukları proteinlerden ayırmak ve bu übikütinlenmiş proteinlere yol göstererek onların protazoma yönlenmelerini sağlamaktır. Übikütinlenmiş proteinler VCP yardımıyla diğer proteinlerden ayrıldıktan sonra, birçok kofaktörün yardımıyla übikütin zincirlerinlerinden uzaklaştırılırlar (deübikütinlenme) [141].

Bu çalışmada, CSN kompleksiyle ilişkide olan Jab1/CSN5'ın ise deübikütinleme aktivitesine sahip olduğu [94] bilindiğinden, Jab1/CSN5'nın VCP'ye bağlı proteinlerin übikütinlenme durumlarını düzenleyip düzenlemeyeceği araştırıldı. Jab1/CSN5 ancak CSN kompleksi içindeyken kendi aktivitelerini gösterdiğinden, sadece Jab1/CSN5'in değil de tüm CSN'nin VCP-poliübikütin etkileşimini etkileyip etkileyemeyeceği RNA interferans ile belirlendi (Şekil 4.3.1). İlk olarak, CSN altbirimlerinden Jab1/CSN5 ve CSN1, HEK 293T hücrelerinde nakdavn (gen susturulması, gen ekspresyonunun azaltılması)

edilmiştir. Bu birimlerden birinin nakdavn edilmesi, CSN kompleksinin stabilizesinin bozulmasına neden oldu. Ayrıca VCP'ye bağlanmış poliübikütinlenmiş proteinler de Jab1/CSN5 and CSN1 nakdovn gruplarında kontrol gruplarıyla karşılaştırıldığında bir birikme görüldü (Şekil 4.3.1B, sıra 6, 7).

Bunlara ek olarak, Jab1/CSN5'nin JAMM motifinin übikütinlenmiş proteinlerin deübikütinlenmesini sağladığı bilindiğinden, Jab1/CSN5'nin JAMM motifi mutant (mCSN5) formu ve wt-Jab1/CSN5, HEK293T hücrelerine transfekte edildi ve VCP'ye bağlı übikütinlenmiş proteinler bu iki grup arasında karşılaştırıldı (Şekil 4.3.1A). Deney sonunda, JAMM motifi mutant (mCSN5) Jab1/CSN5 transfekte edilen grupda, wt Jab1/CSN5 ile transfekte edilen gruba göre VCP'ye bağlanmış übikütinlenmiş proteinlerde bir toplanma gözlendi (Şekil 4.3.1A). Bu deney sonuçları ile JAMM motifi mutant (mCSN5) Jab1/CSN5 ve CSN kompleksinin, VCP'ye bağlanmış übikütinlenmiş proteinlerin deübikütinlenmesinde görev yaptığı kanıtlandı.

CSN'e bağlı olan bir deübikütinlaz USP15'nin de aynı etkiyi gösterip göstermediğini belirlemek amacıyla, USP15, HEK 293T hücrelerinde nakdavn edildi. Aynı CSN1 ve Jab1/CSN5 nakdavn deneylerinde olduğu gibi, USP15 nakdavn edilmiş hücrelerde, VCP'ye bağlı poliübikütinlenmiş proteinlerde bir toplanma gözlendi (Şekil 4.3.1B, sıra 8). Bu nedenle, bu deney, USP15 aktivitesinin de, VCP'ye bağlanmış substratların VCP üzerinde toplanıp toplanmayacağının belirlenmesinde rol oynadığını gösterdi.

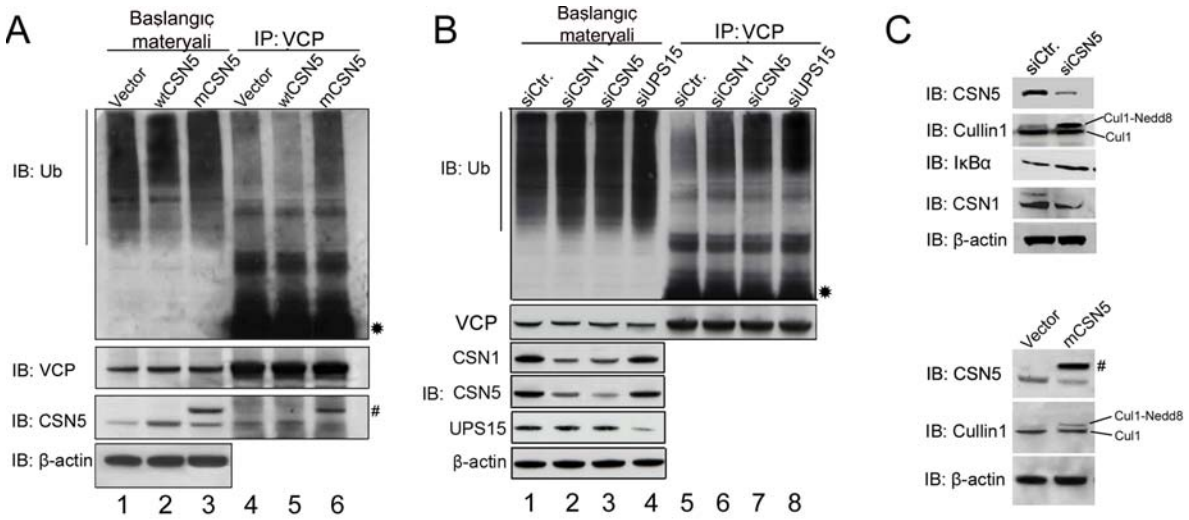

Şekil 4.3.1. CSN kompleksi ve USP15 deübikütinlazın VCP'ye bağlanmış olan poliübikütinlenmiş substratları kontrol etmesi **(A)** HEK293T hücreleri, vektör, Jab1/CSN5 (wtCSN5) ve JAMM mutant Jab1/CSN5 ile transfekte edilip, proteazom inhibitor MG132 ile muamele edildi. Transfekte hücre ekstraktlarından VCP immunoçöktürülerek, çöken proteinler, übikütin, VCP ve CSN5 için geliştirilmiş antikorlar ile saptandı. βeta-aktin, immunoblotda protein yükleme kontrolü olarak kullanıldı. **(B)** HEK293T hücreleri, kontrol, CSN1, CSN5

ve USP15 siRNA'leri ile transfekte edildi. 1 saat proteazom inhibitörü MG132 ile muamele edildikten sonra, hücre ekstraktları spesifik antikorlar ile incelendi. Aynı hücre ekstraktları, VCP immunoçöktürmesi için kullanıldı, VCP'ye bağlı übikütin zincirleri anti-übikütin antikoru ile saptandı. Yıldız: IgG nin ağır zincirini, #: Myc-işaretli CSN5 JAMM mutantını göstermektedir. **(C)** CSN5-nakdavn edilmiş hücreler, CSN5, cullin1, IκBα, CSN1 ve ßeta-aktin için immunoblot analizi ile incelendi (üst panel). Mutant CSN5 ile transfekte edilmiş hücre ekstratları, CSN5, cullin 1 ve ßeta-aktin (alt panel) antikorları ile muamele edildi.

Nakdavnların fonksiyonel olup olmadığı, Jab1/CSN5 nakdavn edilmiş gruplarda incelendi (Şekil 4.3.1C üst panel). Jab1/CSN5'in nakdavn edilen gruplarda, kontrol gruplarına göre nedile edilmiş cullin 1'de bir artış gözlenmiştir ki bu da Jab1/CSN5'in nakdavnu sonucu CSN1 ve ya CSN5'in yeterli düzeyde sentezlenmemesi nedeniyle, CSN fonksiyonunun da bozulduğunu ortaya koydu. Aynı etkiler, JAMM motifi mutant (mCSN5) Jab1/CSN5'in hücrelerde overekspre edildiğinde de gözlenmiştir ki bu da mutant proteinin, CSN'nin denedilaz aktivitesi üzerinde etkili olduğunu gösterdi. Bunlara ek olarak, IκBα'nın da, Jab1/CSN5 nakdavn edilmiş hücrelerde kontrol gruplarına göre bir artış gösterdiği belirlendi.

4.4. MIF, VCP ve Jab1/CSN5'nin Farklı RNAi Stratejeleri İle Nakdavnu

RNA interferans (RNAi), çift zincirli RNA (dsRNA)'nın komplement mRNA sının degradasyonunu hedef alarak genin susturulmasının indüklendiği bir mekanizmadır. Bu mekanizma, ilgili genin hücresel fonksiyonunda da 70-90%'lik bir düşüş sağlar.

Memeli olmayan sistemlerde, uzun çift zincirli RNA (dsRNA)'nın hücrede ekspresyonu RNAi yolağını başlatır. Sitoplazmik nükleaz olan Dicer isimli enzim, uzun dsRNA'leri 21-23bp lik küçük interfering RNA (siRNA)'lara ayırıp, bu siRNA'ların açılımını sağlarlar ve RNA indüklü susturucu kompleksler (RISC) üzerinde toplanırlar. Antisense siRNA zinciri, RISC kompleksinin komplementer RNA molekülü üzerine kaymasını sağlar ve RISC mRNA'yi parçalayarak spesifik gen susturulmasına neden olur. Birçok memeli hücresinde, 30bp den daha uzun dsRNA'lerin hücreye tanıtımı antiviral cevaba neden olduğu için, araştırmacılar, daha çok ya siRNA'leri hücreye transfekte ederek ya da Dicer'lar yardımıyla siRNA moleküllerine dönüştürülen kısa hairpin RNA (shRNA)'ları ekspre etmek için DNA-bazlı vektörler kullanarak RNAi'yi indüklemektedirler.

Bu çalışmada da, memeli hücrelerinde RNAi'yi indükleyebilmek için 2 yöntem kullanıldı: 1. siRNA'ler aracılı 2. shRNA ekspresyon vektörü ile MIF, Jab1/CSN5 ve VCP'nın nakdavnu.

4.4.1. MIF, VCP Ve Jab1/CSN5 Genlerinin shRNA pSUPER Vektörü Yardımıyla Susturulması

pSUPER RNAi sistemi, MIF, VCP ve Jab1/CSN5 genlerinin NIH 3T3, 264.7 RAW makrofajları ve HEKT293 hücrelerindeki nakdavnları için kullanıldı (Deneysel basamakların detayı için metod kısmına bakınız). MIF geninin makrofaj ve NIH3T3 hücrelerindeki nakdavnu Şekil 4.4.1.1'de gösterilmiştir.

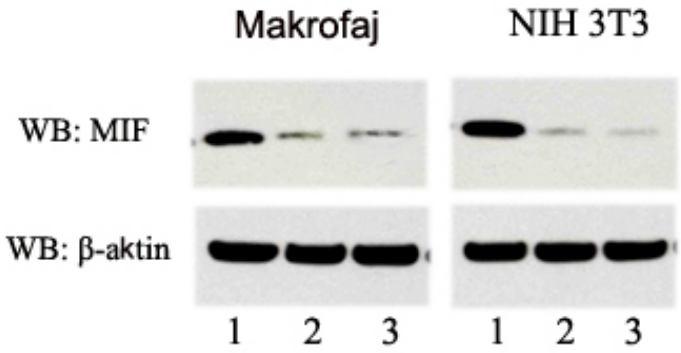

Şekil 4.4.1.1. MIF'in 264.7 RAW makrofaj ve NIH 3T3 hücrelerinde nakdavnu.
264.7 RAW makrofajları ve NIH 3T3 hücreleri ya pSUPER vektörü (sıra 1) ya da MIFsiRNA si (sıra 2 ve 3) ile transfekte edildi. Transfeksiyondan 48 saat sonra, sitoplazmik ekstraktlar Western blot ile analiz edildi. Blot önce MIF sonrada β-aktin antikoru ile inkübe edildi.

4.4.2. VCP ve Jab1/CSN5'nın siRNA'ler İle Nakdavn Edilmesi

Jab1/CSN5 ve VCP gen ekspresyonları, UPS proteinlerinin geri dönüşümlerini göstermek amacıyla özgün siRNA'ler kullanılarak azaltılmıştır. 72 saatlik transfeksiyon sonucu, HEK293T hücre ekstraktları immunoblot ile incelendi. Etkili nakdavnlar, Jab1/CSN5 ve VCP-siRNA'leri ile proteinlerin ekspresyonlarının büyük bir ölçüde baskılanması ile gösterildi. Kontrol siRNA'lerinde ise herhangi bir etki görülmedi (Şekil 4.4.2.1). Jab1/CSN5'ın nakdavn edilmesi, CSN1 ekspresyonunu da baskılamıştır ki, bu da CSN5 subunitesinin nakdavn edilmesinin total CSN üzerinde etkili olduğu görüşünü desteklemektedir [142]. Böylece, CSN subunitelerinden birinin kompleksden ayrılmasının tüm CSN kompleksini etkileyerek bu subunitelerin de ekspresyonlarında bir azalma göstereceğini birkez daha ortaya konuldu. Aynı zamanda CSN fonksiyonunun bozulması, UPS substratlarından Ικβα nın ekspresyon düzeyinde de bir değişiklik yarattı. Ικβα'nın protein miktarı Jab1/CSN5 nakdavn edilmiş hücrelerde bir artış gösterdi (Şekil 4.4.2.1).

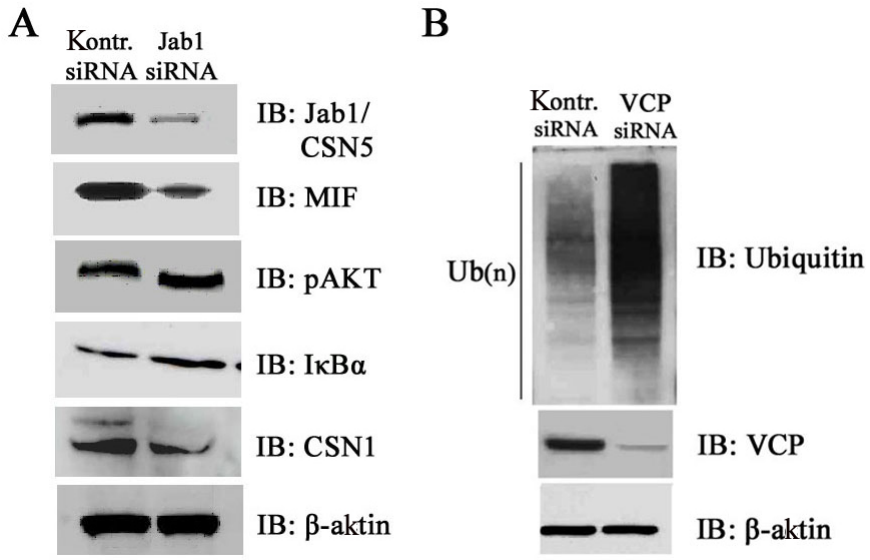

Şekil 4.4.2.1. Jab1/CSN5 and VCP'nin nakdavn edilmesinin etkileri.

(A) HEK293T hücreleri Jab1/CSN5 siRNA ve kontrol siRNA ile transfekte edildi. Transfeksiyondan 72 saat sonra, kontrol ve Jab1/CSN5 nakdovn hücre ekstratları immunoblot ile incelendi. Jab1/CSN5, CSN1, Iκβα, MIF ve pAKT (bakınız sağdaki proteinler) özgün antikorlar kullanılarak saptandı.

(B) HEK293T hücreleri, VCP siRNA ve kontrol siRNA ile transfekte edildi. VCP'nin nakdavnu hücre ekstratlarında immunoblot ile incelendi. Übikütin ve VCP, spesifik antikorlar ile saptandı. βeta-aktin eşit miktardaki protein yüklenmesini göstermektedir.

VCP nakdavnunun übikütinlenmiş proteinler üzerine etkisini görmek amacıyla, HEK293T hücreleri, VCP siRNA ve kontrol siRNA si ile transfekte edildi. VCP'nin nakdavn edilmesi, übikütinlenmiş proteinlerin hücrede toplanmasına neden olmuştur ki, bu da VCP'nin übikütinlenmiş proteinlere yol gösteren önemli bir şaperon olduğu gerçeğini bir kez daha doğruladı [131].

4.5. His-VCP ve GST-Jab1/CSN5'nin Ekspresyonu ve Saflaştırılması

4.5.1. His-VCP ve GST-Jab1/CSN5'nın Ekspresyonu

pET28a $^{(+)}$-VCP ve pGEX-4T$_1$-Jab1/CSN5 konstrakları, *E. coli* BL21 (DE3)'de His-VCP and GST- Jab1/CSN5'nın ekspresyonları için öncelikle bu bakteriyal hücrelere transforme edildi. Protein ekspresyonu için gerekli optimal şartları saptamak amacıyla, bakteriyel hücreler 37°C'de 0.5 mM IPTG ile indüklendi. 3 saatlik bir indükleme sonunda, füzyon proteinleri temel bakteriyel proteini olarak seçildi (Şekil 4.5.1.1A ve B; oklar).

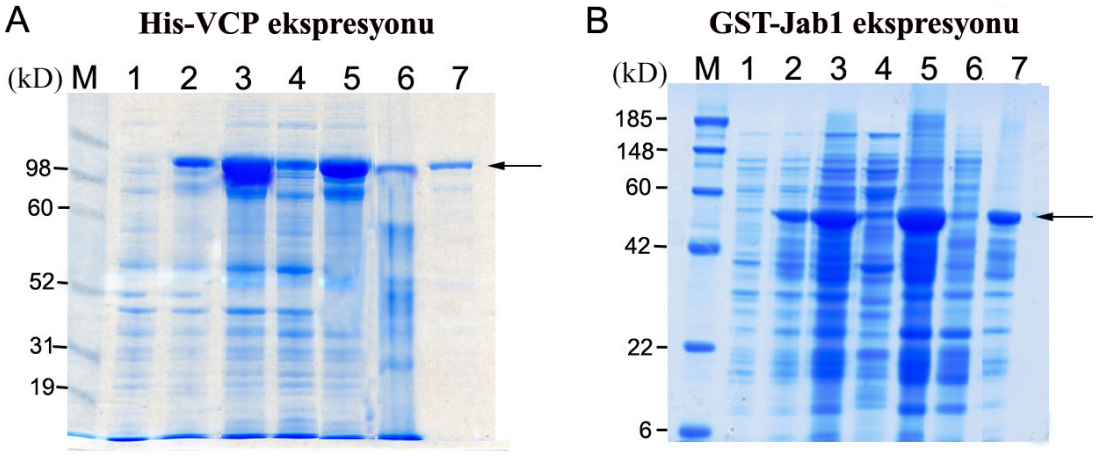

Şekil 4.5.1.1. E. coli'de His-işaretli VCP ve GST-işaretli Jab1/CSN5'nin ekspresyonu.
VCP ekspresyon plasmidini (A, sıra 1) ve Jab1/CSN5 expresyon plasmidini (B, sıra 1) taşıyan 500 ml *E. coli* BL21 (DE3) kültürü 0.5 mM IPTG ile 37°C de indüklendi. 3 saat indüksiyon sonrası (sıra 2) hücreler, 1 mg/ml lizozim ve DNAaz I (sıra 3) ile muamele edildiler. Lizis edilen hücre supernatanları (sıra 4) atıldı. Geriye kalan ve inklüzyon badileri içeren pellet (sıra 5) süspanse edilip, denatürasyon solusyonu ile inkübe edildi ve santrifüj edildiler. Temizlenmiş lizat (sıra 7), PBS'le diyaliz edildi. Diyaliz sonrası herbir fraksiyon, 12.5% SDS-PAGE de yürütülüp, Komasi mavisi ile boyandı. (M) = molekülar ağırlık markerı (kD).

4.5.2. His-VCP ve GST-Jab1/CSN5'nın Saflaştırılması (pürifikasyonu)

His-VCP proteini Nikel agaroz boncukları, GST–Jab1/CSN5 proteini ise glutatyon agaroz boncukları ile saflaştırıldı. Ayrıştırılan (eluye edilen) fraksiyonlar, SDS-PAGE'de yürütüldü (Şekil 4.5.2.1).

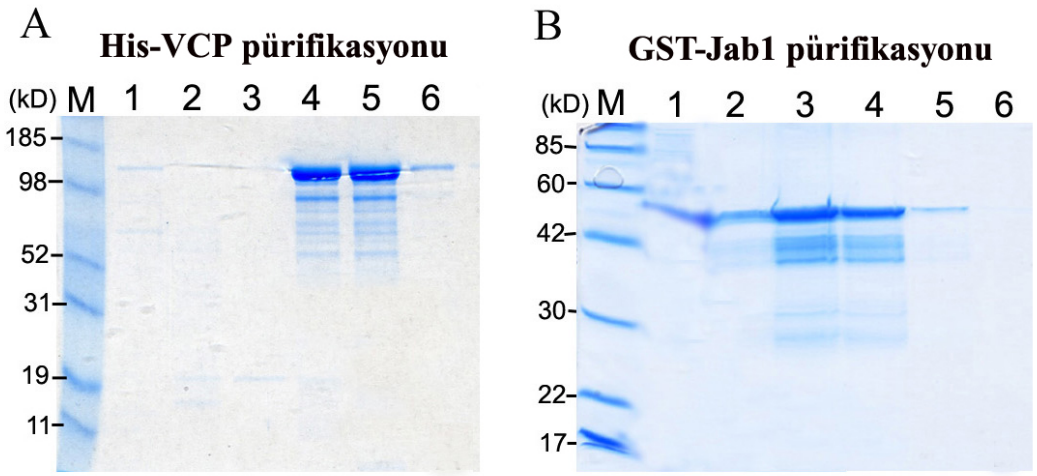

Şekil 4.5.2.1: His işaretli VCP ve GST işaretli Jab1/CSN5'nın saflaştırılması
Ayrıştırılan herbir fraksiyondan (sıra 1- 6) alınan örnekler, 12.5% SDS-PAGE'de yürütülüp, Komasi mavisi ile boyandı.

TARTIŞMA

Makrofaj göçünü engelleyici faktör (MIF), yaklaşık 40 yıl önce keşfedilen ilk immun mediatörlerden birisidir [1, 2]. Daha sonraki yıllarda, makrofajlar tarafından üretildiği [40] ve ön hipofiz hücreleri gibi endokrin ve parankimal hücreler tarafından da ekspre edildiği gösterilmiştir [5]. MIF'in, septik şok [143], romatoid artritis [144], inflamatuvar akciğer hastalıkları [50] ve kanser [145] gibi birçok immun ve inflamatuvar hastalıkta kritik bir molekül olarak görev yaptığı ortaya çıkarılmıştır. Bu nedenle, hem sitokin hem de kemokin olarak görev yapan bir düzenleyici olarak da tanımlanmıştır [146].

MIF ile ilgili proteinlerin keşfedilmesi amacıyla yapılan çalışmalarda, MIF'in tihol-özgün antioksidant bir protein olan çoğalma ile ilişkili gen (PAG: proliferation associated gen)'e bağlandığı bulunmuştur [71]. MIF ile PAG arasındaki bağlanma, PAG'in Cys173 ile MIF'in Cys residuleri arasında olmaktadır ve bu çalışmada MIF'in PAG'ın antioksidant aktivitesini engellediği ortaya çıkarılmıştır. MIF'in aynı zamanda, pankreatik adacıklarının β-hücrelerindeki sekresyon granüllerinde bulunan insülin ile birlikte yerleşim gösterdiği bulunmuştur [57]. PAG ve insüline ek olarak, hepatopetin (HPO), MIF'e direk bağlanarak MIF'in redoks düzenleyici fonksiyonunda görev almaktadır. [72]. MIF'in aynı zamanda, COP9 signalozom (CSN)'in bir parçası olan c-Jun aktiveli domaine bağlanan protein (c-jun activation domain binding protein-1) (JAB1)/CSN5'a bağlandığı bulunmuştur [28]. Bu çalışmada, MIF'in JAB1 aracılı AP-1 aktivasyonunu engellediği ve JAB1 aracılı p27 yıkımını kontrol ettiği gösterilmiştir. Doku uyumlu kompleks ilişkili zincir (Major histocompatibility complex (MHC) class II-associated invariant chain)'in hücre yüzey formu olan CD74'un hücre yüzeyinde MIF'e bağlandığı bulunmuştur [18]. CD74 sinyal iletici domaini olmaması nedeniyle MIF için tanımlanan bir reseptör kabul edilememiştir. Fakat CD74'ün MIF aracılı hücre çoğalması ve MAPK aktivasyonunda görev aldığı ortaya konulmuştur [18]. Bütün bunlara ek olarak, MIF'in apoptozla ilişkili protein, BNIPL'e de bağlandığı ve BNIPL'nin de hücre çoğalmasında görev yapıp, MIF aracılı tümor hücre çoğalmasını engellediği belirlenmiştir [147].

Bugüne kadar yukarıda da belirtildiği gibi MIF ile ilişkili birçok protein tanımlanmış olmasına rağmen, MIF ile ilgili hücre yolakları ve MIF'in bu yolaklardaki fonksiyonu tam olarak anlaşılamamıştır. Bu nedenle, bu çalışma MIF ile ilişkili proteinlerin tanımlanması ve bu proteinlerin hücre içi fonksiyonlarının belirlenmesi amaçlanmıştır.

MIF ile ilişkili yeni proteinlerin tanımlanması amacıyla, MIF'in hücrede sürekli ekspresyonunu sağlayacak *in vivo* biyotinleme yöntemi kullanıldı. Biyotinin avidine

olan yüksek afinitesi bilindiğinden, hedef proteini özgün olarak biyotinlemek amacıyla *in vivo* methodlar geliştirilmiştir [148-151]. Bu çalışmada MIF *in vivo* biyotinlenip, ilişkide olduğu MIF'e bağlanan proteinler streptavidin ile saflaştırıldı. Afinite temelli saflaştırma metodları arasında, biyotin-avidin sisteminin birçok avantajları vardır. Bu çalışmada gösterildiği üzere, biyotinlenmiş MIF hücre ekstratlarından tek bir basamakta direk olarak saflaştırıldı. Oysaki birbiri ardına yapılan afinite saflaştırma (tandem affinity purification tag, TAP) metodu gibi diğer *in vivo* modeller, birçok saflaştırma basamakları içermektedir [152]. Ayrıca, memeli hücresinde çok az sayıda biyotinlenmiş proteinlerin olması özgün olmayan bağlantıları engellemektedir. Avidinin biyotine olan çok yüksek afinitesi aynı zamanda, yıkama basamaklarında daha güçlü ajanların kullanılmasını sağladı. Biyotin ile diğer işaretleyiciler karşılaştırıldığında, biyotinin saflaştırmatırmada kullanılan en iyi işaretleyicilerden biri olduğu gösterilmiştir [153]. Biyotin kısmının alt bölümlerine TEV proteaz kesici alanının yerleştirilmesi, biyotinin uzaklaştırılmasını ve sadece MIF ve MIF ile ilişkili olan proteinlerin ayrılmasını sağladı.

Tüm bunların yanında, biyotin peptit işaretleyicisi MIF'in diğer proteinlerle ilişkiye girmesini engellememiştir ki bu da kullandığımız metodun başarısını ve uygulanabilirliğini göstermektedir. Çalışmamızda kullanılan biyotin ile işaretleme yönteminin yukarıda da belirtilen birçok üstün özelliğinden dolayı bu yöntem tercih edildi.

Bu zamana kadar hiçbir çalışmada, afinite kromatografisi ve kütle spektrometrisi ile birlikte *in vivo* biyotin ile işaretleme metodu MIF ile ilişkide olan proteinleri tanımlamak amacıyla kullanılmadı. Bu çalışmada ise çok sayıda MIF ile ilişkili yeni proteinler tanımlandı. Bunlardan bazıları MIF ile dolaylı olarak ve geçici bir şekilde etkileşmektedirler. Bu yöntemle tanımlanan proteinlerin çoğu, protein-protein bağlantısını bulmada kullanılan maya iki-hibrid (yeast two-hybrid), birlikte immunoçökeltme gibi başka yöntemlerle tanımlanmıştır. *İn vivo* biyotin ile işaretleme yöntemiyle aynı zamanda direk ve ya dolaylı yönden bulunan etkileşimlerin birçoğu saptanabildi. Daha öncesinde bilinen MIF'e bağlanan proteinlerin yanısıra (peroksiredoksin, RPS 19), übikütin protazom sistemine ait (VCP, clatrin, übikütin, protazom subunit α4, β5) ve endoplazmik retikulum ilişkili protein yıkımı (ERAD) kompleksine ait (BIP, ERp57, Sec61 ve T-kompleks protein 1) birçok protein tanımlandı.

UPS'de çalışan çok sayıda proteinlerin MIF'le bağlantıda olabileceğinin belirlenmesi ve kütle spektrometrisi sonucu UPS proteinlerinden VCP'nin yüksek peptid skoru vermesi nedeniyle, çalışmada MIF-VCP bağlantısı üzerinde duruldu. Son bir çalışma [79], MIF'in UPS aktivitesini Jab1/CSN5 aracılı kontrol ettiğini göstermiştir. Bu bulguyla uyumlu bir şekilde, bu çalışmada da MIF'in VCP ile etkileştiğinin bulunması, MIF'in gerçekten de UPS'de önemli rolleri olduğu gerçeğini bir kez daha vurguladı.

Bu çalışmada, MIF ile ilişkide olan bir başka protein ise glikolitik yolakta çalışan fosfogliserat kinaz-1 (Pgk-1) dir. Pgk-1, hipoksiya, tümor gelişimi ve yara iyileşmesinde oldukça çok ekspre edilen bir gen olarak bilinmektedir. Hipoksiya indükleyici transkripsiyon faktörü (HIF-1), hücreler düşük oksijen koşullarına maruz bırakıldığında glikolitik yolağın kontrolünde önemli bir rol oynar. Son çalışmada, HIF-1α'in Pgk-1'i ve glukoz taşıyıcı tip 1(GLUT1) protein ve hekzokinaz 1(HK1)'in düzenlenmesini arttırdığı gösterilmiştir [154]. İlginç olarak, MIF genininde promoter bölgesinde Hipoksiyadan sorumlu bölge (Hipoksiya Response Element, HRE)'in bulunduğu ve hipoksik koşullarda bu genin indüklendiği gösterilmiştir [155-158] Hipoksiyaya neden olan doku yaralanmasında da, monosit ve makrofajların direk devreye girdiği belirlenmiştir [159]. Herhangi bir inflamasyon durumunda, HIF-1α'nın MIF'i upregüle ettiği ve inflamasyon bölgesine inflamatuvar hücreleri çektiği düşünülmektedir. Dahası, MIF kanser hücrelerinde hipoksiya indükleyici bir gen olarak bilinmektedir [156, 160].

Bu bilgiler ışığında, Pgk-1 ve MIF'in hipoksiyada kritik roller oynadığının bulunması, bu çalışma da MIF ve Pgk-1 arasında fonksiyonel bir ilişki olduğunu destekledi.

MIF'in otokrin bir yolla, glukoz indüklü insülin salınımını kontrol ettiği bir başka araştırmada da gösterilmiştir [57] ki bu çalışmada MIF ve Pgk-1 arasındaki etkileşimin var olabileceğini desteklemektedir. MIF'in aynı zamanda glikolitik yolakda çalışan AMP-aktive edici protein kinazı stimüle ederek, iskemik kalpden salındığı da bulunmuştur [34].

MIF ve bu çalışmada yeni keşfedilen MIF'le ilişkili proteinler arasındaki bağlantı, birlikte immunçöktürme ve birlikte yerleşim çalışmaları ile bir kez daha doğrulandı. MIF ve VCP arasındaki bağlantı, NIH 3T3 hücre sitoplazmik ekstratlarında bulunduğu için, immunohistokimyasal analizler her iki proteininde sitoplâzmada yerleşim gösterdiğini ortaya çıkardı. Bu iki protein arasındaki yakın ilişki aynı zamanda floresan rezonans enerji transferi (FRET) ile incelendi. Fakat FRET sonuçları bu iki protein arasında direk bir ilişki olmadığını gösterdi. FRET'inde protein-protein bağlantısını saptamada bir takım dezavantajları vardır. Örneğin, verici ve alıcı florokromların uygun bir şekilde oryante olamaması da pozitif FRET sonucu vermeyebilir. Kısacası, negatif FRET sonucu iki proteinin birbirine bağlanmadığını göstermez.

Bu çalışmada, ektopik olarak ekprese edilmiş MIF ve VCP'nin delesyon mutantları arasındaki bağlantı da *in vivo* olarak incelendi. Fakat VCP'nin hiçbir domainin MIF'e bağlanmadığını ortaya çıkarıldı. Tüm bunlara ek olarak, saflaştırılan rekombinat VCP ve MIF proteinleriyle gerçekleştirilen *in vitro* çökertmede, MIF ve VCP'nin direk bağlanmadıklarını, ancak bağlanmanın bir kofaktör aracılı olabileceğini gösterdi. Kofaktör olarak ise, VCP ile aynı yolakta çalışması nedeniyle Jab1/CSN5 seçildi.

5.1. Jab1/CSN5'ın, VCP'ye Direk olarak *İn vivo* ve *İn vitro* Bağlanması

VCP'nin ardı ardına gelen iki ATPaz domainleri (D1 ve D2) ve de N-terminal domaini (N-domain) bulunmaktadır. VCP'nin kofaktörleri ve übikütinlenmiş proteinlerle nasıl etkileştiği, bilim dünyasında merak konusu olmuştur ve iki mekanizma olabileceği düşünülmektedir. VCP'nin direk olarak N-domaini [126] ile ve ya dolaylı yoldan kofaktörler aracılığıyla [127, 161-164] proteinlere bağlandığı gösterilmiştir. Burada belirtilen ikinci mekânizma yani VCP'nin kofaktörler aracılı diğer proteinlerle etkileştiği, daha kabul görmüş bir mekânizmadır. Bu çalışma da, öngörülen ikinci görüşü destekleyerek, MIF ve VCP arasındaki bağlanmada Jab1/CSN5'in aracı bir molekül olduğunu gösterdi.

VCP'ye bağlanan birçok substratın, VCP'nin übikütin bağlanma domainin S3/S4 kolunu kullandığını belirtmektedir [141]. Bu bağlamda, Jab1/CSN5, VCP'ye bağlanmak için, MPN domainini kullanan tek moleküldür.

VCP-Jab1/CSN5 arasındaki direk ilişki, herbiri için rekombinant proteinlerin saflaştırılmasından sonra incelenerek, bağlanmanın direk olduğu herhangi bir kofaktöre ihtiyaç duyulmadığını ortaya çıkardı. Yapılan birlikte yerleşim ve FRET analizleri sonucu, diğer çalışmalarla uyumlu bir şekilde, Jab1/CSN5'in çekirdek ve sitoplâzmada, VCP'nin ise sitoplâzmada yerleştiği gösterildi [165, 166].

5.2. VCP'nin CSN Kompleksine Bağlanması

Jab1/CSN5'in CSN kompleksine ait olması ve serbest olarak CSN kompleksi dışında fonksiyon gösterememesi nedeniyle, VCP'nin CSN kompleksine de bağlı olabileceği düşünüldü. CSN1 ise, CSN kompleksinin diğer tüm üyeleri ile çöktürüldü [140]. HEK 293T hücre ekstratlarından CSN1 çöktürülerek, VCP'nin tüm kompleksine bağlandığı bu çalışmada ispatlandı. Bu buluş, CSN'nin VCP ile birlikte bir kompleks oluşturabileceği ve bu kompleksinde protazomun regülatör parçasına benzer olduğu hipotezini doğurdu. Yapılan son çalışmada, VCP'nin substrat yönlendirici bir faktör olarak proteinlerin übikütinleme durumlarını belirlemede görev yaptığı gösterilmiştir [141].

Bu tez çalışmasında da, Jab1/CSN5'ın denedilaz aktivitesinin ve deübikütinlaz (DUB) USP15'nin VCP'ye bağlanan übikütinlenmiş proteinlerin kontrolünde görev aldığının bulunması, bir önceki çalışmayı destekleyici yöndedir. Ayrıca diğer deübikütinleyici enzimler de bu kontrolde görev alıyor olabilirler [93, 94].

VCP-Jab1/CSN arasındaki bağlanmanın keşfi, MIF interaktom (MIF ile ilişkili proteinlerin belirlenmesi) taramasından kaynaklanması nedeniyle, bu çalışmanın sonuçları, MIF'in Jab1/CSN5'a bağlanması ile proteinlerin übikütinlenme durumlarını kontrol ettiğini önermektedir.

5.3. Jab1/CSN5'in VCP-poliübikütin Bağlanmasını Kontrol Etmesi

VCP, übikütinlenmiş proteinlere bağlanıp onları protazoma yönlendirir. VCP'ye bağlanmış übikütinlenmiş proteinlerin kaderi VCP'ye bağlanmış faktörler tarafından belirlenir [141, 167]. Bu faktörler, übikütinlenmiş substratların ya poliübikütinlenip protazoma yönelmelerini ya oldukları halde kalmalarını ya da deübikütinlenmelerini (übikütinin uzaklaştırılması) sağlarlar. Bu bağlamda, bu çalışmada Jab1/CSN5-VCP arasındaki ilişkinin, VCP'ye bağlanmış proteinlerin deübikütinlenmesine neden olup olamayacağı araştırıldı. HEK293T hücreleri vahşi-Jab1/CSN5 ve JAMM mutant Jab1/CSN5 ile transfekte edilip, FLAG-VCP hücre ekstratlarından çökeltildi. VCP'ye bağlanmış poliübikütinlenmiş proteinlerin JAMM mutant transfekte hücrelerde arttığı, fakat vahşi tip Jab1/CSN5 transfekte hücrelerde ise poliübikütinlenmiş proteinlerde bir azalma gözlendi. Benzer bir şekilde, CSN1 ve Jab1/CSN5 hücrelerde siRNA ile nakdavn edildiğinde, CSN kompleksinin fonksiyonun bozulduğu ve VCP üzerinde poliübikütinlenmiş proteinlerin toplandığı gözlendi. Sonuç olarak, bu tezde Jab1/CSN5'in JAMM motifinin ve fonksiyonel CSN kompleksinin VCP'ye bağlı übikütinlenmiş proteinlerin deübikütinlenmeleri için gerekli oldukları ortaya çıkardı. CSN aynı zamanda bir deübikütinlaz olan USP15 ile de ilişkili olduğu için [94], bu çalışmada USP15 nakdovn hücrelerinde VCP'ye bağlı poliübikütinlenmiş proteinlerde de bir toplanma görüldü.

Bu nedenle, ilk defa bu çalışmada gösterildiği üzere, USP15 aktivitesinin de VCP'ye bağlı substratların kaderinin belirlenmesinde temel rol oynadığı vurgulandı.

Bu çalışmada kullanılan Jab1/CSN5 nakdavnların ve mutantların fonksiyonlarının belirlenmesi amacıyla HeLa hücreleriyle yapılan deneylerde, Jab1/CSN5 nakdavnlarında nedilenmiş Cullin1'in ekspresyonunda bir artış gözlendi. Aynı etki, JAMM motifi mutant olan Jab1/CSN5 içinde belirlendi. Fakat bu Cullin 1 proteinin nedilasyonu, Jab1/CSN5 nakdavn HEK293T hücrelerinde tam olarak gözlenmedi. Bu sonuçlar, daha önce yayınlanmış sonuçlarla uyumluluk gösterse de HeLa ve HEK293T hücrelerindeki denilasyon arasındaki farklılığın sebebi anlaşılamamıştır [69]. Bunlara ek olarak, Jab1/CSN5 nakdavn grubunda, IκBα proteininde kontrol grubuna göre bir artış görüldü. Bu artışın ise daha öncede belirtildiği üzere USP15'den kaynaklandığı düşünülmektedir [95].

Bunlara ek olarak, bu çalışmada, tek bir CSN subunitesinin nakdavn edilmesinin, tüm CSN kompleksi fonksiyonunu etkilediği gösterilmiştir ki bu sonuçlar diğer çalışmalarla desteklenmiştir [95, 168, 169]. Örneğin, Jab1/CSN5 nakdovnu CSN1 protein ekpresyonunda %50 bir düşüşe neden olmuştur ve bu CSN'nin denedilaz, deübikütinlaz aktivitesinin bozulmasına ve de poliübikütinlenmiş proteinlerin VCP'ye bağlı kalmasına neden oldu.

SONUÇLAR

Sonuç olarak, bu çalışma ile;

1- MIF'in übikütin protazom sistemi (UPS)'ne ait bir protein olan VCP'ye bir kofaktör görevi gören JAB1/CSN5 aracılı bağlandığı;

2- VCP ve JAB1/CSN5 arasındaki bağlanmanın kofaktöre ihtiyaç duymadan direk olduğu ve VCP'nin ND1 domainin, JAB1/CSN5'nin MPN domaini ile etkileştiği;

3- VCP'nin, JAB1/CSN5 sayesinde tüm CSN kompleksi ile ilişki içerisinde olduğu

4- CSN'nin ve CSN bağımlı USP 15'nin VCP'ye bağlanmış poliübikütinlenmiş proteinlerin deübikütinlenmesinde (VCP den ayrılmasında) görev gördüğü;

5- MIF'in JAB1/CSN5 fonksiyonunu engelleyerek VCP üzerinde poliübikütinlenmiş proteinlerin birikimini sağladığı ortaya konulmuştur.

Tüm bu sonuçlar ışığında, protein yıkımı ve übikütin protazom sisteminin birçok hücre yolağındaki önemi düşünüldüğünde, bu çalışmada keşfedilen MIF-JAB1/CSN5-VCP kompleksi arasındaki etkileşim bugüne kadar anlaşılmamış birçok mekanizmanın aydınlanmasını sağlamıştır.

KAYNAKLAR

1. Bloom BR, Bennett B. Mechanism of a reaction in vitro associated with delayed-type hypersensitivity. Science 1966; 153: 80-82.

2. David JR. Delayed hypersensitivity in vitro: its mediation by cell-free substances formed by lymphoid cell-antigen interaction. Proc Natl Acad Sci U S A 1966; 56: 72-77.

3. Weiser WY, Temple PA, Witek-Giannotti JS, Remold HG, Clark SC, David JR. Molecular cloning of a cDNA encoding a human macrophage migration inhibitory factor. Proc Natl Acad Sci U S A 1989; 86: 7522-7526.

4. Bernhagen J, Calandra T, Cerami A, Bucala R. Macrophage migration inhibitory factor is a neuroendocrine mediator of endotoxaemia. Trends Microbiol 1994; 2: 198-201.

5. Bernhagen J, Calandra T, Mitchell RA, Martin SB, Tracey KJ, Voelter W, Manogue KR, Cerami A, Bucala R. MIF is a pituitary-derived cytokine that potentiates lethal endotoxaemia. Nature 1993; 365: 756-759.

6. Esumi N, Budarf M, Ciccarelli L, Sellinger B, Kozak CA, Wistow G. Conserved gene structure and genomic linkage for D-dopachrome tautomerase (DDT) and MIF. Mamm Genome 1998; 9: 753-757.

7. Sugimoto H, Suzuki M, Nakagawa A, Tanaka I, Nishihira J. Crystal structure of macrophage migration inhibitory factor from human lymphocyte at 2.1 A resolution. FEBS Lett 1996; 389: 145-148.

8. Suzuki M, Sugimoto H, Nakagawa A, Tanaka I, Nishihira J, Sakai M. Crystal structure of the macrophage migration inhibitory factor from rat liver. Nat Struct Biol 1996; 3: 259-266.

9. Muhlhahn P, Bernhagen J, Czisch M, Georgescu J, Renner C, Ross A, Bucala R, Holak TA. NMR characterization of structure, backbone dynamics, and glutathione binding of the human macrophage migration inhibitory factor (MIF). Protein Sci 1996; 5: 2095-2103.

10. Sun HW, Bernhagen J, Bucala R, Lolis E. Crystal structure at 2.6-A resolution of human macrophage migration inhibitory factor. Proc Natl Acad Sci U S A 1996; 93: 5191-5196.

11. Rosengren E, Aman P, Thelin S, Hansson C, Ahlfors S, Bjork P, Jacobsson L, Rorsman H. The macrophage migration inhibitory factor MIF is a phenylpyruvate tautomerase. FEBS Lett 1997; 417: 85-88.

12. Bendrat K, Al-Abed Y, Callaway DJ, Peng T, Calandra T, Metz CN, Bucala R. Biochemical and mutational investigations of the enzymatic activity of macrophage migration inhibitory factor. Biochemistry 1997; 36: 15356-15362.

13. Swope M, Sun HW, Blake PR, Lolis E. Direct link between cytokine activity and a catalytic site for macrophage migration inhibitory factor. Embo J 1998; 17: 3534-3541.

14. Kleemann R, Kapurniotu A, Frank RW, Gessner A, Mischke R, Flieger O, Juttner S, Brunner H, Bernhagen J. Disulfide analysis reveals a role for macrophage migration inhibitory factor (MIF) as thiol-protein oxidoreductase. J Mol Biol 1998; 280: 85-102.

15. Kleemann R, Mischke R, Kapurniotu A, Brunner H, Bernhagen J. Specific reduction of insulin disulfides by macrophage migration inhibitory factor (MIF) with glutathione and dihydrolipoamide: potential role in cellular redox processes. FEBS Lett 1998; 430: 191-196.

16. Kleemann R, Kapurniotu A, Mischke R, Held J, Bernhagen J. Characterization of catalytic centre mutants of macrophage migration inhibitory factor (MIF) and comparison to Cys81Ser MIF. Eur J Biochem 1999; 261: 753-766.

17. Mitchell RA, Metz CN, Peng T, Bucala R. Sustained mitogen-activated protein kinase (MAPK) and cytoplasmic phospholipase A2 activation by macrophage migration inhibitory factor (MIF). Regulatory role in cell proliferation and glucocorticoid action. J Biol Chem 1999; 274: 18100-18106.

18. Leng L, Metz CN, Fang Y, Xu J, Donnelly S, Baugh J, Delohery T, Chen Y, Mitchell RA, Bucala R. MIF signal transduction initiated by binding to CD74. J Exp Med 2003; 197: 1467-1476.

19. Hudson JD, Shoaibi MA, Maestro R, Carnero A, Hannon GJ, Beach DH. A proinflammatory cytokine inhibits p53 tumor suppressor activity. J Exp Med 1999; 190: 1375-1382.

20. Mitchell RA, Liao H, Chesney J, Fingerle-Rowson G, Baugh J, David J, Bucala R. Macrophage migration inhibitory factor (MIF) sustains macrophage proinflammatory function by inhibiting p53: regulatory role in the innate immune response. Proc Natl Acad Sci U S A 2002; 99: 345-350.

21. Petrenko O, Fingerle-Rowson G, Peng T, Mitchell RA, Metz CN. Macrophage migration inhibitory factor deficiency is associated with altered cell growth and reduced susceptibility to Ras-mediated transformation. J Biol Chem 2003; 278: 11078-11085.

22. Medzhitov R, Preston-Hurlburt P, Janeway CA, Jr. A human homologue of the Drosophila Toll protein signals activation of adaptive immunity. Nature 1997; 388: 394-397.

23. Medzhitov R. Toll-like receptors and innate immunity. Nat Rev Immunol 2001; 1: 135-145.

24. Takeda K, Kaisho T, Akira S. Toll-like receptors. Annu Rev Immunol 2003; 21: 335-376.

25. Roger T, David J, Glauser MP, Calandra T. MIF regulates innate immune responses through modulation of Toll-like receptor 4. Nature 2001; 414: 920-924.

26. Roger T, Froidevaux C, Martin C, Calandra T. Macrophage migration inhibitory factor (MIF) regulates host responses to endotoxin through modulation of Toll-like receptor 4 (TLR4). J Endotoxin Res 2003; 9: 119-123.

27. Benigni F, Atsumi T, Calandra T, Metz C, Echtenacher B, Peng T, Bucala R. The proinflammatory mediator macrophage migration inhibitory factor induces glucose catabolism in muscle. J Clin Invest 2000; 106: 1291-1300.

28. Kleemann R, Hausser A, Geiger G, Mischke R, Burger-Kentischer A, Flieger O, Johannes FJ, Roger T, Calandra T, Kapurniotu A, Grell M, Finkelmeier D, Brunner H, Bernhagen J. Intracellular action of the cytokine MIF to modulate AP-1 activity and the cell cycle through Jab1. Nature 2000; 408: 211-216.

29. Shaulian E, Karin M. AP-1 as a regulator of cell life and death. Nat Cell Biol 2002; 4: E131-136.

30. Lue H, Thiele M, Franz J, Dahl E, Speckgens S, Leng L, Fingerle-Rowson G, Bucala R, Luscher B, Bernhagen J. Macrophage migration inhibitory factor (MIF) promotes cell survival by activation of the Akt pathway and role for CSN5/JAB1 in the control of autocrine MIF activity. Oncogene 2007; 26: 5046-5059.

31. Song G, Ouyang G, Bao S. The activation of Akt/PKB signaling pathway and cell survival. J Cell Mol Med 2005; 9: 59-71.

32. Wetzker R, Bohmer FD. Transactivation joins multiple tracks to the ERK/MAPK cascade. Nat Rev Mol Cell Biol 2003; 4: 651-657.

33. Bernhagen J, Krohn R, Lue H, Gregory JL, Zernecke A, Koenen RR, Dewor M, Georgiev I, Schober A, Leng L, Kooistra T, Fingerle-Rowson G, Ghezzi P, Kleemann R, McColl SR, Bucala R, Hickey MJ, Weber C. MIF is a noncognate ligand of CXC chemokine receptors in inflammatory and atherogenic cell recruitment. Nat Med 2007; 13: 587-596.

34. Miller EJ, Li J, Leng L, McDonald C, Atsumi T, Bucala R, Young LH. Macrophage migration inhibitory factor stimulates AMP-activated protein kinase in the ischaemic heart. Nature 2008; 451: 578-582.

35. Marsin AS, Bertrand L, Rider MH, Deprez J, Beauloye C, Vincent MF, Van den Berghe G, Carling D, Hue L. Phosphorylation and activation of heart PFK-2 by AMPK has a role in the stimulation of glycolysis during ischaemia. Curr Biol 2000; 10: 1247-1255.

36. Xing Y, Musi N, Fujii N, Zou L, Luptak I, Hirshman MF, Goodyear LJ, Tian R. Glucose metabolism and energy homeostasis in mouse hearts overexpressing dominant negative alpha2 subunit of AMP-activated protein kinase. J Biol Chem 2003; 278: 28372-28377.

37. Sukhodub A, Jovanovic S, Du Q, Budas G, Clelland AK, Shen M, Sakamoto K, Tian R, Jovanovic A. AMP-activated protein kinase mediates preconditioning in cardiomyocytes by regulating activity and trafficking of sarcolemmal ATP-sensitive K(+) channels. J Cell Physiol 2007; 210: 224-236.

38. Lue H, Kleemann R, Calandra T, Roger T, Bernhagen J. Macrophage migration inhibitory factor (MIF): mechanisms of action and role in disease. Microbes Infect 2002; 4: 449-460.

39. Baugh JA, Bucala R. Macrophage migration inhibitory factor. Crit Care Med 2002; 30: S27-S35.

40. Calandra T, Bernhagen J, Mitchell RA, Bucala R. The macrophage is an important and previously unrecognized source of macrophage migration inhibitory factor. J Exp Med 1994; 179: 1895-1902.

41. Bacher M, Meinhardt A, Lan HY, Mu W, Metz CN, Chesney JA, Calandra T, Gemsa D, Donnelly T, Atkins RC, Bucala R. Migration inhibitory factor expression in experimentally induced endotoxemia. Am J Pathol 1997; 150: 235-246.

42. Fingerle-Rowson G, Koch P, Bikoff R, Lin X, Metz CN, Dhabhar FS, Meinhardt A, Bucala R. Regulation of macrophage migration inhibitory factor expression by glucocorticoids in vivo. Am J Pathol 2003; 162: 47-56.

43. Lan HY, Mu W, Yang N, Meinhardt A, Nikolic-Paterson DJ, Ng YY, Bacher M, Atkins RC, Bucala R. De Novo renal expression of macrophage migration inhibitory factor during the development of rat crescentic glomerulonephritis. Am J Pathol 1996; 149: 1119-1127.

44. Nishino T, Bernhagen J, Shiiki H, Calandra T, Dohi K, Bucala R. Localization of macrophage migration inhibitory factor (MIF) to secretory granules within the corticotrophic and thyrotrophic cells of the pituitary gland. Mol Med 1995; 1: 781-788.

45. Calandra T, Bucala R. Macrophage migration inhibitory factor: a counter-regulator of glucocorticoid action and critical mediator of septic shock. J Inflamm 1995; 47: 39-51.

46. Calandra T, Spiegel LA, Metz CN, Bucala R. Macrophage migration inhibitory factor is a critical mediator of the activation of immune cells by exotoxins of Gram-positive bacteria. Proc Natl Acad Sci U S A 1998; 95: 11383-11388.

47. Bacher M, Metz CN, Calandra T, Mayer K, Chesney J, Lohoff M, Gemsa D, Donnelly T, Bucala R. An essential regulatory role for macrophage migration inhibitory factor in T-cell activation. Proc Natl Acad Sci U S A 1996; 93: 7849-7854.

48. Rossi AG, Haslett C, Hirani N, Greening AP, Rahman I, Metz CN, Bucala R, Donnelly SC. Human circulating eosinophils secrete macrophage migration inhibitory factor (MIF). Potential role in asthma. J Clin Invest 1998; 101: 2869-2874.

49. Nishihira J, Koyama Y, Mizue Y. Identification of macrophage migration inhibitory factor in human leukemia HL-60 cells and its induction by lipopolysaccharide. Biochem Mol Biol Int 1996; 40: 861-869.

50. Donnelly SC, Haslett C, Reid PT, Grant IS, Wallace WA, Metz CN, Bruce LJ, Bucala R. Regulatory role for macrophage migration inhibitory factor in acute respiratory distress syndrome. Nat Med 1997; 3: 320-323.

51. Imamura K, Nishihira J, Suzuki M, Yasuda K, Sasaki S, Kusunoki Y, Tochimaru H, Takekoshi Y. Identification and immunohistochemical localization of macrophage migration inhibitory factor in human kidney. Biochem Mol Biol Int 1996; 40: 1233-1242.

52. Lan HY, Yang N, Brown FG, Isbel NM, Nikolic-Paterson DJ, Mu W, Metz CN, Bacher M, Atkins RC, Bucala R. Macrophage migration inhibitory factor expression in human renal allograft rejection. Transplantation 1998; 66: 1465-1471.

53. Tesch GH, Nikolic-Paterson DJ, Metz CN, Mu W, Bacher M, Bucala R, Atkins RC, Lan HY. Rat mesangial cells express macrophage migration inhibitory factor in vitro and in vivo. J Am Soc Nephrol 1998; 9: 417-424.

54. Shimizu T, Ohkawara A, Mizue Y, Nishihira J. Alpha-thrombin stimulates expression of macrophage migration inhibitory factor in skin fibroblasts. Semin Thromb Hemost 1999; 25: 569-573.

55. Shimizu T, Abe R, Ohkawara A, Mizue Y, Nishihira J. Macrophage migration inhibitory factor is an essential immunoregulatory cytokine in atopic dermatitis. Biochem Biophys Res Commun 1997; 240: 173-178.

56. Meinhardt A, Bacher M, McFarlane JR, Metz CN, Seitz J, Hedger MP, de Kretser DM, Bucala R. Macrophage migration inhibitory factor production by Leydig cells: evidence for a role in the regulation of testicular function. Endocrinology 1996; 137: 5090-5095.

57. Waeber G, Calandra T, Roduit R, Haefliger JA, Bonny C, Thompson N, Thorens B, Temler E, Meinhardt A, Bacher M, Metz CN, Nicod P, Bucala R. Insulin secretion is regulated by the glucose-dependent production of islet beta cell macrophage migration inhibitory factor. Proc Natl Acad Sci U S A 1997; 94: 4782-4787.

58. Wistow GJ, Shaughnessy MP, Lee DC, Hodin J, Zelenka PS. A macrophage migration inhibitory factor is expressed in the differentiating cells of the eye lens. Proc Natl Acad Sci U S A 1993; 90: 1272-1275.

59. Matsuda A, Kotake S, Tagawa Y, Matsuda H, Nishihira J. Detection and immunolocalization of macrophage migration inhibitory factor in rat iris and ciliary epithelium. Immunol Lett 1996; 53: 1-5.

60. Bacher M, Meinhardt A, Lan HY, Dhabhar FS, Mu W, Metz CN, Chesney JA, Gemsa D, Donnelly T, Atkins RC, Bucala R. MIF expression in the rat brain: implications for neuronal function. Mol Med 1998; 4: 217-230.

61. Suzuki T, Ogata A, Tashiro K, Nagashima K, Tamura M, Yasui K, Nishihira J. A method for detection of a cytokine and its mRNA in the central nervous system of the developing rat. Brain Res Brain Res Protoc 1999; 4: 271-279.

62. Onodera S, Suzuki K, Matsuno T, Kaneda K, Kuriyama T, Nishihira J. Identification of macrophage migration inhibitory factor in murine neonatal calvariae and osteoblasts. Immunology 1996; 89: 430-435.

63. Hirokawa J, Sakaue S, Tagami S, Kawakami Y, Sakai M, Nishi S, Nishihira J. Identification of macrophage migration inhibitory factor in adipose tissue and its induction by tumor necrosis factor-alpha. Biochem Biophys Res Commun 1997; 235: 94-98.

64. Frenette G, Tremblay RR, Dube JY, Lazure C, Lemay M. High concentrations of the macrophage migration inhibitory factor in human seminal plasma and prostatic tissues. Arch Androl 1998; 41: 185-193.

65. Meyer-Siegler K, Fattor RA, Hudson PB. Expression of macrophage migration inhibitory factor in the human prostate. Diagn Mol Pathol 1998; 7: 44-50.

66. Nishihira J, Koyama Y, Mizue Y. Identification of macrophage migration inhibitory factor (MIF) in human vascular endothelial cells and its induction by lipopolysaccharide. Cytokine 1998; 10: 199-205.

67. Burger-Kentischer A, Finkelmeier D, Thiele M, Schmucker J, Geiger G, Tovar GE, Bernhagen J. Binding of JAB1/CSN5 to MIF is mediated by the MPN domain but is independent of the JAMM motif. FEBS Lett 2005; 579: 1693-1701.

68. Cope GA, Suh GS, Aravind L, Schwarz SE, Zipursky SL, Koonin EV, Deshaies RJ. Role of predicted metalloprotease motif of Jab1/Csn5 in cleavage of Nedd8 from Cul1. Science 2002; 298: 608-611.

69. Cope GA, Deshaies RJ. Targeted silencing of Jab1/Csn5 in human cells downregulates SCF activity through reduction of F-box protein levels. BMC Biochem 2006; 7: 1.

70. Cope GA, Deshaies RJ. COP9 signalosome: a multifunctional regulator of SCF and other cullin-based ubiquitin ligases. Cell 2003; 114: 663-671.

71. Jung H, Kim T, Chae HZ, Kim KT, Ha H. Regulation of macrophage migration inhibitory factor and thiol-specific antioxidant protein PAG by direct interaction. J Biol Chem 2001; 276: 15504-15510.

72. Li Y, Lu C, Xing G, Zhu Y, He F. Macrophage migration inhibitory factor directly interacts with hepatopoietin and regulates the proliferation of hepatoma cell. Exp Cell Res 2004; 300: 379-387.

73. Wadgaonkar R, Dudek SM, Zaiman AL, Linz-McGillem L, Verin AD, Nurmukhambetova S, Romer LH, Garcia JG. Intracellular interaction of myosin light chain kinase with macrophage migration inhibition factor (MIF) in endothelium. J Cell Biochem 2005; 95: 849-858.

74. Nemajerova A, Mena P, Fingerle-Rowson G, Moll UM, Petrenko O. Impaired DNA damage checkpoint response in MIF-deficient mice. Embo J 2007; 26: 987-997.

75. Cardozo T, Pagano M. The SCF übikütin ligase: insights into a molecular machine. Nat Rev Mol Cell Biol 2004; 5: 739-751.

76. Bornstein G, Ganoth D, Hershko A. Regulation of neddylation and deneddylation of cullin1 in SCFSkp2 ubiquitin ligase by F-box protein and substrate. Proc Natl Acad Sci U S A 2006; 103: 11515-11520.

77. Liu J, Furukawa M, Matsumoto T, Xiong Y. NEDD8 modification of CUL1 dissociates p120(CAND1), an inhibitor of CUL1-SKP1 binding and SCF ligases. Mol Cell 2002; 10: 1511-1518.

78. Petroski MD, Deshaies RJ. Function and regulation of cullin-RING übikütin ligases. Nat Rev Mol Cell Biol 2005; 6: 9-20.

79. Nemajerova A, Moll UM, Petrenko O, Fingerle-Rowson G. Macrophage migration inhibitory factor coordinates DNA damage response with the proteasomal control of the cell cycle. Cell Cycle 2007; 6: 1030-1034.

80. Wei N, Chamovitz DA, Deng XW. Arabidopsis COP9 is a component of a novel signaling complex mediating light control of development. Cell 1994; 78: 117-124.

81. Wei N, Deng XW. Making sense of the COP9 signalosome. A regulatory protein complex conserved from Arabidopsis to human. Trends Genet 1999; 15: 98-103.

82. Seeger M, Kraft R, Ferrell K, Bech-Otschir D, Dumdey R, Schade R, Gordon C, Naumann M, Dubiel W. A novel protein complex involved in signal transduction possessing similarities to 26S proteasome subunits. Faseb J 1998; 12: 469-478.

83. Aravind L, Ponting CP. Homologues of 26S proteasome subunits are regulators of transcription and translation. Protein Sci 1998; 7: 1250-1254.

84. Glickman MH, Rubin DM, Fried VA, Finley D. The regulatory particle of the Saccharomyces cerevisiae proteasome. Mol Cell Biol 1998; 18: 3149-3162.

85. Wei N, Tsuge T, Serino G, Dohmae N, Takio K, Matsui M, Deng XW. The COP9 complex is conserved between plants and mammals and is related to the 26S proteasome regulatory complex. Curr Biol 1998; 8: 919-922.

86. Verma R, Aravind L, Oania R, McDonald WH, Yates JR, 3rd, Koonin EV, Deshaies RJ. Role of Rpn11 metalloprotease in deubiquitination and degradation by the 26S proteasome. Science 2002; 298: 611-615.

87. Maytal-Kivity V, Reis N, Hofmann K, Glickman MH. MPN+, a putative catalytic motif found in a subset of MPN domain proteins from eukaryotes and prokaryotes, is critical for Rpn11 function. BMC Biochem 2002; 3: 28.

88. McCullough J, Clague MJ, Urbe S. AMSH is an endosome-associated ubiquitin isopeptidase. J Cell Biol 2004; 166: 487-492.

89. Bellare P, Kutach AK, Rines AK, Guthrie C, Sontheimer EJ. Ubiquitin binding by a variant Jab1/MPN domain in the essential pre-mRNA splicing factor Prp8p. Rna 2006; 12: 292-302.

90. Bech-Otschir D, Kraft R, Huang X, Henklein P, Kapelari B, Pollmann C, Dubiel W. COP9 signalosome-specific phosphorylation targets p53 to degradation by the ubiquitin system. Embo J 2001; 20: 1630-1639.

91. Henke W, Ferrell K, Bech-Otschir D, Seeger M, Schade R, Jungblut P, Naumann M, Dubiel W. Comparison of human COP9 signalsome and 26S proteasome lid'. Mol Biol Rep 1999; 26: 29-34.

92. Zhou C, Wee S, Rhee E, Naumann M, Dubiel W, Wolf DA. Fission yeast COP9/signalosome suppresses cullin activity through recruitment of the deubiquitylating enzyme Ubp12p. Mol Cell 2003; 11: 927-938.

93. Groisman R, Polanowska J, Kuraoka I, Sawada J, Saijo M, Drapkin R, Kisselev AF, Tanaka K, Nakatani Y. The ubiquitin ligase activity in the DDB2 and CSA complexes is differentially regulated by the COP9 signalosome in response to DNA damage. Cell 2003; 113: 357-367.

94. Hetfeld BK, Helfrich A, Kapelari B, Scheel H, Hofmann K, Guterman A, Glickman M, Schade R, Kloetzel PM, Dubiel W. The zinc finger of the CSN-associated deubiquitinating enzyme USP15 is essential to rescue the E3 ligase Rbx1. Curr Biol 2005; 15: 1217-1221.

95. Schweitzer K, Bozko PM, Dubiel W, Naumann M. CSN controls NF-kappaB by deubiquitinylation of IkappaBalpha. Embo J 2007; 26: 1532-1541.

96. Berse M, Bounpheng M, Huang X, Christy B, Pollmann C, Dubiel W. Ubiquitin-dependent degradation of Id1 and Id3 is mediated by the COP9 signalosome. J Mol Biol 2004; 343: 361-370.

97. Callige M, Kieffer I, Richard-Foy H. CSN5/Jab1 is involved in ligand-dependent degradation of estrogen receptor {alpha} by the proteasome. Mol Cell Biol 2005; 25: 4349-4358.

98. Kim BC, Lee HJ, Park SH, Lee SR, Karpova TS, McNally JG, Felici A, Lee DK, Kim SJ. Jab1/CSN5, a component of the COP9 signalosome, regulates transforming growth factor beta signaling by binding to Smad7 and promoting its degradation. Mol Cell Biol 2004; 24: 2251-2262.

99. Li S, Liu X, Ascoli M. p38JAB1 binds to the intracellular precursor of the lutropin/choriogonadotropin receptor and promotes its degradation. J Biol Chem 2000; 275: 13386-13393.

100. Wan M, Cao X, Wu Y, Bai S, Wu L, Shi X, Wang N. Jab1 antagonizes TGF-beta signaling by inducing Smad4 degradation. EMBO Rep 2002; 3: 171-176.

101. Yun J, Tomida A, Andoh T, Tsuruo T. Interaction between glucose-regulated destruction domain of DNA topoisomerase IIalpha and MPN domain of Jab1/CSN5. J Biol Chem 2004; 279: 31296-31303.

102. Wei N, Deng XW. The COP9 signalosome. Annu Rev Cell Dev Biol 2003; 19: 261-286.

103. Ye Y, Meyer HH, Rapoport TA. The AAA ATPase Cdc48/p97 and its partners transport proteins from the ER into the cytosol. Nature 2001; 414: 652-656.

104. Pickart CM. Ubiquitin enters the new millennium. Mol Cell 2001; 8: 499-504.

105. Pickart CM. Mechanisms underlying ubiquitination. Annu Rev Biochem 2001; 70: 503-533.

106. Schnell JD, Hicke L. Non-traditional functions of ubiquitin and ubiquitin-binding proteins. J Biol Chem 2003; 278: 35857-35860.

107. Meusser B, Hirsch C, Jarosch E, Sommer T. ERAD: the long road to destruction. Nat Cell Biol 2005; 7: 766-772.

108. Pickart CM, Cohen RE. Proteasomes and their kin: proteases in the machine age. Nat Rev Mol Cell Biol 2004; 5: 177-187.

109. Schwechheimer C, Deng XW. COP9 signalosome revisited: a novel mediator of protein degradation. Trends Cell Biol 2001; 11: 420-426.

110. Neuwald AF, Aravind L, Spouge JL, Koonin EV. AAA+: A class of chaperone-like ATPases associated with the assembly, operation, and disassembly of protein complexes. Genome Res 1999; 9: 27-43.

111. Maurizi MR, Li CC. AAA proteins: in search of a common molecular basis. International Meeting on Cellular Functions of AAA Proteins. EMBO Rep 2001; 2: 980-985.

112. Ogura T, Wilkinson AJ. AAA+ superfamily ATPases: common structure--diverse function. Genes Cells 2001; 6: 575-597.

113. Vale RD. AAA proteins. Lords of the ring. J Cell Biol 2000; 150: F13-19.

114. Zwickl P, Baumeister W. AAA-ATPases at the crossroads of protein life and death. Nat Cell Biol 1999; 1: E97-98.

115. Frohlich KU, Fries HW, Rudiger M, Erdmann R, Botstein D, Mecke D. Yeast cell cycle protein CDC48p shows full-length homology to the mammalian protein VCP and is a member of a protein family involved in secretion, peroxisome formation, and gene expression. J Cell Biol 1991; 114: 443-453.

116. Pamnani V, Tamura T, Lupas A, Peters J, Cejka Z, Ashraf W, Baumeister W. Cloning, sequencing and expression of VAT, a CDC48/p97 ATPase homologue from the archaeon Thermoplasma acidophilum. FEBS Lett 1997; 404: 263-268.

117. Wang Q, Song C, Yang X, Li CC. D1 ring is stable and nucleotide-independent, whereas D2 ring undergoes major conformational changes during the ATPase cycle of p97-VCP. J Biol Chem 2003; 278: 32784-32793.

118. Wang Q, Song C, Li CC. Molecular perspectives on p97-VCP: progress in understanding its structure and diverse biological functions. J Struct Biol 2004; 146: 44-57.

119. Cao K, Zheng Y. The Cdc48/p97-Ufd1-Npl4 complex: its potential role in coordinating cellular morphogenesis during the M-G1 transition. Cell Cycle 2004; 3: 422-424.

120. Kondo H, Rabouille C, Newman R, Levine TP, Pappin D, Freemont P, Warren G. p47 is a cofactor for p97-mediated membrane fusion. Nature 1997; 388: 75-78.

121. Cao K, Nakajima R, Meyer HH, Zheng Y. The AAA-ATPase Cdc48/p97 regulates spindle disassembly at the end of mitosis. Cell 2003; 115: 355-367.

122. Wojcik C, Yano M, DeMartino GN. RNA interference of valosin-containing protein (VCP/p97) reveals multiple cellular roles linked to ubiquitin/proteasome-dependent proteolysis. J Cell Sci 2004; 117: 281-292.

123. Jarosch E, Taxis C, Volkwein C, Bordallo J, Finley D, Wolf DH, Sommer T. Protein dislocation from the ER requires polyubiquitination and the AAA-ATPase Cdc48. Nat Cell Biol 2002; 4: 134-139.

124. Braun S, Matuschewski K, Rape M, Thoms S, Jentsch S. Role of the ubiquitin-selective CDC48(UFD1/NPL4)chaperone (segregase) in ERAD of OLE1 and other substrates. Embo J 2002; 21: 615-621.

125. Ghislain M, Dohmen RJ, Levy F, Varshavsky A. Cdc48p interacts with Ufd3p, a WD repeat protein required for ubiquitin-mediated proteolysis in Saccharomyces cerevisiae. Embo J 1996; 15: 4884-4899.

126. Dai RM, Li CC. Valosin-containing protein is a multi-ubiquitin chain-targeting factor required in ubiquitin-proteasome degradation. Nat Cell Biol 2001; 3: 740-744.

127. Rape M, Hoppe T, Gorr I, Kalocay M, Richly H, Jentsch S. Mobilization of processed, membrane-tethered SPT23 transcription factor by CDC48(UFD1/NPL4), a ubiquitin-selective chaperone. Cell 2001; 107: 667-677.

128. Hitchcock AL, Krebber H, Frietze S, Lin A, Latterich M, Silver PA. The conserved npl4 protein complex mediates proteasome-dependent membrane-bound transcription factor activation. Mol Biol Cell 2001; 12: 3226-3241.

129. Karin M, Ben-Neriah Y. Phosphorylation meets ubiquitination: the control of NF-[kappa]B activity. Annu Rev Immunol 2000; 18: 621-663.

130. Santoro MG, Rossi A, Amici C. NF-kappaB and virus infection: who controls whom. Embo J 2003; 22: 2552-2560.

131. Dai RM, Chen E, Longo DL, Gorbea CM, Li CC. Involvement of valosin-containing protein, an ATPase Co-purified with IkappaBalpha and 26 S proteasome, in ubiquitin-proteasome-mediated degradation of IkappaBalpha. J Biol Chem 1998; 273: 3562-3573.

132. Mitchell RA. Mechanisms and effectors of MIF-dependent promotion of tumourigenesis. Cell Signal 2004; 16: 13-19.

133. Laemmli UK. Cleavage of structural proteins during the assembly of the head of bacteriophage T4. Nature 1970; 227: 680-685.

134. Blum H, Beier H, Gross H. Improved silver staining of plant proteins, RNA and DNA in polyacrylamide gels. Electrophoresis 1987; 8: 93-99.

135. Shevchenko A, Wilm M, Vorm O, Mann M. Mass spectrometric sequencing of proteins silver-stained polyacrylamide gels. Anal Chem 1996; 68: 850-858.

136. Brummelkamp TR, Bernards R, Agami R. A system for stable expression of short interfering RNAs in mammalian cells. Science 2002; 296: 550-553.

137. Konig P, Krasteva G, Tag C, Konig IR, Arens C, Kummer W. FRET-CLSM and double-labeling indirect immunofluorescence to detect close association of proteins in tissue sections. Lab Invest 2006; 86: 853-864.

138. Truong K, Ikura M. The use of FRET imaging microscopy to detect protein-protein interactions and protein conformational changes in vivo. Curr Opin Struct Biol 2001; 11: 573-578.

139. Deng XW, Dubiel W, Wei N, Hofmann K, Mundt K, Colicelli J, Kato J, Naumann M, Segal D, Seeger M, Carr A, Glickman M, Chamovitz DA. Unified nomenclature for the COP9 signalosome and its subunits: an essential regulator of development. Trends Genet 2000; 16: 202-203.

140. Lyapina S, Cope G, Shevchenko A, Serino G, Tsuge T, Zhou C, Wolf DA, Wei N, Deshaies RJ. Promotion of NEDD-CUL1 conjugate cleavage by COP9 signalosome. Science 2001; 292: 1382-1385.

141. Jentsch S, Rumpf S. Cdc48 (p97): a "molecular gearbox" in the ubiquitin pathway? Trends Biochem Sci 2007; 32: 6-11.

142. Naumann M, Bech-Otschir D, Huang X, Ferrell K, Dubiel W. COP9 signalosome-directed c-Jun activation/stabilization is independent of JNK. J Biol Chem 1999; 274: 35297-35300.

143. Bozza M, Satoskar AR, Lin G, Lu B, Humbles AA, Gerard C, David JR. Targeted disruption of migration inhibitory factor gene reveals its critical role in sepsis. J Exp Med 1999; 189: 341-346.

144. Mikulowska A, Metz CN, Bucala R, Holmdahl R. Macrophage migration inhibitory factor is involved in the pathogenesis of collagen type II-induced arthritis in mice. J Immunol 1997; 158: 5514-5517.

145. Chesney J, Metz C, Bacher M, Peng T, Meinhardt A, Bucala R. An essential role for macrophage migration inhibitory factor (MIF) in angiogenesis and the growth of a murine lymphoma. Mol Med 1999; 5: 181-191.

146. Degryse B, de Virgilio M. The nuclear protein HMGB1, a new kind of chemokine? FEBS Lett 2003; 553: 11-17.

147. Shen L, Hu J, Lu H, Wu M, Qin W, Wan D, Li YY, Gu J. The apoptosis-associated protein BNIPL interacts with two cell proliferation-related proteins, MIF and GFER. FEBS Lett 2003; 540: 86-90.

148. Cronan JE, Jr. Biotination of proteins in vivo. A post-translational modification to label, purify, and study proteins. J Biol Chem 1990; 265: 10327-10333.

149. Beckett D, Kovaleva E, Schatz PJ. A minimal peptide substrate in biotin holoenzyme synthetase-catalyzed biotinylation. Protein Sci 1999; 8: 921-929.

150. de Boer E, Rodriguez P, Bonte E, Krijgsveld J, Katsantoni E, Heck A, Grosveld F, Strouboulis J. Efficient biotinylation and single-step purification of tagged transcription factors in mammalian cells and transgenic mice. Proc Natl Acad Sci U S A 2003; 100: 7480-7485.

151. Smith PA, Tripp BC, DiBlasio-Smith EA, Lu Z, LaVallie ER, McCoy JM. A plasmid expression system for quantitative in vivo biotinylation of thioredoxin fusion proteins in Escherichia coli. Nucleic Acids Res 1998; 26: 1414-1420.

152. Rigaut G, Shevchenko A, Rutz B, Wilm M, Mann M, Seraphin B. A generic protein purification method for protein complex characterization and proteome exploration. Nat Biotechnol 1999; 17: 1030-1032.

153. Tucker J, Grisshammer R. Purification of a rat neurotensin receptor expressed in Escherichia coli. Biochem J 1996; 317 (Pt 3): 891-899.

154. Amin MA, Haas CS, Zhu K, Mansfield PJ, Kim MJ, Lackowski NP, Koch AE. Migration inhibitory factor up-regulates vascular cell adhesion molecule-1 and intercellular adhesion molecule-1 via Src, PI3 kinase, and NFkappaB. Blood 2006; 107: 2252-2261.

155. Maity A, Koumenis C. HIF and MIF--a nifty way to delay senescence? Genes Dev 2006; 20: 3337-3341.

156. Koong AC, Denko NC, Hudson KM, Schindler C, Swiersz L, Koch C, Evans S, Ibrahim H, Le QT, Terris DJ, Giaccia AJ. Candidate genes for the hypoxic tumor phenotype. Cancer Res 2000; 60: 883-887.

157. Bacher M, Schrader J, Thompson N, Kuschela K, Gemsa D, Waeber G, Schlegel J. Up-regulation of macrophage migration inhibitory factor gene and protein expression in glial tumor cells during hypoxic and hypoglycemic stress indicates a critical role for angiogenesis in glioblastoma multiforme. Am J Pathol 2003; 162: 11-17.

158. Yao K, Shida S, Selvakumaran M, Zimmerman R, Simon E, Schick J, Haas NB, Balke M, Ross H, Johnson SW, O'Dwyer PJ. Macrophage migration inhibitory factor is a determinant of hypoxia-induced apoptosis in colon cancer cell lines. Clin Cancer Res 2005; 11: 7264-7272.

159. Karhausen J, Haase VH, Colgan SP. Inflammatory hypoxia: role of hypoxia-inducible factor. Cell Cycle 2005; 4: 256-258.

160. Baugh JA, Gantier M, Li L, Byrne A, Buckley A, Donnelly SC. Dual regulation of macrophage migration inhibitory factor (MIF) expression in hypoxia by CREB and HIF-1. Biochem Biophys Res Commun 2006; 347: 895-903.

161. Meyer HH, Wang Y, Warren G. Direct binding of ubiquitin conjugates by the mammalian p97 adaptor complexes, p47 and Ufd1-Npl4. Embo J 2002; 21: 5645-5652.

162. Richly H, Rape M, Braun S, Rumpf S, Hoege C, Jentsch S. A series of ubiquitin binding factors connects CDC48/p97 to substrate multiubiquitylation and proteasomal targeting. Cell 2005; 120: 73-84.

163. Schuberth C, Richly H, Rumpf S, Buchberger A. Shp1 and Ubx2 are adaptors of Cdc48 involved in ubiquitin-dependent protein degradation. EMBO Rep 2004; 5: 818-824.

164. Hartmann-Petersen R, Wallace M, Hofmann K, Koch G, Johnsen AH, Hendil KB, Gordon C. The Ubx2 and Ubx3 cofactors direct Cdc48 activity to proteolytic and nonproteolytic ubiquitin-dependent processes. Curr Biol 2004; 14: 824-828.

165. Oh W, Lee EW, Sung YH, Yang MR, Ghim J, Lee HW, Song J. Jab1 induces the cytoplasmic localization and degradation of p53 in coordination with Hdm2. J Biol Chem 2006; 281: 17457-17465.

166. Vandermoere F, El Yazidi-Belkoura I, Slomianny C, Demont Y, Bidaux G, Adriaenssens E, Lemoine J, Hondermarck H. The valosin-containing protein (VCP) is a target of Akt signaling required for cell survival. J Biol Chem 2006; 281: 14307-14313.

167. Rumpf S, Jentsch S. Functional division of substrate processing cofactors of the ubiquitin-selective Cdc48 chaperone. Mol Cell 2006; 21: 261-269.

168. Peth A, Berndt C, Henke W, Dubiel W. Downregulation of COP9 signalosome subunits differentially affects CSN complex and target protein stability. BMC Biochem 2007; 8: 27.

169. Peth A, Boettcher JP, Dubiel W. Ubiquitin-dependent proteolysis of the microtubule end-binding protein 1, EB1, is controlled by the COP9 signalosome: possible consequences for microtubule filament stability. J Mol Biol 2007; 368: 550-563.

ÖZGEÇMİŞ

Sevil Çaylı, 1977 yılında Ankara'da doğdu. İlköğrenimini 1988 yılında Ankara Gaziosmanpaşa ilkokulunda, Orta ve Lise öğrenimini 1995 yılında Mustafa Kemal Lisesinde, Lisans eğitimini, 1999 yılında Hacettepe Üniversitesi Fen Fakültesi Biyoloji Bölümünde tamamladı. 1999-2001 yılları arasında Akdeniz Universitesi Sağlık Bilimleri Enstitüsü Histoloji ve Embriyoloji Anabilim Dalında yüksek lisans eğitimini tamamladıktan sonra 2001-2002 yılları arasında Yale Üniversitesi Tıp Fakültesi Sperm Fizyolojisi Laboratuvarında misafir araştırmacı olarak çalıştı.

2003 yılında Akdeniz Üniversitesi Sağlık Bilimleri Enstitüsü Histoloji ve Embriyoloji Anabilim Dalında doktora eğitimine başladı. 2005-2008 yılları arasında Justus Liebig Üniversitesi Tıp Fakültesi Anatomi ve Hücre Biyolojisi bölümünde doktora tez projesine dayalı araştırmalarını tamamladı.

18 tane makale ve çoğu uluslararası kongrelerde olmak üzere 21 tane kongre bildirisi vardır.

Sevil Çaylı, 12 Haziran 2009 tarihinde Akdeniz Universitesi Sağlık Bilimleri Enstitüsü, Histoloji ve Embriyoloji Anabilim Dalında Doktora Tez Savunmasını yapacaktır.

EKLER

The COP9 signalosome interacts ATP-dependently with p97/VCP and controls the ubiquitination status of proteins bound to p97/VCP

Sevil CAYLI[1=], Jörg KLUG[1], Suada FRÖHLICH[1], Gabriela KRASTEVA[2], Lukas OREL[3] and Andreas MEINHARDT[1+]

[1]JLU Giessen, Department of Anatomy and Cell Biology, Unit of Reproductive Biology, Aulweg 123, 35385 Giessen, Germany

[2]JLU Giessen, Department of Anatomy and Cell Biology, Unit of Cardiopulmonary Neurobiology, Aulweg 123, 35385 Giessen, Germany

[3]Medical University of Vienna, Center for Biomolecular Medicine and Pharmacology, Schwarzspanierstraße 17, 1090 Vienna, Austria

[+] Corresponding author. Tel: +49-641-9947024; Fax: +49-641-9947029;

E-mail: andreas.meinhardt@anatomie.med.uni-giessen.de

[=] Future address:

Department of Histology and Embryology, Medical Faculty, Akdeniz University, Antalya, Turkey)

Running title: The CSN and p97/VCP form the CSN particle

THE JOURNAL OF BIOLOGICAL CHEMISTRY VOL. 284, NO. 12, pp. 7977–7985, March 20, 2009

Ribosomal Protein S19 Interacts with Macrophage Migration Inhibitory Factor and Attenuates Its Pro-inflammatory Function*

Received for publication, November 12, 2008, and in revised form, December 24, 2008 Published, JBC Papers in Press, January 20, 2009, DOI 10.1074/jbc.M808620200

Ana-Maria Filip[‡], Jörg Klug[‡], Sevil Cayli[‡], Suada Fröhlich[‡], Tamara Henke[‡], Philipp Lacher[‡], Regina Eickhoff[‡], Patrick Bulau[§], Monika Linder[¶], Christine Carlsson-Skwirut[‖], Lin Leng[**], Richard Bucala[**], Sandra Kraemer[‡‡], Jürgen Bernhagen[‡‡], and Andreas Meinhardt[‡1]

From the [‡]Department of Anatomy and Cell Biology, Unit of Reproductive Biology, [§]Medical Clinic II, and [¶]Department of Biochemistry, Justus-Liebig-University of Giessen, Giessen D-35385, Germany, [‖]Department of Woman and Child Health, Paediatric Endocrinology Unit, Astrid Lindgren Children's Hospital, Karolinska Institute and University Hospital, S-1716 Stockholm, Sweden, [**]Department of Internal Medicine, Yale University School of Medicine, New Haven, Connecticut 06520-8031, and [‡‡]Department of Biochemistry and Molecular Cell Biology, Institute of Biochemistry, University Hospital of the RWTH Aachen, 52074 Aachen Germany

Macrophage migration inhibitory factor (MIF) is a pleiotropic cytokine that has been implicated in the pathogenesis of inflammatory disorders such as infection, sepsis, and autoimmune disease. MIF exists preformed in cytoplasmic pools and exhibits an intrinsic tautomerase and oxidoreductase activity. MIF levels are elevated in the serum of animals and patients with infection or different inflammatory disorders. To elucidate how MIF actions are controlled, we searched for endogenous MIF-interacting proteins with the potential to interfere with key MIF functions. Using *in vivo* biotin-tagging and endogenous co-immunoprecipitation, the ribosomal protein S19 (RPS19) was identified as a novel MIF binding partner. Surface plasmon resonance and pulldown experiments with wild type and mutant MIF revealed a direct physical interaction of the two proteins (K_D = 1.3 × 10^{-6} M). As RPS19 is released in inflammatory lesions by apoptotic cells, we explored whether it affects MIF function and inhibits its binding to receptors CD74 and CXCR2. Low doses of RPS19 were found to strongly inhibit MIF-CD74 interaction. Furthermore, RPS19 significantly compromised CXCR2-dependent MIF-triggered adhesion of monocytes to endothelial cells under flow conditions. We, therefore, propose that RPS19 acts as an extracellular negative regulator of MIF.

A large body of evidence now shows that macrophage migration inhibitory factor (MIF)[2] activates a range of intracellular pathways and plays a key role in host immune and inflammatory responses (1, 2). Certain of the MIF inflammatory functions also have been proposed to be the result of the unusual enzymatic properties of the protein, namely tautomerase and oxidoreductase activities (3–6). Inhibition or deletion of MIF attenuates disease progression in experimental models such as atherosclerosis, arthritis, glomerulonephritis, sepsis, autoimmune encephalitis, and autoimmune diabetes (7–13). A pivotal step in the inflammatory response is the chemokine-governed adherence of monocytes to the endothelial lining which is then followed by their egress from the vasculature at the affected site. Earlier data from $MIF^{-/-}$ mice illustrate a role of MIF in leukocyte recruitment that was recently substantiated by the finding that MIF serves as a chemoattractant for monocytes and T cells by directly binding to the chemokine receptors CXCR2 and CXCR4 (14, 15). On the cell surface MIF also associates with CD74 (invariant chain of major histocompatibility complex class II) which colocalizes with CXCR2 (14, 16). Interaction with different surface molecules is thought to partly explain the wide impact of MIF on cellular pathways.

Despite its role as a key mediator in immune and inflammatory diseases, very little is known of how MIF action is regulated and terminated. Accordingly, we searched for endogenous molecules with the ability to control key steps of MIF signaling (*i.e.* receptor binding and/or receptor-associated functions). In this study, we identified ribosomal protein S19 (RPS19), a component of the small ribosomal subunit that is also released by apoptotic cells (17), as such a candidate.

EXPERIMENTAL PROCEDURES

Identification of MIF-interacting Partners by Coimmunoprecipitation—Mouse NIH 3T3 fibroblasts were grown in Dulbecco's modified Eagle's medium supplemented with 10% heat-inactivated fetal calf serum (PAA Laboratories, Cölbe, Germany) and antibiotics. Cells were lysed in Nonidet P-40 (1% IGEPAL CA-630) buffer containing protease inhibitors. Lysed cells were disrupted by passage through a 21-gauge needle and subjected to sonication by two 10-s bursts at 200–300 watts

* This work was supported by Deutsche Forschungsgemeinschaft Grants Me 1323/2-4 (to A. M.) and SFB 542/TP A7 (J. B.) and a research grant of the University Medical Centre Giessen and Marburg (to A. M.). The costs of publication of this article were defrayed in part by the payment of page charges. This article must therefore be hereby marked "*advertisement*" in accordance with 18 U.S.C. Section 1734 solely to indicate this fact.

[1] To whom correspondence should be addressed: Dept. of Anatomy and Cell Biology, Justus-Liebig-University of Giessen, Aulweg 123, D-35385 Giessen, Germany. Tel.: 49-641-9947024; Fax: 49-641-9947029; E-mail: andreas.meinhardt@anatomie.med.uni-giessen.de.

[2] The abbreviations used are: MIF, migration inhibitory factor; Bis-Tris, 2-[bis(2-hydroxyethyl)amino]-2-(hydroxymethyl)propane-1,3-diol; PBS, phosphate-buffered saline; HPLC, high performance liquid chromatography; RPS19, ribosomal protein S19; MALDI, matrix-assisted laser desorption/ionization; TOF, time of flight; wt, wild type; GST, glutathione *S*-transferase; HAoEC, human aortic endothelial cells; Ni-NTA, nickel-nitrilotriacetic acid; co-IP, co-immunoprecipitation.

separated by a 10-s cooling period. After centrifugation at 12,000 × *g* at 4 °C for 10 min, the supernatant was precleared with 30 μl of protein G-Sepharose 4B Fast Flow beads (GE Healthcare) on a rotating wheel at 4 °C for 1 h before incubation with either rabbit anti-rat MIF antibody or preimmune serum immobilized on 30 μl of protein G-Sepharose commenced at 4 °C for 2 h. After 5 washes with lysis buffer for 10 min each, beads were resuspended in Laemmli sample buffer and boiled for 10 min. Immunoprecipitates were separated on a NuPAGE 4–12% Novex Bis-Tris gel (Invitrogen) and stained with colloidal Coomassie staining solution (Sigma).

Identification of MIF-interacting Partners by in Vivo Biotinylation of Tagged MIF—The method of de Boer *et al.* (18) was employed using the modified tagging construct pN3-CTB developed by Rischitor (19). The rat MIF cDNA insert was produced by standard PCR using the upstream primer C**GAATTC**CGCCACCATGCCTATGTTCATCGTG (EcoRI site in bold) and the downstream primer GAT**GTCGAC**AGCGAAGGTGGAACCGTTCCA (SalI site in bold) and a pGEX-4T-2-MIF full-length expression construct (48) as template. pN3-CTB-MIF was constructed by cloning the EcoRI/SalI-restricted PCR fragment into pN3-CTB. For stable transfection, pBudCE4.1-birA (18) and pN3-CTB-MIF were linearized with XhoI and Eco 01091I, respectively, and transfected together or individually (pBudCE4.1-birA) into NIH 3T3 cells using Lipofectamine (Invitrogen). Antibiotic selection started with 800 μg/ml Geneticin (for pN3-CTB-MIF) and 600 μg/ml zeocin (for pBudCE4.1-birA) and was successively reduced in three steps down to 100 μg/ml Geneticin and 150 μg/ml zeocin after 4 weeks. After 5–8 weeks clones were isolated using small sterile filter discs soaked in trypsin solution. Clones were examined for expression of a biotinylated 22-kDa MIF fusion protein using immunoblots with rabbit anti-rat-MIF antiserum and streptavidin horseradish peroxidase conjugate (Dako, Hamburg, Germany).

One of the clones that strongly expressed the MIF fusion protein and one control clone expressing birA only were cultured in Dulbecco's modified Eagle's medium supplemented with 10% fetal calf serum, biotin (0.1 mg/liter), Geneticin (100 μg/ml), and zeocin (150 μg/ml) at 37 °C. Cells were lysed in 1% IGEPAL CA-630 (v/v), 150 mM NaCl, 50 mM Tris-HCl, pH 8, and proteinase inhibitors and applied to streptavidin-agarose beads (Novagen; 200 μl of bead slurry per mg of cell extract). After 1 h on a rocking platform, beads were washed 3 times with lysis buffer. Bound proteins were eluted by boiling for 10 min in SDS sample buffer, separated by SDS-PAGE on a 4–12% NuPAGE Bis-Tris gel (Invitrogen), and stained with colloidal Coomassie Blue (Sigma). Both lanes were cut into 12 gel slices, and proteins in all slices were digested with trypsin (20). Extracted peptides were separated and sequenced by liquid chromatography-coupled electrospray ionization-tandem mass spectroscopy on a quadrupole-time of flight (TOF) instrument (Q-TOF Ultima, Waters) under standard conditions. Proteins were identified by comparing peptide fragment spectra against all entries in the NCBI nr data base using MASCOT as search engine.

Identification of RPS19 by Matrix-assisted Laser Desorption/Ionization (MALDI)-Mass Spectroscopy Fingerprint Analysis and Peptide Matching—A 16-kDa band identified by co-immunoprecipitation was excised from the gel. The gel piece was washed once with water and twice with 50 mM ammonium hydrogen carbonate:acetonitrile (1:1) and acetonitrile, alternately. Gel pieces were re-swollen in a minimal volume of a 10 ng/μl trypsin solution (sequencing grade, Roche Diagnostics) in 25 mM ammonium hydrogen carbonate and incubated for 16 h at 37 °C. Peptides were extracted with 5 μl of 1% (v/v) trifluoroacetic acid containing 5 mM octylglycoside. 2 μl of the solution were applied to a thin layer of α-cyano-4-hydroxycinnamic acid on an AnchorChip target (Bruker Daltonik, Bremen, Germany). After 10 min the supernatant was removed, and the spot was washed twice with 2 μl of 0.1% (v/v) trifluoroacetic acid. Mass fingerprints of tryptic digests were obtained by MALDI-TOF mass spectrometry using an Ultraflex™ TOF/TOF mass spectrometer (Bruker Daltonik). The identified protein was verified by analyzing selected peptides in LIFT mode (tandem mass spectroscopy), and fragment masses were also submitted to MASCOT.

Expression and Purification of Wild Type and Mutant MIF Proteins—Recombinant rat MIF that differs from mouse MIF by only one amino acid (rat MIF, Ser-54; mouse MIF, Asn-54) was expressed and purified as previously described (21). Possible endotoxin contamination was removed using Detoxi-Gel (Pierce) which was also applied to the wild type human MIF preparation (see below). Human MIF and MIF mutant proteins were obtained from 1 liter of LB cultures of *Escherichia coli* BL21(DE3) transformed with constructs for wild type (wt) MIF and mutants P2A MIF (N-terminal amino acid alanine 2 exchanged for proline), Δ4 MIF (N-terminal four amino acids deleted), and C60S MIF (amino acid cysteine 60 replaced by serine) (22). Expression was induced with 0.5 mM isopropyl 1-thio-β-D-galactopyranoside for 3 h. Cells were harvested, and a lysate was prepared exactly as described (23). Cell lysates were sonicated on ice by five 10-s bursts using a microtip (Sonoplus, Bandelin, Berlin, Germany) and centrifuged at 17,000 × *g* at 4 °C for 30 min. wtMIF and P2A MIF and Δ4 MIF mutants were purified from the soluble fraction of the lysate, whereas the C60S MIF mutant was purified via an inclusion body preparation. The Δ4 MIF mutant was present in comparable portions in soluble and inclusion body fraction alike. Soluble proteins were precipitated with 70% ammonium sulfate (saturation), taken up in PBS, and chromatographed on a Sephacryl S100 HiPrep 16/60 gel filtration column (GE Healthcare) using an ÄKTAbasic UPC10 HPLC system (GE Healthcare). Positive fractions were pooled and passed over directly coupled 1-ml Resource S/Mono Q 5/50 columns (GE Healthcare). In PBS wtMIF, P2A MIF and Δ4 MIF proteins are in the flow-through with the majority of impurities binding to the column.

For the C60S MIF mutant the pellet of the initial lysate was resuspended in 25 ml of 50 mM Tris-HCl, pH 8.0, 10 mM EDTA, 100 mM NaCl, 0.5% (v/v) Triton X-100, and washed 4 times in the same buffer. The washed inclusion bodies were denatured in 6 M guanidine hydrochloride, 100 mM dithiothreitol in PBS. The solubilized protein was dialyzed against 5 mM dithiothreitol, 1 mM phenylmethylsulfonyl fluoride in PBS, cleared by cen-

trifugation, and passed over directly coupled Resource S/Mono Q columns as described above. All proteins had a purity of more than 98% as assessed by SDS-PAGE.

The identity of all purified proteins was confirmed by MALDI-TOF mass spectrometry as described above. Human wtMIF, P2A MIF, and C60S MIF had the N-terminal methionine removed due to a second cleavable residue as predicted (24), whereas the Δ4 MIF mutant had retained this methionine. Because of the internal mutation, the C60S mutant could not be confirmed.

Expression and Purification of GST-RPS19 and RPS19-His—Mouse RPS19 cDNA clone IRAKp961E1430Q was obtained from ImaGenes (Berlin, Germany). The RPS19 cDNA was amplified by PCR with Pfu polymerase (Promega) using forward primer 5′-CGAGGAATTCCCATGCCCGGAGTTACTG-3′ and reverse primer 5′-CGCCTCGAGTAATGCTTCTTGTTGGC-3′ for the glutathione *S*-transferase (GST) tag vector and forward primer 5′-CGCCATATGCCCGGAGTTACTGTAAAA-3′ and reverse primer 5′-GCGAAGCTTATGCTTCTTGTTGGCAGC-3′ for the His tag vector (introduced restriction sites are underlined). EcoRI- and XhoI-restricted PCR fragments were ligated into pGEX-4T-2 (GE Healthcare) yielding pGST-RPS19. Because of an internal NdeI site within the RPS19 cDNA, pET21a(+) (Merck) was restricted with NdeI, blunted, restricted with HindIII, and ligated to the HindIII-restricted PCR fragment. Both inserts plus flanking regions were validated by DNA sequencing (Seqlab, Göttingen, Germany). GST-RPS19 and RPS19-His were expressed in *E. coli* BL21(DE3) by induction with 0.5 mM isopropyl 1-thio-β-D-galactopyranoside at 37 °C for 3 h. For the GST-tagged RPS19 protein, cells were lysed in PBS by sonication and treated with 1% Triton X-100 for 30 min. After centrifugation at 12,000 × *g* for 15 min, the supernatant containing GST-RPS19 was subjected to glutathione-Sepharose 4B (GE Healthcare) chromatography. The purity of the eluted protein was higher than 95% as estimated by SDS-PAGE.

For the His-tagged protein, bacterial cells were lysed with lysozyme followed by sonication, and the native protein was purified from the lysate by standard Ni-NTA chromatography. Bound protein was eluted with 50 mM NaH_2PO_4, 300 mM NaCl, 250 mM imidazole, pH 8.0, and dialyzed against PBS, pH 7.8, containing 0.5 mM phenylmethylsulfonyl fluoride and 1 mM dithiothreitol.

Surface Plasmon Resonance—Biosensor analyses were performed on a BIACORE X system (GE Healthcare). Recombinant MIF dissolved in 0.01 M sodium acetate, pH 4.5, was covalently attached to a CM5 sensor chip (GE Healthcare) by the amine coupling method according to the manufacturer's instructions. Final levels of immobilization were ~5000 response units. 1000 response units correspond to 10 μg/μl on a CM5 chip. Analyses were performed at 25 °C using 0.01 M HEPES, pH 7.4, 0.15 M NaCl, and 0.005% surfactant P20 as a driving buffer at a flow rate of 20 μl/min. All experiments were carried out at 25 °C at a constant flow rate of 20 μl/min HBS-EP buffer. 40 μl of the analyte (RPS19) diluted in HBS-EP buffer (GE Healthcare) were injected over the immobilized MIF followed by a 2-min period when buffer was passed over the surface. Five concentrations of RPS19 were passed over the chip (62.5, 125, 250, 500, and 1000 nM).

Preparation of Antibodies against RPS19 and MIF and Double Immunofluorescence—Antibodies against His-tagged RPS19 or wild type rat MIF were raised in New Zealand White rabbits. In the case of anti-RPS19, serum samples were affinity-purified using His-tagged RPS19 immobilized on Ni-NTA-agarose (25). The purified RPS19 immunoglobulins were dialyzed against water for 1 h and against PBS overnight at 4 °C. A second chicken anti-RPS19 antibody was obtained from Lydie Da Costa (26). The MIF antibody is available through Invitrogen (#36-7401).

Cells were cultured on coverslips and fixed with ice-cold methanol for 10 min. Blocking for 1 h in 5% bovine serum albumin (w/v) and 5% (v/v) normal horse serum was followed by incubation with rabbit anti-mouse RPS19 (1:200) decorated with donkey anti-rabbit IgG conjugated with Cy3 (1:1000) and mouse anti-MIF (1:200, clone 3D9, available by NIH resource sharing) detected by donkey anti-mouse IgG conjugated with fluorescein isothiocyanate (1:1000). Primary antibodies were applied overnight at 4 °C, and both secondary antibodies were incubated for 1 h at room temperature. 4,6-Diamidino-2-phenylindole was used for nuclear staining. Images were acquired with a confocal laser scanning microscope (Leica TCS SP2).

Pulldown Assays—Biotinylation of rat MIF was performed using the ECL protein biotinylation module (GE Healthcare) according to the recommendations of the manufacturer. Nonreacted succinimide ester was separated from biotinylated MIF using Sephadex G-25 columns. Biotinylated MIF was eluted with PBS, pH 7.5, and 2.5 μg were immobilized on 30 μl (50% slurry) of monomeric avidin beads (Pierce) by incubation in 500 μl of PBS at room temperature on a rotating wheel for 30 min. To completely remove free biotinylated MIF, beads were washed with PBS and then incubated in 500 μl of lysis buffer (50 mM Tris-HCl, pH 8.0, 150 mM NaCl, 1% IGEPAL CA-630) with increasing amounts of GST-RPS19 (50, 100, and 200 ng) on a rotating wheel at 4 °C for 1 h. As a control, uncoated avidin beads were incubated with the same amounts of GST-RPS19 alone. Beads were then washed 5 times with lysis buffer and finally boiled in Laemmli sample buffer for 5 min. Protein complexes were separated by SDS-PAGE, transferred onto nitrocellulose membrane, and detected with anti-GST antibody conjugated with peroxidase.

Similarly, RPS19-His (2 μg) was immobilized on Ni-NTA-agarose beads, washed with PBS, and incubated for 1 h with different amounts of recombinant rat MIF or 2 μg of human wild type MIF or P2A MIF, C60S MIF, and Δ4 MIF proteins. As a control, MIF proteins alone were incubated with Ni-NTA-agarose beads. After extensive washing with lysis buffer as described previously or radioimmune precipitation assay buffer (150 mM NaCl, 1% IGEPAL CA-630, 0.5% sodium deoxycholate, 0.1% SDS, 50 mM Tris-HCl, pH 8.0, 1 mM phenylmethylsulfonyl fluoride) in the case of human MIF and MIF mutants, proteins bound to the beads were boiled in Laemmli sample buffer, resolved by SDS-PAGE, and stained with colloidal Coomassie (Sigma) or blotted and probed for RPS19, stripped, and reprobed for MIF.

L-Dopachrome Methyl Ester Tautomerase Assay—The substrate L-dopachrome methyl ester was freshly prepared before each measurement as described but without HPLC purification (27). Enzymatic activity was determined in an 800-μl assay reaction obtained by mixing 400 μl of PBS containing recombinant rat wtMIF at a concentration of 1 μM with 400 μl of crude L-dopachrome methyl ester substrate. In reactions that contained MIF and RPS19, both proteins were preincubated in 400 μl of PBS for 1 h before measurement. As control, SCGB 2A1-His (28), a protein of similar size and with the same tag, was used. Enzyme activity was measured by monitoring the reaction kinetics at 475 nm in an Ultrospec 2100 pro spectrophotometer (GE Healthcare). These conditions resulted in fast and non-linear kinetics leading to a quantitative turnover of the substrate over a time period of 1 min after reaction start. Therefore, the decrease in absorbance from 0 to 4 s, *i.e.* the initial reaction rate, was calculated and defined as tautomerase activity. Unpaired *t* tests were performed to compare the reaction rates +/− RPS19. Differences with a value of $p < 0.05$ were considered statistically different.

Flow Chamber Adhesion Assay—Human aortic endothelial cells (HAoEC; PromoCell, Heidelberg, Germany) were maintained in PromoCell medium and used at passages 3–5. MonoMac6 cells (a gift of Prof. H. W. L. Ziegler-Heitbrock, University of Leicester) were cultured in RPMI 1640 medium supplemented with 10% fetal calf serum, 2 mM L-glutamine, 1% nonessential amino acids, 1 mM sodium pyruvate, and 10 μg/ml human insulin as described (29). The laminar flow assays were performed as described previously (14). Briefly, HAoEC were grown to confluence in 35-mm dishes and preincubated with MIF (50 ng/ml) and RPS19-His (6 μg/ml) or control buffer for 2 h at 37 °C, 5% CO_2. The dishes were assembled at the bottom of a parallel wall flow chamber and mounted on the stage of an Olympus IX71 inverted microscope with 20× and 40× phase contrast objectives. MonoMac6 cells (1×10^6/ml) labeled with calcein-AM were pretreated with a blocking antibody against CXCR2 (R&D Systems, Minneapolis, MN) or matching isotype control IgG (3 μg/ml) and resuspended in assay buffer (1 × Hanks' balanced salt solution, 10 mM Hepes, pH 7.4, 0.5% bovine serum albumin). The cell suspension was supplemented at 37 °C with 1 mM Ca^{2+}/Mg^{2+} shortly before perfusing 5×10^5 cells/ml into the flow chamber at a shear rate of 1.5 dyn/cm^2 for 2 min. The number of adherent monocytes was analyzed in multiple high-power fields using the cell M software (Olympus, Tokyo, Japan). Data are expressed as the means ± S.E. Student's *t* tests (two-sided, unpaired) were performed to compare experimental groups. Differences with a value of $p < 0.05$ were considered statistically different.

MIF-RPS19 Capture Assay—The assay was performed as published (30). Briefly, 96-well plates were coated with 60 μl/well of 26 ng/μl purified soluble CD74 (amino acids 73–232) at 4 °C overnight. After washing 4 times with 250 μl/well Tris-buffered saline, the plates were incubated with 100 μl/well Superblock (Pierce) at 4 °C overnight. Various concentrations of RPS19 were preincubated with 2 ng/μl biotin-MIF (biotin labeling kit from Roche Applied Science) for 1 h at room temperature in the dark. The Superblock was removed and replaced with 120 μl/well of the RPS19 protein/biotin-MIF pre-

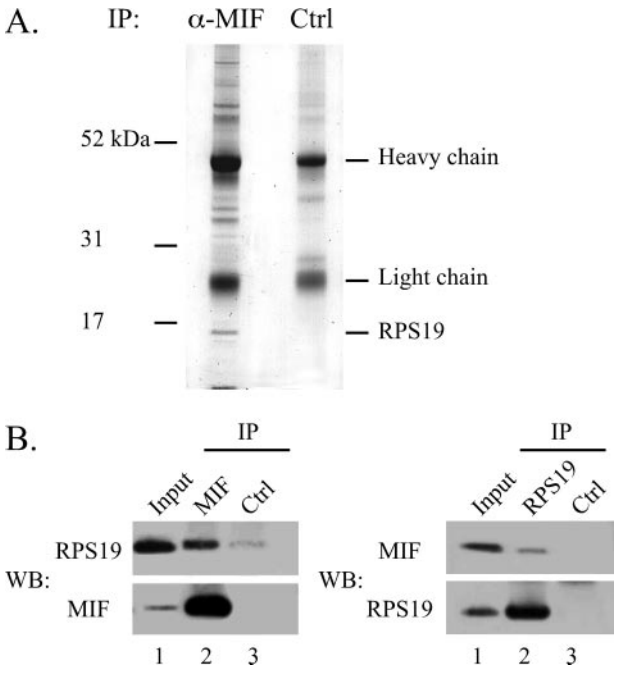

FIGURE 1. **Co-immunoprecipitation of MIF and RPS19.** *A*, extracts from mouse NIH 3T3 fibroblasts were incubated with a polyclonal rabbit anti-rat MIF antibody or with a rabbit IgG polyclonal isotype control antibody before immobilization on protein G-Sepharose beads. Co-immunoprecipitated proteins were separated on a NuPAGE 4–12% Novex Bis-Tris gel and stained with Coomassie. The MIF band is visible at the very *bottom* of the gel (*left lane*). The band at ~16 kDa was excised from the gel and analyzed by tryptic digestion and MALDI-TOF mass spectrometry. *B*, lysates from NIH 3T3 cells were immunoprecipitated (*IP*) with anti-rat MIF antibody (MIF, *left panel*) and anti RPS19 antibody (RPS19, *right panel*) in comparison to an isotype control antibody (*Ctrl*). Separated immunoprecipitates were immunoblotted (*WB*) and probed for RPS19 and, after stripping the membrane, for MIF (*left panel*) or vice versa (*right panel*).

incubated mixture, and incubation was continued in the dark at 4 °C for overnight. After washing the plate 4 times, 60 μl/well of streptavidin-alkaline phosphatase (R&D) was added for 1 h at room temperature in the dark followed by washing of the plate before adding 60 μl/well of PNPP (Sigma) and allowing color to develop in the dark at room temperature and reading at 405 nm. For control, human MIF was denatured by incubation at 100 °C for 5 min.

RESULTS

Identification of RPS19 as a MIF-interacting Protein—A far Western analysis was performed under reducing conditions to evaluate possible sources for the identification of MIF-interacting proteins. As each cell type (PC12, NIH 3T3) or tissue extract (rat and mouse testis) examined exhibited a similar pattern of reactive bands (data not shown), co-immunoprecipitation (co-IP) experiments were performed with endogenous lysates of NIH 3T3 fibroblasts. In co-IPs with a polyclonal MIF antibody a number of putative MIF-interacting proteins were co-precipitated. A prominent band at 16 kDa was readily identified in the anti-MIF precipitate but not in a reaction with an isotype control antibody (Fig. 1*A*). This 16-kDa protein was analyzed by tryptic in-gel digestion followed by MALDI-TOF mass spectrometry and identified as ribosomal protein S19 (RPS19). Confirmation of this finding was provided when the same IP samples were blotted and probed with an RPS19 antibody, stripped,

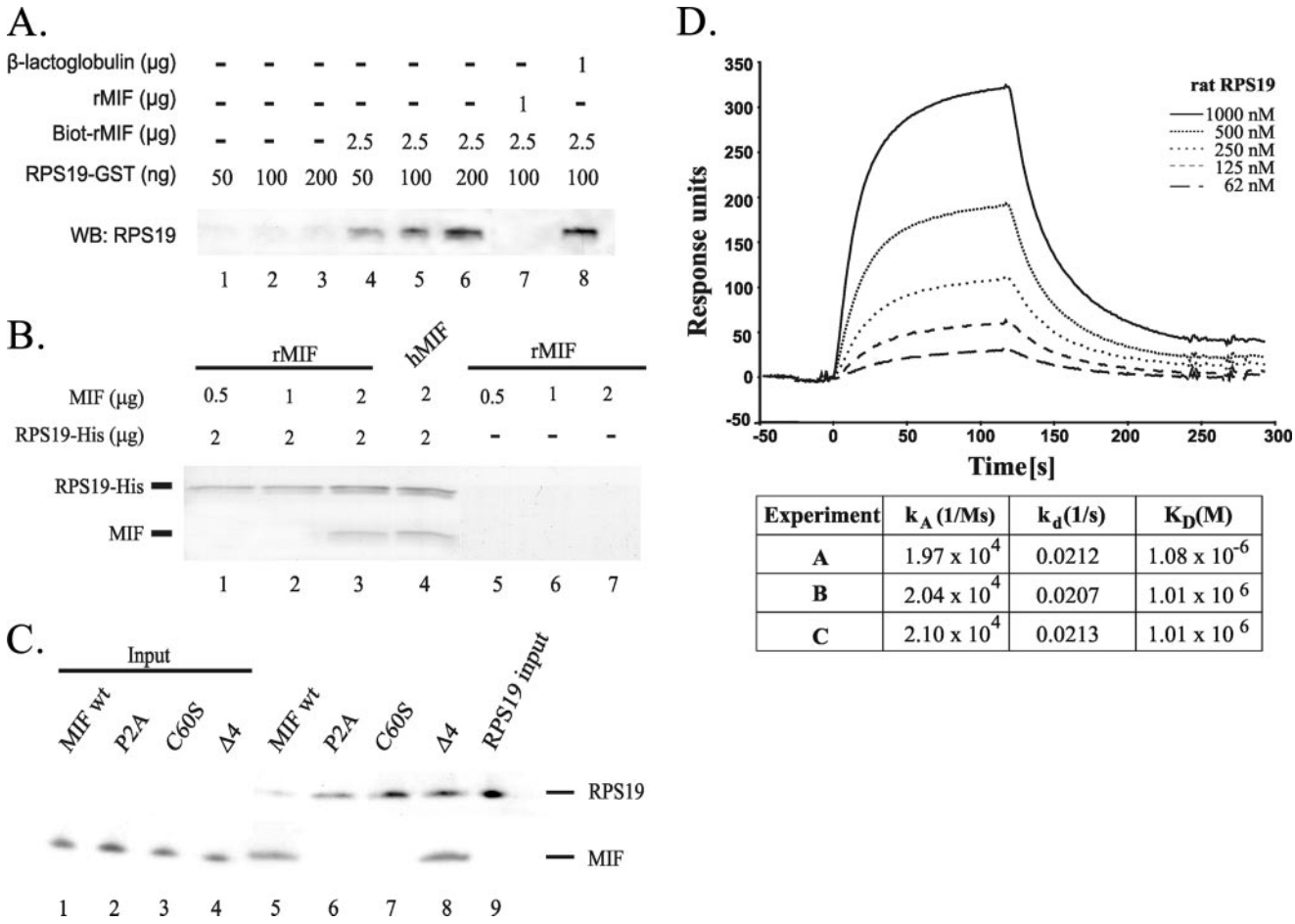

Experiment	k_A (1/Ms)	k_d(1/s)	K_D(M)
A	1.97×10^4	0.0212	1.08×10^{-6}
B	2.04×10^4	0.0207	1.01×10^{6}
C	2.10×10^4	0.0213	1.01×10^{6}

FIGURE 2. **Direct interaction between MIF and RPS19 *in vitro* using pulldown and surface plasmon resonance assays.** *A*, biotinylated rat MIF (*Biot-rMIF*) immobilized on avidin beads was incubated with increasing amounts of RPS19-GST (*lanes 4–6*). As control, unloaded avidin beads were incubated with the same amounts of RPS19-GST (*lanes 1–3*). Preincubation of RPS19 with a 10-fold molar excess of unlabeled soluble MIF prevented a pulldown (*lane 7*), which was not observed when β-lactoglobulin was used in the preincubation (*lane 8*). Detection of recovered RPS19-GST was performed using Western blot (*WB*) analysis with an anti-GST antibody. *B*, His-tagged RPS19 was immobilized on Ni-NTA-agarose beads and incubated with different amounts of recombinant rat MIF (*lane 1–3*) or with human MIF (*lane 4*). As control, recombinant rat MIF was incubated with naked Ni-NTA beads (*lane 5–7*). The immobilized proteins were resolved by SDS-PAGE and stained with Coomassie. *C*, equal amounts of His-tagged RPS19 were immobilized on Ni-NTA-agarose beads and incubated with 2 μg of recombinant human MIF or with human MIF mutants P2A MIF, C60S MIF, and Δ4 MIF (*lanes 5–8*), respectively. As control, all proteins were incubated with naked Ni-NTA matrix (data not shown). Immobilized proteins were resolved by SDS-PAGE, and MIF and RPS19 were detected by immunoblotting. *D*, interaction between RPS19 and recombinant MIF monitored in real time by biosensor analysis. Increasing concentrations of RPS19 (62–1000 nM) were passed over a sensor chip with immobilized MIF for 120 s (association phase) before the flow was switched to buffer alone for another 120 s (dissociation phase). Association and dissociation rate constants were derived using BIAevaluation 4.1 software and a 1:1 curve fitting model. The table provides association and dissociation rate constants (k_a and k_d) and the dissociation equilibrium constant (K_D) derived from three biosensor experiments.

and then re-probed with an antibody against MIF (Fig. 1*B*). Both proteins were detected in the anti-MIF co-IP sample, whereas the control-IP was negative.

Further verification was obtained when RPS19 could also be identified as a MIF-interacting protein in a different screen utilizing a tagged MIF fusion protein that was expressed in NIH 3T3 cells. The C-terminal tag was a peptide that is recognized and biotinylated *in vivo* by the bacterial birA biotin ligase that was stably co-expressed in the same NIH 3T3 clone (18). Biotinylated MIF and associated MIF-interacting proteins were purified in a single step by binding to streptavidin-agarose beads and separated by SDS-PAGE. A stable NIH 3T3 clone that expresses birA ligase only was used as control. Both SDS-PAGE lanes were cut into 12 slices, and proteins within each slice were identified by mass spectrometry. RPS19 was identified among the proteins that were purified from cells expressing biotinylated tagged MIF but not from cells expressing the biotin ligase only. The finding that two independent assays identify RPS19 as an MIF-interacting protein provides robust evidence for a *bona fide* interaction of both proteins.

MIF Directly Interacts with RPS19 in Vitro—Pulldown assays were performed to determine whether the interaction between MIF and RPS19 was direct or indirect (Fig. 2*A*). Biotinylated-MIF immobilized on monomeric avidin beads was incubated with increasing amounts of RPS19-GST (*lanes 4–6*). As a control, unloaded avidin beads were incubated with the same amount of RPS19-GST alone (*lanes 1–3*). Detection of recovered RPS19-GST by GST-immunoblotting confirmed that MIF directly interacted with RPS19, and accordingly, the more RPS19 was added, the more was bound to and recovered from the coated beads. The specificity of this interaction was determined by a competition experiment using rat MIF and β-lactoglobulin. RPS19 and a 10-fold molar excess of unlabeled MIF (*lane 7*) or lactoglobulin (*lane 8*) were preincubated together

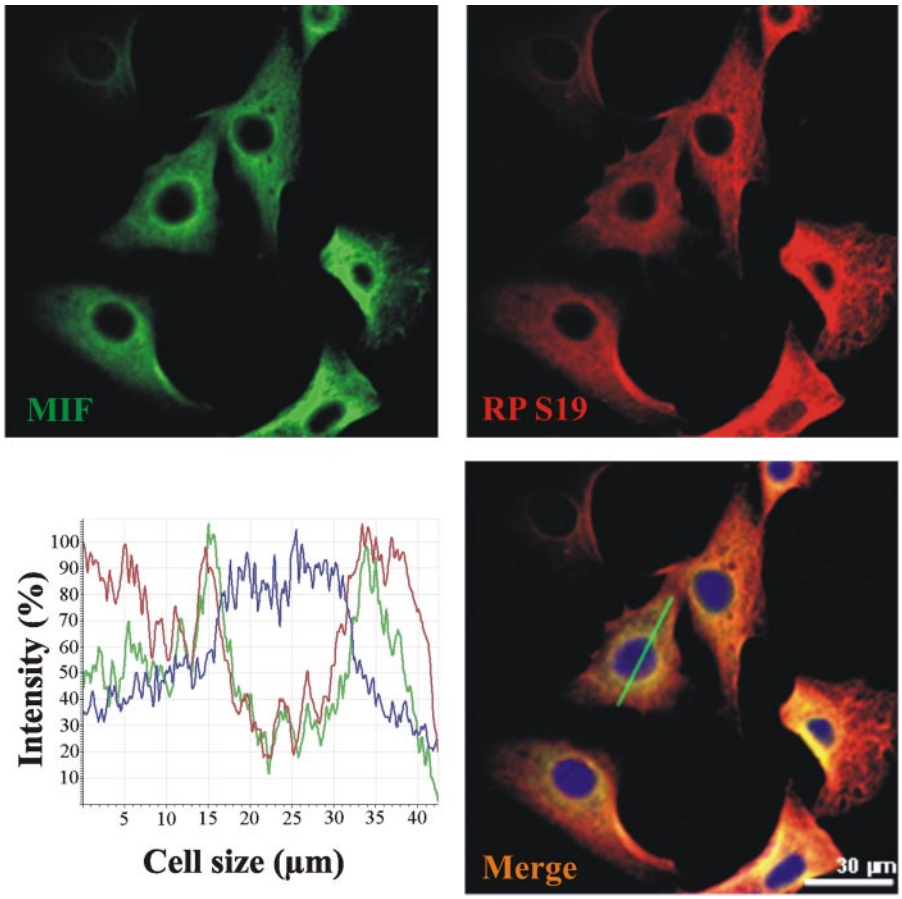

FIGURE 3. **MIF and RPS19 co-localize in NIH 3T3 cells.** Double-labeling immunofluorescence of MIF and RPS19 reveals co-localization in the cytoplasmic compartment of NIH 3T3 cells. Distribution of MIF is shown in *green* (*upper left picture*) and of RPS19 in *red* (*upper right picture*). The *yellow areas* in the merged image indicate colocalization of MIF and RPS19. Cell nuclei are stained *blue* with 4,6-diamidino-2-phenylindole. The graph illustrates the distribution of fluorescence intensities over a virtual cellular cross section (*green line* in the merged image). Colocalization is mostly prominent in the perinuclear region.

before the mixtures were added to avidin beads coated with biotinylated MIF. When RPS19 was preincubated with unlabeled MIF, no RPS19 could be pulled down anymore (*lane 7*), whereas the unspecific competitor lactoglobulin did not affect the interaction of RPS19 with immobilized biotinylated MIF (*lane 8*).

In an independent pulldown assay (Fig. 2*B*), His-tagged RPS19 was immobilized on Ni-NTA-agarose beads and incubated with either increasing amounts of rat MIF (0.5–2 μg) or 2 μg of human MIF. Protein complexes bound to the beads were separated by SDS-PAGE and stained with Coomassie. Rat MIF did not bind to the Ni-NTA matrix (*lanes 5–7*) but was retained on RPS19-coated beads (*lanes 1–3*). RPS19 also directly interacted with human MIF (*lane 4*), which is 95.7% homologous to the rat protein.

To further characterize the nature of the interaction, we also used three MIF mutants in the latter pulldown assay (P2A MIF, Δ4 MIF, and C60S MIF) (22). Whereas the Δ4 MIF mutant was pulled down like the wild type MIF, the P2A MIF and C60S MIF mutants were not bound to RPS19-coated beads (Fig. 2*C*).

Thermodynamic parameters of the formation of the MIF-RPS19 complex were quantified employing surface plasmon resonance. The kinetic data (Fig. 2*D*) were used to determine the association ($k_a = 2.04 \times 10^4 \pm 6.5 \times 10^2$ $(Ms)^{-1}$) and dissociation rate constants ($k_d = 0.021 \pm 3.2 \times 10^{-4}$ s^{-1}) and the dissociation constant $K_D = 1.3 \times 10^{-6} \pm 4 \times 10^{-8}$ M. In summary, interaction of MIF with RPS19 has been shown by four independent methods, namely endogenous co-IP, *in vivo* biotin tagging, pulldown experiments, and surface plasmon resonance.

MIF and RPS19 Co-localize in NIH 3T3 Cells—Two-color immunofluorescence confocal microscopy of NIH 3T3 cells showed that MIF co-localized with RPS19 (Fig. 3). Colocalization of both factors is most prominent in the perinuclear region with varying overlap in the more peripheral cytoplasm. Little (RPS19) or no staining (MIF) was evident in the nucleus. MIF and RPS19 fluorescence intensities monitored along virtual cellular cross-sections indicate overlapping signals (see a typical example in Fig. 3, merged image).

MIF Tautomerase Activity Is Only Moderately Affected by RPS19—Because the tautomerase activity of MIF may play a role in several of its functions as a cytokine (31), we investigated if RPS19 binding to MIF modulates its enzymatic activity. Tautomerization of L-dopachrome methyl ester to 5,6-dihydroxyindole-2-carboxylic acid by MIF was measured in the absence or presence of His-tagged RPS19 (Fig. 4). Increasing concentrations of RPS19 resulted in a dose-dependent but moderate decrease of MIF tautomerase activity, which was statistically significant only at a 3-fold molar excess of RPS19 over MIF but not at any other ratio used. When an excess of His-tagged secretoglobin 2A1 (32), a protein of similar size and without enzymatic activities, was used as control, MIF tautomerase activity was moderately increased, which was statistically significant also at a 3-fold molar excess over MIF but not at a 5-fold molar excess. Therefore, we conclude that overall both proteins have only a marginal effect on MIF tautomerase activity.

RPS19 Inhibits MIF Binding to Its Receptor CD74—To investigate if RPS19 can interfere with the binding of MIF to its receptor CD74, a sensitive capture competition assay system was used. Preincubation of RPS19 to biotin-MIF inhibited the interaction of biotin-MIF with CD74 by 55% at the highest dose. Interestingly, the lowest concentration of RPS19 applied reached already close to maximal inhibition rates (43%), which improved only marginally at higher doses (Fig. 5). As a control,

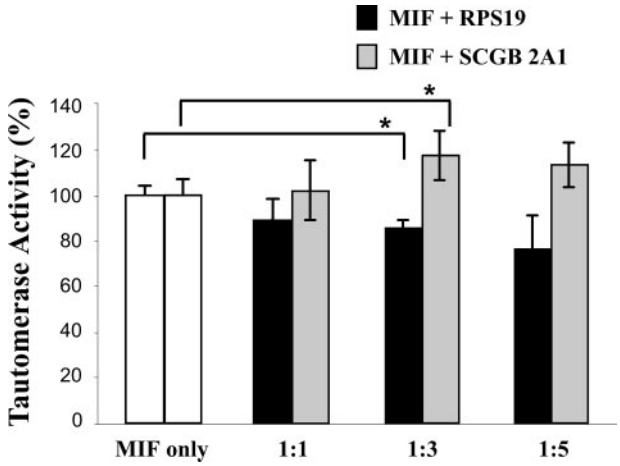

FIGURE 4. **PRS19 has only a moderate effect on the tautomerase activity of MIF.** MIF catalyzes tautomerization of L-dopachrome methyl ester to 5,6-dihydroxyindole-2-carboxylic acid. Reaction kinetics were spectrophotometrically recorded at 475 nm over 1 min. The reaction rate within the initial 4 s was calculated and defined as tautomerase activity (see "Experimental Procedures"). The activity of MIF in the absence of RPS19 was set to 100%. The assay was performed with 1 μM MIF and after preincubation of MIF with a 1-, 3- or 5-fold molar excess (1:1, 1:3, 1:5) of His-tagged RPS19 or His-tagged SCGB 2A1 for 1 h. The control protein SCGB 2A1 is of a similar size like MIF and has no enzymatic activity. Data are expressed as the mean ± S.E. Differences with a value of $p < 0.05$ were considered statistically different and are marked with an *asterisk*.

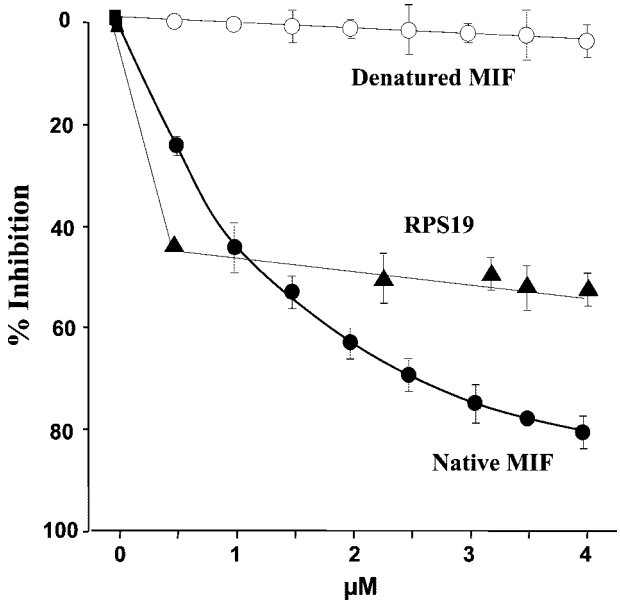

FIGURE 5. **RPS19 inhibits MIF binding to its receptor CD74.** Purified soluble CD74 was immobilized on a plastic matrix. Binding of biotinylated MIF to immobilized CD74 was measured by enzyme-linked immunosorbent assay after preincubation of biotin MIF with increasing amounts of native MIF, denatured human MIF, or RPS19. Data are expressed as the mean ± S.D. of three different experiments. For data points without the error bar the error is less than the width of the symbol.

increasing concentrations of unlabeled human MIF (0.5–4 μM) suppressed the binding of biotin-MIF to immobilized CD74 by 80%, whereas denatured human MIF showed no inhibitory effect (Fig. 5). Of note, the inhibitory effect of RPS19 at the lowest concentration tested (0.5 μM; 43% inhibition) was substantially more effective than the same concentration of human MIF (25% inhibition).

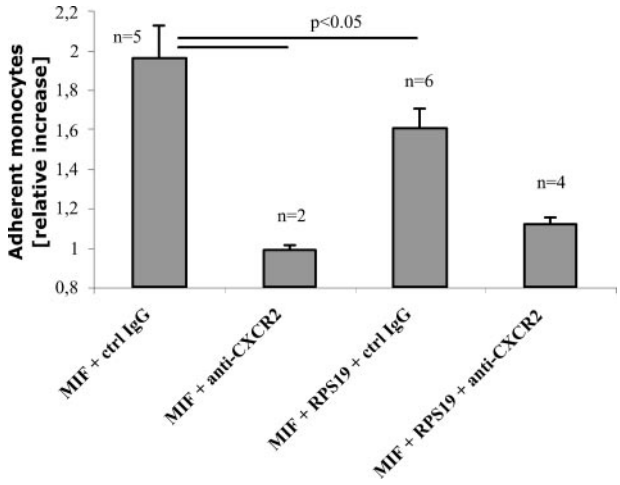

FIGURE 6. **RPS19 inhibits MIF-triggered mononuclear cell arrest.** HAoECs were preincubated with MIF and control IgG, RPS19, and/or anti-CXCR2 antibodies as indicated. After preincubation HAoECs were perfused with calcein-AM labeled mononuclear MonoMac6 cells, and the number of adherent cells was determined. Data are presented as relative increase compared with pretreatment with MIF and anti-CXCR2 antibodies, which was set to 1. Data are expressed as the mean ± S.E. of the indicated number of experiments. Differences with a value of $p < 0.05$ were considered statistically different.

MIF-induced Monocyte Arrest through CXCR2 Is Compromised by RPS19—Recently, it was shown that MIF controls inflammatory and atherogenic leukocyte recruitment through $G\alpha_i$-coupled activities of chemokine receptors CXCR2 and CXCR4 (14).

We used this assay to explore if the number of arrested mononuclear cells can be modified by RPS19. Calcein AM-labeled mononuclear MonoMac6 cells were passed over HAoECs with a defined shear rate. When HAoECs were pretreated with wild type human MIF in the presence of anti-CXCR2 antibodies, the basal level of arrested mononuclear cells was defined (Fig. 6, *second column from left*). Replacement of the specific anti-CXCR2 antibody by mouse IgG control antibodies resulted in a 2-fold MIF-induced increase in the number of arrested cells (*left-most column*). After pretreatment of HAoECs with MIF and RPS19, the number of arrested cells decreased by 39% (*third column from left*). This effect was dose-dependent and statistically significant at a 100-fold molar excess of RPS19 over MIF (data not shown). The addition of anti-CXCR2 antibodies to MIF and RPS19 during pretreatment reduced the number of arrested cells to almost basal levels. This demonstrates that induction of arrest of mononuclear cells by MIF as well as MIF blockage by RPS19 is CXCR2-mediated (Fig. 6, *right-most column*).

DISCUSSION

In the past 20 years significant progress has been made in our understanding of the role MIF plays in normal cellular physiology and in a variety of pathological conditions ranging from infection to autoimmunity and cancer (33, 34). In preclinical studies neutralization of MIF whether by antibodies, gene deletion, or small molecule inhibitors has shown promise as a potential treatment of these diseases (35, 36). As MIF functions within the cytokine cascade to control the initiation and progression of an inflammatory response, any shift toward MIF up-regulation increases the likelihood of systemic inflamma-

tion (37). Consequently, the identification of endogenous proteins that inhibit excess MIF activity is of great interest. Using an established *in vivo* biotinylation tagging approach (18), the RPS19 was identified as a new MIF-interacting partner in NIH 3T3 cells. By using endogenous co-immunoprecipitation as an independent method for the detection of protein-protein interactions, we could confirm RPS19 as an MIF binding partner. The validity of our co-IP approach was corroborated by the co-precipitation of JAB1, a well established MIF-interacting partner (38) (data not shown).

Direct physical interaction was shown by pulldown experiments of purified recombinant proteins and real-time binding analysis by surface plasmon resonance. The dissociation constant of formation of the MIF-RPS19 complex ($K_D = 1.3 \times 10^{-6}$ M) is well within the range of commonly observed and biologically relevant interactions, for instance in intracellular signal transduction cascades or in the binding of peptides to the T cell receptor or major histocompatibility complex. The dissociation rate indicates that 2% of the MIF-RPS19 complex decays per second. This together with a K_D in the micromolar range is strongly indicative of not only a fast but also reversible adjustment of the equilibrium, thereby allowing rapid changes of bioavailable MIF rather than an irreversible blockage of MIF function.

Certain pro-inflammatory activities of MIF are known to be impaired by mutations affecting its enzymatic activity (3, 22, 27). This prompted us to investigate whether critical MIF mutations that abolish these activities impact on RPS19 binding. MIF tautomerase activity is dependent on Pro^2, whereas its thiol-protein oxidoreductase activity is based on the Cys^{57}-Ala-Leu-Cys^{60} (CALC) motif (22).

Pulldown assays showed that the Δ4 MIF mutant had a similar binding affinity as the wild type protein, whereas the P2A and C60S mutants did not bind to RPS19. This suggests that Cys^{60} is essential for a direct interaction. Although the Δ4 and P2A mutants are both missing Pro^2 and, hence, have lost their tautomerase activity (22), they differ in binding to RPS19. Whereas the loss of the first four amino acids does not affect RPS19 binding, an exchange of Pro^2 for alanine prevents binding, indicating that this is caused by the introduced alanine instead by the missing proline. These results suggest that Pro^2 is not required for interaction, which is supported by our results showing that RPS19 only moderately interferes with MIF tautomerase activity. This is in contrast to the synthetic MIF inhibitor ISO-1 which specifically addresses the N terminus of the cytokine (4).

Although considered primarily as a component of the 40 S small subunit of the ribosome and, hence, an integral part of the protein translation machinery, RPS19 also exists in a free form in the cytosol (39). As such, RPS19 has important extraribosomal functions exemplified by its ability to interfere with growth factor signaling via its association with internalized fibroblast growth factor 2 (39, 40) and the PIM-1 oncoprotein (41). A comprehensive analysis of RPS19-binding proteins that were affinity-purified on immobilized GST-RPS19 identified a total of 159 proteins with many non-nucleolar and non-ribosomal factors (42). The list, which comprised many previously identified RPS19 interactors (*e.g.* RPS8), did not include PIM1, fibroblast growth factor 2, or MIF, however. This discrepancy can be attributed to the different methods employed to detect the interacting partners (*i.e.* yeast two-hybrid, co-IP, *in vivo* biotin-tagging).

Interestingly, a transglutaminase cross-linked RPS19 dimer has been described as a selective monocyte chemotactic factor in human rheumatoid arthritis when released by apoptotic cells into the extracellular fluid (43). Like MIF itself, the RPS19 dimer exerts a strong chemotactic stimulus on monocytes by mimicking the complement factor C5a and binding as a ligand to the C5a receptor (CD88) (44). This observation led to the inclusion of RPS19 in the family of chemokine-like function chemokines which also includes C5a and MIF (14, 45). Chemokine-like functions are characteristic for a group of proteins which, although they do not show typical structural chemokine features such as the chemokine-fold or the eponymous cysteine residues, have chemokine-like functions (14, 45). Therefore, we also investigated if MIF can bind to an RPS19 homodimer prepared in a type II transglutaminase reaction with monomeric protein (42). As we could produce only analytical amounts of the dimer (data not shown), we were unable to further investigate interaction of the PRS19 dimer with MIF.

Evidence that RPS19 can indeed be released from cells into extracellular fluids is supported by studies showing that another ribosomal protein, L4, is found in serum of ovarian cancer patients (46). It is tempting to speculate that by inhibiting MIF cytokine activity, monomeric RPS19 may, thus, limit an excessive inflammatory response. This view is supported by the finding that already low concentrations of RPS19 (0.5 μM) resulted in a significant blockage of MIF binding to its receptor CD74 comparable with the concentration of unlabeled MIF required to obtain the same level of inhibition (1 μM). We obtained further support for our hypothesis by investigating the effect of RPS19 on the recently discovered function of MIF as a non-cognate ligand of chemokine receptors CXCR2 and CXCR4 (14). MIF was found to promote the recruitment of monocytes and T lymphocytes by interacting with CXCR2 and CXCR4, a process that also involves CD74. In our flow chamber assays RPS19 significantly inhibited the MIF-dependent adhesion of monocytes to aortic endothelial cells, suggesting that RPS19 limits extracellular bioavailability of MIF for receptor binding. In analogy, Nm23H1, which inhibits MIF-mediated suppression of p53 activity, was recently identified as an intracellular inhibitor of MIF function (47).

In conclusion, our data suggest that RPS19 functions as an extracellular inhibitor of MIF. A shift in equilibrium from free MIF to a MIF·RPS19 complex may counteract excessive MIF function at sites of inflammation and, thus, decrease the likelihood of tissue damage, septic shock, and autoimmune reaction.

Acknowledgments—We thank Dr. Con Mallidis for carefully reading the manuscript, Prof. Guntram Suske for providing pN3-CTB, Dr. Harald Braun for organizing pBudCE4.1-birA, Prof. Gregor Bein for providing buffy coats, Dr. Lydie Da Costa for sending a sample of chicken anti-RPS19 antibody, Dr. Gabriella Krasteva for help at the confocal microscope, Dr. Henning Urlaub for protein identification by mass spectrometry, and Eva Schneider and Dr. Hongqi Lue for expert technical assistance.

REFERENCES

1. Calandra, T., and Roger, T. (2003) *Nat. Rev. Immunol.* **3,** 791–800
2. Hoi, A. Y., Iskander, M. N., and Morand, E. F. (2007) *Inflamm. Allergy Drug Targets* **6,** 183–190
3. Swope, M., Sun, H. W., Blake, P. R., and Lolis, E. (1998) *EMBO J.* **17,** 3534–3541
4. Al-Abed, Y., Dabideen, D., Aljabari, B., Valster, A., Messmer, D., Ochani, M., Tanovic, M., Ochani, K., Bacher, M., Nicoletti, F., Metz, C. N., Pavlov, V. A., Miller, E. J., and Tracey, K. J. (2005) *J. Biol. Chem.* **280,** 36541–36544
5. Rosengren, E., Bucala, R., Aman, P., Jacobsson, L., Odh, G., Metz, C. N., and Rorsman, H. (1996) *Mol. Med.* **2,** 143–149
6. Thiele, M., and Bernhagen, J. (2005) *Antioxid. Redox Signal.* **7,** 1234–1248
7. Lan, H. Y., Bacher, M., Yang, N., Mu, W., Nikolic-Paterson, D. J., Metz, C., Meinhardt, A., Bucala, R., and Atkins, R. C. (1997) *J. Exp. Med.* **185,** 1455–1465
8. Bernhagen, J., Calandra, T., Mitchell, R. A., Martin, S. B., Tracey, K. J., Voelter, W., Manogue, K. R., Cerami, A., and Bucala, R. (1993) *Nature* **365,** 756–759
9. Pan, J. H., Sukhova, G. K., Yang, J. T., Wang, B., Xie, T., Fu, H., Zhang, Y., Satoskar, A. R., David, J. R., Metz, C. N., Bucala, R., Fang, K., Simon, D. I., Chapman, H. A., Libby, P., and Shi, G. P. (2004) *Circulation* **109,** 3149–3153
10. Leech, M., Metz, C., Santos, L., Peng, T., Holdsworth, S. R., Bucala, R., and Morand, E. F. (1998) *Arthritis Rheum.* **41,** 910–917
11. Denkinger, C. M., Denkinger, M., Kort, J. J., Metz, C., and Forsthuber, T. G. (2003) *J. Immunol.* **170,** 1274–1282
12. Stosic-Grujicic, S., Stojanovic, I., Maksimovic-Ivanic, D., Momcilovic, M., Popadic, D., Harhaji, L., Miljkovic, D., Metz, C., Mangano, K., Papaccio, G., Al-Abed, Y., and Nicoletti, F. (2008) *J. Cell. Physiol.* **215,** 665–675
13. Hoi, A. Y., Hickey, M. J., Hall, P., Yamana, J., O'Sullivan, K. M., Santos, L. L., James, W. G., Kitching, A. R., and Morand, E. F. (2006) *J. Immunol.* **177,** 5687–5696
14. Bernhagen, J., Krohn, R., Lue, H., Gregory, J. L., Zernecke, A., Koenen, R. R., Dewor, M., Georgiev, I., Schober, A., Leng, L., Kooistra, T., Fingerle-Rowson, G., Ghezzi, P., Kleemann, R., McColl, S. R., Bucala, R., Hickey, M. J., and Weber, C. (2007) *Nat. Med.* **13,** 587–596
15. Gregory, J. L., Morand, E. F., McKeown, S. J., Ralph, J. A., Hall, P., Yang, Y. H., McColl, S. R., and Hickey, M. J. (2006) *J. Immunol.* **177,** 8072–8079
16. Leng, L., Metz, C. N., Fang, Y., Xu, J., Donnelly, S., Baugh, J., Delohery, T., Chen, Y., Mitchell, R. A., and Bucala, R. (2003) *J. Exp. Med.* **197,** 1467–1476
17. Nishimura, T., Horino, K., Nishiura, H., Shibuya, Y., Hiraoka, T., Tanase, S., and Yamamoto, T. (2001) *J. Biochem.* (*Tokyo*) **129,** 445–454
18. de Boer, E., Rodriguez, P., Bonte, E., Krijgsveld, J., Katsantoni, E., Heck, A., Grosveld, F., and Strouboulis, J. (2003) *Proc. Natl. Acad. Sci. U. S. A.* **100,** 7480–7485
19. Rischitor, G. (2005) *Transcription Factor Sp3 as Target for SUMOylation in Vivo*. Ph.D. thesis, Philipps-Universität Marburg, Marburg, Germany
20. Shevchenko, A., Wilm, M., Vorm, O., and Mann, M. (1996) *Anal. Chem.* **68,** 850–858
21. Berndt, K., Kim, M., Meinhardt, A., and Klug, J. (2008) *Mol. Cell. Biochem.* **307,** 265–271
22. Kleemann, R., Rorsman, H., Rosengren, E., Mischke, R., Mai, N. T., and Bernhagen, J. (2000) *Eur. J. Biochem.* **267,** 7183–7193
23. Sambrook, J., and Russell, D. W. (2001) *Molecular Cloning*, 3rd Ed., pp. 15.51, Cold Spring Harbor Laboratory Press, Cold Spring Harbor, New York
24. Sherman, F., Stewart, J. W., and Tsunasawa, S. (1985) *BioEssays* **3,** 27–31
25. Gu, J., Stephenson, C. G., and Iadarola, M. J. (1994) *Biotechniques* **17,** 257, 260, and 262
26. Da Costa, L., Tchernia, G., Gascard, P., Lo, A., Meerpohl, J., Niemeyer, C., Chasis, J. A., Fixler, J., and Mohandas, N. (2003) *Blood* **101,** 5039–5045
27. Bendrat, K., Al-Abed, Y., Callaway, D. J., Peng, T., Calandra, T., Metz, C. N., and Bucala, R. (1997) *Biochemistry* **36,** 15356–15362
28. Xiao, F., Mirwald, A., Papaioannou, M., Baniahmad, A., and Klug, J. (2005) *Mol. Endocrinol.* **19,** 2964–2978
29. Weber, C., Aepfelbacher, M., Haag, H., Ziegler-Heitbrock, H. W., and Weber, P. C. (1993) *Eur. J. Immunol.* **23,** 852–859
30. Kamir, D., Zierow, S., Leng, L., Cho, Y., Diaz, Y., Griffith, J., McDonald, C., Merk, M., Mitchell, R. A., Trent, J., Chen, Y., Kwong, Y. K., Xiong, H., Vermeire, J., Cappello, M., McMahon-Pratt, D., Walker, J., Bernhagen, J., Lolis, E., and Bucala, R. (2008) *J. Immunol.* **180,** 8250–8261
31. Swope, M. D., and Lolis, E. (1999) *Rev. Physiol. Biochem. Pharmacol.* **139,** 1–32
32. Ni, J., Kalff-Suske, M., Gentz, R., Schageman, J., Beato, M., and Klug, J. (2000) *Ann. N. Y. Acad. Sci.* **923,** 25–42
33. Bucala, R., and Lolis, E. (2005) *Drug News Perspect.* **18,** 417–426
34. Morand, E. F., Leech, M., and Bernhagen, J. (2006) *Nat. Rev. Drug Discov.* **5,** 399–410
35. Leech, M., Metz, C., Bucala, R., and Morand, E. F. (2000) *Arthritis Rheum.* **43,** 827–833
36. Santos, L., Hall, P., Metz, C., Bucala, R., and Morand, E. F. (2001) *Clin. Exp. Immunol.* **123,** 309–314
37. Baugh, J. A., and Bucala, R. (2002) *Crit. Care Med.* **30,** 27–35
38. Kleemann, R., Hausser, A., Geiger, G., Mischke, R., Burger-Kentischer, A., Flieger, O., Johannes, F. J., Roger, T., Calandra, T., Kapurniotu, A., Grell, M., Finkelmeier, D., Brunner, H., and Bernhagen, J. (2000) *Nature* **408,** 211–216
39. Soulet, F., Al Saati, T., Roga, S., Amalric, F., and Bouche, G. (2001) *Biochem. Biophys. Res. Commun.* **289,** 591–596
40. Wool, I. G. (1996) *Trends Biochem. Sci.* **21,** 164–165
41. Chiocchetti, A., Gibello, L., Carando, A., Aspesi, A., Secco, P., Garelli, E., Loreni, F., Angelini, M., Biava, A., Dahl, N., Dianzani, U., Ramenghi, U., Santoro, C., and Dianzani, I. (2005) *Haematologica* **90,** 1453–1462
42. Orru, S., Aspesi, A., Armiraglio, M., Caterino, M., Loreni, F., Ruoppolo, M., Santoro, C., and Dianzani, I. (2007) *Mol. Cell. Proteomics* **6,** 382–393
43. Nishiura, H., Shibuya, Y., Matsubara, S., Tanase, S., Kambara, T., and Yamamoto, T. (1996) *J. Biol. Chem.* **271,** 878–882
44. Nishiura, H., Shibuya, Y., and Yamamoto, T. (1998) *Lab. Investig.* **78,** 1615–1623
45. Degryse, B., and de Virgilio, M. (2003) *FEBS Lett.* **553,** 11–17
46. Chatterjee, M., Mohapatra, S., Ionan, A., Bawa, G., Ali-Fehmi, R., Wang, X., Nowak, J., Ye, B., Nahhas, F. A., Lu, K., Witkin, S. S., Fishman, D., Munkarah, A., Morris, R., Levin, N. K., Shirley, N. N., Tromp, G., Abrams, J., Draghici, S., and Tainsky, M. A. (2006) *Cancer Res.* **66,** 1181–1190
47. Jung, H., Seong, H. A., and Ha, H. (2008) *J. Biol. Chem.* **283,** 32669–32679
48. Kim, M. (2003) *Expression Cloning and Purification of Macrophage Migration Inhibitory Factor*. Diploma thesis (M.Sc) Philipps-University, Marburg, Germany

Placenta (2006), **27**, 648–659
doi:10.1016/j.placenta.2005.05.013

Spatial and Temporal Distribution of Tie-1 and Tie-2 During Very Early Development of the Human Placenta

U. A. Kayisli[a], S. Cayli[a], Y. Seval[a], F. Tertemiz[a], B. Huppertz[b] and R. Demir[a,*]

[a] Department of Histology and Embryology, Faculty of Medicine, Akdeniz University, Antalya, Turkey;
[b] Department of Anatomy II, University Hospital RWTH Aachen, Germany

Paper accepted 14 May 2005

Vasculogenesis in the human placenta comprises differentiation and growth of newly forming blood vessels derived from hemangiogenic stem cells within the mesenchymal core of villi. In a second stage, angiogenesis leads to the expansion and remodeling of the already existing vessels. At present, relatively little is known about the regulatory mechanisms of vasculogenesis and angiogenesis during very early placentation. Using placental villous tissues from days 22 to 48 of pregnancy, we analyzed the spatial and temporal expression of Tie-1 and Tie-2 in parallel to vascular maturation in the human placenta. In immunohistochemistry both receptors, Tie-1 and Tie-2 show a cell and villous type specific expression during this early phase of placental development. Especially, cytotrophoblast and hemangiogenic cell cords in mesenchymal villi and Hofbauer cells in immature intermediate villi have the strongest immunoreactivities. Western blot analysis showed that no significant changes were detected for Tie-1 and Tie-2 as pregnancy advanced. Moreover, phospho-Tie-2 levels did not change significantly in parallel to pregnancy ages. We conclude that both receptors are involved in angiogenesis as well as vascular modulation of early vessels. Due to their spatial distribution we speculate on an additional role in regulation of villous and extravillous trophoblastic behavior.
Placenta (2006), **27**, 648–659

Keywords: Tie-1; Tie-2; Human placenta; Angiogenesis; Invasion; Extravillous trophoblasts; Early pregnancy

INTRODUCTION

In the human placenta vasculogenesis comprises the differentiation and growth of blood vessels derived from hemangiogenic stem cells, which derived from indifferent mesenchymal cells of extra-embryonic mesenchymal tissue [1]. Subsequently, angiogenesis is responsible for the remodeling and expansion of an already existing vascular network. At present, relatively little is known about the regulatory mechanisms of vasculogenesis and angiogenesis. And present information on production, release and action of angiogenic growth factors in the first stages of human placental vasculogenesis is not detailed enough to explain the molecular mechanisms of this process.

At the beginning of the third week of development, vasculogenesis inside chorionic villi leads to the formation of first placental vessels. Villous trophoblast may control the development of blood vessels inside the villous stroma [2], and it is likely that a multidirectional regulation influences the function of each other, trophoblast and stromal cells, including paracrine and autocrine pathways [3]. The early appearance of macrophages (Hofbauer cells) in the villous core suggests a paracrine role for these cells during the first stages of placental vasculogenesis [4,5]. Previous studies have reported that Hofbauer cells express angiogenic growth factors such as vascular endothelial growth factor (VEGF) [3,6] and have been described as sources of VEGF in villi from early placenta [5,7].

Tie-1 and Tie-2 proteins were first identified as orphan receptors with an essential role in embryogenic angiogenesis. The angiopoietins include a receptor activator (Angiopoietin-1; Ang-1) and a receptor antagonist (Angipoietin-2; Ang-2) for Tie-2 [8–10]. Ang-1 by binding to Tie-2 remodels the primitive vessels and provokes the stability of the maturing vessels by regulating the interactions between endothelial cells and surrounding matrix and cells [8,9,11,12]. Thus, in addition to the vital role of VEGF and its receptors [13], Tie-1 and Tie-2 can be regarded as one of the main molecules in vasculogenesis during very early placentation.

In knockout mice Tie-1 deficiency resulted in a poor capillary integrity whereas Tie-2 deficiency revealed an uncompleted capillary network, in the embryo as well as in the yolk sac placenta [9,14]. In human placental tissues, expression of Tie-1 and Tie-2 has been detected at both protein and mRNA levels [15,16].

So far the exact localization of both receptors is unclear during vasculogenesis in very early stages of placentation. We hypothesize that the spatial and temporal expression of Tie-1 and Tie-2 parallels vascular maturation in the human placenta.

* Corresponding author. Tel./fax: +90 242 227 44 86.
E-mail address: rdemir@akdeniz.edu.tr (R. Demir).

0143–4004/$–see front matter

Therefore, we investigated Tie-1 and Tie-2 expression in human placenta and evaluated their expression in different cell types of the villous tree that are at different stages of maturation, using immunohistochemistry and Western blot analysis.

MATERIALS AND METHODS

Samples of human placental tissue were obtained after legal termination of pregnancy by curettage for medical or psychosocial reasons, which were unlikely to affect placental structure and function. None of the normal pregnancies were receiving hormone treatment. Tissues were supplied from the Department of Obstetrics and Gynecology, Medical Faculty, Akdeniz University, and Clinic of Obstetrics and Gynecology, Government Hospital, Antalya. Written consent was obtained from patients before the procedure. Consent forms and protocols to use the tissue were approved by the Ethical Committee of the Medical Faculty of Akdeniz University.

Tissue collection and storage

Samples of human placental tissues were studied from 23 women with uncomplicated normal pregnancies. Tissue samples were obtained form curettage material, which was collected due to social and medical reasons during early periods of pregnancy (from days 22 to 48 days post conception, p.c.). Eight placental samples from the 4th week (aged 22–27 days p.c.), six samples from the 5th week (aged 29–36 days p.c.), five samples from the 6th week (aged 37–41 days p.c.) and four samples from the 7th week (aged 42–48 days p.c.) were examined. Placental specimens were classified as described in our previous study [1] and by studying embryonic developmental details following the Carnegie classification [17]. Immediately after vacuumed aspiration of the conceptus (no application of prostaglandins), placental samples were collected (1) for paraffin treatment for further immunohistochemical reaction, (2) were snap-frozen in liquid nitrogen in PBS and stored at −80 °C for further investigation, and (3) were double fixed in glutaraldehyde and osmium tetroxide for electron microscopic examination. For paraffin section analysis, tissue samples were fixed with 4% neutral paraformaldehyde for about 6 h before dehydration and paraffin embedding.

Immunohistochemistry

Serial sections were collected on poly-L-lysine coated slides (Sigma, St. Louis, MO, USA) and incubated overnight at 40 °C. Tissue sections were dewaxed, dehydrated, and placed in citrate buffer (pH 6; 2.1 g/l citric acid, 15 ml/l NaOH). To unmask antigenic sites in the tissues, antigen retrieval was performed, by treating the samples in a microwave oven at 750 W for 5 min twice. After cooling for 20 min at room temperature, the sections were washed in phosphate buffered saline (PBS; pH 7.4). To block endogenous peroxidase activity, sections were kept in 3% hydrogen peroxide (Dako A/S, Glostrup, Denmark) for 30 min and washed with PBS three times. The following primary antibodies were used: rabbit anti-Tie-1 (1:200, polyclonal, C-18, SC-342; Santa Cruz Biotechnology Inc, Santa Cruz, CA, USA), rabbit anti-Tie-2 (1:200, polyclonal, C20, SC-324; Santa Cruz), mouse anti-human Tie-1 (25 μg/ml, monoclonal, MAB619, R&D Systems), and goat anti-human Tie-2 (25 μg/ml, monoclonal, AF313, R&D Systems).

After blocking with normal serum for 30 min at room temperature, sections were incubated at 4 °C overnight with the primary antibodies, followed by sequential incubations with biotinylated polyvalent antibodies (Dako A/S, Glostrup, Denmark) and peroxidase-labeled streptavidin (Dako A/S). Immunohistochemistry was performed using a horseradish peroxidase-labeled streptavidin biotin (HRP-LSAB) kit (Dako) according to the manufacturer's instructions. The resulting signal was developed with diaminobenzidine (DAB) (Dako). All incubations were performed in a moist chamber at room temperature, using PBS for washes between the incubation steps. The sections were counterstained with Mayer's hematoxylin solution (Merck) and mounted with glycerol gelatin (Dako). Negative control staining was performed by replacing the primary antibodies with non-immune rabbit IgG. Photomicrographs were taken with an Axioplan microscope (Zeiss, Oberkochen, Germany). Tissue sections from different pregnancy days were evaluated for protein localization and intensity. All samples for each individual antibody were exposed to the same protocol and were stained using the same incubation periods of staining. To test the antigenic specificity of the antibodies, Tie-1 and Tie-2 primary antibodies were preincubated with their specific peptides (10 μg/ml dilution for Tie-1P (C-18), and 10 μg/ml Tie-2P (C20), Santa Cruz) for 1 h at 37 °C. Then, the same protocol was applied.

The intensity of immunoreactivity was semi-quantitatively evaluated as follows. Positively stained cells were grouped according to the following categories: − (no staining), 1+ (weak but detectable), 2+ (moderate or distinct), 3+ (intense). For each tissue, an HSCORE value was calculated by summing the percentages of cells grouped in one intensity category and multiplying this number with the weighted intensity of the staining, using the formula [HSCORE = P_i (i + l)], where i represents the intensity scores and P_i is the corresponding percentage of the cells. In each slide, five different areas were evaluated under a microscope using 400× original magnification, the percentage of the cells for each intensity within these areas was determined by two investigators who were blinded to slides and gestational age, and the average score was used [18].

Western blot analysis

From placental tissues total protein was extracted using a lysis buffer (50 mM HEPES, pH 7.4, 150 mM NaCl, 10% glycerol, 1% Triton X-100, 1.5 mM $MgCl_2$, 1 mM EGTA, 100 mM NaF, 10 mM sodium pyrophosphate and protease inhibitors,

1 mM Na_3VO_4, 10 mg/ml leupeptin, 10 mg/ml aprotinin, and 4 mM PMSF). The protein concentration was determined by a detergent compatible protein assay (Bio-Rad Laboratories, Hercules, CA, USA). Samples (20 μg) were loaded and separated by non-reducing SDS-polyacrylamide gel electrophoresis using 7.5–12% Tris–HCl ready gels (Bio-Rad Laboratories) and electroblotted onto Hybond ECL nitrocellulose membrane (Amersham Pharmacia Biotech, Buckinghamshire, England). The membrane was blocked with 5% non-fat dry milk in TBS-T buffer (0.05% Tween-20 in TBS, pH 7.4) for 1 h to reduce non-specific binding. Afterwards, the membrane was incubated for 1 h with polyclonal antibodies against Tie-1 (1/200; Santa Cruz Biotechnology) and Tie-2 (1/200; Santa Cruz Biotechnology) and phospho-Tie-2 (1/500, Cell Signaling Inc., Beverly, MA). Following rinses with TBS-T for 15 min once and 10 min twice, the membranes were further incubated for 1 h with peroxidase-labeled anti-rabbit IgG (Vector Laboratories) diluted at 1:10 000 and subsequently washed with TBS-T for 15 min once and 10 min twice. The immunoblot was developed using a chemiluminescent kit (NEN Life Science, Boston, MA). After stripping, the same membranes used for Tie-1 and Tie-2 were also used to immunoblot β-actin (1/7000; clone no. mAbcam 8226; Abcam, Cambridge, MA).

To test the antigenic specificity of the antibodies, Tie-1 and Tie-2 primary antibodies were preincubated with their specific peptides (10 μg/ml dilution for Tie-1P (C-18), and 10 μg/ml Tie-2P (C20), Santa Cruz) for 1 h at 37 °C. Then the same protocol was applied. Equal loading was confirmed using Ponceau staining (Molecular Dynamics, Sunnyvale, CA). The bands were quantified using the Image J software provided by NIH.

Statistical analysis

Statistical analyses for immunohistochemical data and Western blot results were normally distributed (tested by Kolmogorov–Smirnov test) throughout the pregnancy days. Analysis of variance (ANOVA) and the Tukey test were carried out for statistical analysis and pairwise multiple comparisons. Statistical calculations were performed using Sigmastat for Windows, version 2.0 (Jandel Scientific Corporation, San Rafael, CA, USA).

RESULTS

Results of Tie-1 and Tie-2 immunoreactivities in the villous tree were evaluated in two categories, according to cell types and villous types. Moreover, total levels of these proteins were analyzed using Western blot analysis.

The specificity of the antibodies for Tie-1 and Tie-2 was evaluated by a pre-absorption test utilizing the specific antigens (10 μg/ml) for both Western blot analysis (Figure 1) and immunohistochemistry (Figure 2a–d). Moreover, expression of each Tie receptor was also examined with two different antibodies obtained from different companies (Figure 2e–h).

Besides the morphological appearance, the angioblastic and hematopoietic characteristics of the cells in the villous core were further confirmed by the intensity of the immunoreactivity with anti-CD34 and anti-CD31 antibodies in parallel to antibodies against Tie-1 and Tie-2 (Figure 3a–d).

In general, the total immunoreactivities for Tie-1 and Tie-2 did not change significantly as pregnancy progressed. However, Tie-1 immunoreactivity was stronger than Tie-2 in all pregnancy days evaluated (Figure 4a–c).

Tie-1 expression

Cell types

Cytotrophoblast and angiogenic cells showed the strongest Tie-1 immunoreactivity, which did not change significantly as pregnancy progressed. Among the cells of the villous stroma Hofbauer cells revealed a moderate immunoreactivity while mesenchymal cells displayed weak staining and no significant

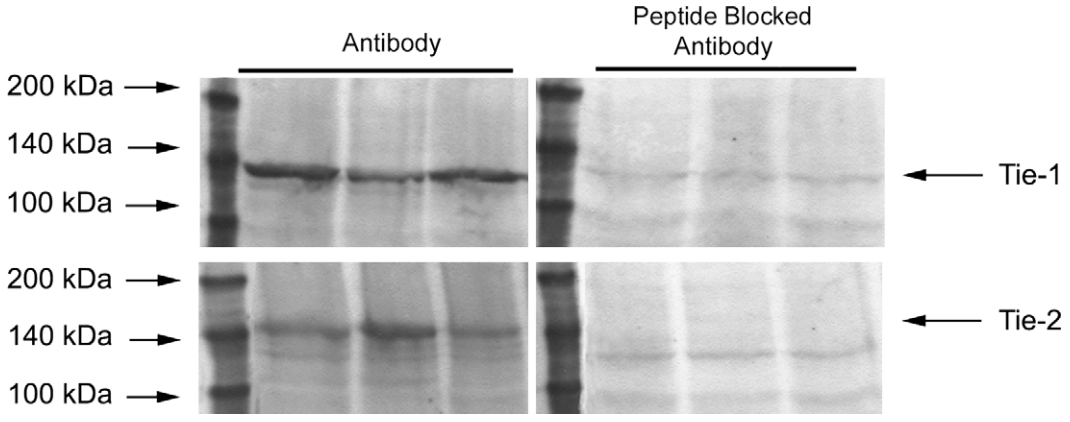

Figure 1. Western blot analysis of Tie-1 and Tie-2 expressions in the presence and absence of their blocking peptides in three samples from different pregnancy days. Tie-1 and Tie-2 revealed 126-kDa 140-kDa bands, respectively. When pre-absorbed with their specific antigens Tie-1 and Tie-2 antibodies revealed very weak bands with the same samples.

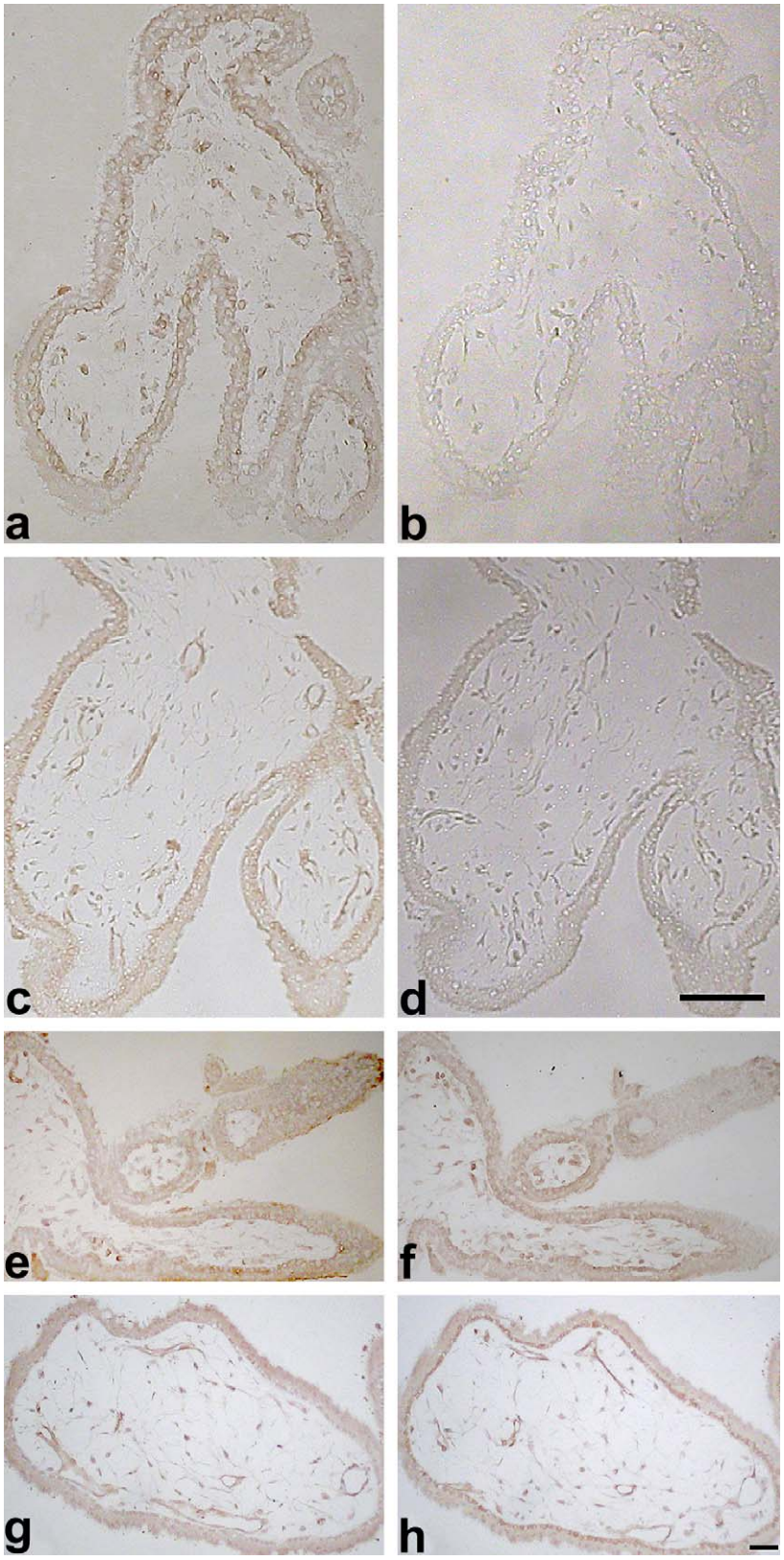

Figure 2. Immunohistochemical analysis of Tie-1 and Tie-2 antibodies in the presence and absence of their blocking peptides. (a, c) Tie-1 and Tie-2 immunoreactivities are seen, respectively. (b, d) When Tie-1 and Tie-2 antibodies were pre-absorbed with their specific antigens no immunoreactivity was detected in early placental villi. (e–h) Representative pictures for Tie-1 and Tie-2 immunohistochemistry. Similar immunoreactivities were detected for Tie-1 (e, Santa Cruz; f, R&D Systems) and Tie-2 (g, Santa Cruz; h, R&D Systems) using primary antibodies purchased from different companies. (a–d) Scale bar = 100 μm; (e–h), scale bar = 50 μm.

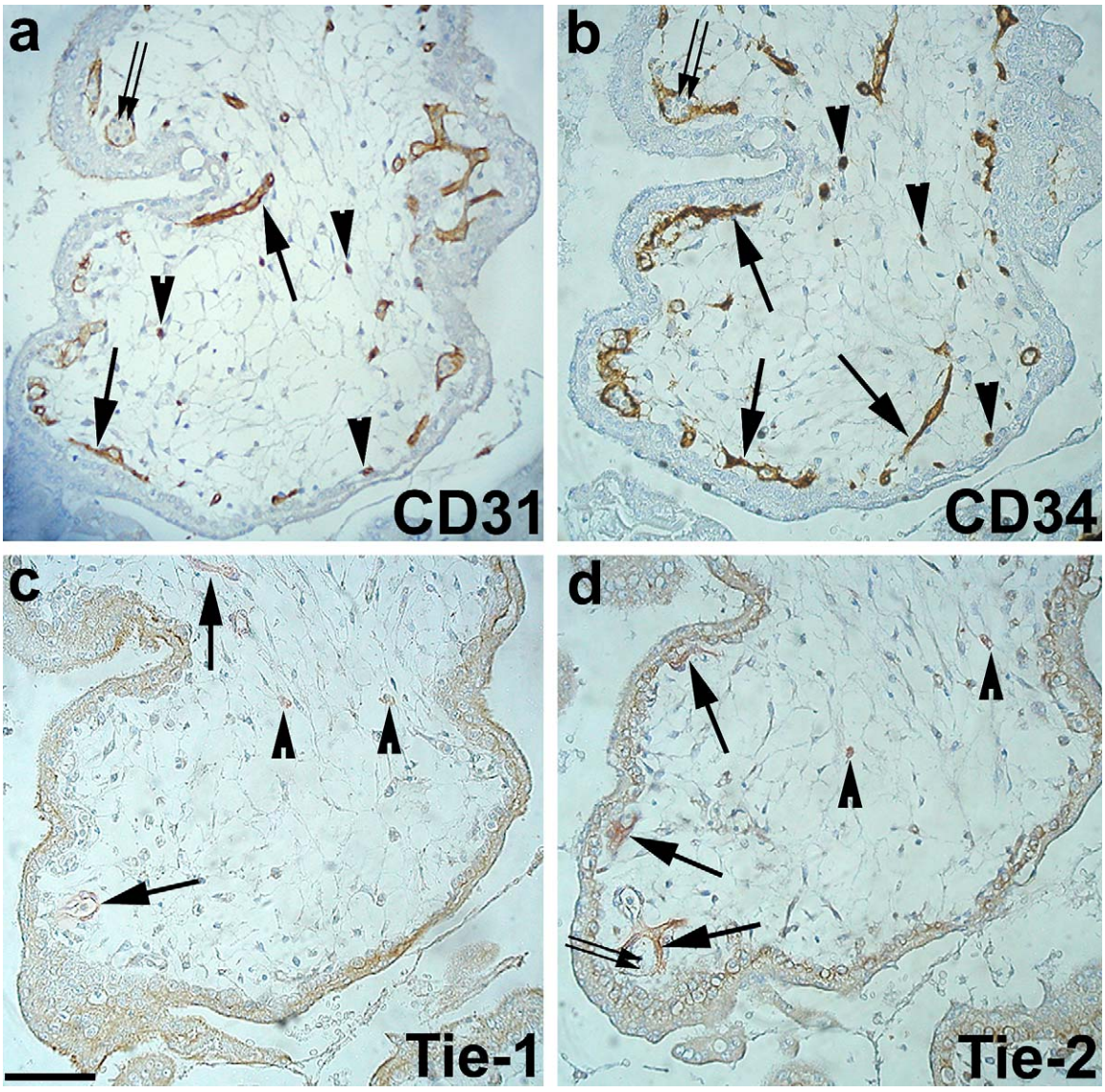

Figure 3. Analysis of CD31 and CD34 immunoreactivities in parallel to Tie-1 and Tie-2 immunostaining in human placental villi. (a, b) Angioblastic cells (arrowheads) and cell cords (arrows) are positive for both CD31 and CD34 while the hematopoietic progenitor cells (double arrows) in the primitive vascular lumen do not stain positive for CD31 and CD34. (c, d) In parallel sections to CD 31 and CD34 immunostaining in placental villi Tie-1 and Tie-2 immunostaining are seen. Tie-1 and Tie-2 expression in angioblastic cell cords and presumptive vascular endothelium (arrows), and in some angioblastic cells in stroma (arrowheads) are seen whereas hematopoietic cells in primitive vascular tubes are immunonegative (double arrows). Scale bar = 100 μm.

modification was noted as pregnancy progressed. Interestingly, vascular endothelium revealed weaker immunoreactivity than angiogenic cells in all pregnancy weeks evaluated (Figure 5a, c, d).

Villous types

Mesenchymal villi expressed a moderate to strong immunoreactivity for Tie-1. However, Tie-1 immunoreactivity revealed a gradual decrease from mesenchymal villi towards stem villi in parallel to villous maturation but not to the weeks of pregnancy (Figure 5b—d). Differential expression of Tie-1 in cytotrophoblast and angioblastic cells cords originates from the difference of their location in progressively maturing villous types (Figure 5b—d).

Western blot analysis of total Tie-1 expression in placental villi

Western blot analysis of Tie-1 expression in placental villi was performed to evaluate total Tie-1 protein levels. Immunoblotting of placental lysates revealed a 120-kDa band for Tie-1. No significant changes were found for Tie-1 expression related to week of pregnancy. Equal loading of samples was confirmed by β-actin immunolabeling of the same membrane used for Tie-1 immunoblotting (Figure 6a).

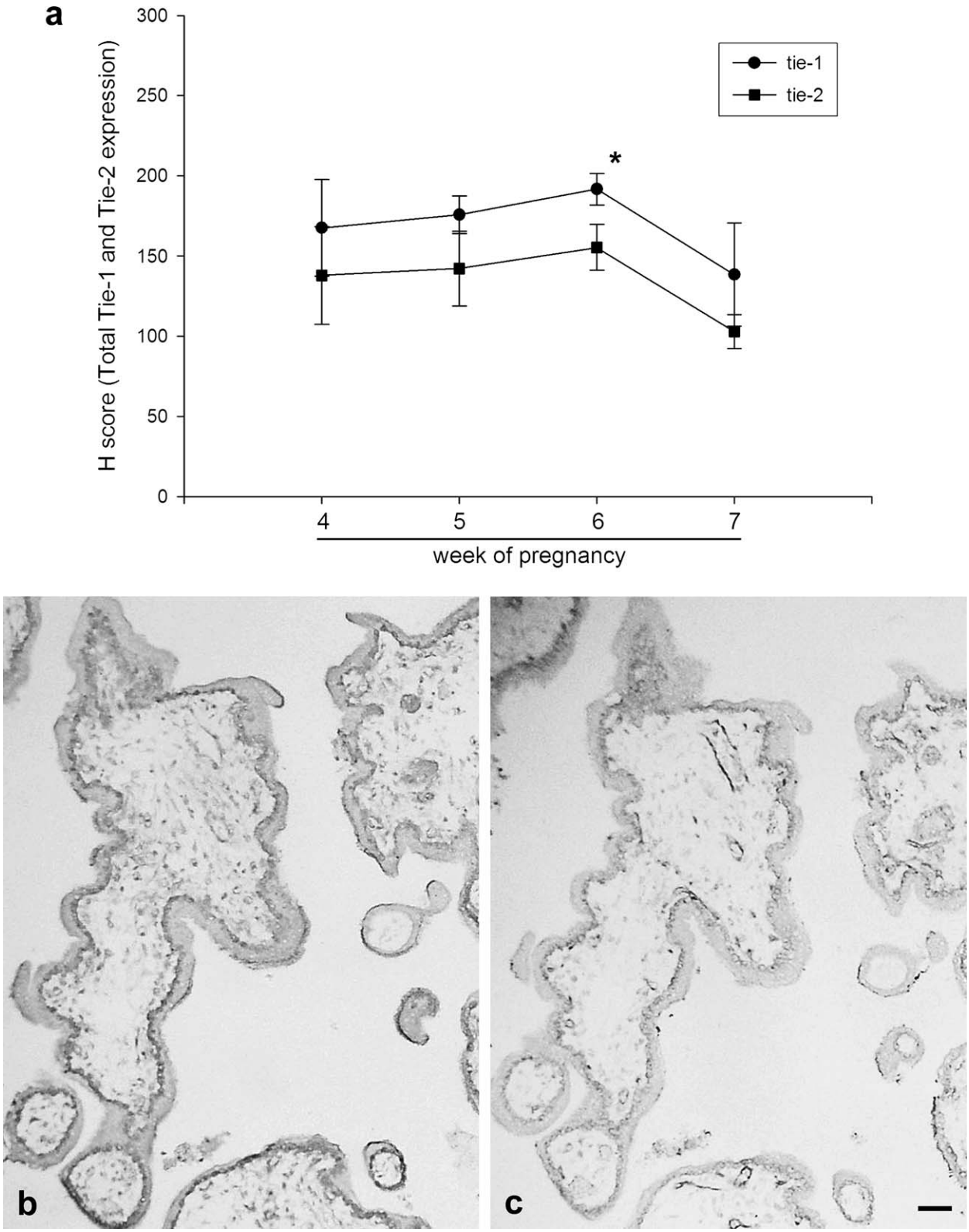

Figure 4. Analysis of Tie-1 and Tie-2 expression in early placental villi. (a) Semi-quantitative evaluation of changes in total Tie-1 and Tie-2 expression between week 4 and week 7 of pregnancy. Note higher Tie-1 expressions in all pregnancy weeks. (b) Tie-1 and (c) Tie-2 immunoreactivities are seen in placental villi at 4 weeks of pregnancy. (b, c) Scale bar = 100 μm. (a) The asterisk at week 6 represents significantly higher Tie-1 expression when compared to Tie-2 ($p < 0.05$).

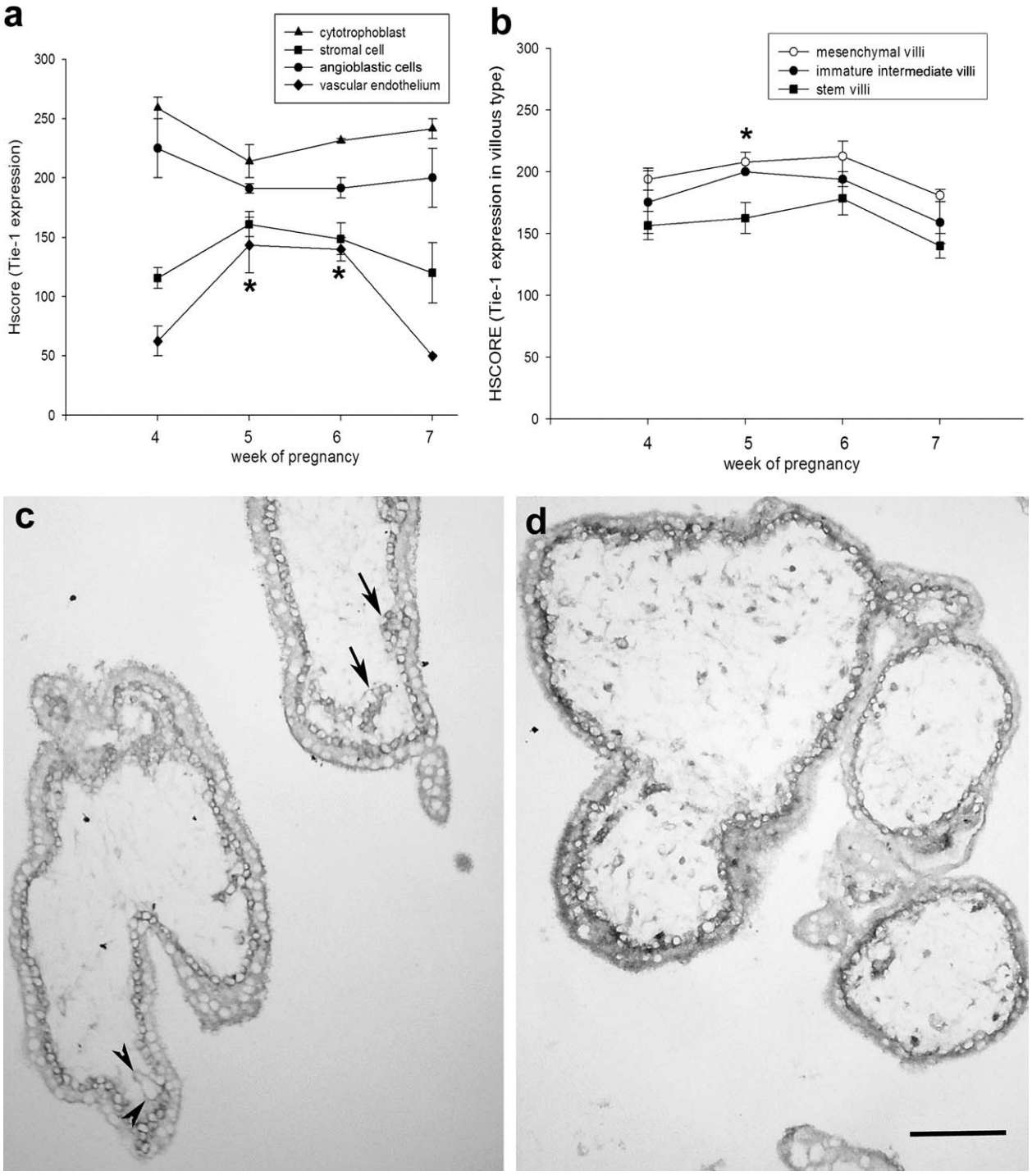

Figure 5. Analysis of Tie-1 expression in early placental villi. (a) Semi-quantitative evaluation of changes in Tie-1 expression in different cell types between week 4 and week 7 of pregnancy. Asterisk represents significantly higher Tie-1 immunoreactivity in vascular endothelium compared to that of weeks 4 and 7 ($p < 0.05$). (b) Semi-quantitative evaluation of changes in Tie-1 expression in different villous types between week 4 and week 7 of pregnancy. The asterisk represents significantly higher Tie-1 immunoreactivity in mesenchymal and immature intermediate villi compared to that in stem villi ($p < 0.05$). (c, d) are from weeks 4 and 6 p.c., respectively. Changes of Tie-1 expression in placental villi from week 4 to week 6 of pregnancy can be seen (arrows, angioblastic cells; arrowheads, presumptive endothelium); scale bar = 100 μm.

Tie-2 expression

Cell types

Cytotrophoblast and angiogenic cells exhibited a moderate to weak immunoreactivity for Tie-2 without significant alterations related to the week of pregnancy. Interestingly, vascular endothelium displayed a gradual decrease from strong to weak, while stromal cells revealed a gradual increase from absent to moderate for Tie-2 immunoreactivity as pregnancy advanced (Figure 7a, c, d).

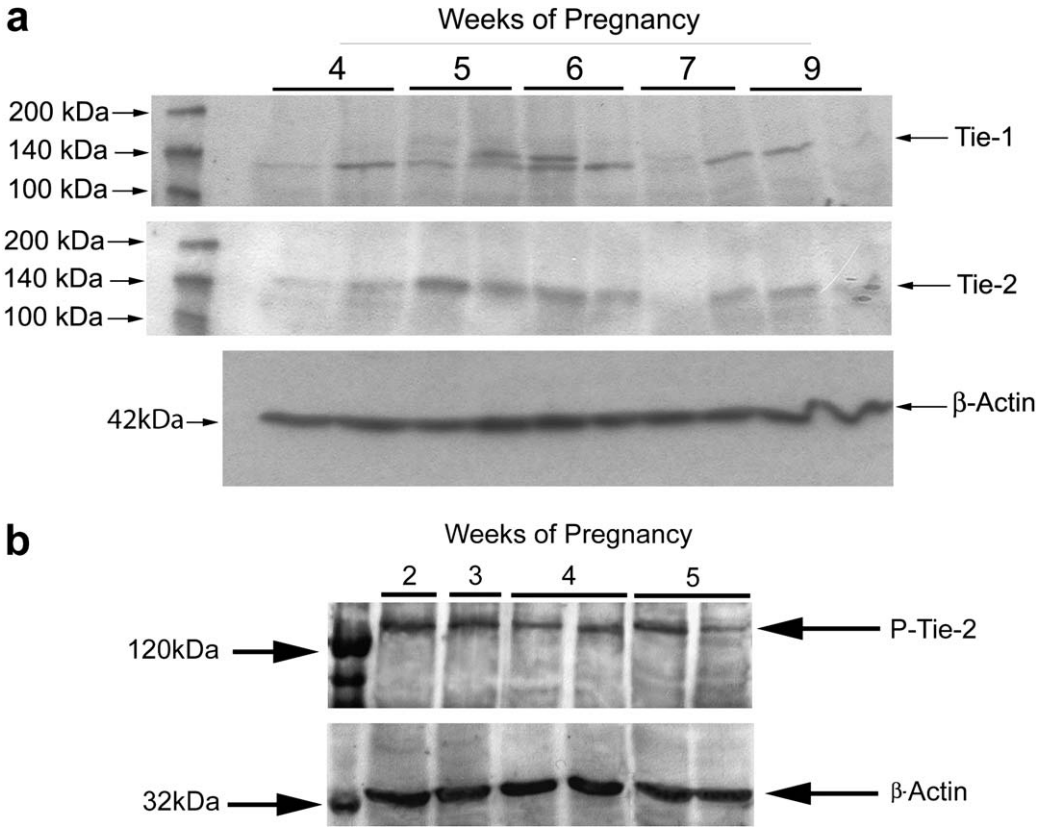

Figure 6. Western blot analysis of Tie-1, Tie-2 and phospho-Tie-2 expression in early placental villi. Two placental samples from each week are shown. (a) An immunoblot signal at around 120 kDa was detected for Tie-1 and around 140 kDa for Tie-2 showing a gradual increase in expression as pregnancy progressed. When dividing the signals by the β-actin bands, no statistically significant differences can be obtained from the Tie-1 and Tie-2 bands. Two bands for Tie-1 were detected from placental lysates of 5 and 6 weeks of pregnancy. (b) Phospho-Tie-2 and β-actin revealed bands around 160 kDa and 40 kDa, respectively. When normalized to β-actin, no significant difference was observed in phospho-Tie-2 expressions among the pregnancy weeks.

Villous type

Cells of mesenchymal villi expressed the weakest immunoreactivity for Tie-2 in all pregnancy days evaluated, while in immature intermediate villi Tie-2 immunoreactivity was moderate. In stem villi Tie-2 revealed a gradual increase in parallel to pregnancy weeks, except for the 7th week of pregnancy (Figure 7b—d).

Western blot analysis of total Tie-2 expression in placental villi

Western blot analysis of Tie-2 expression in placental villi was performed to evaluate total Tie-2 protein levels. Immunoblotting of placental lysates revealed a 140-kDa band for Tie-2. No significant changes were found for Tie-2 expression related to week of pregnancy. Equal loading of the samples was confirmed by β-actin immunolabeling of the same membrane used for Tie-2 immunoblotting (Figure 6a). Phospho-Tie-2 expression was also analyzed by Western blot. No significant difference in phospho-Tie-2 levels was observed among the weeks of pregnancy when normalized to β-actin (Figure 6b).

Tie-1 and Tie-2 expression by extravillous trophoblast

The distribution and intensity for both receptors were also evaluated in extravillous trophoblast cells in cell columns. Tie-1 immunoreactivity was strong in the proximal part of the cell columns and gradually decreased towards the distal part of the column (Figure 8a, c). On the other hand, Tie-2 immunoreactivity revealed a homogenous weak and mostly membranous immunoreactivity throughout the cell columns (Figure 8b, d).

DISCUSSION

Tie-1 and Tie-2 are crucial proteins for vascularization. Angiopoietin-1 (Ang-1) and angiopoietin-2 (Ang-2) actions are transformed by binding to their receptor tyrosine kinase (Tie-2). Both Tie-2 ligands are antagonists to each other while the Tie-1 ligand is still not known. In the present study we evaluated both Tie-1 and Tie-2 in different stages of vasculogenesis related to cell type, villous maturation and pregnancy age during very early placental development.

Angiogenic precursor cells differentiated from pluripotent mesenchymal cells initiate the first molecular and morphological signals of vascularization in placental villi just after the development

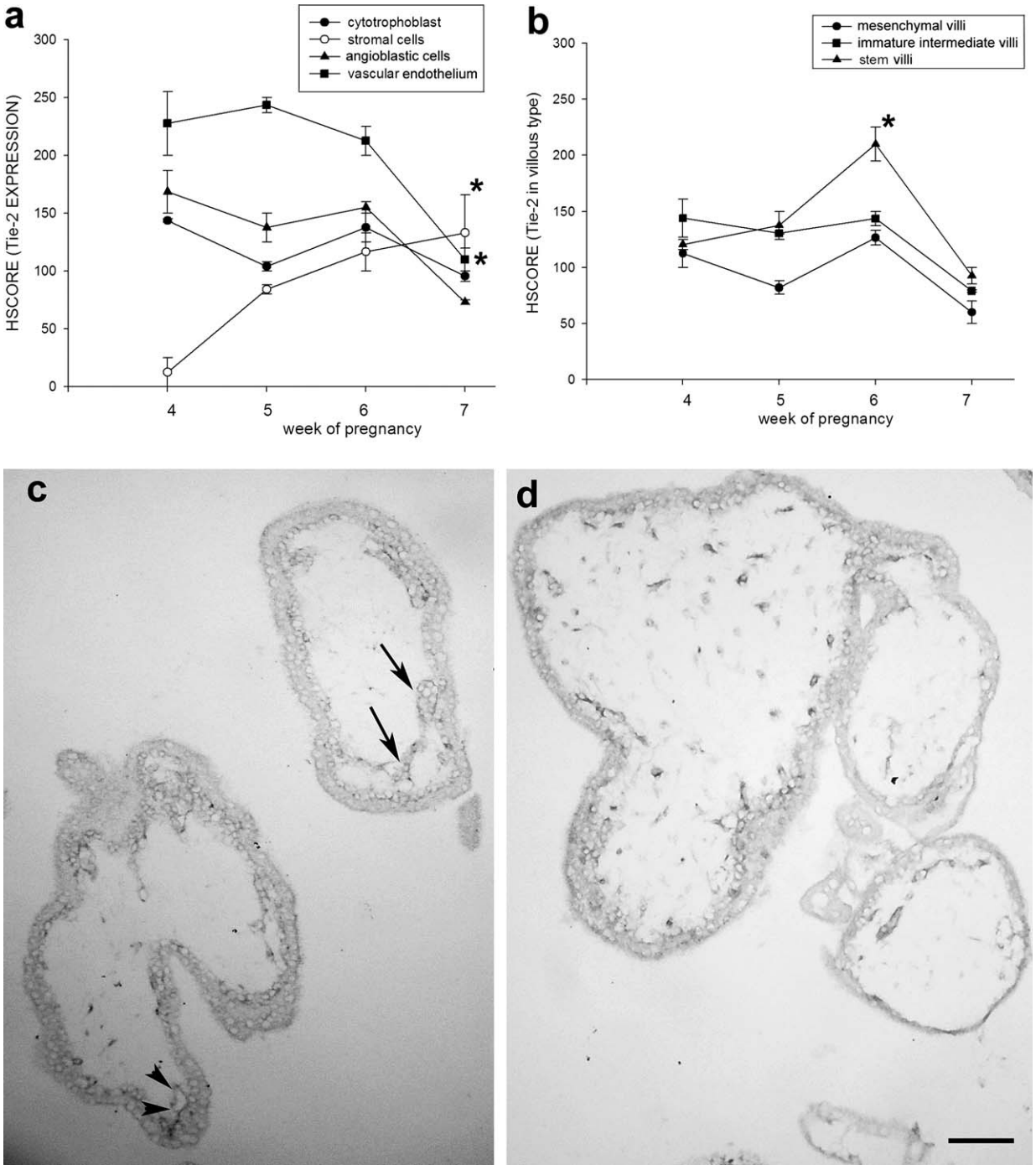

Figure 7. Analysis of Tie-2 expression in early placental villi. (a) Semi-quantitative evaluation of changes in Tie-2 expression in different cell types between week 4 and week 7 of pregnancy. Asterisk represents significantly higher Tie-2 immunoreactivity in stromal cells and decreasing Tie-2 immunoreactivity in vascular endothelium compared to other weeks ($p < 0.05$). (b) Semi-quantitative evaluation of changes in Tie-2 expression in different villous types between week 4 and week 7 of pregnancy. Asterisk represents significantly higher Tie-2 immunoreactivity in stem villi compared to that in mesenchymal and immature intermediate villi ($p < 0.05$). (c, d) are from week 4 and 6 p.c., respectively. Changes of Tie-2 expression in placental villi from week 4 to week 6 of pregnancy can be seen (arrows, angioblastic cells; arrowheads, presumptive endothelium); scale bar = 100 μm.

of tertiary villi. The exact mechanisms of how these cells differentiate or what signals induce differentiation of these cells are still not known. Because of new vessel formation and development, placental angiogenesis necessitates a source of cell type with pluripotent characteristics of differentiation, proliferation and migration. Therefore, placental angiogenesis is different from conventional angiogenesis as shown by different investigators [19–21]. The results of the present study suggest that both Tie-1 and Tie-2 take part in the modulation of placental angiogenesis and vasculogenesis starting from earliest steps of placental angiogenesis. Moreover, our results also show that there is a cell and villous type specific expression for both receptors.

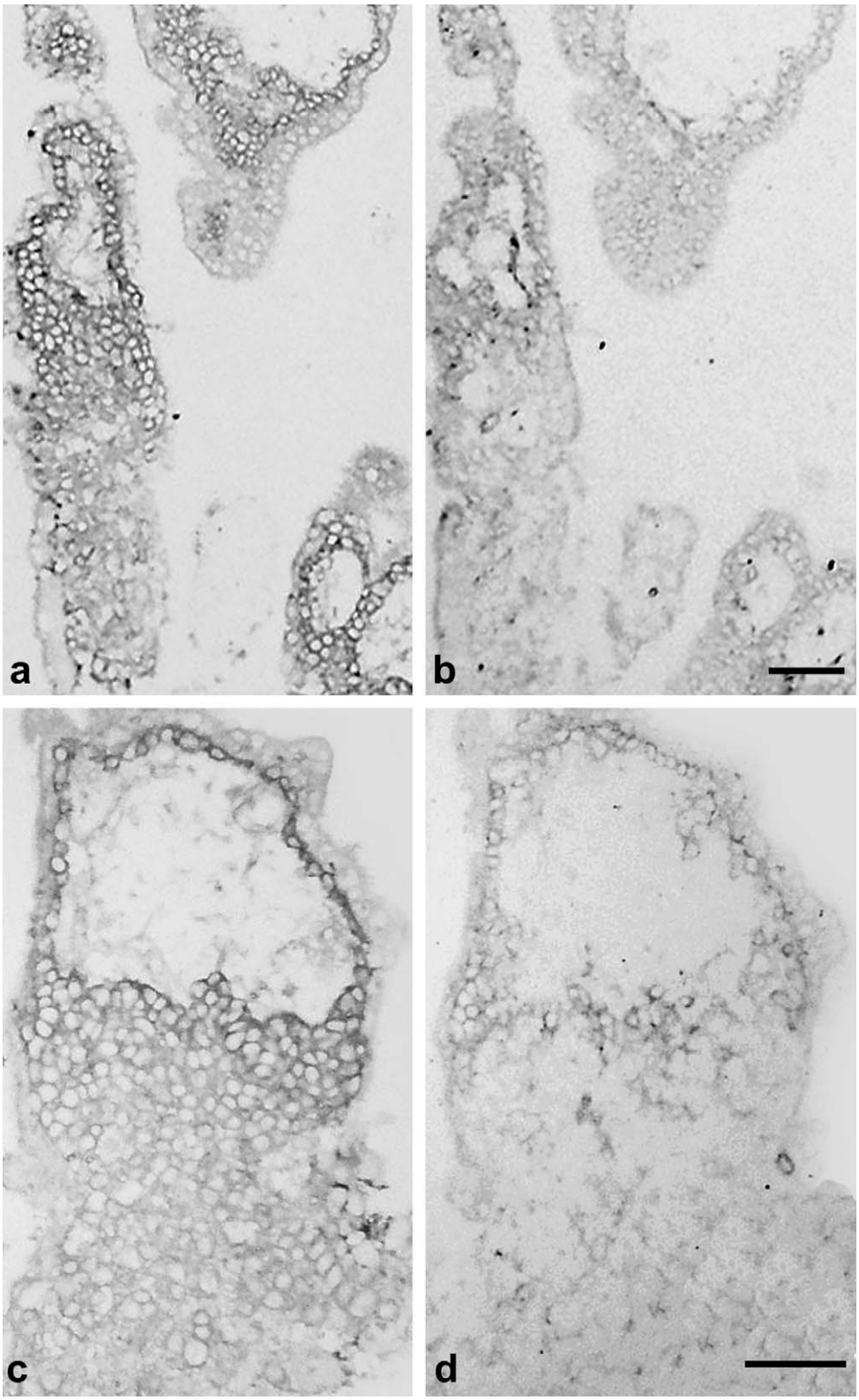

Figure 8. Analysis of Tie-1 and Tie-2 expression of extravillous trophoblast cells in early placental cell columns. (a, c) A gradual decrease of Tie-1 expression from the proximal to the distal part of the cell column can be seen. (b, d) Comparing to the Tie-1 expression pattern, Tie-2 expression is only weak and more homogenous. (a, b) are from week 4; (c, d) are from week 7; scale bars = 50 μm.

Higher Tie-1 expression in angioblastic cell cords suggests that Tie-1 is likely to be involved in early angiogenic events such as cell–cell contact, angiogenic differentiation and proliferation. The observation of double bands for Tie-1 in Western blot analysis of some samples may be due to the hyper-phosphorylation of Tie-1 that may represent an increased activation of Tie-1 at these days of pregnancy. On the other hand, increasing expression of Tie-2 in endothelium in parallel to vascular maturation suggests a function in later stages of angiogenesis such as vascular branching and/or vascular tube formation. In our previous ultrastructural and immunohistochemical observations [1,22] we suggested that these angiogenic cells and cell cords turn to main vessels and route to new vascular branching by cell protrusions and by connecting other main vessels via angiogenic bridge cells. Thus, the primitive structure of a vascular network is set up [13]. In the molecular mechanisms of this differentiation process, a variety of proteins such as VEGF and its receptors play crucial roles [13]. The results of this study suggest that Tie-1 also provokes this process possibly participating to form new main vascular patterns.

Although there are changes in Tie-1 and Tie-2 expression from week to week of pregnancy investigated, the changes in either total Tie-1 or Tie-2 expression levels did not reach a statistically significant value according to HSCORE results and Western blot analysis. Therefore, the changes may reflect a switching mechanism from one cell type to the other in parallel to villous maturation. Increasing levels of Tie-2 expression in stromal cells from mesenchymal villi to stem villi suggest that Tie-2 expression is related to villous maturation and may indicate a mesenchymal cell differentiation towards primitive perivascular cells such as progenitors of pericyte and/or vascular smooth muscle cells. These findings are in agreement with data from Brown et al. [23] and own results [5,13,22]. Brown et al. [23] suggested that VEGF is released during angiogenesis implicating that VEGF is involved in autocrine regulation of angiogenesis with an additional paracrine regulation of angiogenesis in embryonic development. Presenting a moderate immunoreactivity for Tie-1, Hofbauer cells are likely to regulate vascularization in villous stroma by interacting with perivascular mesenchymal cells or by taking over the paracrine effect from the cytotrophoblast.

Tie-1 expression in villous cytotrophoblast but not syncytiotrophoblast as well as its differential expression pattern related to the villous type suggests a specific role for these cells. Dunk et al. [10] showed that Ang-1 and Tie-2 mRNA are present in both layers of villous trophoblast in first trimester placenta, while Ang-2 mRNA is present only in the cytotrophoblast. Previously, Ang-1, Ang-2 and Tie-2 expression were analyzed in first trimester and term placentas at both mRNA and protein levels [24,25]. It is reported that although Ang-2 was mainly localized in syncytiotrophoblast, no signal was detected for Ang-1 throughout the gestation by in situ hybridization. Moreover, Tie-2 was mainly localized to endothelial cells of villi. They also showed that Ang-2 mRNA but not Ang-1 mRNA reduced in preeclamptic placentas [24]. However, Wulff et al. [25] have shown that Ang-1 is mainly expressed in syncytiotrophoblast and Ang-2 is highly expressed at 10 weeks of gestation. Moreover, Tie-2 was localized to cytotrophoblasts and vascular cells. Significantly, lower levels of Tie-1 in cytotrophoblast from recurrent miscarriage and missed abortion [26] present evidence for a vital role of Tie-1 in pregnancy.

Our finding regarding a strong expression of Tie-1 in extravillous trophoblast cells of the proximal parts of cell columns may represent an additional role for Tie-1 in proliferation or in keeping the stem cell phenotype of these cells. The decreased levels of Tie-1 in the distal parts of cell columns support this hypothesis since the distal cells have invasive rather than proliferative features. Since Tie-2 shows a weak but constant expression throughout the cell columns, the balance between Tie-1 and Tie-2 expressions in these cells may regulate their invasive and proliferative behavior. Moreover, expressing angiogenic factors and their receptors may be part of their differentiation process towards maternal endothelial cells. Goldman-Wohl et al. [27] showed that endovascular trophoblast cells express Tie-2 during the acquisition of an endothelial phenotype.

In conclusion, our results show that both Tie-1 and Tie-2 are involved in early angiogenic events and vascular modulation as well as in regulation of villous and extravillous trophoblastic behavior. Furthermore, the villous maturation-dependent localization and expression levels of the two receptors may point to a spatial role in vascular maturation, although no significant changes can be detected in their temporary expression during these very early stages of pregnancy. However, functional studies need to be done to further support our findings.

ACKNOWLEDGMENTS

Umit A. Kayisli and Sevil Cayli have equal contribution to this study. Akdeniz University Scientific Research Project Units supported this study.

REFERENCES

[1] Demir R, Kaufmann P, Castellucci, Erbengi T, Katowski A. Fetal vasculogenesis and angiogenesis in human placental villi. Acta Anat (Basel) 1989;139:190–203.

[2] Kingdom J, Huppertz B, Seaward G, Kaufmann P. Development of the placental villous tree and its consequences for fetal growth. Eur J Obstet Gynecol Reprod Biol 2000;92:35–43.

[3] Cervar M, Blaschitz G, Dohr G, Desoye G. Paracrine regulation of distinct trophoblast functions in vitro by placental macrophages. Cell Tissue Res 1999;295:297–305.

[4] Demir R, Erbengi T. Some new findings about Hofbauer cells in the chorionic villi of the human placenta. Acta Anat (Basel) 1984;119:18–26.

[5] Demir R, Kosanke G, Kohnen G, Kertschanska S, Kaufmann P. Classification of human placental stem villi: structural and functional aspects – a review. Microsc Res Tech 1997;38:29–41.

[6] Clark DE, Smith SK, Licence D, Evans AL, Charnock-Jones DS. Comparison of expression patterns for placenta growth factor, vascular endothelial growth factor (VEGF), VEGF-B and VEGF-C in the human placenta throughout gestation. J Endocrinol 1998;159:459–67.

[7] Kayisli UA, Demir R, Erguler G, Arici A. Vasodilator-stimulated phosphoprotein expression and its cytokine-mediated regulation in vasculogenesis during human placental development. Mol Hum Reprod 2002;8:1023–30.

[8] Suri C, Jones PF, Patan S, Bartunkova S, Maisonpierre PC, Davis S, et al. Requisite role of angiopoietin-1, a ligand for the Tie-2 receptor, during embryonic angiogenesis. Cell 1996;87:1171–80.

[9] Maisonpierre PC, Suri C, Jones PF, Bartunkova S, Wiegand SJ, Radziejewski C, et al. Angiopoietin-2 a natural antagonist for Tie2 that disrupts in vivo angiogenesis. Science 1997;277:55–60.

[10] Dunk C, Shams M, Nijjar S, Rhaman M, Qiu Y, Bussolati B, et al. Angiopoietin-1 and angiopoietin-2 activate trophoblast Tie-2 to promote growth and migration during placental development. Am J Pathol 2000; 156:2185–99.

[11] Suri C, McClain J, Thurtson G, McDonald MD, Zhou H, Oldmixon EH, et al. Increased vascularization in mice overexpressing angiopoietin-1. Science 1998;282:468–71.

[12] Holash J, Wiegand SJ, Yancopoulos GD. New model of tumor angiogenesis: dynamic balance between vessel regression and growth mediated by angiopoietins and VEGF. Oncogene 1999;18: 5356–62.

[13] Demir R, Kayisli UA, Seval Y, Celik-Ozenci C, Korgun ET, Demir-Weusten AY, et al. Sequential expression of VEGF and its receptors in human placental villi during very early pregnancy: differences between placental vasculogenesis and angiogenesis. Placenta 2004;25:560–72.

[14] Sato TN, Qin Y, Kozak CA, Audu KL. Tie-1 and Tie-2 define another class of putative receptor tyrosine kinase genes expressed in early embryonic vascular system. Proc Natl Acad Sci U S A 1993;90: 9355–8.

[15] Vuorela P, Hatva E, Lymboussaki A, Kaipainen A, Joukov V, Persico GM, et al. Expression of vascular endothelial growth factor and placental growth factor in human placenta. Biol Reprod 1997;56: 489–94.

[16] Ziegler SF, Bird TA, Schneringer JA, Schooley KA, Baum PR. Molecular cloning and characterization of novel receptor protein tyrosine kinase from human placenta. Oncogene 1993;8:663–70.

[17] O'Rahilly R. Developmental stages in human embryos, part A. Washington: Carnegie Institute; 1973 [Publ. 631].

[18] Selam B, Kayisli UA, Mulayim N, Arici A. Regulation of Fas ligand expression by estradiol and progesterone in human endometrium. Biol Reprod 2001;65:979–85.

[19] Risau W, Lemmon V. Changes in the vascular extracellular matrix during embryonic vasculogenesis and angiogenesis. Dev Biol 1998;125:441–50.

[20] Risau W, Flamme I. Vasculogenesis. Annu Rev Cell Dev Biol 1995;11: 73–91.

[21] Hanahan D. Signaling vascular morphogenesis and maintenance. Science 1997;277:48–50.

[22] Demir R, Kaufmann P, Erbengi T. Ultrastructural observations on angiogenetic cells formation and differentiation toward vascular endothelium in human placental villi. In: Catravas JD, Callow AD, Ryan US, editors. Vascular endothelium: physiological basis of clinical problems I. New York and London: Plenum Press; 1992, p. 240–2 [NATO Scientific Affairs Division].

[23] Brown KJ, Maynes SF, Bezos A, Maguire DJ, Ford MD, Parish CR. A novel in vitro assay for human angiogenesis. Lab Invest 1996;75: 539–55.

[24] Zhang EC, Smith KS, Baker PN, Charnock-Jones SD. The regulation and localization of angiopoietin-1, -2 and their receptor Tie-2 in normal and pathologic human placentae. Mol Med 2001;7:624–35.

[25] Wulff C, Wilson H, Dickson SE, Wiegand SJ, Fraser HM. Hemochorial placentation in the primate: expression of vascular endothelial growth factor, angiopoietins, and their receptors throughout pregnancy. Biol Reprod 2002;66:802–12.

[26] Vuorela P, Carpen O, Tulppala M, Halmesmaki E. VEGF, its receptors and the tie receptors in recurrent miscarriage. Mol Hum Reprod 2000;6: 276–82.

[27] Goldman-Wohl DS, Ariel I, Greenfield C, Lavy Y, Yagel S. Tie-2 and angiopoietin-2 expression at the fetal–maternal interface: a receptor ligand model for vascular remodelling. Mol Hum Reprod 2000;6:81–7.

Molecular Human Reproduction Vol.10, No.5 pp. 365–372, 2004 DOI: 10.1093/molehr/gah050

Cellular maturity and apoptosis in human sperm: creatine kinase, caspase-3 and Bcl-$_{XL}$ levels in mature and diminished maturity sperm

Sevil Cayli[1,3], Denny Sakkas[2], Lynne Vigue[1], Ramazan Demir[3] and Gabor Huszar[1,4]

[1]Sperm Physiology and [2]IVF Laboratories, Department of Obstetrics and Gynecology, Yale University School of Medicine, New Haven, CT 06525 USA and [3]Department of Histology and Embryology, Akdeniz University, Antalya, 07070, Turkey

[4]To whom correspondence should be addressed at: Sperm Physiology Laboratory, Department of Obstetrics and Gynecology, Yale School of Medicine, 333 Cedar Street, New Haven, CT 06510, USA. E-mail: gabor.huszar@yale.edu

The relationship between human sperm maturity and apoptosis is of interest because of the persistence of immature sperm in ejaculates in spite of various apoptotic processes during spermatogenesis. We assessed sperm maturity by HspA2 chaperone levels, and plasma membrane maturity by sperm binding to immobilized hyaluronic acid (HA). We also utilized objective morphometry. Sperm were stained with three antibody combinations: active caspase-3/creatine kinase (CK, a marker of cytoplasmic retention), caspase-3/the antiapoptotic Bcl-$_{XL}$, and CK/Bcl-$_{XL}$. In semen, 13% of sperm stained with CK, caspase-3 or Bcl-$_{XL}$, and 28% had stained with two markers. In the mature HA-bound sperm fraction, <4% were single- or double-stained. Regarding sperm regions, CK staining, whether alone or as double staining, occurred in the head and midpiece (15–20%), whereas caspase-3 and Bcl-$_{XL}$ were primarily (>80% of sperm) in the midpiece. Morphometrical attributes of clear, single- and double-stained sperm, in line with their more pronounced maturation arrest, showed an incremental increase in head size (due to cytoplasmic retention) and shorter tail length. We hypothesize that during faulty sperm development, three alternatives may occur: (i) elimination of aberrant germ cells by apoptosis; (ii) in surviving immature cells, caspase-3 is activated, and in response the antiapoptotic Bcl-$_{XL}$, and perhaps HspA2, provide protection; (iii) in a third type of immature sperm, in addition to the CK, caspase-3 and Bcl-$_{XL}$ expression, there are related manifestations of increased head size and shorter tail length. Thus, immature sperm may vary in the type of developmental arrest and in protection mechanisms for apoptosis. These variations are likely to explain the persistence of immature sperm in the ejaculate.

Key words: apoptosis/hyaluronic acid/maturity/morphometry/spermatogenesis/HspA2

Introduction

Spermatogenesis, a complex process of male germ cell development, encompasses spermatogonial proliferation, meiosis and spermiogenesis. The spermiogenetic events that eliminate the surplus cytoplasm, such as development of the acrosome, tail growth, along with cytoplasmic extrusion, result in mature sperm (de Kretser *et al*., 1998; Huszar *et al*., 2000). Developmental defects may occur in both the cytoplasmic or nuclear compartments, which can result in the production of immature sperm.

Creatine kinase (creatine phosphokinase, CK) in human sperm is a marker of cytoplasmic retention and, thus, diminished sperm maturity (Huszar and Vigue, 1990, 1993). In unison with cytoplasmic extrusion, there is also a remodelling of the sperm plasma membrane (Huszar *et al*., 1997). Functional evidence for the remodelling process originates in studies of CK-immunostained sperm–hemizona (halved unfertilized human oocytes) complexes. Immature sperm with cytoplasmic retention were not able to bind to the zona pellucida, suggesting that the formation of the zona-binding site(s) is part of the membrane remodelling process (Huszar *et al*., 1994, 1997). Subsequently, we have also demonstrated that synthesis of the binding sites for hyaluronic acid (HA), a component of the female reproductive tract, is also regulated by the plasma membrane-remodelling events (Huszar *et al*., 1990; Sbracia *et al*., 1997). Mature sperm that bind to HA do not show cytoplasmic retention, are of normal morphology, have high DNA integrity and a low frequency of chromosomal aneuploidies (Huszar *et al*., 1997, 1998, 2003; Kovanci *et al*., 2001).

In addition, independent observations in our laboratory have indicated that sperm shape is very closely related to maturity. Sperm of diminished maturity have larger, rounder and amorphous heads due to the cytoplasmic retention (Huszar and Vigue, 1993). As sprouting of the tail is also a spermiogenetic event, immature sperm also show shorter tail lengths. In two studies, the ratio of tail length:long head axis was shown to be a very sensitive marker of sperm maturity (Gergely *et al*., 1999; Celik-Ozenci *et al*., 2003). Furthermore, mature sperm that are able to bind to HA compared to the non-binding sperm significantly differ in all tail, head, tail:head long axis ratio parameters (Celik-Ozenci *et al*., 2002). This relationship is also demonstrated in the present work.

Another important marker of sperm maturation is the testis-specific Hsp70-2, a member of the highly conserved Hsp70 family of chaperone proteins. In mice, the targeted disruption of the HSP70-2 gene caused the fragmentation of the synaptonemal complexes (structures formed between homologous chromosomes during the meiotic process), and a failure of desynapsis of the paired chromosomes (Dix *et al*., 1996). A second wave of 70 kDa chaperone

expression (hsc70t in mice) was also demonstrated during terminal spermiogenesis (Dix *et al*., 1996; Eddy, 1999). In addition to the meiotic support, the chaperone proteins are also responsible for the transport and folding of proteins, such as DNA repair enzymes, or the proteins for sperm membrane remodelling. HSP70-2 also exhibits an anti-apoptotic function (Buzzard *et al*., 1998; Garrido *et al*., 2001; Parcellier *et al*., 2003). Indeed, in Hsp70-2 knockout mice, in addition to arrested meiosis, there is increased germ cell apoptosis with the characteristic apoptotic DNA degradation pattern (Dix *et al*., 1996).

The role of the Hsp70 chaperone proteins in regulating the apoptotic process is well studied in somatic cells. In cell cultures, Hsp70 antisense oligomer caused an inhibition of Hsp70-1 expression and promoted apoptosis, whereas heat or other stress induced Hsp70 synthesis with a reduction of apoptosis (Wei *et al*., 1994, 1995). The mechanism of Hsp70 action in apoptosis is related to the apoptotic enzymes caspase-3 and -9. Activated caspase-9 is associated with cytochrome c that is released from the mitochondria. Both the apoptosis-triggering effect of cytochrome c upstream and the recruitment of caspase-9 to the apoptosis activating complex downstream, are inhibited by the C-terminal region of Hsp70. Thus, the Hsp70 chaperones, such as the homologous HSP70-2 as well as the human HspA2, are likely inhibitors of the apoptotic process (Beumer *et al*., 2000; Li *et al*., 2000).

The identity of HspA2 and the two-wave expression pattern of the testis-specific chaperone proteins in spermatogenesis and spermiogenesis has been established in men (Huszar *et al*., 2000). HspA2 first appears in the primary and secondary spermatocytes as a component of the synaptonemal complex. The second wave of HspA2 (perhaps hsc70t as in the mouse) expression occurs in elongating spermatids, simultaneously with cytoplasmic extrusion and plasma membrane remodelling. In ejaculated human sperm with low levels of HspA2, there are several other markers that reflect diminished maturity. These include cytoplasmic retention and consequential abnormal sperm head shape, diminished binding to the zona pellucida and HA, increased rate of chromosomal aneuploidies caused by meiotic defects, increased levels of DNA fragmentation, retarded histone-protamine replacement, and shape attributes detected by objective morphometry that are characteristic for immature sperm (Celik-Ozenci *et al*., 2003; Huszar *et al*., 2003; Kovanci *et al*., 2001; Óvári *et al*., 2003).

Several studies have focused on various aspects of sperm immaturity, DNA damage and apoptosis in sperm (Aitken *et al*., 1994; Huszar and Vigue 1994; Manicardi *et al*., 1995, 1998; Huszar *et al*., 1998; Sakkas *et al*., 1999a,b; Gandini *et al*., 2000; Irvine *et al*., 2000; Aitken and Krausz, 2001; Ricci *et al*., 2002; Shen *et al*., 2002). In line with the general notion that the proportion of immature sperm is higher in samples with lower sperm concentration, Sakkas *et al.* (2002) have demonstrated an inverse correlation between sperm concentrations and a number of apoptotic marker proteins; however, a potential link between the morphological attributes of such sperm and their apoptotic profile is yet unexplored.

In considering the relationship between apoptosis and diminished sperm maturity, we hypothesized that there may be a relationship between cytoplasmic retention, larger heads and shorter tails and the presence of various apoptotic proteins in the same sperm. In the present study we have therefore investigated the relationship between diminished sperm maturity and apoptosis. We have applied double immunostaining for combinations of CK/caspase-3, Bcl-$_{XL}$/caspase-3 and CK/Bcl-$_{XL}$ in mature and diminished maturity sperm fractions characterized by their level of CK and HspA2 content. Subsequently, we determined the morphometrical attributes of sperm with various staining patterns originating in semen and in the HA-bound mature sperm fractions.

Materials and methods

Patient population

The study samples originated from the leftover portion of semen submitted for semen analysis at the Sperm Physiology Laboratory, Department of Obstetrics and Gynecology, Yale University of Medicine. Samples were collected by masturbation after 2 days of abstinence, and were allowed to liquefy for 30–60 min. All studies were approved by the Yale School of Medicine Human Investigation Committee.

After determination of sperm concentration and motility according to World Health Organization (1999) criteria, the semen was diluted with 3 volumes of human tubal fluid medium (HTF; Irvine Scientific, USA) containing 0.5% bovine serum albumin (BSA). The diluted semen was centrifuged at 500 *g* for 15 min at room temperature. The sperm pellet was resuspended in HTF, and aliquots were taken for CK activity and HspA2 ratio determinations. Sperm smears were prepared for various studies, including CK immunocytochemistry for cytoplasmic retention and determination of Bcl-$_{XL}$ and active caspase-3 expression levels by immunocytochemistry. For preparation of the HA-bound mature sperm fractions, 7 µl aliquots were applied to HA-coated glass slides (Biocoat, Inc., USA). After incubation for 10 min in a humidity chamber, the slides were washed gently in order to remove the unbound sperm (Huszar *et al*., 2003). The smears of unselected and HA-selected sperm fractions were air-dried and fixed with formaldehyde for the CK, caspase-3 and Bcl-$_{XL}$ immunocytochemical assessments.

In the initial and respective HA-bound sperm fractions, we evaluated 200 cells for staining intensity as light mature (L), slightly dark (S) or dark immature (D), whether the slides were processed for CK retention or Bcl-$_{XL}$ immunocytochemistry.

CK activity and HspA2 ratio measurements

These assays were carried out by standard procedures as described previously (Huszar and Vigue, 1990; Huszar *et al*., 1992). Aliquots of semen were washed with 10–15 vols of 4°C 0.15 mol/l NaCl and 30 mmol/l imidazole (buffer, pH 7.0) at 5000 *g* in order to remove seminal fluid. The sperm pellets were disrupted by vortexing in 0.1% Triton, 30 mmol/l imidazole (pH 7.0), 10% glycerol, and 5 mmol/l dithiothreitol. The homogenate was clarified by centrifugation at 5000 *g*, and aliquots of the extract were subjected to CK activity determinations by a spectrophotometric CK kit (Sigma, USA).

The sperm CK-B isoform and the HspA2 were separated by electrophoresis on precast Agarose gels (Helena Laboratories, USA). The separated proteins were detected by overlaying the gel with a fluorescent ATP substrate. The fluorescent bands corresponding to CK-B and HspA2 were quantified under long-wave UV light with a scanning fluorometer. The HspA2 ratio is expressed as % (HspA2/HspA2 + CK-B).

Immunostaining of sperm for CK, Bcl-x_L and caspase-3

The CK immunocytochemistry procedures have been described previously (Huszar and Vigue, 1993; Huszar *et al*., 1994). Both the initial semen and the HA-selected sperm fractions were fixed with 3.7% formaldehyde in phosphate buffer/sucrose (PB-suc) for 20 min at room temperature. After removal of the formalin, the slides were allowed to air dry. After three washing steps with PB-suc, the sperm were exposed to a 3% BSA (blocking solution) in PB-suc at room temperature. After further washing with PB-suc, the slides were covered with 1:1000 dilution of either of polyclonal anti-CK-B antiserum (Chemicon Co., USA), 1:1000 dilution of active caspase-3 (PharMingen, USA), or 1:100 dilution of monoclonal anti-Bcl-$_{XL}$ antibody (Transduction Laboratories, USA) and incubated overnight at 4°C. After the washing steps, single staining of CK, Bcl-$_{XL}$ and caspase-3 was carried out with second antibodies and the slides were visualized with light microscopy. The specificity of the staining was established by using preimmune serum in place of the first antibody, or by applying the second antibody only.

In order to visualize the simultaneous presence of caspase-3 activity and CK retention or Bcl-$_{XL}$ levels in semen sperm or HA-bound sperm fractions, double labelling was performed with antisera in the same dilution as for single staining. In order to visualize the CK/*Caspase-3*, *Caspase-3*/Bcl-x_L and CK-Bcl-$_{XL}$ double markers, caspase-3 immunoreaction was detected by using a 1/400 dilution of alexa flour-350 goat anti-rabbit secondary antibody (Molecular Probes, USA), CK immunoreaction was detected by using a biotinylated anti-goat second antibody (Vector Laboratories, USA) at a 1:1000 dilution and a

1:200 dilution of F/TC (fluorescein isothiocyanate)-labelled avidin (Vector Laboratories) and Bcl-$_{XL}$ immunoreaction was detected by using a 1:200 dilution of PE (phycoerythrin)-labelled goat anti-mouse secondary antibody (Molecular Probes, USA).

Objective morphometry measurements by Metamorph

This computer-based program was developed by Universal Imaging Co. (USA). The details of the methods, along with the validation information, are described in Celik-Ozenci *et al*. (2003).

Briefly, calibration of the system was performed by viewing an objective micrometer scale (OB-M 1/100) at ×100 magnification, and digitizing the image with the Metamorph™ program. The automated conversion of pixels to μm was 0.13 μm/pixel.

After capturing and digitizing the images, Metamorph™ overlay tools were used to delineate the head versus tail regions of individual sperm in order to measure head and tail parameters separately. In the assessment of head parameters, Metamorph™ recognizes the following elements: area (area of entire head); perimeter (distance around edge of head, measuring from midpoints of each pixel that defines its border); long head axis (length of longest diameter); short head axis (width measured perpendicular to the longest diameter); shape factor (a value from 0 to 1 representing how closely the object represents a circle, with 1 being a perfect circle). For the sperm tail measurements, Metamorph™ distinguishes the fibre length (the length of an object, assuming that it is a fibre). In addition, in our laboratory, we have developed a parameter which is not standard to the Metamorph™ program, but which reflects well sperm cellular maturity (Gergely *et al*., 1999): tail length/long head axis. These additional parameters were calculated using Microsoft Excel.

Statistical analysis

In order to compare the various sperm attributes—sperm concentrations and other semen parameters, CK-activity, HspA2 ratios, the staining intensity of the CK and Bcl$_{XL}$ biochemical markers (darkness factor as described in Results), and the morphometry measures—we used the *t*-test analysis and non-parametric comparisons, with the computer-based SigmaStat program (Version 2.0; Jandel Scientific Corp., USA). In testing the various correlations, we have used Pearson correlation analysis utilizing the SigmaStat program. $P < 0.05$ was accepted as significant.

Results

Cytoplasmic retention and Bcl-x_L expression in sperm of various maturity

In focusing upon the relationship between the expression levels of Bcl-$_{XL}$ and of other biochemical markers in human sperm, we studied 30 men, sperm concentration 34.8 ± 4.1×10^6 (min–max: 10–106×10^6), motility 53.3 ± 2.5% (min–max: 27–72%, all data mean ± SEM). Based on the sperm HspA2 ratios, we divided the men into three maturity groups: low (n = 10), intermediate (n = 10) and high (n = 10). The sperm maturity markers of HspA2 ratio and CK activity were significantly different in the three groups, whereas sperm concentrations, motility and total motile sperm concentration were similar (Table I). These data are in agreement with our consistent findings: sperm maturity is largely independent of the sperm concentrations (Huszar and Vigue, 1990, 1993; Huszar *et al*., 1994).

From each sample, we prepared sperm smears and the HA-bound mature sperm fractions. Further, we subjected the slides to immunostaining for CK or Bcl-x_L, and evaluated the proportion of sperm according to their staining intensity. In each sample, we assessed 200 sperm (800 sperm/man, 24 000 sperm in 30 men). The staining intensity of sperm was quantified by the 'darkness factor' using the following scale: unstained clear sperm = 0, partially or slightly stained sperm = 1.5, and darkly stained sperm = 3. For instance, considering 200 sperm: 160 clear, 36 slightly stained, and 4 dark, would yield a darkness factor of 66 (36×1.5 + 4×3). The values reported in Table II are based on the cumulative staining intensity of 200 cells in each sample. The clear, slightly or darkly stained sperm are easily distinguishable when all three types are observed on the same slide (Figure 1).

Table I. The mean HspA2 levels and semen parameters in samples with low, intermediate and high HspA2 ratios

	Low HspA2 (n = 10)	Intermediate HspA2 (n = 10)	High HspA2 (n = 10)
HspA2 (%)	**17.8 ± 1.5**	**31.8 ± 1.6**	**60.5 ± 2.6**
CK activity (IU/10^8)	3.2 ± 0.8	2.3 ± 0.9	0.7 ± 0.2[a]
Sperm concentration (10^6/ml)	27.3 ± 5.9	33.6 ± 3.6	43.6 ± 10.3
Total motile sperm (10^6/ml)	13.6 ± 4.1	19.1 ± 2.5	25.8 ± 6.6
Motility (%)	47.4 ± 4.7	56.8 ± 3.7	56.8 ± 3.7

Values are mean ± SEM.
Values in bold: $P < 0.001$ in all comparisons.
[a]$P < 0.05$ high HspA2 versus intermediate HspA2 and low HspA2 (*t*-test).

Table II. The creatine kinase (CK) and Bcl-x_L darkness factor in the semen and HA-selected sperm fractions

	Low HspA2 (n = 10)	Intermediate HspA2 (n = 10)	High HspA2 (n = 10)
Semen			
CK	**61.3 ± 5**[a]	38.5 ± 3.5[a]	38.2 ± 5[a]
Bcl-x_L	**57.5 ± 5**[b]	33.2 ± 4.2[b]	31.9 ± 5.1[b]
HA-bound			
CK	**25.8 ± 4.1**[a]	20.2 ± 3.3[a]	18.5 ± 3.4[a]
Bcl-x_L	**28.0 ± 5**[b]	17.8 ± 2.3[b]	17.0 ± 3.5[b]

Values are mean ± SEM.
Values in bold: $P < 0.05$, low HspA2 versus intermediate HspA2 and high HspA2 ratios (horizontal comparisons).
[a] and [b]$P < 0.001$ in the respective CK and Bcl-$_{XL}$ values of the semen and HA-bound sperm fractions (vertical comparisons), *t*-test.

The study of the sperm populations arising from semen and of the mature sperm selected by HA binding has further supported the relationship between sperm maturity, the expression levels of CK content (cytoplasmic retention) and Bcl-$_{XL}$ expression levels (Table II). Regarding the three HspA2 maturity groups, both the CK and Bcl-$_{XL}$ darkness factors reflected the maturity-related differences, as they were significantly higher in the low versus the less mature intermediate and high staining intensity groups (Table II, horizontal comparisons). The staining intensity in the vertical comparisons between the sample pairs is substantially lower in the HA-bound versus the semen sperm fraction ($P < 0.001$, Table II).

These staining differences between the low, intermediate and high maturity groups arise because in the semen fractions, there is a mixture of sperm with various degrees of maturity. However, in the respective HA-bound sperm fractions, the staining pattern is lighter by virtue of the plasma membrane maturity and higher HA receptor density, which in turn lead to a higher uniformity of the HA-bound sperm (Huszar *et al*., 1994, 1997, 2003).

The common maturity-related origin among CK activity (cytoplasmic retention), HspA2 ratio and Bcl-x_L expression levels were also reflected by the significant correlations between these markers: in semen (CK versus Bcl-$_{XL}$ $r = 0.71$, $P < 0.001$; HspA2 versus Bcl-$_{XL}$ $r = -0.52$, $P = 0.003$; CK versus HspA2 ratio $r = -0.55$, $P = 0.001$). In the HA-bound sperm fraction: CK versus Bcl-$_{XL}$ $r = 0.75$, $P < 0.001$.

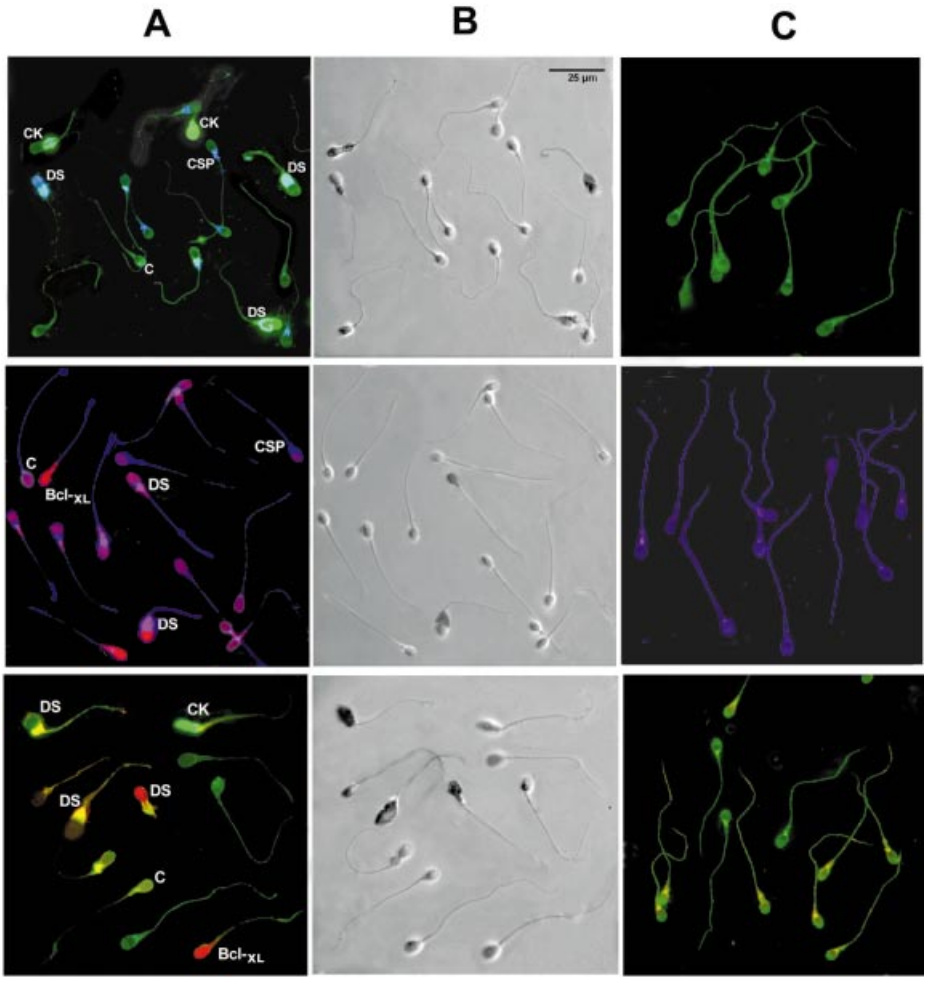

Figure 1. Sperm single- or double-stained for creatine kinase (CK), Bcl-x_L and caspase-3. The fluorescent colour labels are the following: upper row: CK/caspase-3 (green–blue); middle row: caspase-3/Bcl-x_L (blue–red); and lower row: CK/Bcl-x_L (green–red)]. Column A represents sperm originating in semen samples; column B demonstrates the same sperm cells under phase contrast microscopy; and column C represents the respective HA-bound sperm fractions. C = clear; CK = CK positive; CSP = caspase-3 positive; Bcl-$_{XL}$ = Bcl-$_{XL}$ positive; DS = double-stained sperm.

Sperm maturity and levels of active caspase-3 and Bcl-x_L expression

In the next set of experiments, we examined the hypothesis that sperm with diminished maturity may arise either from apoptosis as indicated by the presence of Bcl-$_{XL}$ and active caspase-3, or from a sperm population with a more retarded development exhibiting cytoplasmic retention. We have double-stained semen sperm and their respective HA-bound fractions with the three immuno-marker combinations of *CK/active caspase-3*, *active caspase-3*/Bcl-$_{XL}$ and *CK*/Bcl-$_{XL}$ (Figure 1 upper, middle and lower rows). In the semen fraction (Figure 1A), one can identify sperm with three distinct patterns: clear sperm, single marker-stained sperm with CK, caspase-3 or Bcl-$_{XL}$, and double-stained sperm with the various marker combinations. In the HA-bound mature sperm (Figure 1C), almost all sperm are the clear type.

In order to better understand the respective association between the immunostaining patterns, the HA-binding characteristics and the morphometrical attributes of sperm, we considered three aspects: (i) the types of staining patterns and the proportion of sperm exhibiting particular staining patterns; (ii) the head and midpiece distribution of CK, caspase-3 [with our antibody we are detecting active caspase); (iii) the morphometrical attributes of sperm with various staining patterns.

Staining patterns with CK and active caspase-3 (Figure 1, upper panel)

In the semen fractions we have identified clear sperm, CK-only-stained sperm, caspase-3-only-stained sperm, and sperm that were stained with both CK and caspase-3. In the HA-bound sperm fraction there were a few lightly stained sperm, but no sperm with substantial cytoplasmic retention or caspase activity. This finding is in line with our hypothesis; sperm that stained either for CK or caspase-3 only likely represent sperm subpopulations that are immature due to an early and compensated apoptotic process during spermatogenesis. Conversely, sperm that are double-stained with both CK (cytoplasmic retention) and caspase-3 most likely arise from a combination of arrested development and apoptosis. Finally, it is of note that sperm, whether with the single- or double-staining patterns, are immature as they have not completed membrane remodelling thus are deficient in HA binding.

Sperm double-stained for Bcl-$_{XL}$ and caspase-3, or for CK and Bcl-$_{XL}$ (Figure 1, middle and lower rows), similar to the CK and

Table III. Morphometrical attributes of sperm fractions with various staining patterns (n = 1200 sperm evaluated mean ± SEM)

	Tail length (μm)	Head area (μm²)	Perimeter (μm)	Long axis (μm)	Short axis (μm)	Shape factor	Tail:long axis ratio	n
HA-bound	**62.1 ± 0.2**	**20.6 ± 0.2**	**17.9 ± 0.1**	**6.5 ± 0.03**	**4.5 ± 0.02**	0.82 ± 0.0	**9.7 ± 0.0**	450
Clear	56.3 ± 0.4	21.8 ± 0.3	18.5 ± 0.1	6.6 ± 0.05	4.7 ± 0.04	0.81 ± 0.0	8.6 ± 0.1	180
Caspase-3 only	**46.5 ± 0.5**	**24.0 ± 0.4**	**20.1 ± 0.3**	**7.2 ± 0.08**	4.8 ± 0.05[a]	**0.76 ± 0.01**	**6.6 ± 0.1**	190
CK only	**45.5 ± 0.5**	**26.2 ± 0.5**	**21.1 ± 0.3**	**7.7 ± 0.1**	4.9 ± 0.08[a]	**0.74 ± 0.0**	**6.4 ± 0.1**	140
Bcl-$_{XL}$ only	**45.6 ± 0.3**	21.7 ± 0.6	18.8 ± 0.3	6.8 ± 0.1	4.6 ± 0.9	0.77 ± 0.0[a]	**6.9 ± 0.1**	100
Double-stained sperm	**43.6 ± 0.6**	**28.1 ± 0.7**	**22.2 ± 0.4**	**8.0 ± 0.1**	**5.1 ± 0.09**	**0.72 ± 0.01**	**5.6 ± 0.1**	140

The attributes in each column are compared to respective 'clear' type sperm (underlined).
Values in bold: $P < 0.001$; [a]$P < 0.05$ compared to 'clear' (paired t-test).

caspase-3 staining, showed the four types of pattern, with sperm heads of clear, caspase-3-only, CK-only, Bcl-$_{XL}$-only, or the Bcl-$_{XL}$-caspase-3 and CK-Bcl-x$_L$ double-staining.

Proportions of sperm that showed the various staining patterns

With respect to the proportion of various staining patterns, we have found a remarkable consistency with the three pairs of immunomarker combinations. In the semen fraction, whether with the CK/caspase-3, caspase-3/Bcl-$_{XL}$ or CK/Bcl-$_{XL}$ combinations (Figure 1, upper, middle and lower rows), the mean proportions of clear and double-stained sperm were 45.1 ± 1.0 and 27.7 ± 0.9% (half of the stained sperm), whereas the single-stained sperm with the various probe combinations in the upper, middle and lower rows represented 20.5 ± 1.5, 14.1 ± 2.1 and 6.5 ± 0.5% respectively.

In each study, 300–500 sperm were evaluated in five randomly chosen men. It is of interest that at least two-thirds of semen sperm that stained with caspase-3 were also double-stained with Bcl-$_{XL}$. In the respective HA-bound mature sperm fractions, >90% of the sperm were the clear type. The other four sperm staining patterns, caspase-3-only, CK-only, Bcl-$_{XL}$-only and double-stained sperm, occurred only at a mean <4% incidence.

Regarding the staining in the sperm head or midpiece or in both regions with the various immunomarkers, the CK staining, representing cytoplasmic retention, was localized in the head (25%), in the midpiece (>60%) and in the head + midpiece (18–20% of sperm, Figure 2). This is in agreement with our previous data (Huszar and Vigue, 1993; Gergely *et al*., 1999). Caspase-only staining in the midpiece has occurred with a >92% incidence, whereas the Bcl-$_{XL}$ only pattern in the midpiece was detected in 75–80% of the sperm. Others also noted the prevalence of caspase-3 midpiece staining (Weng *et al*., 2002).

Morphometrical attributes

Regarding sperm dimensions, there were distinct maturity-related differences between the clear and the caspase-3-only, CK-only, Bcl-$_{XL}$-only and double-stained sperm populations. These morphometrical attributes of the sperm populations have provided independent supporting evidence for our hypothesis regarding the different mechanism of how sperm that are single- or double-stained evolve (1200 sperm originating in five men, Table III). The clear sperm had significantly longer tails, smaller and better-shaped heads, as well as higher tail length:long head axis ratios. The sperm with the three types of single staining patterns had tail and head morphometrical attributes that were consistent with diminished maturity sperm compared to both classes of clear mature sperm. Furthermore, the double-stained sperm had significantly shorter tail length and larger head area, circumference and long axis dimensions ($P < 0.001$), indicating a distinct

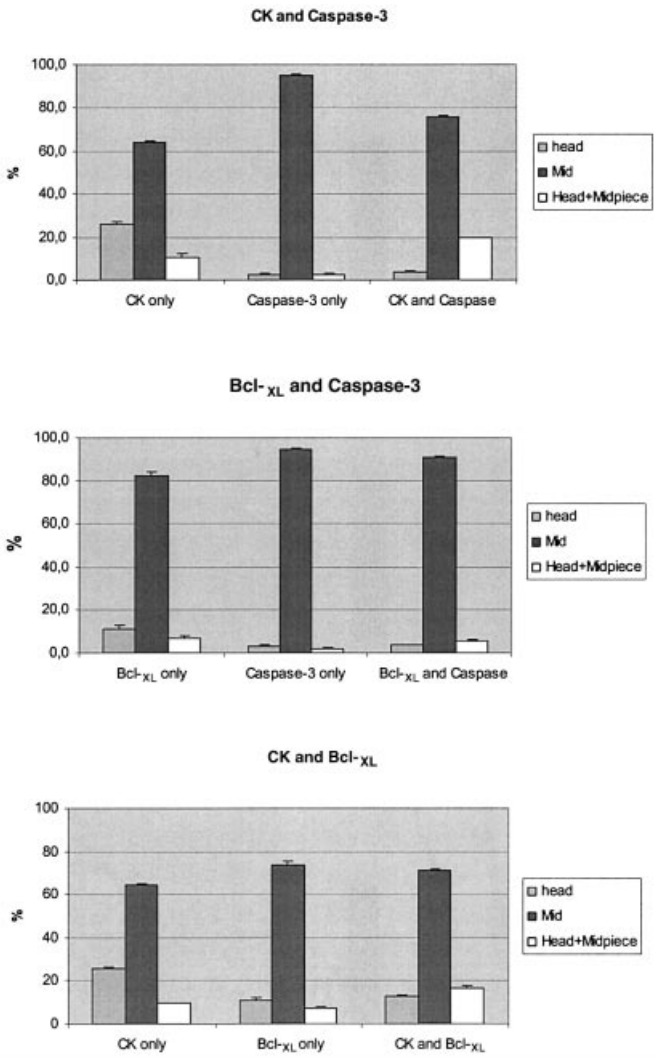

Figure 2. The distribution of head and midpiece staining patterns in sperm exhibiting single or double staining with creatine kinase (CK), Bcl-$_{XL}$ and caspase-3 antisera.

difference between the single-stained and even less mature double-stained sperm population. The sperm populations double-stained with CK/caspase-3, caspase-3/Bcl-$_{XL}$ or with CK/Bcl-$_{XL}$ firmly support the morphometrical and maturity-related differences between the single-stained versus double-stained sperm.

It is of further interest that the HA-bound clear sperm had longer tails, smaller heads and a smaller SEM in all parameters compared to

the clear sperm of semen (Table III). These differences are due to the heterogeneity of clear sperm in semen compared to the uniformity of HA-bound sperm, which is the most mature sperm population selected by the highest density of HA receptor.

The maturation-related decline of tail length and increase in head parameters of area, perimeter and long axis in the five types of sperm are most impressive (Table III). Indeed, the tail of the clear semen sperm is >25% longer and the HA-bound clear sperm are 31% longer than that of the mean of the three classes of stained immature sperm. The head area, perimeter and long head axis is ~15% larger in the stained versus the clear sperm fractions. The maturity-related dimensional differences are best demonstrated by the decline of tail length:long head axis ratios in the HA-bound clear, clear, single-stained or double-stained sperm populations (ratios. 9.1 ± 0.0, 8.6 ± 0.1, 6.6 ± 0.1, 5.6 ± 0.1 respectively, independently from the probe combinations used). The ratio of the double-stained sperm is 35% shorter than that of the clear semen sperm, and 44% shorter compared to populations of HA-bound and clear sperm.

The dimensions of the double-stained sperm whether by the CK/caspase-3, Bcl-$_{XL}$/caspase-3 and CK/Bcl-$_{XL}$ combinations were comparable both in the head and in the tail length:long head axis ratio dimensions. This indicates that these double-stained sperm by the various markers are actually 'triple-stained', i.e. the combination of all these markers, CK, caspase-3 and Bcl-x_L staining. This idea is further supported by the dimensions of the CK/Bcl-$_{XL}$-stained sperm compared to the mean of the CK/caspase-3 and caspase-3/Bcl-$_{XL}$ sperm (in parentheses): tail length: 44.9 μm (44.1); head area: 26.2 μm^2 (27.5); perimeter: 20.0 μm (21.1); long axis 7.3 μm (7.9); short axis 5.0 μm (5.1); shape factor 0.78 (0.72); and tail length/head axis ratio: 6.2 (5.8).

Discussion

During spermatogenesis and spermiogenesis, apoptosis, the controlled degradation of sperm DNA, has been suggested to play a key role in adjusting the appropriate number of proliferating germ cells associated with the surrounding Sertoli cells (Blanco-Rodriguez, 1998; Li *et al*., 2000; Print and Loveland, 2000; Kaufmann *et al*., 2001). The regulation of apoptosis is based on the intracellular dominance of various proteins that induce or inhibit the apoptotic process, such as BAX, Bcl-$_{XL}$, caspase-3 and several key enzymes. Bcl-$_{XL}$ has been previously observed in ejaculated sperm (Sakkas *et al*., 2002). In samples with low sperm concentrations that also have higher incidence of immature sperm, a proportionally higher Bcl-$_{XL}$ expression occurs (Huszar *et al*., 1988; Huszar and Vigue, 1990; Sakkas *et al*., 2002). In the current study, we have found that immature sperm show a proportionally higher level of Bcl-$_{XL}$ and caspase-3 expression. Although the current and previous Bcl-$_{XL}$ data suggest that this anti-apoptotic protein is an important factor in the survival of immature germ cells, and this finding is also supported by the regulation of mouse germ cell survival, it is clear that the balance of both pro- and anti-apoptotic members of the Bcl-2 family are involved in the fate of immature sperm that would otherwise be eliminated by apoptosis (Rucker *et al*., 2000; Sakkas *et al*., 2002).

Our laboratory has focused upon the objective biochemical markers, such as CK-activity and HspA2 ratios, for the evaluation of sperm maturity, function and male fertility (Huszar and Vigue, 1993; Huszar *et al*., 1994, 2000; Ergur *et al*., 2002). It has been shown that diminished expression of the HspA2 chaperone protein is associated with cytoplasmic retention and consequential abnormal morphology, along with changes detectable with objective morphometry, such as the increase in head size or shorter tail length (Gergely *et al*., 1999). The correlation between sperm CK activity and HspA2 ratios was consistently close in several studies ($r \approx -0.7$, $P < 0.001$; Huszar *et al*., 1992; Lalwani *et al*., 1996; Ergur *et al*., 2002). The HspA2 family of chaperone proteins facilitates the intracellular transport of proteins in the elongating spermatids, the repair of DNA strand breaks, and likely supports plasma membrane remodelling and the collection and externalization of surplus cytoplasm (Dix *et al*., 1996; Eddy, 1999; Huszar *et al*., 2000). Diminished maturity sperm with low HspA2 levels have extensive DNA fragmentation, increased rates of aneuploidy and diminished fertility (Huszar *et al*., 1994; Kovanci *et al*., 2001). Mature sperm that are able to bind HA show none of the markers of diminished maturity (Huszar *et al*., 2003). In two blinded studies, we have demonstrated that low levels of sperm HspA2 predicts the failure of pregnancies in couples treated with IVF (Huszar *et al*., 1992; Ergur *et al*., 2002).

The present work has furthered our knowledge on the relationship between sperm maturity and the expression levels of CK, caspase-3 and Bcl-$_{XL}$. We were interested in the mechanism which would allow the conservation of grossly immature sperm in the ejaculate. These sperm cells would be expected to be eliminated in the adluminal area or the epididymis by the ongoing apoptotic process. Focusing on maturity, we divided the 30 men into three groups based on their high, intermediate and low HspA2 levels. The data of Table II clearly indicate that there was a relationship between the HspA2 ratios and the biochemical markers in the three maturity groups and also in semen versus the HA-bound sperm fractions. Another relevant aspect, which highlights the factor of maturity, is the correlations between the darkness factor and HspA2 ratios on one hand and of the various apoptotic markers on the other hand. Furthermore, the most mature sperm fractions bound to HA, which have completed membrane remodelling and have a higher density of HA receptors, showed a very low expression of CK, caspase-3 and Bcl-$_{XL}$ (Figure 1C; Huszar *et al*., 1997, 2003).

Regarding the staining patterns, we have observed sperm that were clear and sperm stained exclusively with CK, caspase-3 or Bcl-$_{XL}$, or were double-stained with the CK/caspase-3, caspase-3/Bcl-$_{XL}$ or CK/Bcl-x_L combinations (Figure 1). It is of interest that the proportions of sperm that were clear, or stained with a single or two markers, were consistent with the various probe combinations. Also, >90% of the HA-bound mature sperm were the clear type (Table III).

The regional distribution of the markers in the various sperm types was also different. The midpiece-stained sperm with caspase-3 occurs with a >90% incidence, whereas the Bcl-$_{XL}$ in the sperm midpiece pattern occurs >75% of the time. However, CK staining, representing cytoplasmic retention, is present in the head only or in head and midpiece in ~60% of the CK-containing sperm (Figure 2). These variations in patterns also indicate that the origin of defect that leads to caspase-3/Bcl-$_{XL}$ or CK expression is different. The dimensions of sperm with single- or double-stained patterns were different from that of the clear sperm, whether one considers the 28% decline in tail length or the 15% increase in the head parameters of area, perimeter and long axis (Table III). Thus, if sperm were stained with single or double markers, they were of lesser maturity compared to the clear sperm populations, as is further indicated by the substantial decline in tail length:long head axis ratios in sperm with arrested maturation.

The uniformity in size of the clear, single- and double-stained sperm by the various probe combinations suggests that the double-stained sperm actually contain all three markers, or 'triple-stained', as they are the very same immature sperm highlighted independently by the three sets of biochemical markers. These staining patterns, regional differences and the morphometrical attributes all support the idea that immature sperm, if they are single- or double (most likely triple)-stained may differ in pathogenesis and extent of compensation in the apoptotic process.

We suggest that the data are consistent with the following concepts. When spermatogenesis, spermiogenesis and sperm maturation proceed normally, the process will yield mature fertilizing sperm with a high level of genetic and functional integrity. However, when sperm development becomes faulty, three alternatives may occur. (i) There is early apoptosis in developing germ cells within the adluminal area. These sperm are eliminated and are not present in the ejaculate. (ii) In other immature cells, caspase-3 is activated, and in response Bcl-$_{XL}$ is also expressed which provides a protective effect that substitutes the presence of HspA2. Other immature sperm (caspase-3 only) may survive without any compensatory Bcl-$_{XL}$ expression, most likely because these cells contain HspA2. The continuing development of immature sperm has been observed in the acrosome formation of the HSP70-2 knockout mice in which the meiotic process is interrupted (Mori *et al*., 1999). (iii) In a third type of sperm with diminished maturity that proceeds to elongated spermatids, there are secondary effects of diminished HspA2 chaperone activity, such as cytoplasmic retention, larger and amorphous heads, lack of sperm membrane remodelling and retarded tail sprouting. These immature sperm are more severely affected, and in these 'triple-stained' sperm there is CK retention, in addition to the caspase-3 and Bcl-$_{XL}$ expression. In general, it is unclear what proportion of developing sperm is represented by the apoptotic and immature ejaculated sperm, and what proportion of the total germ cell population is eliminated by apoptosis prior to ejaculation.

In addition to the consistency of the proportions and dimensions of single or double-stained sperm with the CK/caspase-3, caspase-3/Bcl-$_{XL}$ and CK/ combinations, these diminished maturity sperm have all failed to bind to HA. From the point of view of reproduction, this indicates that the CK-, caspase-3- or Bcl-x_L-stained immature sperm are non-fertilizing in conventional conception based on sperm–zona pellucida interaction.

Future studies will aim to further define the DNA integrity in the different types of sperm observed. The CK-containing sperm, due to their higher level of lipid peroxidation (Aitken *et al*., 1994; Huszar *et al*., 1994) may contain randomly fragmented DNA, whereas the caspase-3-stained sperm may show DNA degradation with a pattern more closely related to apoptosis. The relative proportions of the subpopulations of mature and diminished maturity sperm in the ejaculate are important in defining why men with similar sperm concentrations have different chances of reproductive success. However, it is clear that not all the immature sperm are eliminated during spermatogenesis and spermiogenesis, and that immature sperm may vary in the type of developmental arrest and in protection mechanisms for apoptosis. These variations are likely to explain the persistence of immature sperm in the ejaculate and contribute to sperm polymorphism.

Acknowledgements

This work was supported by the NIH (OH-04061, HD-19505).

References

Aitken RJ, Krausz CS and Buckhinham D (1994) Relationship between biochemical markers for residual cytoplasm, reactive oxygen species generation, and the presence of leukocytes and precursor germ cells in human sperm suspensions. Mol Reprod Dev 39,268–279.

Aitken RJ and Krausz C (2001) Oxidative stress, DNA damage and the Y chromosome. Reproduction 122,497–506.

Beumer TL, Roepers-Gajadien HL, Gademan IS, Lock TM, Kal HB and De Rooij DG (2000) Apoptosis regulation in the testis: involvement of Bcl-2 family members. Mol Reprod Dev 56,353–359.

Blanco-Rodriguez J (1998) A matter of death and life: the significance of germ cell death during spermatogenesis. Int J Androl 21,236–248.

Buzzard KA, Giacca AJ, Killender M and Anderson RL (1998) Heat shock protein 70 modulates pathways of stress-induced apoptosis. J Biol Chem 273,17147–17153.

Celik-Ozenci C, Jakab A, Vigue L, Demir R and Huszar G (2002) Mature and fertile sperm selectively bind to hyaluronic acid: cytoplasmic content, HspA2 levels, chromatin maturity, shape and ICSI sperm selection. J Gynecol Invest 9(49th SGI annual meeting; No. 1, Suppl 849),340A.

Celik-Ozenci C, Catalanotti J, Jakab A, Aksu C, Ward D, Bray-Ward P, Demir R and Huszar G (2003) Human sperm maintain their shape following decondensation and denaturation for FISH: shape analysis and objective morphometry. Biol Reprod 69,1347–1355.

De Kretser DM, Loveland KL, Meihardt A, Simorangkir D and Wreford N (1998) Spermatogenesis. Hum Reprod 13,1–8.

Dix DJ, Allen JW, Collins BW, Mori C, Nakamura N, Poorman-Allen P, Goulding EH and Eddy EM (1996) Targeted gene disruption of Hsp70-2 results in failed meiosis, germ cell apoptosis, and male infertility. Proc Natl Acad Sci USA 93,3264–3268.

Eddy EM (1999) Role of heat shock protein HSP70-2 in spermatogenesis. Rev Reprod 4,23–30.

Ergur AR, Dokras A, Giraldo JL, Habana A, Kovanci E and Huszar G (2002) Sperm maturity and treatment choice of in vitro fertilization (IVF) or intracytoplasmic sperm injection: diminished sperm HspA2 chaperone levels predict IVF failure. Fertil Steril 77,910–918.

Gandini L, Lombardo F, Paoli D, Caponecchia L, Familiari G, Verlengia C, Dondero F and Lenzi A (2000) Study of apoptotic DNA fragmentation in human spermatozoa. Hum Reprod 15,830–839.

Garrido C, Gurbuxani S, Ravagnan L and Kroemer G (2001) Heat shock proteins: endogenous modulators of apoptotic cell death. Biochem Biophys Res Commun 286,433–442.

Gergely A, Kovanci E, Senturk L, Cosmi E, Vigue L and Huszar G (1999) Morphometric assessment of mature and diminished-maturity human spermatozoa: sperm regions that reflect differences in maturity. Hum Reprod 14,2007–2014.

Huszar G and Vigue L (1990) Spermatogenesis-related change in the synthesis of the creatine kinase B-type and M-type isoforms in human spermatozoa. Mol Reprod Dev 25,258–262.

Huszar G and Vigue L (1993) Incomplete development of human spermatozoa is associated with increased creatine phosphokinase concentration and abnormal head morphology. Mol Reprod Dev 34,292–298.

Huszar G. and Vigue L (1994) Correlation between the rate of lipid peroxidation and cellular maturity as measured by creatine kinase activity in human spermatozoa. J Androl 15,71–77.

Huszar G, Corrales M and Vigue L (1988) Correlation between sperm creatine phosphokinase activity and sperm concentrations in normospermic and oligospermic men. Gamete Res 19,67–75.

Huszar G, Vigue L and Morshedi M (1992) Sperm creatine phosphokinase M-isoform ratios and fertilizing potential of men: a blinded study of 84 couples treated with in vitro fertilization. Fertil Steril 57,882–888.

Huszar G, Vigue L and Oehninger S (1994) Creatine kinase immunocytochemistry of human sperm-hemizona complexes: selective binding of sperm with mature creatine kinase-staining pattern. Fertil Steril 61,136–142.

Huszar G, Sbracia M, Vigue L, Miller DJ and Shur BD (1997) Sperm plasma membrane remodeling during spermiogenetic maturation in men: relationship among plasma membrane beta 1,4-galactosyltransferase, cytoplasmic creatine phosphokinase, and creatine phosphokinase isoform ratios. Biol Reprod 56,1020–1024.

Huszar G, Stone K, Dix D and Vigue L (2000) Putative creatine kinase M-isoform in human sperm is identified as the 70-kilodalton heat shock protein HspA2. Biol Reprod 63,925–932.

Huszar G, Celik-Ozenci C, Cayli S, Zavaczki Z, Hansch E and Vigue L (2003) Hyaluronic acid binding by human sperm indicates cellular maturity, viability and unreacted acrosomal status. Fertil Steril 79,1616–1624.

Irvine DS, Twigg JP, Gordon EL, Fulton N, Milne PA and Aitken RJ (2000) DNA integrity in human spermatozoa: relationships with semen quality. J Androl 21,33–44.

Kaufmann SH and Hengartner MO (2001) Programmed cell death: alive and well in the new millennium. Trends Cell Biol 11,526–534.

Kovanci E, Kovacs T, Moretti E, Vigue L, Bray-Ward P, Ward DC and Huszar G (2001) FISH assessment of aneuploidy frequencies in mature and immature human spermatozoa classified by the absence or presence of cytoplasmic retention. Hum Reprod 16,1209–1217.

Lalwani S, Sayme N, Vigue L, Corrales M and Huszar G (1996) Biochemical markers of early and late spermatogenesis: relationship between the lactate

dehydrogenase-X and creatine kinase-M isoform concentrations in human spermatozoa. Mol Reprod Dev 43,495–502.

Li CY, Lee JS, Ko YG, Kim J and Seo JS (2000) Heat shock protein 70 inhibits apoptosis downstream of cytochrome c release and upstream of caspase-3 activation. J Biol Chem 275,25665–25671.

Manicardi GC, Bianchi PG, Pantano S, Azzoni P, Bizzaro D, Bianchi U and Sakkas D (1995) Presence of endogenous nicks in DNA of ejaculated human spermatozoa and its relationship to chromomycin A3 accessibility. Biol Reprod 52,864–867.

Manicardi GC, Tombacco A, Bizzaro D, Bianchi U, Bianchi PG and Sakkas D (1998) DNA strand breaks in ejaculated human spermatozoa: comparison of susceptibility to the nick translation and terminal transferase assays. Histochem J 30,33–39.

Mori C, Allen JW, Dix DJ, Nakamura N, Fujioka M, Toshimori K and Eddy EM (1999) Completion of meiosis is not always required for acrosome formation in HSP70-2 null mice. Biol Reprod 61,813–822.

Óvári L, Vigue L, Stronk J, Borsos A, Ward D, Ward P and Huszar G (2003) Detection of numerical chrosomal aberrartions and nuclear immaturity within in the same spermatozoa: a study of FISH and Aniline blue staining. Hum Reprod 18(Suppl 1), p. xviii, 79.

Parcellier A, Gurbuxani S, Schmitt E, Solary E and Garrido C (2003) Heat shock proteins, cellular chaperones that modulate mitochondrial cell death pathways. Biochem Biophys Res Commun 304,505–512.

Print CG and Loveland KL (2000) Germ cell suicide: new insights into apoptosis during spermatogenesis. Bioessays 25,423–430.

Ricci G, Perticarari S, Fragonas E, Giolo E, Canova S, Pozzobon C, Guaschino S and Presani G (2002) Apoptosis in human sperm: its correlation with semen quality and the presence of leukocytes. Hum Reprod 17,2665–2672.

RuckerIII EB, Dierisseau P, Wagner K-U, Garrett L, Wynshaw-Boris A, Flaws JA and Henninghausen L (2000) Bcl-x and BAX regulate mouse primordial germ cell survival and apoptosis during embryogenesis. Mol Endocrinol 14,1038–1052.

Sakkas D, Mariethoz E and St John JC (1999a) Abnormal sperm parameters in humans are indicative of an abortive apoptotic mechanism linked to the Fas-mediated pathway. Exp Cell Res 251,350–355.

Sakkas D, Mariethoz E, Manicardi G, Bizzaro D, Bianchi PG and Bianchi U (1999b) Origin of DNA damage in ejaculated human spermatozoa. Rev Reprod 4,31–37.

Sakkas D, Moffatt O, Manicardi GC, Mariethoz E, Tarozzi N and Bizzaro D (2002) Nature of DNA damage in ejaculated human spermatozoa and the possible involvement of apoptosis. Biol Reprod 66,1061–1067.

Sbracia M, Grasso J, Sayme N, Stronk J and Huszar G (1997) Hyaluronic acid substantially increases the retention of motility in cryopreserved/thawed human spermatozoa. Hum Reprod 12,1949–1954.

Shen HM, Dai J, Chia SE, Lim A and Ong CN (2002) Detection of apoptotic alterations in sperm in subfertile patients and their correlations with sperm quality. Hum Reprod 17,1266–1273.

Steger K, Klonisch T, Gavenis K, Drabent B, Doenecke D and Bergmann M (1998) Expression of mRNA and protein of nucleoproteins during human spermiogenesis. Mol Hum Reprod 4,939–945.

Wei YQ, Zhao X, Kariya Y, Fukata H, Teshigawara K and Uchida A (1994) Induction of apoptosis by quercetin: involvement of heat shock protein. Cancer Res 54,4952–4957.

Wei YQ, Zhao X, Kariya Y, Teshigawara K and Uchida A (1995) Inhibition of proliferation and induction of apoptosis by abrogation of heat-shock protein (HSP) 70 expression in tumor cells. Cancer Immunol Immunother **40**,73–78.

Weng SL, Taylor SL, Morshedi M, Schuffner A, Duran EH, Beebe S and Oehninger S (2002) Caspase activity and apoptotic markers in ejaculated human sperm. Mol Hum Reprod 8,984–991.

World Health Organization (1999) WHO Laboratory Manual for the Examination of Human Semen and Sperm–Cervical Mucus Interaction. 4th edn, Cambridge University Press, Cambridge, UK.

Submitted on January 20, 2004; accepted on February 19, 2004

RBM Online - Vol 7. No 4. 462–468 Reproductive BioMedicine Online; www.rbmonline.com/Article/1020 on web 12 August 2003

Article

Biochemical markers of sperm function: male fertility and sperm selection for ICSI

Dr Gabor Huszar

The senior author, Gabor Huszar, is Senior Research Scientist, and Director of Male Infertility and of the Sperm Physiology Laboratory at the Department of Obstetrics and Gynecology, Yale University School of Medicine, USA. His scientific goal is to develop concepts in the laboratory that are directly applicable to patient care. Dr Huszar has contributed to three different fields: (i) to muscle diseases by discovering tissue, species, and developmental differences in myosin structure; (ii) preterm labour and the concept of common regulation of the myometrium and cervix in pregnancy and labour; (iii) the objective biochemical markers of sperm maturity and function, and male infertility. Dr Huszar's group found a relationship between genetic integrity and membrane structure in human spermatozoa, a concept that led to an ICSI selection method that eliminates spermatozoa with disomies, diploidies and fragmented DNA.

S Cayli[1,3], A Jakab[4], L Ovari[4], E Delpiano[5], C Celik-Ozenci[3], D Sakkas[1], D Ward[2], G Huszar[1,6]
[1]The Sperm Physiology and IVF Laboratories, Department of Obstetrics and Gynecology, [2]Department of Genetics Yale University School of Medicine, 333 Cedar Street, New Haven, CT 06510 USA
[3]Akdeniz University, Antalya, Turkey
[4]Department of Obstetrics and Gynaecology, University of Debrecen, Hungary
[5]Department of Obstetrics and Gynaecology, University of Torino, Italy
[6]Correspondence: Tel: +1 203 7854010; Fax: +1 203 7371200; e-mail: gabor.huszar@yale.edu

Abstract

The expression of a 70 kDa chaperone protein, HspA2 (formerly called CK-M), has been identified in mature human spermatozoa. The central role of HspA2 has been established, as the expression level of this protein is related to sperm cellular maturity, DNA integrity, chromatin maturity, chromosomal aneuploidy frequency and sperm function, including fertilizing potential. The spermiogenetic events of cytoplasmic extrusion and remodelling of the plasma membrane, which facilitate the formation of zona pellucida binding site(s) in human spermatozoa, are related. Finally, the presence of the hyaluronic acid (HA) receptor on the plasma membrane of mature sperm coupled with the HA-coated slide sperm-binding assay, facilitates the testing of infertile men and the selection of single mature spermatozoa for ICSI. Because mature spermatozoa have no residual cytoplasm, the HA-bound sperm fraction is also enriched in spermatozoa that are normal by the Kruger strict morphology method.

Keywords: *chromosomal aneuploidies, human sperm function, hyaluronic acid binding, ICSI sperm selection, maturity, strict morphology*

Introduction

Much research is being focused on the objective biochemical markers of sperm maturity and function. In the past 3 years, advances have been made on the clinical application of the hyaluronic acid (HA) binding assay of human spermatozoa, a test of sperm maturity and fertilizing potential, which also reflects DNA integrity and aneuploidy frequency. Sperm–HA binding also facilitates the selection of individual mature spermatozoa for intracytoplasmic sperm injection (ICSI). The following key points will be discussed: (i) cytoplasmic retention as an evidence of sperm immaturity, and the two-wave expression pattern of the testis-specific HspA2 chaperone protein during meiosis and late spermiogenesis; (ii) cellular maturation, plasma membrane remodelling and their contributions to fertilization function of human spermatozoa; (iii) relationship between sperm immaturity and increased frequencies of chromosomal aneuploidy; (iv) relationship between diminished sperm cellular maturity, persistent histones and diminished DNA integrity; (v) semen analysis and assessment of sperm maturity by HA binding in a double chamber device; (vi) relationship between HA-binding ability of spermatozoa and Kruger strict morphology parameters; and (vii) selection of mature individual spermatozoa with low levels of chromosomal aneuploidy and high DNA integrity.

Biochemical markers of sperm cellular maturation

The primary interest of this research has been the development of objective biochemical markers of human sperm maturity and function, which would predict male fertility, independently from the traditional semen criteria of sperm concentration and motility. In measurements of sperm creatine-N-phosphotransferase or creatine kinase (CK), significantly higher sperm CK activities have been found in men

with diminished fertility (Huszar *et al*., 1988a,b). The research has addressed reasons underlying the sperm CK activity differences by direct visualization of the CK in individual spermatozoa with CK immunocytochemistry (Huszar and Vigue, 1993). The autoradiographic and CK immunostaining patterns indicated that the high sperm CK activity was a direct consequence of increased cytoplasmic protein and CK concentrations in the spermatozoon. The combination of increased CK and protein concentrations, coupled with the diminished fertility, suggested the identification of a sperm developmental defect in the last phase of spermiogenesis when the cytoplasm (unnecessary for the mature spermatozoon) normally is extruded and left in the adluminal area as 'residual bodies' (Clermont, 1963).

Following electrophoretic analysis of human sperm extracts, in addition to the CK-B isoform, another ATP-containing protein was found, which was proportional to the incidence of mature spermatozoa characterized by low CK activity and no cytoplasmic retention in the semen samples (Huszar and Vigue, 1990). This developmentally regulated protein has been identified as the 70 kDa testis-expressed chaperone protein, which in humans is called HspA2 (Huszar *et al*., 2000). The close inverse correlation between the proportions of spermatozoa with cytoplasmic retention and low expression of HspA2 and those spermatozoa with lack of cytoplasmic retention and increased expression of HspA2 indicated that cytoplasmic extrusion and commencement of the HspA2 synthesis are related, developmentally regulated spermiogenetic events. In three independent studies, the correlation between HspA2 levels and CK activity was $r = -0.69, -0.71$ and -0.76 ($P < 0.001$, $n = 159$, 134, and 119) (Huszar *et al*., 1990; Lalwani *et al*., 1996; Ergur *et al*., 2002). It was established that all sperm maturational events related to the decline of CK activity and increase in HspA2 expression are completed by the time the spermatozoa enter the caput epididymidis (Huszar *et al*., 1998).

HspA2 which, due to its electrophoretic properties and ATP content, was initially assumed to be an unusual form of sperm specific CK-M isoform (several properties have also indicated that it was not a conventional CK-M; Huszar and Vigue, 1990), proved to be a most useful objective biochemical marker. It has been shown that mature and immature spermatozoa are different with respect to HspA2 ratio, as expressed by the concentrations of sperm CK and HspA2 [%HspA2/(HspA2 + CK-B)], morphological and morphometrical attributes, zona pellucida-binding properties and fertility (Huszar *et al*., 1992, 1994). Furthermore, it has been established that in spermiogenesis, simultaneously with cytoplasmic extrusion and the commencement of HspA2 synthesis, the sperm plasma membrane also undergoes maturation-related remodelling. This remodelling step facilitates the formation of the sites and receptors for zona binding and for hyaluronic acid binding in mature spermatozoa (Huszar *et al*., 1997).

Sperm maturity and fertilization function

The predictive value of CK activity, representing cytoplasmic retention, was tested in couples with oligozoospermic husbands treated with intrauterine insemination. In spite of identical sperm concentration and motility parameters in husbands of those couples that have or have not achieved pregnancy, those with pregnancies had four times lower sperm CK activity ($P < 0.001$). In addition, a logistic regression analysis indicated that sperm CK activity, but not sperm concentrations, contributed significantly to the predictive power (Huszar *et al*., 1990).

The validity of HspA2 ratio in the assessment of male fertility was tested in two blinded studies of couples undergoing IVF. In the first, 84 husbands from two different IVF centres were classified (without any information on their semen parameters or reproductive histories) based only on their sperm HspA2 ratios into 'high likelihood' (>10% HspA2 ratio) and 'low likelihood' (<10% HspA2 ratio) for fertility groups. All pregnancies occurred in the 'high likelihood' group. No pregnancy occurred in the 'low likelihood' group. In the 'high likelihood' group, if at least one oocyte was fertilized, indicating the lack of oocyte defects in the wife, the predictive rate of HspA2 ratio for pregnancy was a very high 30.4% per cycle. An additional important utility of the HspA2 ratio became apparent: nine of the 22 'low likelihood' men were normozoospermic, but had diminished fertility. Thus, the HspA2 ratio provided, for the first time, a diagnostic tool for unexplained male infertility (infertile men with normal semen, Huszar *et al*., 1992).

Morphometrical differences have also been demonstrated between mature and diminished maturity spermatozoa (Gergely *et al*., 1999). More recently, the utility of CK-M ratios in predicting IVF failure has been examined in 119 couples treated at Yale. Similar to the 1992 study, none of the 25 men with <10% CK-M ratios was able to father children, whether they had low or high sperm concentrations (Ergur *et al*., 2002). The value of sperm CK studies has also been confirmed by other laboratories (Gomez *et al*., 1996; Orlando *et al*., 1994; Sidhu *et al*., 1998).

It has also been established that sperm samples with high CK activities and cytoplasmic retention have proportionally higher levels of lipid peroxidation (Aitken *et al*., 1994; Huszar and Vigue, 1994). Due to the high level of reactive oxygen species, there is increased degradation of DNA, which contributes to the diminished ability of the spermatozoon to provide the paternal contribution to the zygote. The high level of lipid peroxidation has not affected normal spermatozoa without cytoplasmic retention, even if incubated in sperm pellets with high reactive oxygen species producing spermatozoa. For this reason, it has been concluded that the high level of lipid peroxidation in spermatozoa is an 'inborn' error, rather than an 'acquired' property (Huszar and Vigue, 1994). In a recent review, the factors that characterize immature spermatozoa with defective function, such as cytoplasmic retention and consequential abnormal sperm morphology, high level of lipid peroxidation, DNA fragmentation and aneuploidies, were cited as key elements in the aetiology of human infertility and genetic mutations in the offspring (Aitken *et al*., 2003). It is of interest that the potential relationship between diminished sperm maturity and aspects of male germ cell apoptosis is not yet understood (Henkel *et al*., 2003; Oehninger *et al*., 2003).

To identify the steps in the fertilization process at which the low HspA2 immature spermatozoa are deficient, human sperm–oocyte binding was explored. With the study of sperm–hemizona complexes, it was established that only the

clear headed (low CK), mature spermatozoa were able to bind to the zona (Huszar *et al*., 1994; **Figure 1**). Spermatozoa with retained cytoplasm were deficient in the oocyte binding site. In a further study, it was confirmed that plasma membrane remodelling occurs in human spermatozoa, simultaneously with cytoplasmic extrusion, during spermiogenetic maturation. This was demonstrated by the close correlation (r = 0.8) between CK concentration or the HspA2 ratio and the density of the sperm plasma membrane-specific enzyme $\beta_{1,2}$-galactosyltransferase in sperm fractions of various maturities (Huszar *et al*., 1997). Such remodelling apparently facilitates the formation of the zona pellucida- and hyaluronic acid-binding sites. This finding explains two major characteristics of spermatozoa with diminished maturity: cytoplasmic retention and deficiency in zona pellucida binding (Huszar and Vigue 1993, 1994; Huszar *et al*. 2000).

In general, chaperone proteins facilitate the assembly and intracellular transport of proteins. Indeed, the expression of HspA2 is simultaneous with major sperm protein movements underlying cytoplasmic extrusion and remodelling of the human sperm plasma membrane. This in turn facilitates the development of zona pellucida-binding site(s). It is thought that retention of the cytoplasm, and the lack of zona-binding sites in immature spermatozoa, are probably related to the diminished expression of HspA2, and also to diminished DNA integrity, as a consequence of the impaired delivery of DNA repair enzymes during and following meiosis. In order to confirm findings regarding the expression of HspA2 during terminal spermiogenesis, the expression pattern of HspA2 in human testicular tissue was also examined (**Figure 2**). Varying low levels of immunostaining were evident in spermatocytes and spermatids, reflecting the presence of HspA2, which was also identified in mouse spermiogenesis in the synaptonemal complexes. However, the staining was particularly striking in the cytoplasm of elongating spermatids and mature spermatozoa about to be released from the adluminal compartment (Huszar and Vigue, 1990; Huszar *et al*., 2000).

From the perspective of male infertility, it is important that synthesis of the 70 kDa family of testis-specific chaperone proteins is developmentally regulated. In the mouse, the chaperone protein homologous to HspA2 is the Hsp70-2, which arises from a different gene. Another member of this family is hsc70, which in the mouse is expressed in terminal spermiogenesis, and has not yet been identified in human testis (Eddy, 2002). Hsp70-2 in mice appears during meiotic prophase as a component of the synaptonemal complexes. The apparent functions of Hsp70-2 are maintaining the synaptonemal complexes and assisting chromosome crossing over during meiosis and spermatocyte development (Allen *et al*., 1996). Accordingly, the targeted disruption of the *hsp70-2* gene causes arrested sperm maturation and azoospermia (Dix, 1997). These events could be related to faulty meiotic recombination in spermatocytes, disruption of the meiotic cell cycle regulatory machinery, or perhaps to a more direct disruption of the apoptotic machinery in spermatocytes or even in spermatids or ejaculated immature spermatozoa (Dix, 1997). Regarding human spermatozoa, this was the first demonstration of the expression pattern of the HspA2 protein in human testis and spermatozoa and correlation of the expression level of HspA2 to sperm function (Huszar *et al*., 2000). Because maturational differences in cytoplasmic content, plasma membrane remodelling, DNA integrity and aneuploidy rates had already been identified, subsequent studies explored whether the plasma membrane structure differences and features specific for mature spermatozoa could facilitate the selection of mature spermatozoa for ICSI.

Diminished sperm maturity: DNA integrity and chromosomal aneuploidies

Because HspA2 is a component of the synaptonemal complex, it was postulated that the frequency of chromosomal aneuploidies will be higher in immature versus mature spermatozoa (Kovanci *et al*., 2001). This question has been examined in spermatozoa from semen and from 80% Percoll pellets (enhanced in mature spermatozoa) of the same ejaculate in 10 oligozoospermic men. Immature spermatozoa with retained cytoplasm, which signifies spermiogenetic arrest, were identified by immunocytochemistry. Approximately 7000 sperm nuclei were evaluated with fluorescence in-situ hybridization (FISH) in each of the 20 fractions (142,086 spermatozoa in all) using centromeric probes for the X, Y, and 17 chromosomes. The proportions of immature spermatozoa (as detected by cytoplasmic retention) were 45.4 ± 3.4 versus 26.6 ± 2.2% in the two groups (medians: 48.2 versus 25%, $P <$ 0.001, n = 300 spermatozoa evaluated per fraction, 6000 spermatozoa in all). There was also a concomitant decline in total disomy, total diploidy and total aneuploidy frequencies in the 80% Percoll versus semen fractions (0.17 versus 0.54%, 0.14 versus 0.26% and 0.31 versus 0.81%, respectively, $P <$ 0.001 in all comparisons). The mean decline of aneuploidies was 2.7-fold. Regarding the hypothesis that aneuploidies are related to sperm immaturity, there was a close correlation between the incidence of immature spermatozoa and disomies ($r = 0.7, P < 0.001$), indicating that disomies originate primarily in immature spermatozoa. Thus, the idea that the common factor underlying sperm immaturity and aneuploidies is the diminished expression of the HspA2 appears to be valid (Huszar *et al*., 2000; Kovanci *et al*., 2001).

In another study, it was found that the elimination of disomic spermatozoa with diminished maturity was more effective with gradient centrifugation, whereas spermatozoa with diploidy were more reduced in semen fractions prepared by the swim-up approach (Jakab *et al*., 2003).

Association between chromosomal aneuploidies and nuclear immaturity

As discussed, during spermiogenesis there are concurrent nuclear and cytoplasmic processes in the developing male germ cell, including histone–protamine replacement, cytoplasmic extrusion, plasma membrane remodelling and formation of the acrosome and tail.

Studies have looked for a relationship between numerical chromosomal aberrations and persistent histones, potentially indicating that errors in the spermatogenetic and spermiogenetic phases simultaneously occur in immature spermatozoa.

In seven moderately oligozoospermic men, an average of 8399 spermatozoa (58,793 spermatozoa in all) were evaluated for aniline blue staining pattern as light (L, most mature spermatozoa), intermediate (IN) and dark (D, immature spermatozoa). The FISH patterns of sperm nuclei were scored by strict criteria. The images of the aniline blue-treated spermatozoa were digitized and saved, along with their field locations on the slides, using the Metamorph program (Universal Imageing Co., PA, USA) for identification following FISH step as spermatozoa having normal, disomic or diploid nuclei. It was found that immature sperm cells with D aniline blue histone staining showed no FISH signals. It is unclear whether this was due to a failure of DNA uncoiling during decondensation, or to a high degree of DNA degradation, which is known to occur in immature spermatozoa. The spermatozoa with L and IN patterns showed normal decondensation and easily evaluable FISH signals. There was an aggregate five-fold increase in the frequency of disomies in the IN versus the mature L pattern spermatozoa. The relationship between disomies and nuclear immaturity was further emphasized by the close correlation between proportions of spermatozoa with the IN pattern and total disomy rates ($r = 0.76$, $P < 0.05$; Óvári *et al*., 2003).

These results, using double nuclear detection probes of human spermatozoa, indicate that diminished maturity spermatozoa show defects in both the spermatogenetic and spermiogenetic phases of male germ cell development. The close relationship between occurrence of persistent histones and chromosomal disomies further points to the common origin of the defects: low expression levels of the HspA2 chaperone protein.

Sperm–HA-binding assay: a test of sperm maturity and fertility

Current ideas on sperm maturation in men are summarized in **Figure 3**. Looking for the reason underlying for diminished zona binding by immature spermatozoa, it has been established that in spermiogenesis, simultaneously with cytoplasmic extrusion and the commencement of HspA2 synthesis, the sperm plasma membrane also undergoes maturation-related remodelling that promotes the formation of zona-binding and HA-binding sites. Thus, in immature spermatozoa with cytoplasmic retention, there is a low density of zona-binding sites and also of HA receptors (Huszar *et al*., 1997, 2003).

Based on the above concepts, three questions were examined. Firstly, would spermatozoa bind permanently to solid state hyaluronic acid? Secondly, the diagnostic utility of sperm binding to HA was examined, in a double chamber device in which the A side provided the measures of sperm concentration and motility (thus motile sperm concentration), and the B side was coated with HA in order to test the proportion of mature sperm exhibiting HA binding. Finally, the potential correlation between sperm CK activity or sperm HspA2 expression (proven clinical utility in predicting diminished fertility), increase in the proportion of sperm with strict morphology within the HA-bound sperm fraction, and the rate of sperm binding to HA were studied. The results are described below.

Sperm binds to HA

There were three sperm populations: (i) spermatozoa permanently bound to HA; (ii) spermatozoa exhibiting no binding; (iii) a small proportion of spermatozoa (<5%) that has initially bound to HA, was released shortly, and rebound again. These three patterns were interpreted as mature spermatozoa with high density HA receptor, immature spermatozoa with deficient maturity and plasma membrane remodelling, and spermatozoa of intermediate maturity with a low density of HA receptors (**Figure 4**). The specificity of HA binding has been determined by two methods. First, HA was left out from the slide coating mixture. Spermatozoa no longer bound to the slide. Using various polymers, similar to HA, in the coating mixture did not result in sperm binding. Adding HA to the solution, thus saturating the HA receptors, caused a decline in binding efficiency. Unfortunately, no specific antibodies to the HA receptor are yet available, thus it was impossible to perform definitive binding inhibition experiments. These experiments will be performed as soon as the reagents are available (Huszar *et al*., 2003).

In the HA-binding experiments, points of further interest have been found. If the spermatozoa were non-viable, they did not bind to HA. Thus, membrane integrity is closely related to binding ability. The potential relationship between HA binding and acrosomal integrity has also been explored, by following the FITC–*Pisum sativum* fluorescence pattern. The data indicate that spermatozoa with intact or slightly reacted acrosomal cap are able to bind to HA. However, spermatozoa with a further advanced activation state are non-binders. Thus it appears, in line with the top of the cap binding pattern, that the HA receptors are localized on the acrosomal membrane.

Correlation of binding with sperm maturity markers

When the relationship between sperm binding and CK activity ($n = 50$ men) was studied, a strong correlation ($r = -0.56$, $P < 0.001$) was found, which is a well-characterized sperm maturity marker (**Figure 5**). The fact that the correlation was closer with CK activity, as compared with the HspA2 ratio (data not shown), is an expected effect because the membrane remodelling and the formation of the HA receptor sites occur simultaneously with cytoplasmic extrusion, whereas HspA2 expression occurs in two waves (in meiotic spermatocytes as a part of the synaptenomal complex and in terminal spermatogenesis when the cytoplasm is extruded); thus it is not directly related to membrane remodelling.

Diagnostic utility of sperm binding to HA

Finally, CK activities, HspA2 ratios and per cent binding of spermatozoa to HA-coated slides were evaluated in 46 men. With respect to binding, sperm populations were classified as follows: >90% ($n = 26$) were excellent, between 60–90% ($n = 12$) were intermediate, and <60% ($n = 8$) were diminished binders. In line with previous findings with respect to CK and HspA2, the sperm binding scores were largely independent from sperm concentration. Among men within the $<20 \times 10^6$ spermatozoa/ml concentration range ($n = 14$ of 56 men), three excellent, five moderate, and six diminished HA binders were identified.

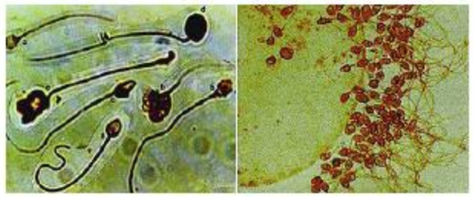

Figure 1. *Left*, panel of immature/mature sperm after CK immunostaining of the retained cytoplasm. *Right*, CK immunostained sperm–hemizona complex. Observe that only the clear headed mature spermatozoa without cytoplasmic retention are able to bind.

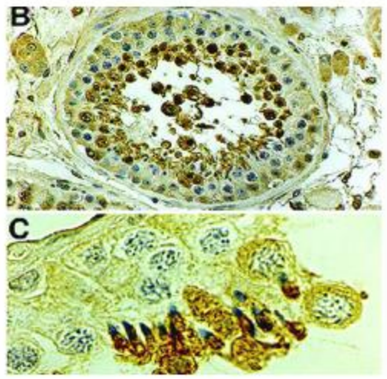

Figure 2. Human testicular biopsy tissues immunostained with human HspA2 antiserum. Sections B and C in the composites represent different magnifications to illustrate the tubular structure, and the staining pattern of the adluminal area. HspA2 expression begins in meiotic spermatocytes, but is predominant during terminal spermiogenesis in the elongated spermatids and spermatozoa.

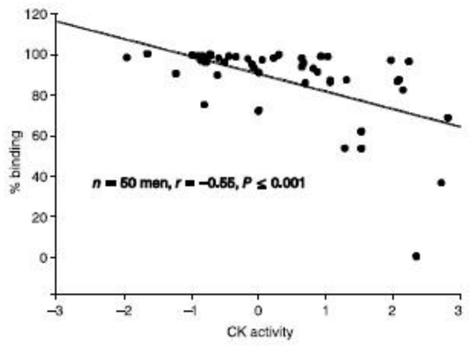

Figure 5. Correlation between HA binding and CK activity.

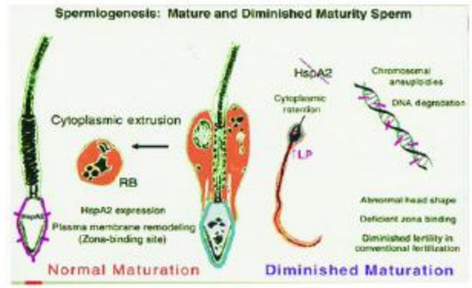

Figure 3. A model of normal and diminished maturation of human spermatozoa. In normal sperm maturation, HspA2 is expressed in the synaptonemal complex of spermatocytes, supporting meiosis. HspA2 is probably also involved in the processes of late spermiogenesis, such as cytoplasmic extrusion (represented by the loss of residual body, RB), plasma membrane remodelling, and the formation of the zona pellucida-binding site (change from the blue to the red membrane and the stubs). Diminished maturity spermatozoa lack HspA2 expression, which causes meiotic defects and a higher rate of retention of CK and other cytoplasmic enzymes, increased levels of lipid peroxidation (LP) and consequent DNA fragmentation, abnormal sperm morphology and deficiency in zona-binding and HA-binding sites.

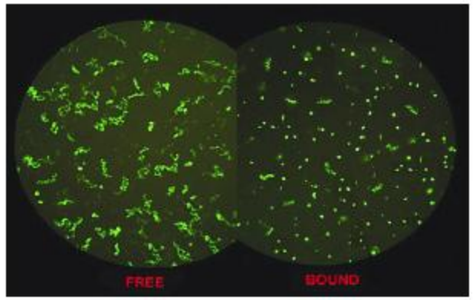

Figure 4. Sperm movement patterns in the double chamber device. A side: uncoated glass chamber with patterns of motile sperm. B side: mature spermatozoa are bound, and diminished motility spermatozoa remain motile in the HA-coated chamber. Spermatozoa are stained with Cyber green DNA stain (Molecular Probes, Eugene, Oregon) that permeates viable spermatozoa.

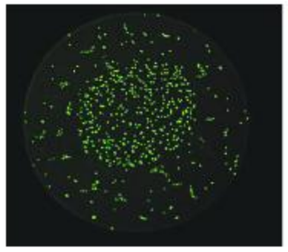

Figure 6. Spermatozoa approach from the periphery, and then bind to the HA spot on a Petri dish.

Sperm–HA binding and strict morphology

Based on current understanding of sperm cellular maturity, it was postulated that HA-bound spermatozoa will show an improved strict morphology score. Twenty-four men were studied (concentration 57.2 ± 10.4 × 10^6 spermatozoa/ml; motility: 55.3 ± 2.8%, all data mean ± SEM). For the HA-binding assay, CellVu double chamber slides were used. On the A side, motile sperm concentration was assessed. HA binding was measured on the HA-coated B side, by calculating the percentage of spermatozoa that remained unbound after 15 min incubation. Semen was added to the A and B sides of another slide, and after 15 min the non-bound spermatozoa on the B side were gently washed off with human tubal fluid (HTF). Spermatozoa on both sides were fixed and stained with DiffQuik. Kruger strict morphology was performed on spermatozoa from all 24 men by two investigators who evaluated 200 spermatozoa on both the A and the B sides (Zavaczki *et al*., 2003).

The proportion of normal spermatozoa was higher in the HA-bound population on the B side as compared with semen on the A side (18.1 ± 1.3% versus 7.8 ± 0.8% $P < 0.001$, $n = 400$ spermatozoa evaluated in each man). The mean strict morphology score improvement on the B versus A sides was 2.6 ± 1.0-fold (range: 1.6–6.3). The proportion of spermatozoa that did not bind to HA was related to the improvement in morphology on the B versus the A side ($r = 0.48$, $P < 0.02$).

The HA-binding ability of spermatozoa is related to sperm maturity and Kruger strict morphology. There was a significant improvement in the proportion of normal spermatozoa in the HA-selected population. HA binding was also related to the objective morphometry attributes that have been shown to reflect sperm maturity, as measured by the biochemical markers of CK activity and HspA2 ratio (Gergely *et al*., 1999). The relationship with strict morphology further indicates that the sperm–HA-binding test is a quick and effective assessment that may be used in the offices of physicians treating male infertility.

Selection of spermatozoa with low aneuploidy frequencies for ICSI

Previously, it was found that mature, but not immature, spermatozoa in response to HA showed increased velocity and retention of long-term motility (Sbracia *et al*., 1997). It was suggested that this effect was receptor mediated. Based on the association between sperm maturation and plasma membrane remodelling, it has been suggested that the presence of the HA receptor in mature, but not in immature spermatozoa, and a respective device with HA-coated surface, will facilitate the selection of single mature spermatozoa with high DNA integrity and low frequency of chromosomal aneuploidies for ICSI (Huszar *et al*., 2003).

As discussed, there is a relationship between the proportion of immature spermatozoa with cytoplasmic retention and frequency of chromosomal aneuploidies in human spermatozoa (Kovanci *et al*., 2001). This relationship is based on the dual role of the HspA2 chaperone, which supports meiosis as a component of the synaptonemal complex, and facilitates plasma membrane remodelling as well as the formation of the zona pellucida and HA-binding sites during spermiogenesis (**Figure 3**). The increased rate of chromosomal aberrations and other potential consequences of using immature spermatozoa for ICSI are of major concern. Data have been presented to show that HA-selected mature spermatozoa show a low frequency of chromosomal aberrations comparable to that of sperm selected by the zona pellucida in conventional fertilization. HA is a normally occurring component of the female reproductive tract; thus there should not be any ethical concerns (**Figure 6**).

In ongoing studies, the efficiency of sperm selection with respect to elimination of spermatozoa with chromosomal aneuploidies and diploidies has been tested. Washed spermatozoa of eight moderately oligozoospermic men (OS, sperm concentration ± SEM: 20.6 ± 1.7 × 10^6/ml, motility: 54.1 ± 2.5%) and 80% isolate gradient sperm pellets from seven normozoospermic IVF patients (ISL80, sperm concentration 118 ± 21.4 × 10^6/ml, motility: 59.1 ± 4.9%) were studied. Spermatozoa suspended in HTF were placed over HA spots bonded to Petri dishes (Biocoat Co., PA, USA). After incubation for 15 min, the HA-attached spermatozoa were collected using an ICSI micropipette. Aliquots of the sperm suspension and HA-bound spermatozoa were examined after FISH, using centromeric probes for the X, Y and 17 chromosomes. Data were analysed by chi-squared analysis.

In each man, the initial sperm suspension (mean: 3000 spermatozoa, 45,000 spermatozoa in the 15 men) was evaluated, and all HA-bound spermatozoa collected in the eight OS men (mean: 753, range: 224–1142) and seven ISL80 men (mean: 644, range 224–1128). In the OS group, the proportion of disomies showed a mean 6.9-fold reduction, and the sex chromosome disomies alone a 3.6-fold reduction. Diploidies in the HA-selected samples were 6.4-fold lower compared with the initial semen sample. With respect to the ISL80 group, the disomy rates declined in the HA-bound fractions (**Table 1**). The decrease for sex chromosomes was approximately four-fold, even though that the ISL80 samples were 80% isolate pellets of normozoospermic men (thus an 'ideal sperm' fraction). The incidence of diploid sperm decreased six-fold in both groups ($P < 0.001$).

It can be concluded that HA selection eliminated spermatozoa with disomy and diploidy. The four-fold decline of sex chromosome disomies is consistent with the increase of

Table 1. Reduction of sperm nuclei with disomy and diploidy in the HA-bound fractions.

	Group OS		
	Disomy		*Diploidy*
	Sex	*17*	
Initial (%)	0.35	0.23	0.81
HA-bound (%)	0.09	0.04	0.13
Reduction	4.0×	5.3×	6.1×
P (chi-squared)	<0.001	<0.001	<0.001

OS = oligozoospermic men.

chromosomal aberrations in ICSI children. In spite of the sample differences, the aneuploidy and diploidy rates in the HA-bound fraction declined to a narrow and low 0.04–0.13% range, which is comparable to normal fertile men. Thus, HA sperm selection provides a new, safe and efficient method for selection of mature spermatozoa for ICSI.

Acknowledgements

This work was supported by NIH (HD-19505, OH-04061). All experiments performed in the Huszar laboratory were approved by the Yale School of Medicine Human Investigation Committee.

References

Aitken J, Krausz C, Buckingham D 1994 Relationships between biochemical markers for residual sperm cytoplasm, reactive oxygen species generation, and the presence of leukocytes and precursor germ cells in human sperm suspensions. *Molecular Reproduction and Development* **39**, 268–279.

Aitken RJ, Baker MA, Sawyer D 2003 Oxidative stress in the male germ line and its role in the aetiology of male infertility and genetic disease. *Reproductive BioMedicine Online* **7**, 63–68.

Allen JW, Dix DJ, Collins BW *et al*. 1996 HSP70–2 is a part of the synaptonemal complex in mouse and hamster spermatocytes. *Chromosoma* **104**, 414–421.

Clermont Y 1963 The cycle of the seminiferous epithelium in man. *American Journal of Anatomy* **112**, 35–51.

Dix DJ 1997 Hsp70 expression and function during gametogenesis. *Cell Stress Chaperones* **2**, 73–77.

Eddy ME 2002 Male germ cell expression. *Recent Progress in Hormone Research* **57**, 103–128.

Ergur AR, Dokras A, Giraldo JR *et al*. 2002 Sperm maturity and treatment choice of IVF or ICSI: Diminished sperm HspA2 chaperone levels predict IVF failure. *Fertility and Sterility* **77**, 910–918.

Gergely A, Kovanci E, Senturk L *et al*. 1999 Morphometric assessment of mature and diminished-maturity human spermatozoa: sperm regions that reflect differences in maturity. *Human Reproduction* **14**, 2007–2014.

Gomez E, Buckingham DW, Brindle J *et al*. 1996 Development of an image analysis system to monitor the retention of residual cytoplasm by human spermatozoa: correlation with biochemical markers of the cytoplasmic space, oxidative stress, and sperm function. *Journal of Andrology* **17**, 276–287.

Henkel R, Kierspel E, Hajimohammade M *et al*. 2003 DNA fragmentation of spermatozoa and ART. *Reproductive BioMedicine Online* **7**, 477–484.

Huszar G, Vigue L 1990 Spermatogenesis-related change in the synthesis of the creatine kinase B-type and M-type isoforms in human spermatozoa. *Molecular Reproduction and Development* **25**, 258–262.

Huszar G, Vigue L 1993 Incomplete development of human spermatozoa is associated with increased creatine phosphokinase concentration and abnormal head morphology. *Molecular Reproduction and Development* **34**, 292–298.

Huszar G, Vigue L 1994 Correlation between the rate of lipid peroxidation and cellular maturity as measured by creatine kinase activity in human spermatozoa. *Journal of Andrology* **15**, 71–77.

Huszar G, Corrales M, Vigue L 1988a Correlation between sperm creatine phosphokinase activity and sperm concentrations in normospermic and oligospermic men. *Gamete Research* **19**, 67–75.

Huszar G, Vigue L, Corrales M 1988b Sperm creatine phosphokinase activity as a measure of sperm quality in normospermic, variablespermic, and oligospermic men. *Biology of Reproduction* **38**, 1061–1066.

Huszar G, Vigue L, Corrales M 1990 Sperm creatine kinase activity in fertile and infertile oligospermic men. *Journal of Andrology* **11**, 40–46.

Huszar G, Vigue L, Morshedi M 1992 Sperm creatine phosphokinase M-isoform ratios and fertilizing potential of men: a blinded study of 84 couples treated with in vitro fertilization. *Fertility and Sterility* **57**, 882–888.

Huszar G, Vigue L, Oehninger S 1994 Creatine kinase immunocytochemistry of human sperm–hemizona complexes: selective binding of sperm with mature creatine kinase-staining pattern. *Fertility and Sterility* **61**, 136–142.

Huszar G, Sbracia M, Vigue L *et al*. 1997 Sperm plasma membrane remodeling during spermiogenetic maturation in men: relationship among plasma membrane beta 1,4-galactosyltransferase, cytoplasmic creatine phosphokinase, and creatine phosphokinase isoform ratios. *Biology of Reproduction* **56**, 1020–1024.

Huszar G, Patrizio P, Vigue L *et al*. 1998 Cytoplasmic extrusion and the switch from creatine kinase B to M isoform are completed by the commencement of epididymal transport in human and stallion spermatozoa. *Journal of Andrology* **19**, 11–20.

Huszar G, Stone K, Dix D, Vigue L 2000 Putative creatine kinase M-isoform in human sperm is identified as the 70-kilodalton heat shock protein HspA2. *Biology of Reproduction* **63**, 925–932.

Huszar G, Celik-Ozenci C, Cayli S *et al*. 2003 Hyaluronic acid binding by human sperm indicates cellular maturity: viability and unreacted acrosomal status. *Fertility and Sterility* **79** (suppl. 3), 1616–1624.

Jakab A, Kovacs T, Zavaczki Z *et al*. 2003 Efficiency of the swim-up method in eliminating sperm with diminished maturity and aneuploidy. *Human Reproduction* **18**, 1481–1488.

Kovanci E, Kovacs T, Moretti E *et al*. 2001 FISH assessment of aneuploidy frequencies in mature and immature human spermatozoa classified by the absence or presence of cytoplasmic retention. *Human Reproduction* **16**, 1209–1217.

Lalwani S, Sayme N, Vigue L *et al*. 1996 Biochemical markers of early and late spermatogenesis: relationship between the lactate dehydrogenase-X and creatine kinase-M isoform concentrations in human spermatozoa. *Molecular Reproduction and Development* **43**, 495–502.

Oehninger S, Morshedi M, Weg S-L *et al*. (2003) Presence and significance of somatic cell apoptosis markers in human ejaculated spermatozoa. *Reproductive BioMedicine Online* **7**, in press.

Orlando C, Krausz C, Forti G, Casano R 1994 Simultaneous measurement of sperm LDH, LDH-X, CPK activities and ATP content in normospermic and oligozoospermic men. *International Journal of Andrology* **17**, 13–18.

Óvári L, Vigue L, Stronk L *et al*. 2003 Detection of numerical chromosomal aberrations and nuclear immaturity within the same spermatozoa: a study of FISH and aniline blue staining. In: Abstracts from 19th Annual Meeting of the ESHRE, Madrid, Spain; 29 June – 2 July 2003. *Human Reproduction* **18** (suppl. 1), O–230 (abstr.).

Sbracia M, Grasso J, Sayme N *et al*. 1997 Hyaluronic acid substantially increases the retention of motility in cryopreserved/thawed human spermatozoa. *Human Reproduction* **12**, 1949–1954.

Sidhu RS, Sharma RK, Agarwal A 1998 Relationship between creatine kinase activity and semen characteristics in subfertile men. *International Journal of Fertility* **43**, 192–197.

Zavaczki Z, Cayli S, Celik-Ozenci C *et al*. 2003 Correlation between hyaluronic acid binding and shape attributes of human sperm: hyaluronic acid binding score, strict morphology and objective morphometry. In: Abstracts from 19th Annual Meeting of the ESHRE, Madrid, Spain; 29 June – 2 July 2003. *Human Reproduction* **18** (suppl. 1), O–024 (abstr.).

Paper based on contribution presented at the 'TWIN–Meeting Alpha–Andrology 2003' in Antwerp, Belgium, September 2003.

Received 21 May 2003; refereed 16 July 2003; accepted 21 July 2003.

acta histochem. 104(3) 271–277 (2002)

http://www.urbanfischer.de/journals/actahist

acta histochemica

Distribution patterns of PCNA and ANP in perinatal stages of the developing rat heart

Sevil Çayli, İsmail Üstünel, Çiler Çelik-Özenci, Emin Türkay Korgun, and Ramazan Demir*

Department of Histology and Embryology, Akdeniz University, Antalya, Turkey

Received 4 December 2001 and in revised form 25 March 2002 and 22 April 2002; accepted 29 April 2002

Summary

Distribution patterns of proliferating cell nuclear antigen (PCNA) and atrial natriuretic peptide (ANP) were determined immunohistochemically and morphometrically in atrium and ventriculum of the developing rat heart in different stages of the perinatal period. During the prenatal period, PCNA and ANP were localized in opposite patterns, particularly in trabecular myocytes. A distinct reduction in the percentage of PCNA-positive nuclei was detected starting at day 19 of the prenatal period, and these cells were rarely observed on postnatal days 30 and 60. In cardiomyocytes, a distinct increase in ANP positivity was found, whereas PCNA positivity was very low. It is concluded that PCNA expression gradually decreased from prenatal day 19 onwards, whereas ANP expression increased in atria throughout the prenatal and postnatal periods, except for a decrease in ANP expression in ventricles from prenatal day 21 onwards. The opposite expression patterns of PCNA and ANP in trabecular myocytes of ventricles indicate that ANP may have antimitogenic/antiproliferative effects in trabecular myocytes.

Key words: heart – PCNA – ANP – immunohistochemistry – development – rat

Introduction

Proliferating cell nuclear antigen (PCNA) is a marker for the cell cycle. It is an accessory protein that is necessary for DNA synthesis in mammalian cells (Jonsson and Hubscher, 1997; Kelman, 1997), since a lack of this protein prevents a cell to undergo cell division (Bravo and Macdonald-Bravo, 1987; Prelich et al., 1987). Besides, PCNA also has a role in DNA repair and control of the cell cycle (Tsurimoto et al., 1998). Ki-67, which is also a proliferation marker, has a shorter half life than PCNA. For this reason, the labelling index (LI) of Ki-67 correlates better with the BrdU LI than the PCNA LI does (Scott et al., 1991; Mokry and Nemecek, 1995).

DNA synthesis ceases in mice hearts when the animals are 4 months of age (Petersen and Baserga, 1965), in chicks after birth (Clark and Fischman, 1983), and cell division does not occur in the adult myocardium (Zak, 1984; Bugaisky and Zak, 1986). In rats, it was found that cardiac muscle cells do not have the ability to divide at 4 weeks after birth and as the cells increase in volume, they do not produce PCNA any longer (Anversa et al., 1980; Claycomb, 1992).

ANP has been found in granules in mammalian heart myocytes and has natriuretic, diuretic, vasodilator and hypotensive effects (Forssmann, 1986; Rebuffat et al., 1989; Mifune et al., 1991; Mochizuki et al., 1991; Ram-

*Correspondence to: Prof. Dr. Ramazan Demir, Department of Histology and Embryology, Faculty of Medicine, Akdeniz University, 07070 Campus, Antalya, Turkey; tel and fax: + 90 242 2274486; e-mail: demir@med.akdeniz.edu.tr

0065-1281/02/104/03-271 $ 15.00/0

say, 1991). In adult males, these granules are more apparent in right atrial cardiomyocytes, and are densely packed in perinuclear, intermyofibrillar and subsarcolemmal compartments in myocytes (Forssmann, 1986; Lee and Lee, 1990; Mifune et al., 1991). It has been suggested that ANP starts to be produced during very early embryonic stages in fetal rat heart. ANP granules appear immediately after organogenesis, and this early secretory activity of ANP is directly related to either the development or the functioning of the heart (Thompson et al., 1986; Scott and Jennes, 1988). On the other hand, it has been determined that ANP plays a growth-regulatory role in tissues, such as brain and bone and in some cell types such as myocytes, and endothelial cells. In vascular smooth muscle cells, it has an antimitogenic/antiproliferative effect and thus inhibits cell proliferation (Appel, 1992). However, the exact mechanisms of the growth-regulatory role of ANP has not yet been elucidated completely.

Thus far, it has not been investigated what the regional distribution patterns are of PCNA and ANP-producing cells in prenatal and postnatal periods of rat heart and whether there is a relationship between their distributions patterns. In the present study, the relevance of the distribution patterns of PCNA and ANP in rat heart are investigated in different perinatal stages in its development.

Material and methods

Tissue preparation

Fourty-eight female and 24 male adult rats (Rattus norvegicus), weighing 190–230 g, were used and none of them had mated before the present study was performed. The rats were fed with normal rat chow and tap water and 2 females and 1 male were kept overnight in one cage. The following morning, vaginal smears were prepared and when sperm was found by microscopical examination, that day was designated as the first day of pregnancy. Pregnant rats were anaesthetized with ether, their abdomens were opened, and embryos and fetuses were removed by excising uterine horns. Of 30 pregnant rats, 24 fetuses were removed on days 15, 17, 19, and 21 and 6 embryos were removed on day 13. Additionally, 6 rats were used on days 10, 30 and 60 after birth.

Hearts of 13-day embryos, 15, 17, 19, and 21-day fetuses and 10, 30 and 60-day old rats were removed and fixed in Holland's fixative consisting of 4% formaldehyde, 1–5 ml glacial acetic acid, 4 g picric acid, 2.5 g cupric acetate in 100 ml distilled water. After dehydration, tissues were cleared in acetone and embedded in paraffin, and subsequently, serial sections (5–7 μm thick) were collected on poly-L-lysine-coated slides (Sigma, St. Louis MO, USA) and incubated overnight at 40 °C.

Immunohistochemistry

After dehydrating, heat-induced antigen retrieval was performed by boiling the sections in citrate buffer, pH 6.0, in a microwave oven as described by Cattoretti et al. (1993). Sections were then washed 3 times in PBS (pH 7.4). To block endogenous peroxidase activity, sections were incubated in an aqueous solution of 3% H_2O_2 for 20 min at room temp and afterwards, washed 3 times with PBS. Sections were then incubated with primary undiluted rabbit anti-PCNA antibodies (Dako, Glostrup, Denmark) and anti-ANP antibodies (Chemicon, Temecula CA, USA) in an 1:500 dilution. Negative control incubations were performed by using normal rabbit IgG

Fig. 1. PCNA and ANP immunohistochemistry in prenatal rat heart (day 13). **a.** PCNA-positive interphase nuclei (arrow) and PCNA-positive cytoplasm of a cell in prophase (p) are present. **b.** PCNA positivity is present in a metaphase (m) in the left ventricle. **c.** A PCNA-positive cell in anaphase (a). **d.** Negative control incubation. **e.** Telophase (t) in the right atrium. **f.** ANP-positive trabecular myocytes (arrows) of the left ventricle. Magnifications, **a–e** ×250; **f**, ×50.

Fig. 2. Comparison of PCNA and ANP staining in the left ventricle in a prenatal rat heart (day 15). **a.** Density of PCNA-positive nuclei increases from the inner to the outer part of the ventricular wall (as indicated by the arrows) and its density is lowest in trabecular myocytes. **b.** Density of ANP-positive cells decreases from the inner to the outer part of the ventricular wall and its density is highest in trabecular myocytes (tm). **c.** Negative control incubation. Magnifications, ×50.

Fig. 3. Density of PCNA-positive cells is low in prenatal rat heart at day 19. Magnification, ×50.

Fig. 4. Immunohistochemical staining of ANP in prenatal rat heart at day 21. ANP-positive cardiomyocytes (arrows) are present throughout the right atrial wall. Magnification, ×100.

Fig. 5. Immunohistochemical staining of PCNA (**a**) and ANP (**b**) in rat heart at postnatal day 10. **a.** High frequency of cells that are PCNA positive (arrows) is found in the atrioventricular (AV) valve and cells with dense ANP staining (arrows) are present in the left atrium. Magnification, ×50.

Fig. 6. Immunohistochemical staining of PCNA in rat heart at postnatal day 30. Strong PCNA staining is present in mesenchymal cells of the right ventricle (arrows) and scarce PCNA immunostaining is present in cardiomyocytes in mitosis (double arrows). Magnification, ×100.

Fig. 7. Immunohistochemistry of PCNA (**a**) and ANP (**b,c**) in rat heart at postnatal day 60. **a.** PCNA-positive cardiomyocytes (arrows) are hardly present in the outer part of the left ventricle. **b.** Very dense ANP staining is present in the left atrium (arrows) when compared to previous days. **c.** ANP-positive Purkinje cells are present in the left ventricle (arrows). Magnifications, **a**, ×50; **b**, ×250; **c**, ×100.

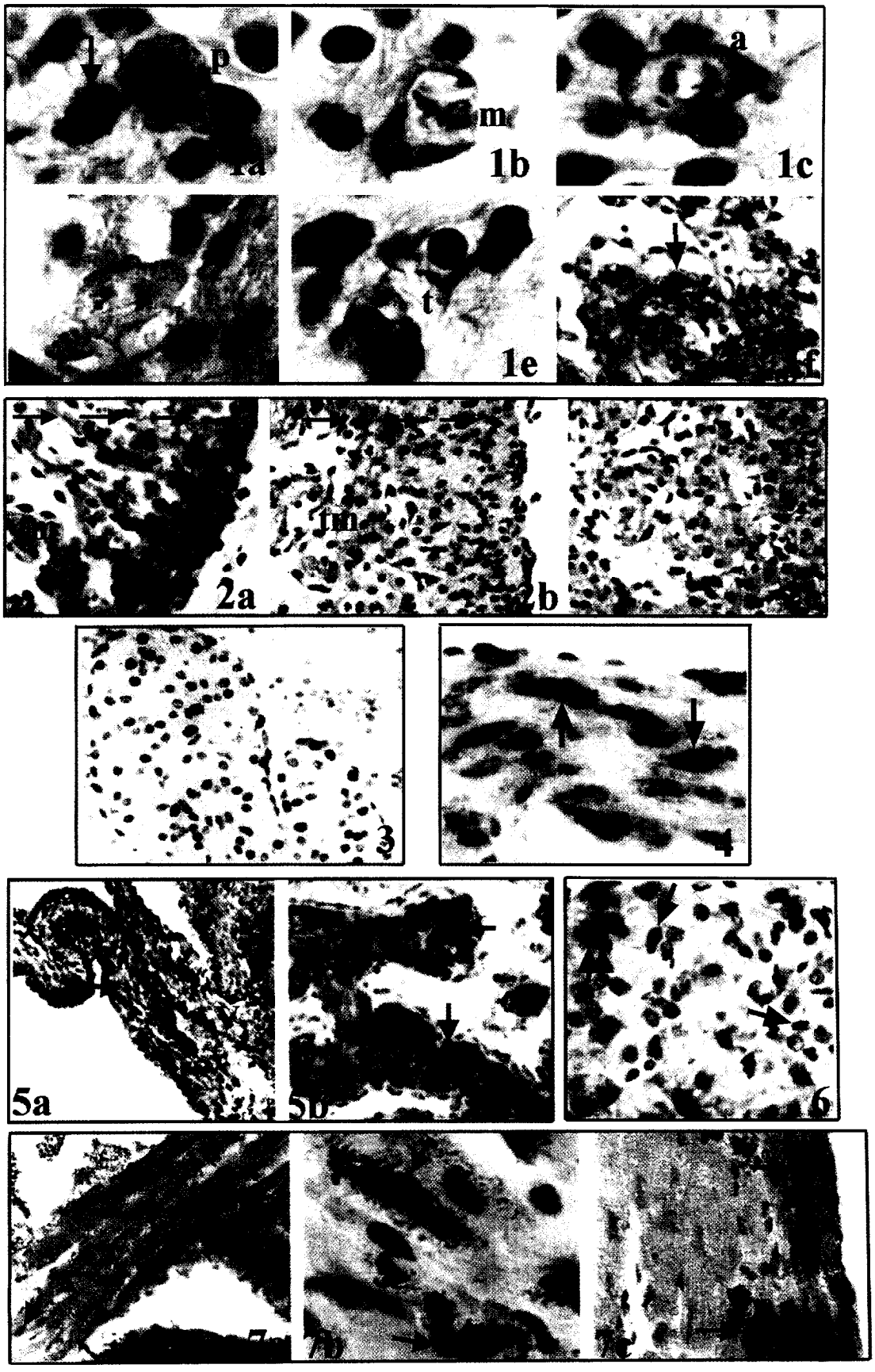

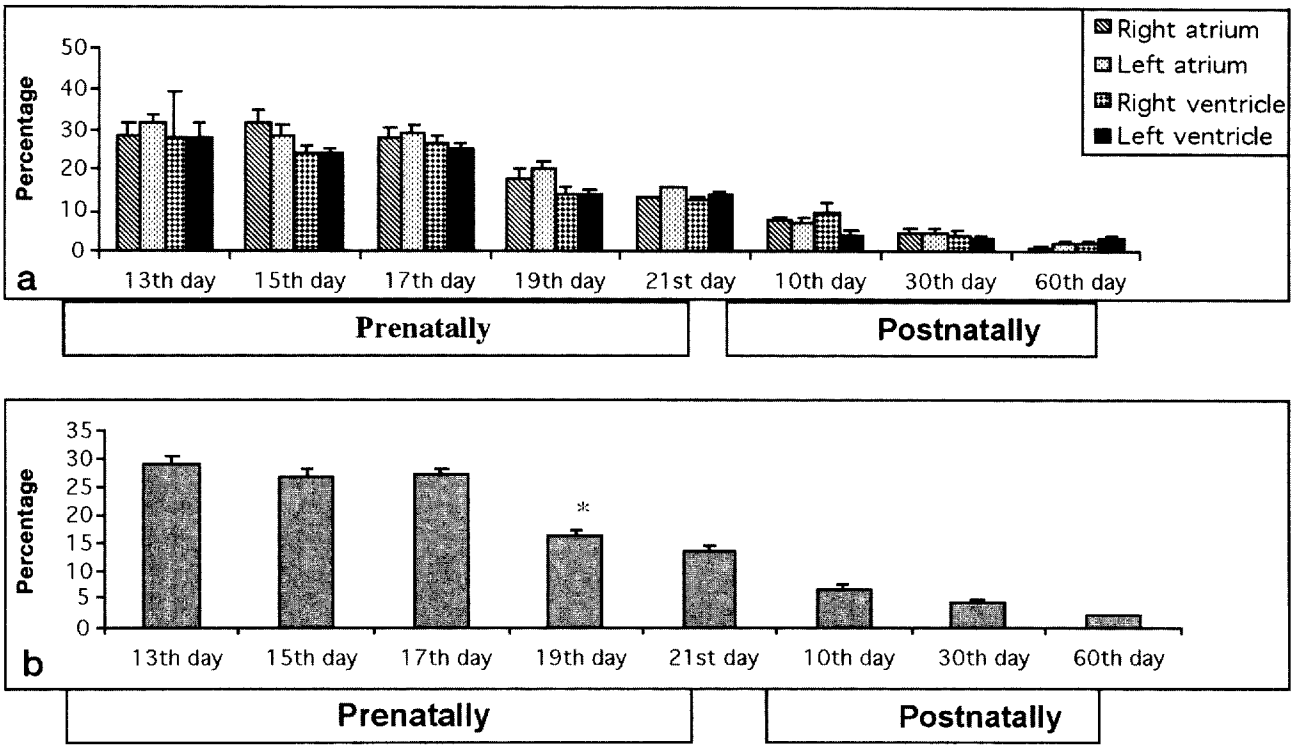

Fig. 8. Distribution patterns of PCNA-positive cells in atria and ventricles of rat heart (**a**) and total PCNA-positive cell frequency in developing rat heart (**b**). *, Statistically significant difference with the value at day 13.

in the same concentration as the primary antibody. A secondary anti-rabbit antibody conjugated with biotin and horseradish-peroxidase-labelled streptavidin (HRP-LSAB kit, Dako) were applied according to manufacturer's instructions. Peroxidase activity was visualized with 3-amino-9-ethylcarbozole (AEC; Dako) and H_2O_2 as substrates. All incubations were performed in a moist chamber at room temp, using PBS for washes between incubation steps. The sections were counterstained with hematoxylin, dehydrated and mounted in mounting medium (Biogenex, San Ramon CA, USA).

Photomicrographs were taken with an Axioplan microscope (Zeiss, Oberkochen, Germany) and original magnifications were calculated.

Morphometric analysis

Six rat hearts were evaluated for each time point. Twenty areas were selected consisting of 5 regions that were analyzed morphometrically for each heart compartment (2 atria and 2 ventricles). Morphometry was performed light microscopically with a 0.01 mm^2 ocular scale bar, and PCNA-positive and ANP-positive cardiomyocytes in a 1 cm^2 field at X200 original magnification were counted and their percentages were determined. The means at each prenatal and postnatal day were calculated as means (SD and were compared statistically using the Student's t-test. All statistical comparisons were made with 95% as level of significance.

Results

PCNA immunopositivity was strong in cardiomyocytes on day 13 of gestation. Various stages of mitosis were observed in large amounts of cardiomyocytes throughout the hearts. Interphase nuclei and cells in mitosis showed strong PCNA expression (Fig. 1a). Most of the PCNA-positive cells were localized in the outer parts of the heart walls. Immunostaining was present in cells in prophase, metaphase, anaphase and telophase (Fig. 1). Immunostaining of PCNA was more extensive in atria than in ventricles (Fig. 8a).

Myocardial cardiomyocytes of atria and ventricles were strongly stained for ANP and were found close to the ventricular chamber, especially in trabecular myocytes (Fig. 1f). ANP granules were particularly localized in perinuclear regions. The percentages of ANP-positive cells were highest in trabecular regions of the left atrium and left ventricle whereas the right ventricule contained the lowest amount of ANP-positive cells (Fig. 9a).

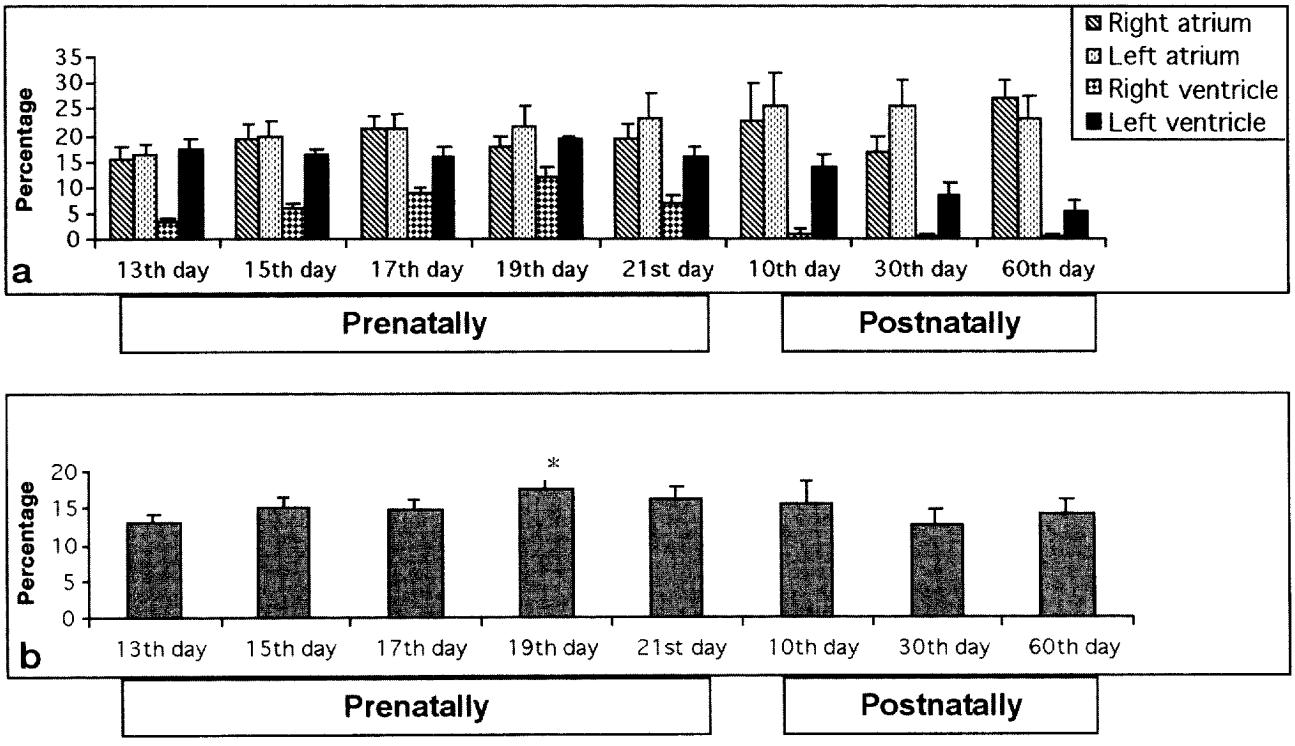

Fig. 9. Distribution patterns of ANP-positive cells in atria and ventricles of rat heart (**a**) and total ANP-positive cell frequency in developing rat heart (**b**). *, Statistically significant difference with the value at day 13.

On day 15 of gestation, the percentage of PCNA-positive nuclei in atrial and ventricular walls was elevated and increased from the inner to the outer wall of the myocardium. The frequency of PCNA-positive trabecular myocytes was lower than the frequency of other PCNA-positive myocardial myocytes (Fig. 2a). In contrast, ANP immunostaining decreased from the inner to the outer wall of the myocardium (Fig. 2b). The percentage of PCNA-positive nuclei was distinctly higher in atria than in ventricles and atria showed the highest amounts of ANP immunostaining in parallel with PCNA staining.

On day 17 of gestation, PCNA immunostaining was similar to that on day 15 of embryonic heart development and the percentage of PCNA-positive nuclei was not significantly different from that on days 13 and 15. Thus, highest percentages of PCNA-positive cells were found on days 13, 15 and 17 of the prenatal phase (Fig. 8b). In this period, ANP immunostaining increased continuously in the atrial wall and was highest in the left atrium.

On day 19 of gestation, there was a significant decrease in the densities of PCNA-positive cells (Figs. 3 and 8), whereas the total percentage of ANP-positive cells was highest (Fig. 9b). The increase was statistically significant when compared with day 13 of gestation ($p<0.05$). ANP immunostaining was still intense in almost every region of the atria.

On day 21 of gestation, most of the PCNA-positive nuclei were found in the medial and outer parts of the myocardium, whereas ANP immunostaining was not present in these regions except for cardiomyocytes in subendocardial regions of the left ventricle and the papillar muscle. However, in the pectinate muscles of the atria, dense ANP immunostaining was observed in cardiomyocytes throughout the myocardial wall (Fig. 4).

After birth on postnatal day 10, the number of PCNA-positive nuclei in atrial and ventricular walls was strongly reduced, whereas the atrioventricular wall still contained cells positive for PCNA (Fig. 5a). There was a slight decrease in the number of ANP-positive cells in ventricles of the rat hearts that was not statistically significant ($p>0.05$) whereas the atria were still immunopositive for ANP (Figs. 5b and 9a).

On postnatal day 30, PCNA immunostaining was strong in mesenchymal cells of the heart, whereas there was less immunopositivity in cardiomyocytes (Fig. 6). The total percentage of PCNA-positive cells continued to decline (Fig. 8b). The percentage of ANP-positive cells did not change significantly, but its decline in the ventricles continued (Fig. 9a). Finally, on postnatal day 60, hardly any PCNA-positive cardiomyocytes were

found (Figs. 7a and 8), whereas ANP immunopositivity was most intense when compared with the previous days. Both atrial myocytes and Purkinje cells of the ventricles were stained strongly for ANP (Fig. 7b,c).

Discussion

The present study shows that the number of PCNA-positive nuclei in the outer part of atrial and ventricular myocardium is higher than in other parts of the developing rat heart. PCNA positivity decreased towards the trabecular myocytes that are found near the ventricular chamber. Because trabecular myocytes develop from myocytes in the outer compact layer of the ventricle wall (Wenink et al., 1996; Sedmera et al., 2000), our study suggests that PCNA-negative trabecular myocytes of the ventricular myocardium differentiate from PCNA-positive cardiomyocytes localized in the outer layer of ventricular myocardium. Therefore, these PCNA-negative trabecular myocytes are differentiated rather than proliferating.

It has been established that ANP has antimitogenic/antiproliferative effects in tissues such as brain, bone, myocytes, and red blood cell precursors (Appel, 1992). The present study shows that ANP immunostaining, but not PCNA immunostaining is present in trabecular myocytes in the prenatal period which is in agreement with the findings of Appel (1992). It may be assumed that ANP has antimitogenic/antiproliferative effects on cardiac myocytes of rats as well. The percentage of PCNA-positive cells was highest on prenatal days 13, 15, 17 and decreased after prenatal day 17. In contrast, the number of ANP-positive cells was highest on prenatal day 19, indicating that ANP has an antimitogenic effect on cardiomyocytes. In the postnatal period, a similar contrast in percentages of PCNA-positive and ANP-positive cells was found as well. PCNA immunostaining decreased and ANP immunostaining increased with age.

PCNA-positive interphase nuclei have been found in other studies as well (Mathews et al., 1984; Waseem and Lane, 1990) and indicate that PCNA is necessary for both DNA replication and cell division (Bravo and Macdonald-Bravo, 1987; Prelich et al., 1987). PCNA immunostaining during the various stages of mitosis was present only in the cytoplasm, implying that the protein was synthesized in the interphase and during mitosis expressed in the cytoplasm. Moreover, PCNA-positive interphase nuclei were mainly localized in the outer part of the ventricle, indicating that this part of the ventricular wall serves as a source of new cells.

In contrast with the findings of Marino et al. (1996), we found that PCNA-positive cardiomyocytes are still present on postnatal days 30 and 60, indicating that cardiomyocytes continue to divide at least up to 2 months postnatally.

During development, ANP-positive cells were lowest in number in the right ventricle. During the postnatal period, ANP-immunostaining in the ventricles decreased whereas in the atria it increased continuously. The decrease in ANP immunostaining in ventricular myocytes in the postnatal period may be related to increased sympathetic innervation in this region. A number of studies report increased ANP levels after sympathectomy in rat ventricles (Albino-Teixeri et al., 1990; Hansson et al., 1998; Hansson, 2001). ANP production may be limited in the ventricular myocardium and conduction system due to sympathetic innervation or other factors. However, it is not clear why ANP expression in the atrium is continuous during development. In the postnatal period, ANP staining is reduced in the left ventricle and is only present in the Purkinje cells, which are part of the conducting system. These findings are in line with other studies (Thompson et al., 1986; Toshimori et al., 1987; Benvenuti et al., 1997). Our findings show that ANP-positive cardiomyocytes of the left ventricle are differentiated cells of the conducting system of the ventricle in the postnatal period, and ANP has an important role in the conducting process in heart.

In conclusion, immunostaining of ANP and PCNA was observed in trabecular myocytes and various cell types of the heart wall and showed opposite distribution patterns, thus ANP may have a negative growth-regulatory effect in developing rat heart.

Acknowledgment

This study was supported by the Research Fund of Akdeniz University, Antalya, Turkey, grant no: 20.01.0122.01, and was part of Sevil Çayli's thesis for a master of science degree.

References

Albino-Teixeira A, Polonia JJ, and Azevedo I (1990) Sympathetic denervation causes atrial natriuretic peptide-storing granules to appear in the ventricular myocardium of the rat. Naunyn-Schmiedebergs Arch Pharmacol **342**: 241–244

Anversa P, Olivetti G, and Loud AV (1980) Morphometric study of early postnatal development in the left and right ventricular myocardium of the rat. I. Hypertrophy, hyperplasia, and binucleation of myocytes. Circ Res **46**: 495–502

Appel RG (1992) Growth-regulatory properties of atrial natriuretic factor. Am J Physiol **262**: 911–918

Benvenuti LA, Aiello VD, Higuchi MDL, and Palomino SA (1997) Immunohistochemical expression of atrial natriuretic peptide (ANP) in the conducting system and internodal atrial myocardium of human hearts. Acta Histochem **99**: 187–193

Bravo R, and Macdonald-Bravo H (1987) Existence of two populations of cyclin/proliferating cell nuclear antigen during the cell cycle: association with DNA replication sites. J Cell Biol **105**: 1549–1554

Bugaisky LB, and Zak R (1986) Biological mechanism of hypertrophy. In: Fozzard HA, Haber E, Jennings RB, Katz AM and Morgan HE (Eds) The heart and the cardiovascular system. Raven Press, New York NY, pp 1491–1506

Cattoretti G, Pileri S, Parravicini C, Becker MH, Poggi S, Bifulco C, Key G, D'Amato L, Sabattini E, and Feudale E (1993) Antigen unmasking on formalin-fixed, paraffin-embedded tissue sections. J Pathol **171**: 83–98

Clark WA, and Fischman DA (1983) Analysis of population cytokinetics of chick myocardial cells in tissue culture. Dev Biol **97**: 1–9

Claycomb WC (1992) Control of cardiac muscle cell division. Cardiovasc Med **2**: 231–236

Forssmann WG (1986) Cardiac hormones. I. Review on the morphology, biochemistry and molecular biology of the endocrine heart. Eur J Clin Invest **16**: 439–451

Hansson M, Kjorell U, and Forsgren S (1998) Increased immunoexpression of atrial natriuretic peptide in the heart conduction system of the rat after cardiac sympathectomy. J Mol Cell Cardiol **30**: 2047–2057

Hansson M, Kjorell U, and Forsgren S (2001) Ingrowth of sympathetic innervation occurs concomitantly with a decrease of ANP in the growing rat cardiac ventricles. Anat Embryol **203**: 35–44

Jonsson ZO, and Hubscher U (1997) Proliferating cell nuclear antigen: more than a clamp for DNA polymerases. Bioessays **19**: 967–975

Kelman Z (1997) PCNA: structure, functions and interactions. Oncogene **14**: 629–640

Lee YS, and Lee CP (1990) Secretory granules containing atrial natriuretic polypeptide in human ventricular cardiomyocytes. An electron microscopic immunocytochemical study. Jpn Heart J **31**: 661–670

Marino TA, Cao W, Lee J, and Courtney R (1996) Localization of proliferating cell nuclear antigen in the developing and mature heart cell. Anat Rec **245**: 677–684

Mathews MB, Bernstein RM, Franza BRJr, and Garrels JI (1984) Identity of the proliferating cell nuclear antigen and cyclin. Nature **309**: 374–376

Mifune H, Suzuki S, Noda Y, Mohri S, and Mochizuki K (1991) Fine structure of atrial natriuretic peptide (ANP) granules in the atrial cardiocytes in the pig, cattle and horse. J Vet Med Sci **53**: 561–568

Mochizuki N, Sawa H, Yasuda H, Shinohara T, Nagashima K, Yamaji T, Ohnuma N, and Hall WW (1991) Distribution of atrial natriuretic peptide in the conduction system and ventricular muscles of the human heart. Virch Arch **418**: 9–16

Mokry J, and Nemecek S (1995) Immunohistochemical detection of proliferative cells. Sb Ved Pr Lek Fak Karlovy Univerzity Hradci Kralove **38**: 107–113

Petersen RO, and Baserga R (1965) Nucleic acid and protein synthesis in cardiac muscle of growing and adult mice. Exp Cell Res **40**: 340–352

Prelich G, Tan CK, Kostura M, Mathews MB, So AG, Downey KM, and Stillman B (1987) Functional identity of proliferating cell nuclear antigen and a DNA polymerase-delta auxiliary protein. Nature **326**: 517–520

Ramsay LE, and Ramsay YWW (1991) First line treatment in hypertension. Brit Med J **302**: 352–353

Rebuffat P, Mazzocchi G, Coi A, Gottardo G, and Nussdorfer GG (1989) A stereologic study of the granule population of rat atrial myoendocrine cells: effects of chronic water/sodium restriction and acute water/sodium load. Anat Anz **169**: 149–155

Scott JN, and Jennes L (1988) Development of immunoreactive atrial natriuretic peptide in foetal hearts of spontaneously hypertensive and Wistar-Kyoto rats. Anat Embryol (Berl) **178**: 359–363

Scott RJ, Hall PA, Haldane JS, van Noorden S, Price Y, Lane DP, and Wright NA (1991) A comparison of immunohistochemical markers of cell proliferation with experimentally determined growth fraction. J Pathol **165**: 173–178

Sedmera D, Pexieder T, Vuillemin M, Thompson RP, and Anderson RH (2000) Developmental patterning of the myocardium. Anat Rec **258**: 319–337

Thompson RP, Simson JA, and Currie MG (1986) Atriopeptin distribution in the developing rat heart. Anat Embryol (Berl) **175**: 227–233

Toshimori H, Toshimori K, Oura C, and Matsuo H (1987) Immunohistochemical study of atrial natriuretic polypeptides in the embryonic, foetal and neonatal rat heart. Cell Tissue Res **248**: 627–633

Tsurimoto T (1998) PCNA, a multifunctional ring on DNA. Biochim Biophys Acta **1443**: 23–39

Waseem NH, and Lane DP (1990) Monoclonal antibody analysis of the proliferating cell nuclear antigen (PCNA). Structural conservation and the detection of a nucleolar form. J Cell Sci **96**: 121–129

Wenink AC, Knaapen MW, Vrolijk BC, and Van Groningen JP (1996) Development of myocardial fiber organisation in rat heart. Anat Embryol (Berl) **193**: 559–567

Zak R (1984) Factors controlling cardiac growth. In: Zak R (Ed) Growth of the heart in health and disease. Raven Press, New York NY, pp 165–185